

VOLUME 87 NO. ST7

OCTOBER 1961

PART 1

**JOURNAL of the**

***Structural***

***Division***

---

**PROCEEDINGS OF THE**



**AMERICAN SOCIETY**

**OF CIVIL ENGINEERS**

## BASIC REQUIREMENTS FOR MANUSCRIPTS

Original papers and discussions of current papers should be submitted to the Manager of Technical Publications, ASCE. Authors should indicate the technical division to which the paper is referred. The final date on which a discussion should reach the Society is given as a footnote with each paper. Those who are planning to submit material will expedite the review and publication procedures by complying with the following basic requirements:

1. Titles must have a length not exceeding 50 characters and spaces.
2. A summary of approximately 50 words must accompany the paper, a 300-word synopsis must precede it, and a set of conclusions must end it.
3. The manuscript (an original ribbon copy and two duplicate copies) should be double-spaced on one side of 8½-inch by 11-inch paper. Three copies of all illustrations, tables, etc., must be included.
4. The author's full name, Society membership grade, and footnote reference stating present employment must appear on the first page of the paper.
5. Mathematics are recomposed from the copy that is submitted. Because of this, it is necessary that letters be drawn carefully, and that special symbols be properly identified. The letter symbols used should be defined where they first appear, in the illustrations or in the text, and arranged alphabetically in an Appendix.
6. Tables should be typed (an original ribbon copy and two duplicate copies) on one side of 8½-inch by 11-inch paper. Specific illustrations and explanation must be made in the text for each table.
7. Illustrations must be drawn in black ink on one side of 8½-inch by 11-inch paper. Because illustrations will be reproduced with a width of between 3-inches and 4½-inches, the lettering must be large enough to be legible at this width. Photographs should be submitted as glossy prints. Explanations and descriptions must be made within the text for each illustration.
8. The desirable average length of a paper is about 12,000 words and the absolute maximum is 18,000 words. As an approximation, each full page of typed text, table, or illustration is the equivalent of 300 words.
9. Technical papers intended for publication must be written in the third person.
10. The author should distinguish between a list of "Reading References" and a "Bibliography," which would encompass the subject of his paper.

---

Reprints from this Journal may be made on condition that the full title, name of author, name of publication, page reference, and date of publication by the Society are given. The Society is not responsible for any statement made or opinion expressed in its publications.

This Journal is published bi-monthly by the American Society of Civil Engineers. Publication office is at 2500 South State Street, Ann Arbor, Michigan. Editorial and General Offices are at United Engineering Center, 345 East 47th Street, New York 17, N. Y. \$4.00 of a member's dues are applied as a subscription to this Journal. Second-class postage paid at Ann Arbor, Michigan.

The index for 1960 was published as ASCE Publication 1961-15 (list price \$2.00); indexes for previous years are also available.



---

Journal of the  
STRUCTURAL DIVISION  
Proceedings of the American Society of Civil Engineers

---

STRUCTURAL DIVISION  
EXECUTIVE COMMITTEE

Emerson J. Ruble, Chairman; Nathan D. Whitman, Jr., Vice Chairman;  
Robert D. Dewell; Theodore R. Higgins; John D. Haltiwanger, Secretary  
Elmer K. Timby, Board Contact Member

COMMITTEE ON PUBLICATIONS

Gerald F. Borrmann, Chairman; Phil M. Ferguson; Abbott Frank;  
William J. Hall; Roy G. Johnston; William T. K. May; William H.  
Munse; Sidney Shore; George S. Vincent

CONTENTS

October, 1961

Papers

	Page
Prestressed Bowstring Arch by Movses J. Kaldjian . . . . .	1
Dynamic Response of Highway Bridges by John F. Fleming and James P. Romualdi . . . . .	31
String Polygon Analysis of Frames with Straight Members by Jan J. Tuma and John T. Oden . . . . .	63
Stresses at a Re-Entrant Corner of a Plate by Mario G. Salvadori . . . . .	91
Vibration Analysis for Structural Floor Systems by Lawrence R. Burkhardt . . . . .	97
(over)	

Copyright 1961 by the American Society of Civil Engineers.

Note.—Part 2 of this Journal is the 1961-37 Newsletter of the Structural Division.

The three preceding issues of this Journal are dated April 1961, June 1961, and August 1961.

	Page
Multiple Ribless Shells by Anton Tedesco . . . . .	107
Deflection Theory of Arches by S. O. Asplund . . . . .	125
Strength of Plate Girders in Shear by Konrad Basler . . . . .	151
Strength of Plate Girders Under Combined Bending and Shear by Konrad Basler . . . . .	181
Recent Advances in the Design and Behavior of Concrete Bridges by Hubert Rüschi . . . . .	199
Folded Plate Structures of Light Gage Steel by Arthur H. Nilson . . . . .	215

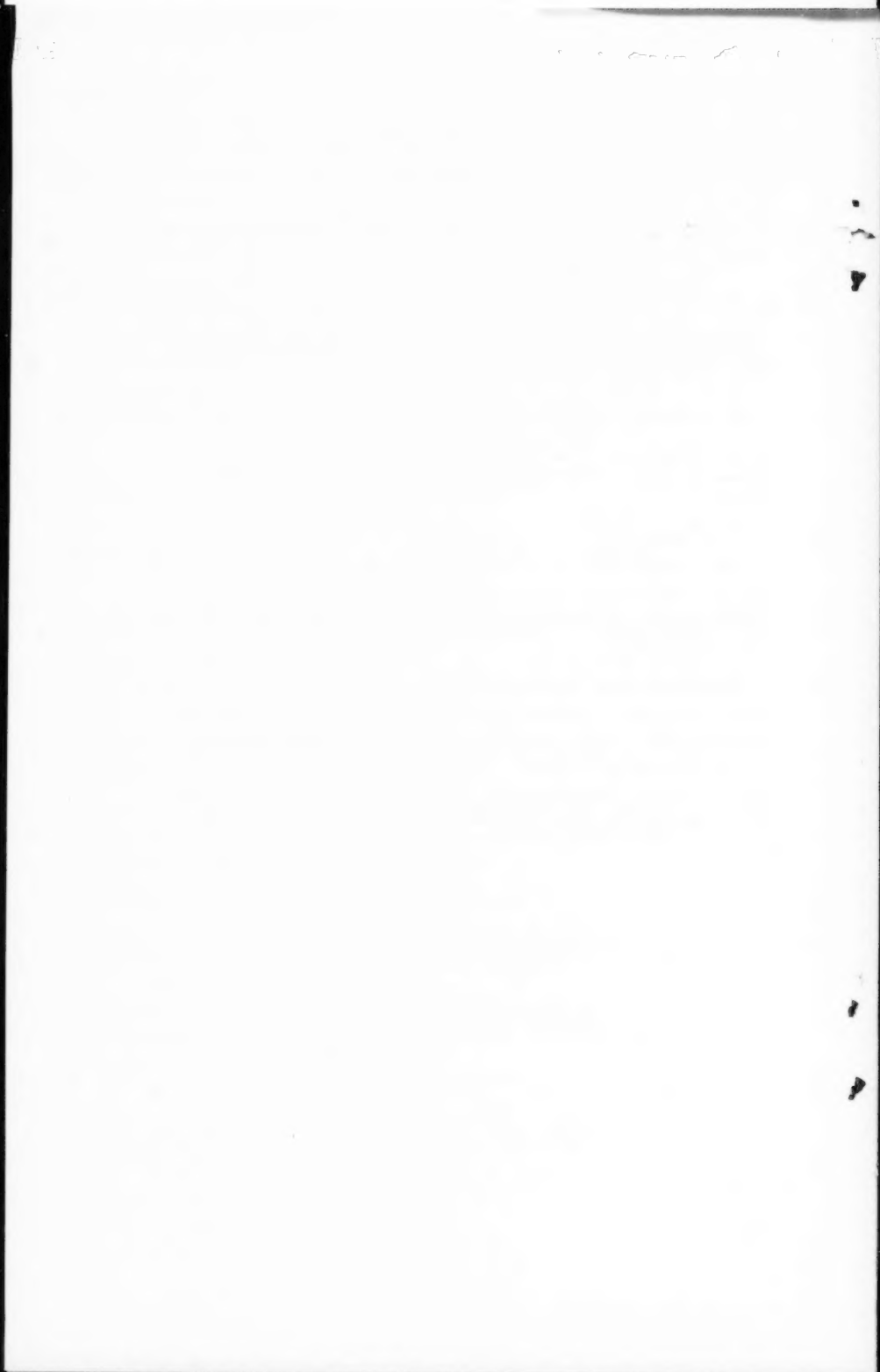
---

## DISCUSSION

---

Secondary Stresses in Parallel Wire Suspension Cables, by Thomas A. Wyatt. (July, 1960. Prior discussion: February, 1961. Discussion closed.) by Thomas A. Wyatt (closure). . . . .	241
Method for Analysis of Multibeam Bridges, by John E. Duberg, Narbey Khachaturian, and Raul E. Fradinger. (July, 1960. Prior discussion: February, 1961. Discussion closed.) by John E. Duberg, Narbey Khachaturian, and Raul E. Fradinger (closure). . . . .	243
Basic Column Strength, by Lynn S. Beedle and Lambert Tall. (July, 1960. Prior discussion: February, 1961. Discussion closed.) by Lynn S. Beedle and Lambert Tall (closure). . . . .	245
Shear Diaphragms of Light Gage Steel, by Arthur H. Nilson. (November, 1960. Prior discussion: None. Discussion closed.) by J. Morley English. . . . .	247
Periods of Framed Buildings for Earthquake Analysis, by M. G. Salvadori and E. Heer. (December, 1960. Prior discussion: May, 1961. Discussion closed.) by M. G. Salvadori and E. Heer (closure). . . . .	261
Movements of a Cable Due to Changes in Loading, by James Michalos and Charles Birnstiel. (December, 1960. Prior discussion: May, 1961. Discussion closed.) by D. M. Brotton, N. W. Williamson, and M. Millar . . . . .	263
by Hannsharl Bandel . . . . .	267
by W. E. Adams . . . . .	270
by Jackson L. Durkee . . . . .	271

	Page
Structural Model Analysis by Means of Moire Fringes, by A. J. Durelli and I. M. Daniel. (December, 1960. Prior discussion: May, 1961. Discussion closed.)	281
by A. J. Durelli and T. M. Daniel (closure) . . . . .	
Static and Dynamic Analysis of Guy Cables, by Donald L. Dean. (January, 1961. Prior discussion: May, 1961. Discussion closed.)	283
by A. H. Brownfield . . . . .	286
by John H. Wells . . . . .	
Analysis of Structures by Combining Redundants, by Peter P. Gillis and Kurt H. Gerstle. (January, 1961. Prior discussion: March, 1961. Discussion closed.)	293
by B. J. Hartz . . . . .	295
by Phillip L. Gould . . . . .	
Recent Trends in Ultimate Strength Design, by Phil M. Ferguson. (January, 1961. Prior discussion: March, 1961. Discussion closed.)	305
by John G. Merkle . . . . .	308
by M. Gregory . . . . .	310
by A. A. Eremin . . . . .	
Moment-Distribution Constants from Cardboard Analogs, by Otakar Ondra. (January, 1961. Prior discussion: None. Discussion closed.)	313
by Paul H. Reimer, Jr. . . . .	314
by Miguel Angel Macias-Rendón . . . . .	
Matrix Analysis of Structures Curved in Space, by Frank Baron (March, 1961. Prior discussion: None. Discussion closed.)	321
by Alfredo H.-S. Ang . . . . .	
Steel Frame Folded Plate Roof, by Oliver A. Baer. (June, 1961. Prior discussion: None. Discussion closes November 1, 1961.)	323
by E. I. Fiesenheiser . . . . .	



---

Journal of the  
STRUCTURAL DIVISION  
Proceedings of the American Society of Civil Engineers

---

PRESTRESSED BOWSTRING ARCH

By Movses J. Kaldjian<sup>1</sup>

---

SYNOPSIS

A general expression for solving prestressed bowstring arches with extensible suspension rods is derived from the strain energy of the structure. Specific equations are then obtained. A simplified membrane-analogy method of solving the bowstring arch is also introduced. A laboratory investigation of several 49-in.-span aluminum models is described briefly. Experimental and analytical work is compared, and the accuracy of the latter is shown.

---

INTRODUCTION

The ever-increasing use of prestressed concrete in construction makes the analysis of the prestressed bowstring arch valuable to the structural engineer. Here the term "bowstring arch" denotes a combination of an arch rib with a tie girder. These elements are fastened to one another at the supports and connected to each other through equally spaced vertical suspension rods. Any load on the tie girder is resisted jointly, both by the tie girder and the arch rib, making the structure highly indeterminate.

The analysis presented in this paper is that of determining redundant forces even when the forces applied are those of prestressing.

---

Note.—Discussion open until March 1, 1962. To extend the closing date one month, a written request must be filed with the Executive Secretary, ASCE. This paper is part of the copyrighted Journal of the Structural Division, Proceedings of the American Society of Civil Engineers, Vol. 87, No. ST 7, October, 1961.

<sup>1</sup> Asst. Prof. of Engrg. Mechanics, Univ. of Michigan, Ann Arbor, Mich.



*Notation.*—The letter symbols adopted for use in this paper are defined where they first appear, in the illustrations or in the text, and are arranged alphabetically, for convenience of reference, in Appendix II.

### THE STRAIN ENERGY METHOD

*Derivation of the Equation for a Bowstring Arch Having Any Number of Suspension Rods.*—Fig. 1 shows a fixed-end bowstring arch with equally spaced vertical suspension rods. "Cuts" or "hinges," as the case may be, are imagined to be inserted at suitable places in the structure to make it statically determinate (see Fig. 2). Moments and forces are then applied to both sides

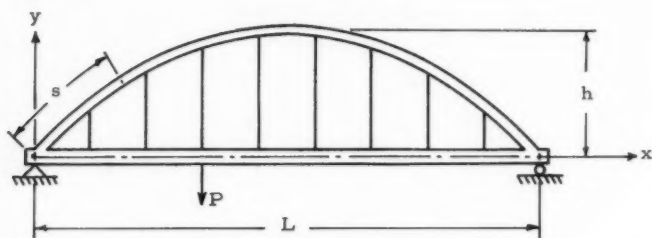


FIG. 1

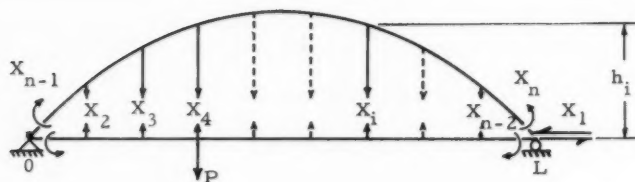


FIG. 2

of these "cuts" or "hinges" to restore the structure to its initial condition. The total strain energy  $U$ , which is a function of all the forces and moments acting on the structure, can now be expressed in terms of these same forces and moments.

The terms  $X_1, X_2, X_3, \dots, X_n$  denote the unknown forces and bending moments to restore the structure to its original condition (Fig. 2). Let  $M$  and  $N$  denote, respectively, the bending moment and the axial force on the "cut" structure produced by the externally applied loads,  $P$ ; and let  $M'$  and  $N'$  be the bending moment and the axial force caused by the unknown forces  $X_1, X_2, X_3, \dots, X_n$ . The total strain energy (neglecting shear and torsion) is

$$\begin{aligned}
 U = & \int_0^L \frac{(M_a + M_a')^2}{2 E_a I_a} ds + \int_0^L \frac{(N_a + N_a')^2}{2 E_a A_a} ds + \int_0^L \frac{(M_g + M_g')^2}{2 E_g I_g} dx \\
 & + \int_0^L \frac{(N_g + N_g')^2}{2 E_g A_g} dx + \sum_{i=2}^{(n-2)} \frac{(X_i)^2 h_i}{2 E_r A_r} \dots \dots \dots (1)
 \end{aligned}$$

in which  $L$  denotes the span length between supports,  $M$  is the bending moment,  $N$  refers to the axial force,  $E$  is the modulus of elasticity,  $I$  refers to the moment of inertia,  $X$  denotes an unforce or moment,  $A$  is the cross sectional area and the subscripts "a," "g" and "r" represent, respectively, the arch rib, the tie girder, and the suspension rod.

The relative deflection or rotation at the  $i$ -th "cut" is

$$\Delta X_i = \frac{\partial U}{\partial X_i} \dots \dots \dots (2)$$

in which  $U$  denotes the strain energy. By means of Eq. 1, Eq. 2 can be expressed in the form

$$\begin{aligned}
 \Delta X_i = & \int_0^L \frac{(M_a + M_a')}{E_a I_a} \frac{\partial M_a'}{\partial X_i} ds + \int_0^L \frac{(N_a + N_a')}{E_a A_a} \frac{\partial N_a'}{\partial X_i} ds \\
 & + \int_0^L \frac{(M_g + M_g')}{E_g I_g} \frac{\partial M_g'}{\partial X_i} dx + \int_0^L \frac{(N_g + N_g')}{E_g A_g} \frac{\partial N_g'}{\partial X_i} dx \\
 & + \sum_{i=2}^{(n-2)} \frac{X_i h_i}{E_r A_r} \dots \dots \dots (3)
 \end{aligned}$$

in which  $h_i$  is the height of the arch at the  $i$ th suspension rod. If now, the summation is used for the integration, the expression for  $\Delta X_i$  becomes:

$$\begin{aligned}
 \Delta X_i = & \sum_0^L \frac{(M_a + M_a')}{E_a I_a} \frac{\partial M_a'}{\partial X_i} \Delta s + \sum_0^L \frac{(N_a + N_a')}{E_a A_a} \frac{\partial N_a'}{\partial X_i} \Delta s \\
 & + \sum_0^L \frac{(M_g + M_g')}{E_g I_g} \frac{\partial M_g'}{\partial X_i} \Delta x + \sum_0^L \frac{(N_g + N_g')}{E_g A_g} \frac{\partial N_g'}{\partial X_i} \Delta x \\
 & + \sum_{i=2}^{(n-2)} \frac{X_i h_i}{E_r A_r} \dots \dots \dots (4)
 \end{aligned}$$

in which  $\Delta s$  denotes the length along the centerline of the arch, and  $\Delta x$  refers to the length along the girder or horizontal projection of  $\Delta X$ .

Eq. 4 gives "n" independent equations as "i" assumes values of 1, 2, 3, . . . n, respectively (that is, one equation per "cut"). Thus, one gets as many equations as there are unknowns in the system. If there is no initial lack of fit of members,  $(\Delta X_i)$ s are equal to zero (or a predetermined quantity). These "n" equations now can be solved simultaneously, and the values of  $(X_i)$ s are obtained. Once the unknown forces are determined, it is a simple matter to find the actual bending moment, the axial forces, and the shear, at any section in the structure.

*Sign Convention.*—Bending moments producing compression on the upper fibers of the arch rib and the tie girder are considered positive throughout this paper.

*Solution of Hinged-End Bowstring Arch Having Six Suspension Rods.*—The arch being studied is parabolic in form and has the dimensions shown in Fig.

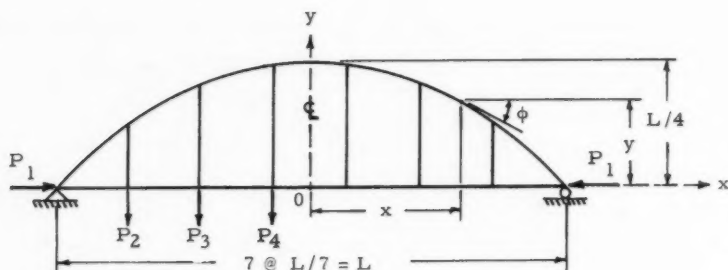


FIG. 3

3. For a 1-to-4 rise-to-span ratio, the equation of the centerline of the arch with its origin at midpoint of the tie girder is

$$y = -\frac{x^2}{L} + \frac{L}{4} \quad \dots \dots \dots (5)$$

Further, the cross-sectional area of the arch  $A_a$  and the length along the centerline of arch  $\Delta s_a$  are assumed, respectively, to vary according to equations

$$A_a = A_c \sec \phi \quad \dots \dots \dots (6a)$$

and

$$\Delta s_a = \Delta s_c \sec \phi = \Delta x \sec \phi \quad \dots \dots \dots (6b)$$

in which  $\phi$  is the slope along the centerline of the arch rib and the subscript "c" denotes crown; and taking the width of the arch to be constant throughout, the moment of inertia of the arch is given by

$$I_a = I_c \sec^3 \phi \quad \dots \dots \dots (7)$$

To evaluate Eq. 4 for this case, three tables have been prepared. Tables 1, 2, and 3 show all the forces acting on the structure, as well as the bending moments successively produced in the arch and in the tie girder by all the redundants  $X_1, X_2, \dots, X_7$  and the external forces  $P_1, P_2, P_3$ , and  $P_4$ .

TABLE 1.—BENDING MOMENTS AND AXIAL FORCES WITH PARTIAL DERIVATIONS IN ARCH

Load	$(M_a + M_b) \text{ \& } \frac{\partial M_1}{\partial X_1}$		Mult. Factor for $\frac{\partial M_1}{\partial X_1}$		$N_a \text{ \& } \frac{\partial N_1}{\partial X_1}$		Mult. Factor for $\frac{\partial N_1}{\partial X_1}$	
			$(M_a + M_b)$	$\frac{\partial M_1}{\partial X_1}$	$N_a$	$\frac{\partial N_1}{\partial X_1}$	$N_a$	$\frac{\partial N_1}{\partial X_1}$
	3.25 8.25 11.25 12.25 11.25 8.25 3.25		$X_1 \cdot \frac{L}{49}$	$\frac{L}{49}$	-.75927 -.55780 -.07089 -.09266 -.09266 -.07089 -.55780 -.75927		$X_1$	1
	3.0 5.5 4.5 3.5 2.5 1.5 0.5		$X_2 \cdot \frac{L}{49}$	$\frac{L}{49}$	.55780 .35445 -.07851 0 0 -.07851 -.35445 -.55780		$X_2$	1
	2.5 7.5 9.0 7.0 5.0 3.0 1.0		$X_3 \cdot \frac{L}{49}$	$\frac{L}{49}$	.46484 .35445 -.07851 0 0 -.07851 -.35445 -.46484		$X_3$	1
	2.0 6.0 10.0 10.5 7.5 4.5 1.5		$X_4 \cdot \frac{L}{49}$	$\frac{L}{49}$	.37187 .28356 .15703 .11777 .11777 .28356 .37187		$X_4$	1
	1.5 4.5 7.5 10.5 10.0 6.0 2.0		$X_5 \cdot \frac{L}{49}$	$\frac{L}{49}$	.27890 .21267 .11777 0 0 -.28356 -.37187		$X_5$	1
	1.0 3.0 5.0 7.0 9.0 7.5 2.5		$X_6 \cdot \frac{L}{49}$	$\frac{L}{49}$	.18593 .14178 .07851 0 0 -.07851 -.14178 -.18593		$X_6$	1
	0.5 1.5 2.5 3.5 4.5 5.5 3.0		$X_7 \cdot \frac{L}{49}$	$\frac{L}{49}$	.09297 -.07089 -.03926 0 0 -.07089 -.09297		$X_7$	1

Using these tables, and letting

$$m_g = \frac{A_g E_g}{A_c E_a} \dots \dots \dots (8a)$$






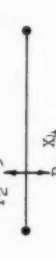
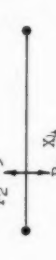
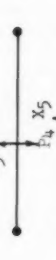
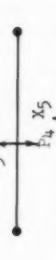
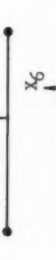
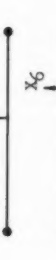


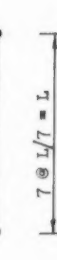
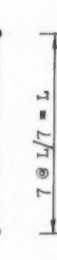
$$m_r = \frac{A_r E_r}{A_c E_a} \dots \dots \dots (8b)$$

and

$$m_I = \frac{I_g E_g}{I_c E_a} \dots \dots \dots (8c)$$

and by recognizing that  $(L/r_c)^2$  is identical to  $\frac{I_c}{L^2 A_c}$  (in which  $r_c$  is the radius of gyration of the arch rib at the crown), and that  $\Delta X_1, \Delta X_2, \dots, \Delta X_7$

TABLE 2.—BENDING MOMENTS AND AXIAL FORCES WITH PARTIAL DERIVATIVES IN THE GIRDER

Load	$(M_g + M_g^*)$ & $\frac{\partial M_g^*}{\partial X_1}$	Mult. Factor for $(M_g + M_g^*)$	$(N_g + N_g^*)$ & $\frac{\partial N_g^*}{\partial X_1}$	Mult. Factor for $(N_g + N_g^*)$
		0		1
		$(P_2 - X_2) \cdot \frac{L}{49}$	$N_{11}$	0
		$(P_3 - X_3) \cdot \frac{L}{49}$	$N_{11}$	0
		$(P_4 - X_4) \cdot \frac{L}{49}$	$N_{11}$	0
		$-X_5 \cdot \frac{L}{49}$	$N_{11}$	0
		$-X_6 \cdot \frac{L}{49}$	$N_{11}$	0
		$-X_7 \cdot \frac{L}{49}$	$N_{11}$	0



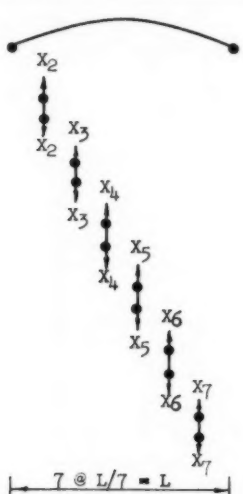
are all equal to zero, a set of seven equations, Eq. 9, is obtained to solve for the values of  $X_1, X_2, \dots, X_7$ .

$$\sum_{n=1}^7 a_{mn} x_n + c_m = 0 \quad (m = 1, 2, \dots, 7) \dots \dots \dots (9)$$

in which  $a_{mn} = a_{nm}$ . (See Appendix I for the values of  $a_{mn}$  and  $c_m$ ).

The numerical values of  $X_1, X_2, \dots, X_7$  of Eq. 9 depend, no doubt, on the external load,  $L/r_c$ ,  $m_g$ ,  $m_r$  and  $m_l$ . Once these parameters are known their values can be determined.

TABLE 3.—AXIAL FORCES WITH PARTIAL DERIVATIVES IN SUSPENSION-RODS

Load	$X_1$ & $\frac{\partial X_1}{\partial X_i}$	Mult. Factor for	
		$X_1$	$\frac{\partial X_1}{\partial X_i}$
	(1) 0 0 0 0 0 0	- $X_2$	-1
	0 (1) 0 0 0 0	- $X_3$	-1
	0 0 (1) 0 0 0	- $X_4$	-1
	0 0 0 (1) 0 0	- $X_5$	-1
	0 0 0 0 (1) 0	- $X_6$	-1
	0 0 0 0 0 (1)	- $X_7$	-1

When additional prestressing of the tie girder is desired, a specified initial (vertically restrained) horizontal gap  $\Delta$  is provided between the ends of the arch rib and the tie girder. Then a horizontal force  $X_1$ , just large enough to close this gap completely, is applied. Because there is a relative motion now between the ends of the arch and the tie girder, a different set of equations must be obtained. This is done by satisfying the new geometric boundary conditions and by setting all the external forces  $P_1, P_2, P_3$  and  $P_4$  equal to zero.

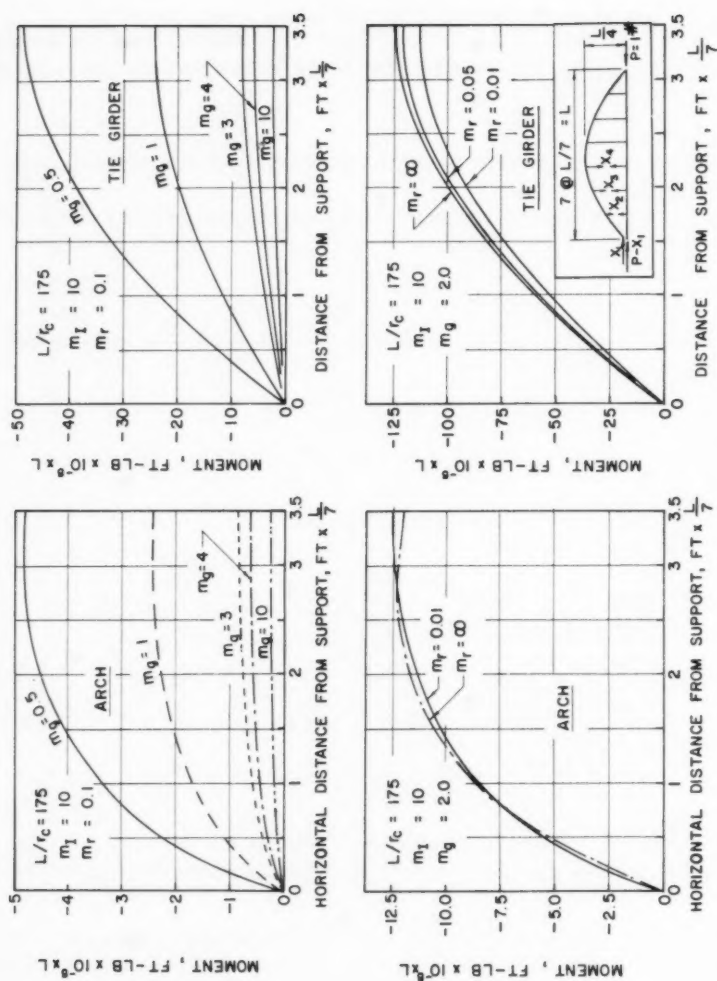


FIG. 4.—BENDING MOMENT ALONG ARCH AND GIRDER FOR DIFFERENT  $m_g$  AND  $m_r$  VALUES

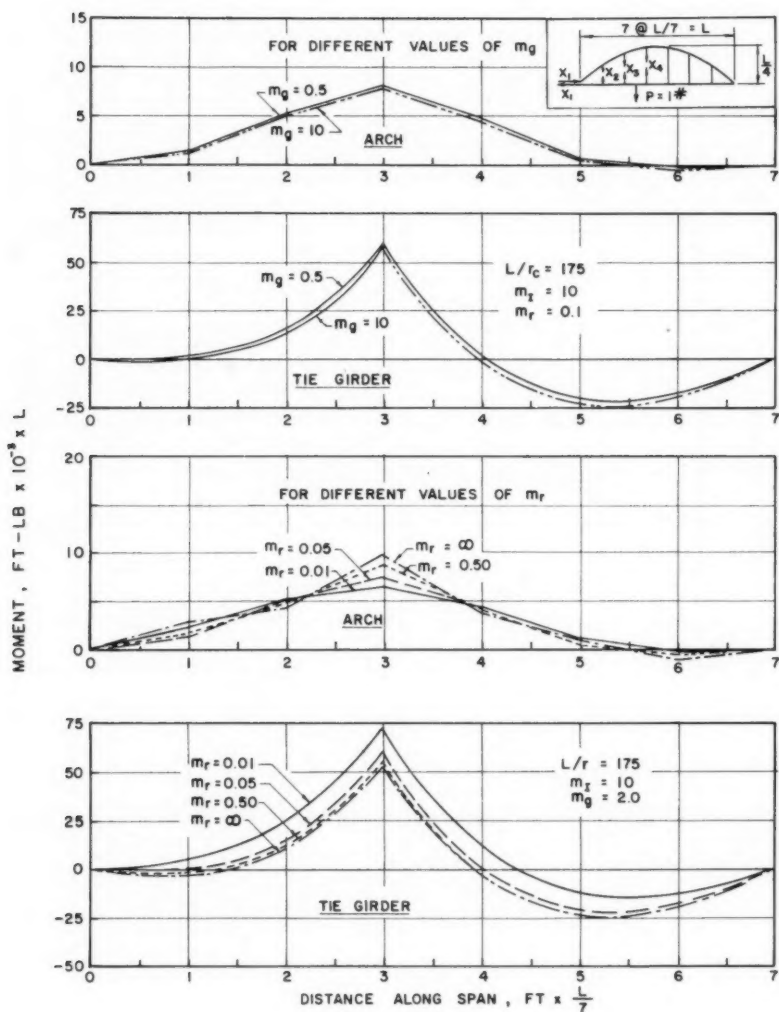


FIG. 5.—INFLUENCE LINES FOR BENDING MOMENT AT PANEL POINT  $X_4$  FOR DIFFERENT  $m_g$  AND  $m_r$  VALUES

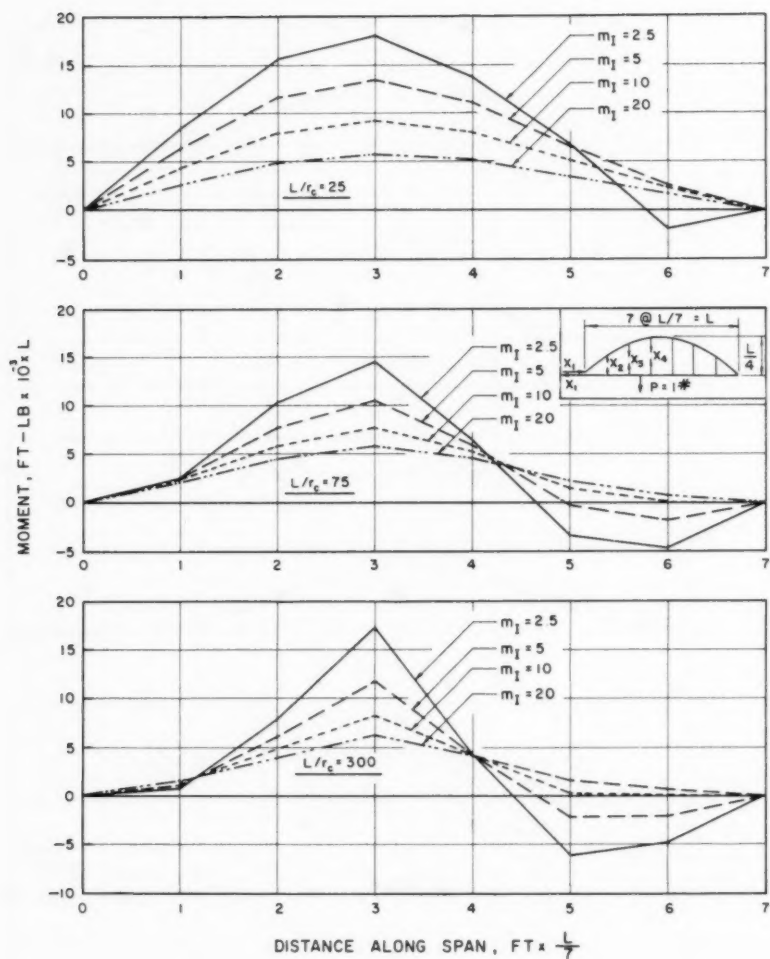


FIG. 6.—INFLUENCE LINES FOR BENDING MOMENT AT PANEL POINT  $X_4$  FOR ARCH

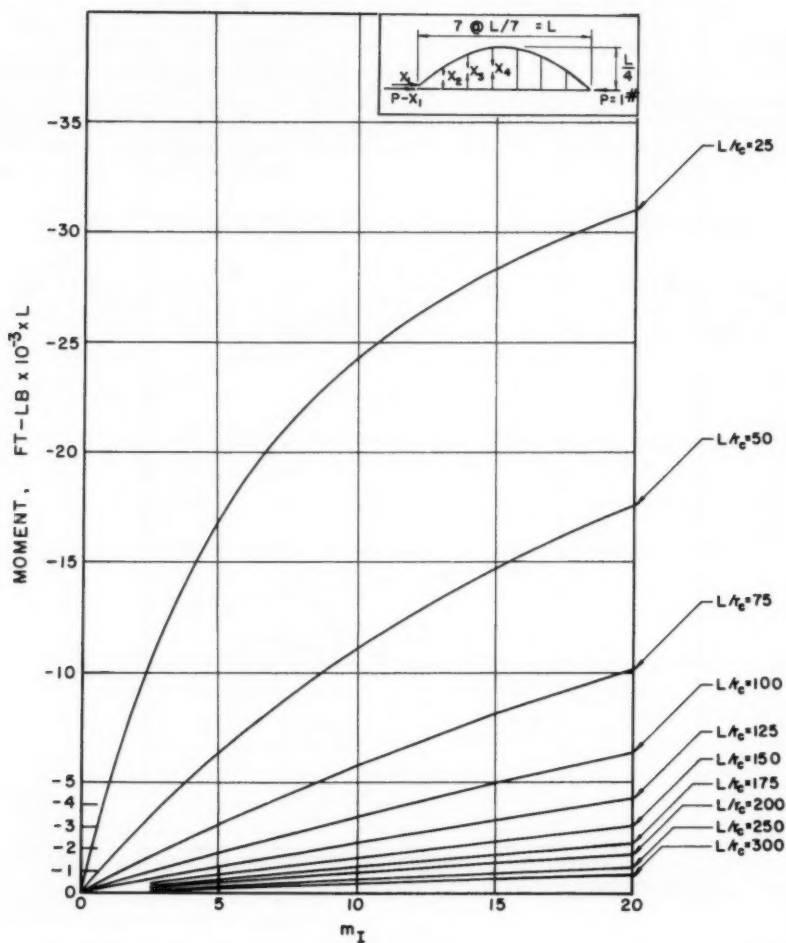


FIG. 7.—BENDING MOMENT AT PANEL POINT  $X_4$  FOR DIFFERENT VALUES OF  $L/r_c$  AND  $m_I$  FOR TIE GIRDER



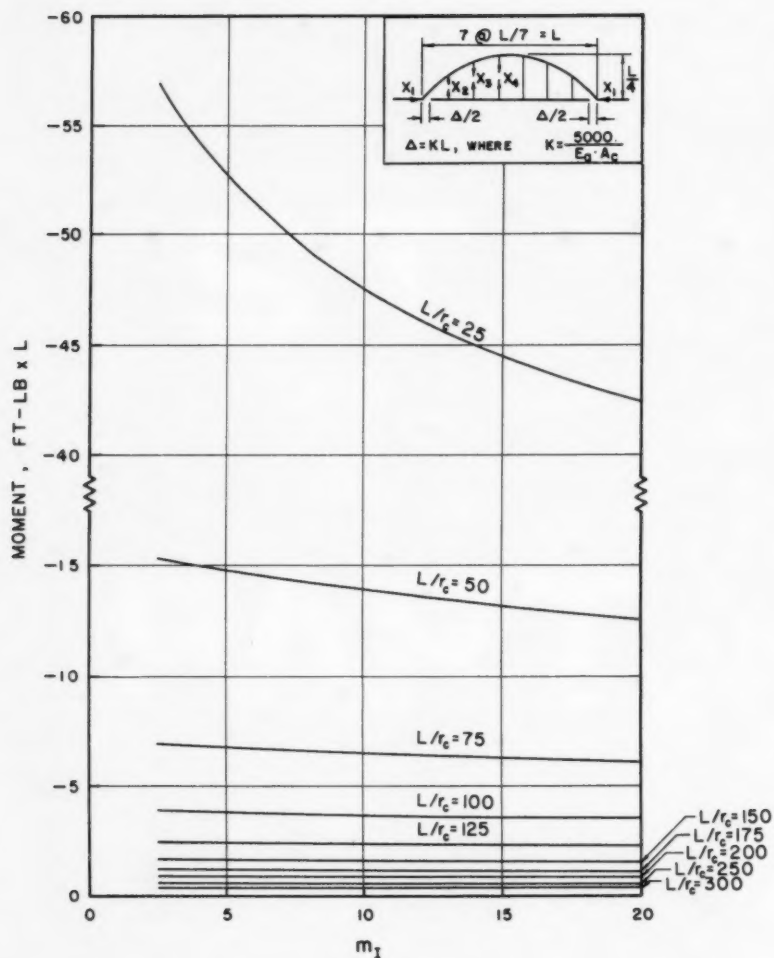


FIG. 8.—BENDING MOMENT AT CROWN FOR DIFFERENT VALUES OF  $L/r_c$  AND  $m_I$  FOR ARCH

Thus, for the case with a gap, Eq. 9 becomes

$$\sum_{n=1}^7 b_{mn} x_n + d_m = 0 \quad (m = 1, 2, \dots, 7) \dots\dots\dots(10)$$

in which  $b_{mn} = b_{nm}$ . (See Appendix I for the values of  $b_{mn}$  and  $d_m$ ).

To facilitate the preliminary design of bowstring arches, some fifty bending moment and axial force diagrams were prepared from Eqs. 9 and 10 for various parameters. A small sample of these diagrams is indicated in Figs. 4 through 8. The electronic computing facilities of the University of Michigan, Ann Arbor, Mich. were used to obtain the data for these diagrams. Eqs. 9 and 10 were solved 420 times.

### THE MEMBRANE-ANALOGY METHOD<sup>2</sup>

*For a Concentrated Vertical Force on the Girder.*—The membrane-analogy method may be used to generalize sufficiently the analysis of the hinged-end

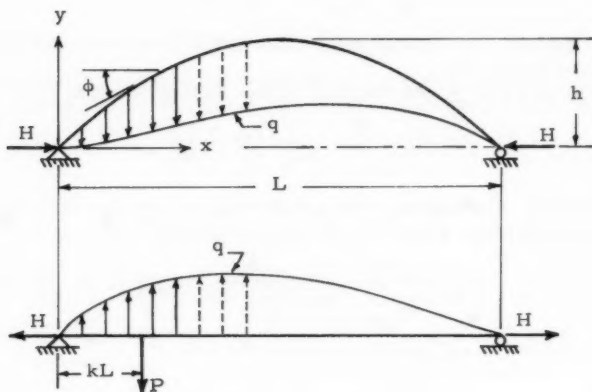


FIG. 9

bowstring arch so that it may apply to any desired number of suspension rods and to all rise-to-span ratios.

It is assumed that the arch and the tie girder are connected by an inextensible membrane, so that the deflections of the arch rib and the tie girder are the same. Therefore, the vertical force  $q$  in the membrane may be expressed as a simple continuous function as shown in Fig. 9.

<sup>2</sup> "A Study of the Bowstring Arch Having Extensible Suspension Rods and Different Ratios of Tie-Beam to Arch-Rib Stiffness," by S. Chandrangu and S. R. Sparkes, Proceedings, ICE, Vol. 3, No. 2, August, 1954, Paper No. 5966.

The arch is assumed to be of parabolic form

$$y = 4h \left[ \left( \frac{x}{L} \right) - \left( \frac{x}{L} \right)^2 \right] \dots\dots\dots(11)$$

in which  $h$  refers to the rise at the crown. The moment of inertia and the cross-sectional area of the arch vary, respectively, as

$$\text{and} \quad \begin{matrix} I_a = I_c \sec \phi \\ A_a = A_c \sec \phi \end{matrix} \left. \vphantom{\begin{matrix} I_a \\ A_a \end{matrix}} \right\} \dots\dots\dots(12)$$

The arch is then separated from the girder as in Fig. 9. The term  $P$  in Fig. 9 is any vertical load applied on the girder.

The vertical deflection of the arch due to the membrane force  $q$  may be obtained from the equations

$$q = E I_a \cos \phi \frac{d^4 \Delta_q}{dx^4} \dots\dots\dots(13)$$

and

$$M^q = E I_a \cos \phi \frac{d^2 \Delta_q}{dx^2} \dots\dots\dots(14)$$

in which  $\Delta_q$  denotes the vertical deflection and  $M^q$  the bending moment due to the membrane force only.

This deflection can be represented by the Fourier series:

$$\Delta_q = \sum_{n=1}^{\infty} \frac{a_n}{E I_c} \sin \frac{n \pi x}{L} \dots\dots\dots(15)$$

Differentiating  $\Delta_q$  successively and substituting it and Eq. 12 into Eqs. 13 and 14, the membrane force  $q$  and the bending moment  $M^q$  are found.

$$M^q = - \sum_{n=1}^{\infty} a_n \left( \frac{n \pi}{L} \right)^2 \sin \frac{n \pi x}{L} \dots\dots\dots(16)$$

and

$$q = \sum_{n=1}^{\infty} a_n \left( \frac{n \pi}{L} \right)^4 \sin \frac{n \pi x}{L} \dots\dots\dots(17)$$

The accuracy of the membrane force  $q$  no doubt depends on the number of terms considered in Eq. 17.

The vertical deflection of the arch and the girder is the same at a given section. In the arch it is equal to the sum of the deflections produced by the horizontal force  $H$  and the membrane force  $q$ ; that is

$$\Delta = \Delta_H + \Delta_q \dots\dots\dots(18)$$

The deflection due to  $H$  is given by

$$\frac{d^2 \Delta_H}{dx^2} = \frac{H y}{E I_c} = \frac{4 H h}{E I_c} \left[ \frac{x}{L} - \left( \frac{x}{L} \right)^2 \right] \dots\dots\dots(19)$$

Integrating this equation and applying the end conditions that  $\Delta_H = 0$  at  $x = 0$  and  $x = L$  yields

$$\Delta_H = -\frac{H h L^2}{3 E I_c} \left[ \left(\frac{x}{L}\right)^4 - 2\left(\frac{x}{L}\right)^3 + \left(\frac{x}{L}\right) \right] \dots \dots \dots (20)$$

Hence, from Eqs. 15 and 20

$$\Delta = -\frac{H h L^2}{3 E I_c} \left[ \left(\frac{x}{L}\right)^4 - 2\left(\frac{x}{L}\right)^3 + \left(\frac{x}{L}\right) \right] + \sum_{n=1}^{\infty} \frac{a_n}{E I_c} \sin \frac{n \pi x}{L} \dots \dots (21)$$

Hence, when  $x = k L$ , the deflection  $\Delta_P$  under the load  $P$  is

$$\Delta_P = -\frac{H h L^2}{3 E I_c} (k^4 - 2 k^3 + k) + \sum_{n=1}^{\infty} \frac{a_n}{E I_c} \sin n \pi k \dots \dots \dots (22)$$

$H$  and the coefficients  $a_n$  remain to be determined.

Because the relative horizontal movement on each side of the cut section at  $H$  is zero,

$$\delta_H = \delta_{OH} + H \delta_{HH} = 0 \dots \dots \dots (23)$$

from which

$$H = -\frac{\delta_{OH}}{\delta_{HH}} \dots \dots \dots (24)$$

The terms  $\delta_{OH}$  and  $\delta_{HH}$  denote, respectively, the horizontal movement of the arch at  $H$  due to the membrane load force  $q$  and to the load  $H$  taken as unity.

$$\delta_{OH} = -\frac{16}{E I_c} \frac{h}{L} \sum_{1.3.5}^{\infty} a_n \left(\frac{1}{n \pi}\right) \dots \dots \dots (25a)$$

and

$$\delta_{HH} = \frac{8}{15 E I_c} h^2 L \dots \dots \dots (25b)$$

Substituting Eqs. 25 in Eq. 24 and reducing, yields

$$H = 30 \frac{L}{h} \sum_{1.3.5}^{\infty} \frac{a_n}{L^3} \left(\frac{1}{n \pi}\right) \dots \dots \dots (26)$$

Eq. 26 can be solved once the Fourier constants are known. This is done by the energy method. A small increment  $da_i$  in the Fourier coefficient  $a_i$  will produce small stress changes in the system, and this, in turn, will cause small deformations in the structure. Equilibrium conditions require that the change in the internal energy of the system equal the change in the external work due to  $P$ . Thus

$$\frac{\partial U}{\partial a_i} da_i = P \frac{\partial \Delta_P}{\partial a_i} da_i \dots \dots \dots (27)$$

The total internal energy in the system (neglecting shear and torsion and axial force in the arch due to membrane load  $q$ ) is

$$U = \int_0^L \frac{M_a^2}{2 E I_c} dx + \int_0^L \frac{M_g^2}{2 E_g I_g} dx + \int_0^L \frac{(H \cos \phi)^2}{2 E A_c} dx + \int_0^L \frac{(-H)^2}{2 E_g A_g} dx \dots \dots (28)$$

in which

$$M_a = H y - \sum_{n=1}^{\infty} a_n \left( \frac{n\pi}{L} \right)^2 \sin \frac{n\pi x}{L} \dots\dots\dots (29)$$

and

$$\begin{aligned} M_g &= P(1-k)x - \sum_{n=1}^{\infty} a_n \left( \frac{n\pi}{L} \right)^2 \sin \frac{n\pi x}{L} \text{ for } 0 \leq x \leq kL \\ &= Pk(L-x) - \sum_{n=1}^{\infty} a_n \left( \frac{n\pi}{L} \right)^2 \sin \frac{n\pi x}{L} \text{ for } kL \leq x \leq L \dots\dots (30) \end{aligned}$$

From Eq. 11, for  $L/h = 4$ ,

$$\int_0^L \cos^2 \phi \, dx = \frac{\pi}{4} L \dots\dots\dots (31)$$

Substituting these values into Eq. 28, and integrating, after simplification, gives

$$\begin{aligned} U &= \frac{1}{2EI_c} \left[ \frac{8}{15} H^2 h^2 L - \frac{32 H h}{L} \sum_{n=1}^{\infty} a_n \frac{1}{n\pi} + \frac{1}{2L^3} \sum_{n=1}^{\infty} a_n^2 (n\pi)^4 + \frac{\pi}{4} H^2 r_c^2 L \right] \\ &+ \frac{1}{2m_I EI_c} \left[ \frac{P^2 k^2 L^3}{3} (1-k)^2 - 2P \sum_{n=1}^{\infty} a_n \sin(n\pi k) \right. \\ &\left. + \frac{1}{2} \sum_{n=1}^{\infty} \frac{a_n^2}{L^3} (n\pi)^4 + H^2 r_g^2 L \right] \dots\dots\dots (32) \end{aligned}$$

in which  $r_c$  and  $r_g$  are, respectively, the radius of gyration of the arch at the crown and of the girder.

Substituting for  $H$  in Eq. 32, differentiating with respect to  $a_i$  and multiplying this by  $da_i$ , gives the first term of Eq. 27.

$$\begin{aligned} \frac{\partial U}{\partial a_i} da_i &= \frac{1}{2EI_c} \left\langle \frac{a_i}{L^3} \right\} (i\pi)^4 - \frac{1}{(i\pi)^2} \left[ 960 - 1800 \frac{\pi}{4} \left( \frac{r_c}{h} \right)^2 \right] \left\{ \right. \\ &\left. + \frac{1}{m_I} \left\{ -2P \sin(i\pi k) + \frac{a_i}{L^3} \left[ (i\pi)^4 + \frac{1800}{(i\pi)^2} \left( \frac{r_g}{h} \right)^2 \right] \right\} \right\} da_i \dots\dots (33) \end{aligned}$$

Similarly, Eq. 22, after being multiplied by  $P$ , gives the second term of Eq. 27.



$$P \frac{\partial \Delta P}{\partial a_i} da_i = \frac{P}{E I_c} \left[ -\frac{10}{i \pi} (k^4 - 2k^3 + k) + \sin(i \pi k) \right] da_i \dots (34)$$

Finally, substituting Eqs. 33 and 34 into Eq. 27 and simplifying it gives the value for  $a_i$ ; that is

$$a_i = 2 P L^3 \frac{\frac{m_I + 1}{m_I} \sin(i \pi k) - \frac{10}{i \pi} (k^4 - 2k^3 + k)}{\frac{m_I + 1}{m_I} (i \pi)^4 - \frac{120}{(i \pi)^2} \alpha_P} \dots (35)$$

in which

$$\alpha_P = 8 - 15 \left[ \frac{\pi}{4} \left( \frac{r_c}{h} \right)^2 + \frac{1}{m_I} \left( \frac{r_g}{h} \right)^2 \right] \dots (36)$$

With the Fourier constants now known, Eqs. 16, 17 and 26 can be used to give, respectively,  $M^q$ ,  $q$  and  $H$ . Suspension rod forces are found by integrating Eq. 17 between the proper limits, and the bending moment in the arch and the girder are given by:

$$M_a = H y - \sum_{n=1}^{\infty} a_n \left( \frac{n \pi}{L} \right)^2 \sin \frac{n \pi}{L} x \dots (37)$$

and

$$M_g = M_P - \sum_{n=1}^{\infty} a_n \left( \frac{n \pi}{L} \right)^2 \sin \frac{n \pi}{L} x \dots (38)$$

in which  $M_P$  equals simple beam moment produced by  $P$ .

*For a Prestressing Force  $F$  As Shown in Fig. 10.*—All dimensions and assumptions are the same as in the previous case. The difference is in the manner in which the external load is applied, as shown in Fig. 10.

Because the analysis of this case is very similar to (a), only the results are presented here. They are as follows:

$$H = \frac{1}{\alpha_F} \left[ \frac{1}{m_g} \left( \frac{r_g}{L} \right)^2 + 16 \frac{h}{L} \sum_{n=1}^{\infty} \frac{a_n}{1.3 \cdot 5} \left( \frac{1}{n \pi} \right) \right] \dots (39)$$

in which

$$\alpha_F = \frac{8}{15} \left( \frac{h}{L} \right)^2 + \frac{1}{m_I} \left( \frac{r_g}{L} \right)^2 \dots (40)$$

and

$$a_i = F L^3 \frac{\frac{8}{m_I (i \pi)} \left( \frac{r_g}{L} \right)^2 \frac{h}{L} \beta_F}{\frac{m_I + 1}{m_I} (i \pi)^4 \alpha_F - \frac{128}{(i \pi)^2} \left( \frac{h}{L} \right)^2 \beta_F} \dots (41)$$

in which

$$\beta_F = 4 - \frac{4}{\alpha_F} \left( \frac{\pi}{4} \right) \left( \frac{r_c}{L} \right)^2 \dots (42)$$

As before, Eq. 41 can be used in Eqs. 16 and 17 to give  $M^q$  and  $q$ . Suspension rod forces are also found similarly. The bending moments in the arch and the girder are

$$M_a = Hy - \sum_{n=1}^{\infty} a_n \left( \frac{n\pi}{L} \right)^2 \sin \frac{n\pi}{L} x \dots \dots \dots (43)$$

and

$$M_g = - \sum_{n=1}^{\infty} a_n \left( \frac{n\pi}{L} \right)^2 \sin \frac{n\pi}{L} x \dots \dots \dots (44)$$

*For an Initial Predetermined Gap  $\Delta_G$ .*—All previous assumptions and dimensions apply for an initial predetermined gap  $\Delta_G$  also. There exists now a

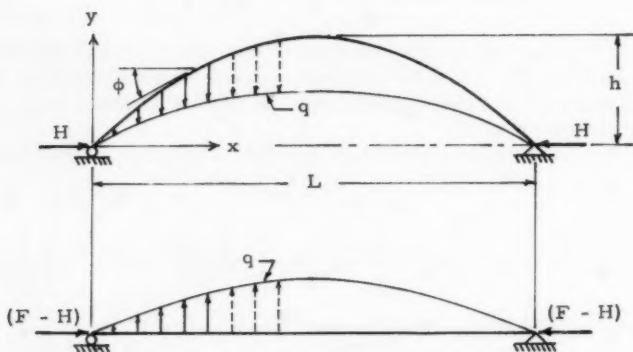


FIG. 10

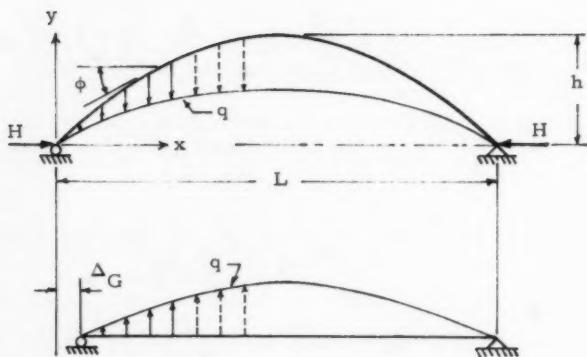


FIG. 11

relative horizontal movement  $\Delta_G$  on each side of the cut section at the origin "O," as shown in Fig. 11.

Here, too, a similar analysis is followed, and the results are as follows:

$$H = \frac{15}{8} \left( \frac{E I_c}{h^2 L} \right) \Delta_G + 30 \frac{L}{h} \sum_{1.3.5}^{\infty} \frac{a_n}{L^3} \left( \frac{1}{n \pi} \right) \dots \dots \dots (45)$$

and

$$a_i = L^3 \frac{\frac{30}{(i \pi)} \alpha_G \left( \frac{E I_c}{h L^2} \right) \Delta_G}{\frac{m_I + 1}{m_I} (i \pi)^4 - \frac{480}{(i \pi)^2} \alpha_G} \dots \dots \dots (46)$$

in which

$$\alpha_G = 2 - \frac{15}{4} \left( \frac{\pi}{4} \right) \left( \frac{r_c}{h} \right)^2 \dots \dots \dots (47)$$

From Eq. 46, the Fourier constants can now be substituted in Eq. 45 to give H. Eqs. 16, 17, 43 and 44 can be used to give, respectively,  $M_a^q$ ,  $q$ ,  $M_a$  and  $M_g$ . The suspension rod forces, as before, are given by integrating Eq. 17 between the proper limits.

#### EXPERIMENTAL STUDY

The experimental work was performed on an aluminum model of 49 in. c to c of span and 12-1/4 in. rise. See Figs. 12 and 13.

*Dimensions.*—The arch rib, cut from 1-in. thick aluminum (6061-T6) plate, was 1 sq in. at the crown and varied according to  $A_a = A_c \sec \phi$  toward the abutments (making  $L/r_c = 169.74$  and  $I_a = I_c \sec^3 \phi$ ). The interchangeable tie girders were made of extruded aluminum (6063-T5) rectangular tubing. There were two different sizes, 1-1/2 x 1-1/2 x 1/8 in. for two, and 1-1/2 x 2 x 1/8 in. for one tie girder. One of the former was for the case with an initial gap. This had horizontally slotted holes at each end to permit relative horizontal motion between the ends of the arch and the tie girder. The suspension rods were made of 7/32-in. diameter brass rods and spaced 7 in. apart.

*Loading and Measurements.*—The model, in vertical position, was loaded in two increments of 100 lb at each panel point, and strains of a total of twenty-five points were measured by SR-4 electric strain gages after the application of each increment of load.

The horizontal prestressing load was applied in increments of 1000 lb to a maximum of 4000 lb. This was done with the help of a hydraulic jack, a calibrated 3/4-in. diameter load rod, prestressing wire that ran concentrically inside the tie girder, and anchor plates. As with the panel point loading, strain measurements were taken after every increment of load.

For the case with the initial gap, the relative horizontal deflections were varied in different increments to a maximum of  $181.7 \times 10^{-3}$  in., and the corre-

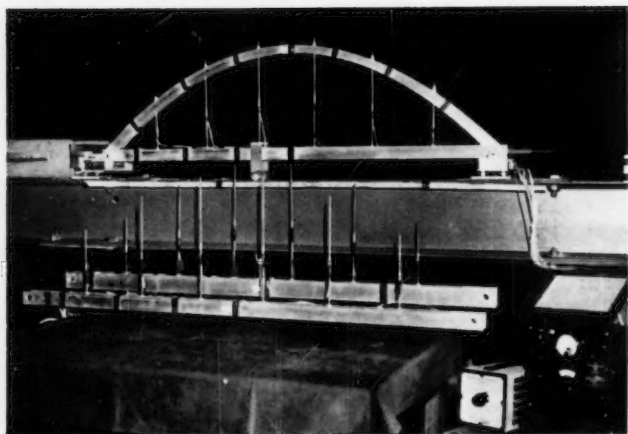


FIG. 12.—MODEL AND INTERCHANGEABLE GIRDERS

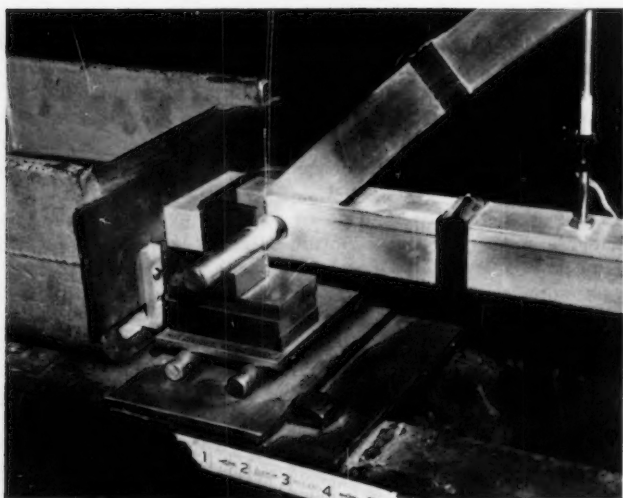
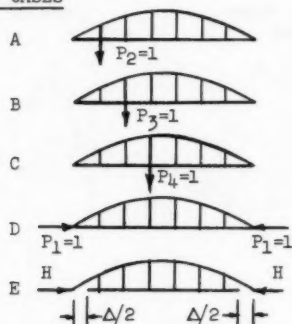


FIG. 13.—END DETAIL

TABLE 4.—ANALYTICAL AND EXPERIMENTAL VALUES OF HORIZONTAL FORCE  $X_1$  COMPARED

## LOAD CASES



$$\Delta = KL \text{ \& } K = \frac{5000}{E_a A_c}$$

Load Case	$m_I$	Horizontal Force		
		By Energy Method	By Membrane Analogy	By Experiment
A	2.62	0.3329	0.3296	0.3300
B		0.5999	0.6064	0.5892
C		0.7482	0.7662	0.7161
D		0.005615	0.005422	
E		19.41	18.74	20.14
A	5.30	0.3304	0.3190	0.3304
B		0.5938	0.6000	0.5648
C		0.7390	0.7682	0.7114
D		0.008061	0.007915	
E		33.01	32.41	

- — Indicates Experimental Values  
 △ — Indicates Membrane Analogy Values  
 Bending Moments are in units of in-lb x 49

$$m_I = 2.62$$

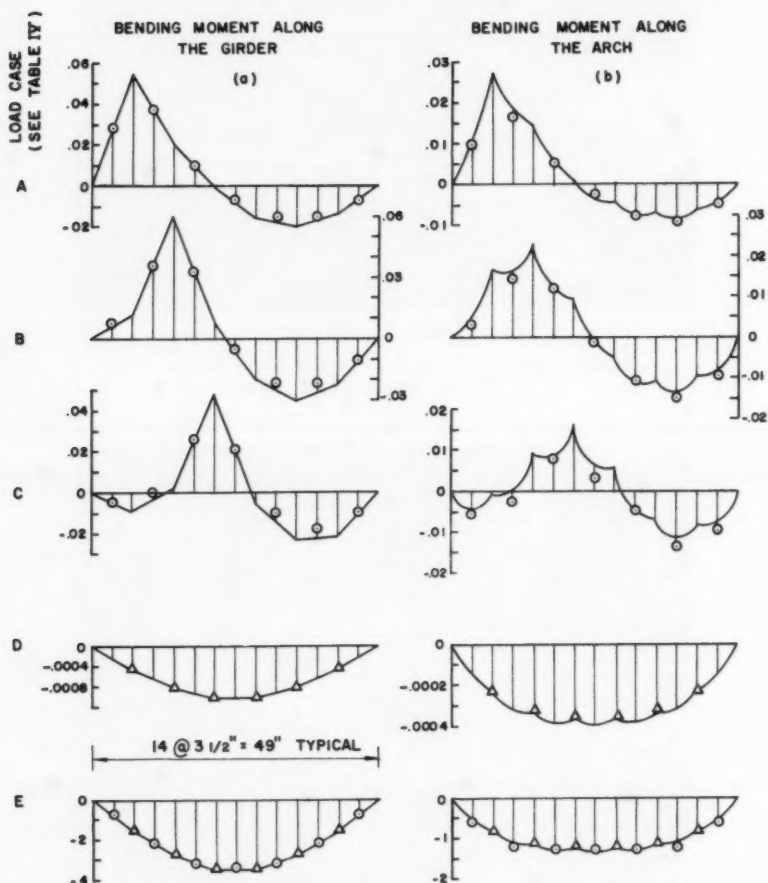


FIG. 14.—ANALYTICAL AND EXPERIMENTAL VALUES OF BENDING MOMENTS COMPARED FOR  $m_I = 2.62$

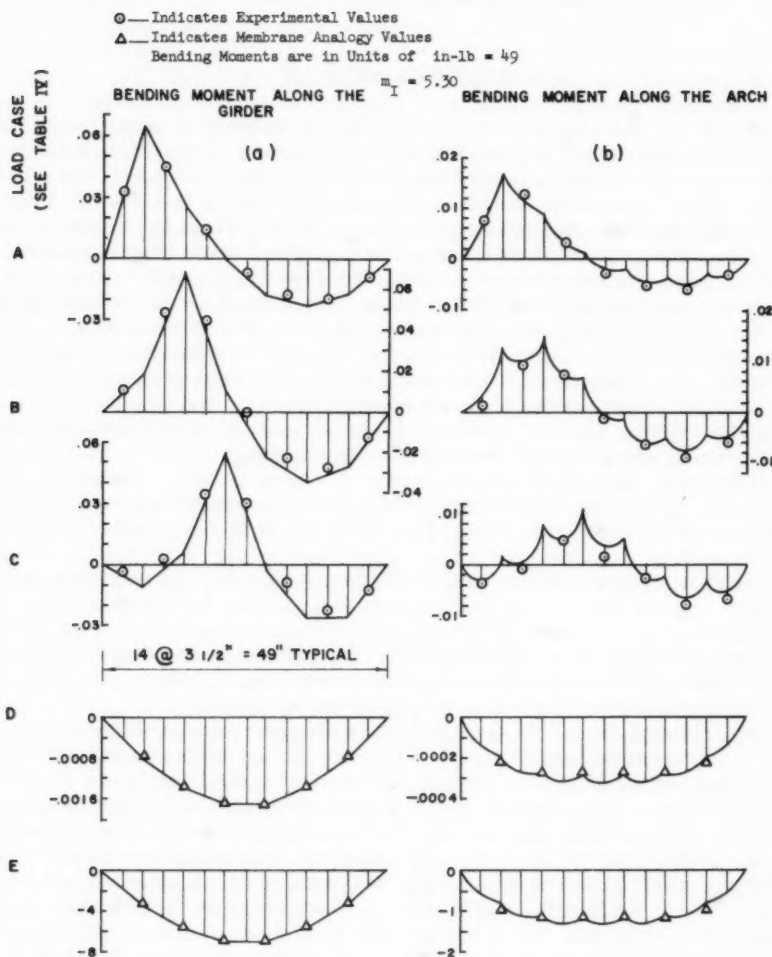


FIG. 15.—ANALYTICAL AND EXPERIMENTAL VALUES OF BENDING MOMENTS COMPARED FOR  $m_I = 5.30$

sponding horizontal force and strain measurements were taken. The theoretical and experimental values of the horizontal force and bending moments in the arch and the tie girder are shown compared in Table 4 and Figs. 14 and 15. For Figs. 14 and 15 the full lines show bending moments calculated by the energy method with extensible suspension rods.

### ANALYSIS OF RESULTS

(1) That the total moment at a section (simple bending moment minus  $H y$ ) seems to be distributed between the rib and the girder according to their respective moment of inertia is quite justified. For horizontal loading, the error in the maximum moment, for the preceding observation, is within 2% (Figs. 14 and 15); for vertical loading the error is around 10% at the load point, at best, but away from the load there is a much larger error (Figs. 14 and 15).

(2) A good correspondence between the results of strain-energy and membrane-analogy methods (Table 4 and Figs. 14 and 15) seems to suggest that the assumption of inextensible suspension rods in simplified design is not unreasonable. (This can also be due in part to point 3.) Suspension rods were assumed to be extensible in the former and inextensible in the latter.

(3) The manner in which  $I_a$  varied along the arch rib did not affect the results appreciably. ( $I_a$  was assumed to be  $I_c \sec^3 \phi$  in the strain-energy method and  $I_c \sec \phi$  in the membrane-analogy method).

(4) Omitting the axial strain energy in the arch rib, caused by the suspension-rod force components, produced only a maximum error of 0.3% anywhere in the bowstring arch. This item can safely be omitted from the design.

(5) For horizontal loading, an inverse linear variation was noticed to exist between  $m_g$  and the bending moment in both the girder and the arch (Fig. 4). The maximum error in this assumption, as  $m_g$  varied from 0.5 to 10, was 1.0%. For vertical loads, the same variation in  $m_g$  changes the bending moment by only -3.3% in the arch and by -5.6% in the girder (Fig. 5) (that is, the effect of varying  $m_g$  on vertical loads can be totally neglected).

(6) Varying  $m_r$  from 0.05 to  $\infty$  produced a maximum bending moment change of -2.4% in the arch and 2.7% in the girder for the horizontal loads, and 26.7% in the arch and -9.8% in the girder for the vertical loads (Figs. 4 and 5). This same variation in  $m_r$  caused in the largest of the suspension-rod forces an increase of about 21%. In practice the percentages mentioned above can be considerably less, for  $m_r$  may take values a few times larger than 0.05.

(7) For vertical loads: The horizontal force in the arch and the bending moment along the girder were found to be very sensitive to variations in  $m_I$  when  $L/r_c$  was small, but for large values of  $L/r_c$ , changing  $m_I$  had very little effect on the bending moment and practically none on the horizontal force.

Suspension-rod and horizontal forces were directly proportional to  $L/r_c$  and, inversely, to  $m_I$ . They never changed sign.

The bending moment varied with  $m_I$  directly in the girder and inversely in the arch (Fig. 6). As  $L/r_c$  increased, along the girder, the (-) bending moment increased and the (+) moment decreased.

For horizontal loads: Suspension-rod and horizontal forces as well as the bending moments both in the arch and in the girder were all found to vary inversely with  $L/r_c$  and except for the bending moment in the arch, directly



with  $m_I$ . They were very sensitive to changes in  $L/r_c$  when the latter had low values and became insensitive as  $L/r_c$  took on large values (Figs. 7 and 8).

(8) As a whole, the results of the analytical methods showed very good agreement with those of the experimental work. The maximum error in the horizontal force, using the actual test structure as the standard for comparison, was 4.5% for the strain-energy method and 8.0% for the membrane-analogy method. (See Table 4.) For the vertical loading, the bending-moment curve of the strain-energy method showed a small shift downwards along the girder and upwards along the arch (Figs. 14 and 15).

The bending moment along the arch (Figs. 14(b) and 15(b)) was not a smooth curve, whereas upper- and lower-envelope curves, if drawn, tend to be smooth. Fig. 4 shows upper-envelope curves only.

(9) The membrane-analogy method yielded very satisfactory results. The maximum error in the bending moments for horizontal loading did not exceed 2.6% along the girder and 6.6% along the arch (Figs. 14 and 15) compared with the results of the strain-energy method. It was further observed that, as  $m_I$  increased, the error in the bending moment increased in the arch and decreased in the girder in a linear fashion. This can be attributed to the assumption that the suspension rods were inextensible.

In some cases the results from the membrane-analogy method can be obtained by using only the first term of the series. This is especially true for finding the horizontal force for all types of loading and the bending moment along the girder and the arch for horizontal loads. In other cases, for example, to find the bending moment for a vertical load, because here the series does not converge so rapidly, a few more terms of the series must be used. The latter will no doubt depend on the accuracy desired. One can assume ( $I_a = I_c \sec \phi$ ) variation without introducing any error that is significant for preliminary design.

(10) When a uniform load is applied over the entire length of the bowstring arch, the bending moment along the arch is found to be positive (Fig. 6). On the other hand, prestressing the bowstring arch, with or without gap, by a horizontal force always produces a negative bending moment in the arch rib (Figs. 4 and 8). Thus, prestressing the bowstring arch to counteract the dead-load bending moment is very advantageous for the arch rib.

In the tie girder for low  $L/r_c$  values the bending moment is also positive when  $m_I$  is approximately 10 or larger. Here again there is an advantage to prestressing for the dead-load bending moment. When  $L/r_c$  has large values, the girder part of the structure does not profit from this combined prestressing; it may even suffer. In this case, the gap prestressing system may be followed and the suspension rods released when the gap is being closed. After prestressing, the suspension rods are fastened back. This will allow one to get the benefit of prestressing without its harmful effect. If the tie girder is to be made of prestressed concrete, the two prestressing operations can be performed in one.

It may be of interest also to mention here that for short spans, the roadway floor may be designed as part of the tie girder itself.

## CONCLUSIONS

The assumption that the total moment at a section (simple beam moment minus  $H \cdot y$ ) is distributed between the rib and the girder according to their

respective moment of inertia is quite justified. So also is the assumption of inextensible suspension rods in simplified design.

The good agreement between the test results and the theoretical analyses highly recommends the membrane-analogy method for preliminary work and the strain-energy method for final design.

Finally, the definite advantages to prestressing the bowstring arch, within the limits described, suggest that this procedure is feasible in actual engineering practice.

---

#### APPENDIX I.—CONSTANTS

---

$$\begin{aligned}
 a_{11} &= 498.8567 + \frac{13228.3095}{(L/r_c)^2} + \frac{16807}{m_g(L/r_c)^2} \\
 a_{12} = a_{17} &= 165.7657 - \frac{1186.3341}{(L/r_c)^2} \\
 a_{13} = a_{16} &= 303.2085 - \frac{2220.6849}{(L/r_c)^2} \\
 a_{14} = a_{15} &= 382.4850 - \frac{2855.2692}{(L/r_c)^2} \\
 a_{22} = a_{77} &= 66.5788 + \frac{799.2929}{(L/r_c)^2} + \frac{80.50}{m_I} + \frac{2058.8575}{m_r(L/r_c)^2} \\
 a_{23} = a_{67} &= 112.5944 + \frac{642.7477}{(L/r_c)^2} + \frac{131.25}{m_I} \\
 a_{24} = a_{57} &= 129.5393 + \frac{544.5468}{(L/r_c)^2} + \frac{147.00}{m_I} \\
 a_{25} = a_{47} &= 119.6737 + \frac{472.2767}{(L/r_c)^2} + \frac{134.75}{m_I} \\
 a_{26} = a_{37} &= 89.4689 + \frac{374.0758}{(L/r_c)^2} + \frac{101.50}{m_I} \\
 a_{27} &= 47.2175 + \frac{217.5306}{(L/r_c)^2} + \frac{54.25}{m_I} \\
 a_{33} = a_{66} &= 200.3580 + \frac{981.2887}{(L/r_c)^2} + \frac{227.50}{m_I} + \frac{3430.3087}{m_r(L/r_c)^2} \\
 a_{34} = a_{56} &= 239.2140 + \frac{845.8723}{(L/r_c)^2} + \frac{266.00}{m_I}
 \end{aligned}$$

$$a_{35} = a_{46} = 224.4488 + \frac{762.3175}{(L/r_c)^2} + \frac{248.50}{m_I}$$

$$a_{36} = 169.0053 + \frac{626.6610}{(L/r_c)^2} + \frac{189.00}{m_I}$$

$$a_{44} = a_{55} = 300.7027 + \frac{912.8602}{(L/r_c)^2} + \frac{329.00}{m_I} + \frac{4116.0343}{m_r(L/r_c)^2}$$

$$a_{45} = 293.0846 + \frac{876.3650}{(L/r_c)^2} + \frac{320.25}{m_I}$$

$$c_1 = \frac{16807}{m_g(L/r_c)^2} P_1$$

$$c_2 = -\frac{1}{m_I} (80.50 P_2 + 131.25 P_3 + 147.00 P_4)$$

$$c_3 = -\frac{1}{m_I} (131.25 P_2 + 227.50 P_3 + 266.00 P_4)$$

$$c_4 = -\frac{1}{m_I} (147.00 P_2 + 266.00 P_3 + 329.00 P_4)$$

$$c_5 = -\frac{1}{m_I} (134.75 P_2 + 248.50 P_3 + 320.25 P_4)$$

$$c_6 = -\frac{1}{m_I} (101.50 P_2 + 189.00 P_3 + 248.50 P_4)$$

$$c_7 = -\frac{1}{m_I} (55.25 P_2 + 101.50 P_3 + 134.75 P_4)$$

$$b_{mn} = a_{mn} \text{ (see Eq. 9) except for } b_{11}$$

$$b_{11} = 498.8567 + \frac{13228.3095}{(L/r_c)^2}$$

$$d_1 = -\frac{7^5 E_a I_c}{L^3} \Delta$$

$$d_2 = d_3 = d_4 = d_5 = d_6 = d_7 = 0$$

---

#### APPENDIX II.—NOTATION

---

The following symbols, adopted for use in the paper and for the guidance of discussers conform essentially with "American Standard Letter Symbols for Structural Analysis" (ASA Z10.8-1961), prepared by a committee of the Ameri-

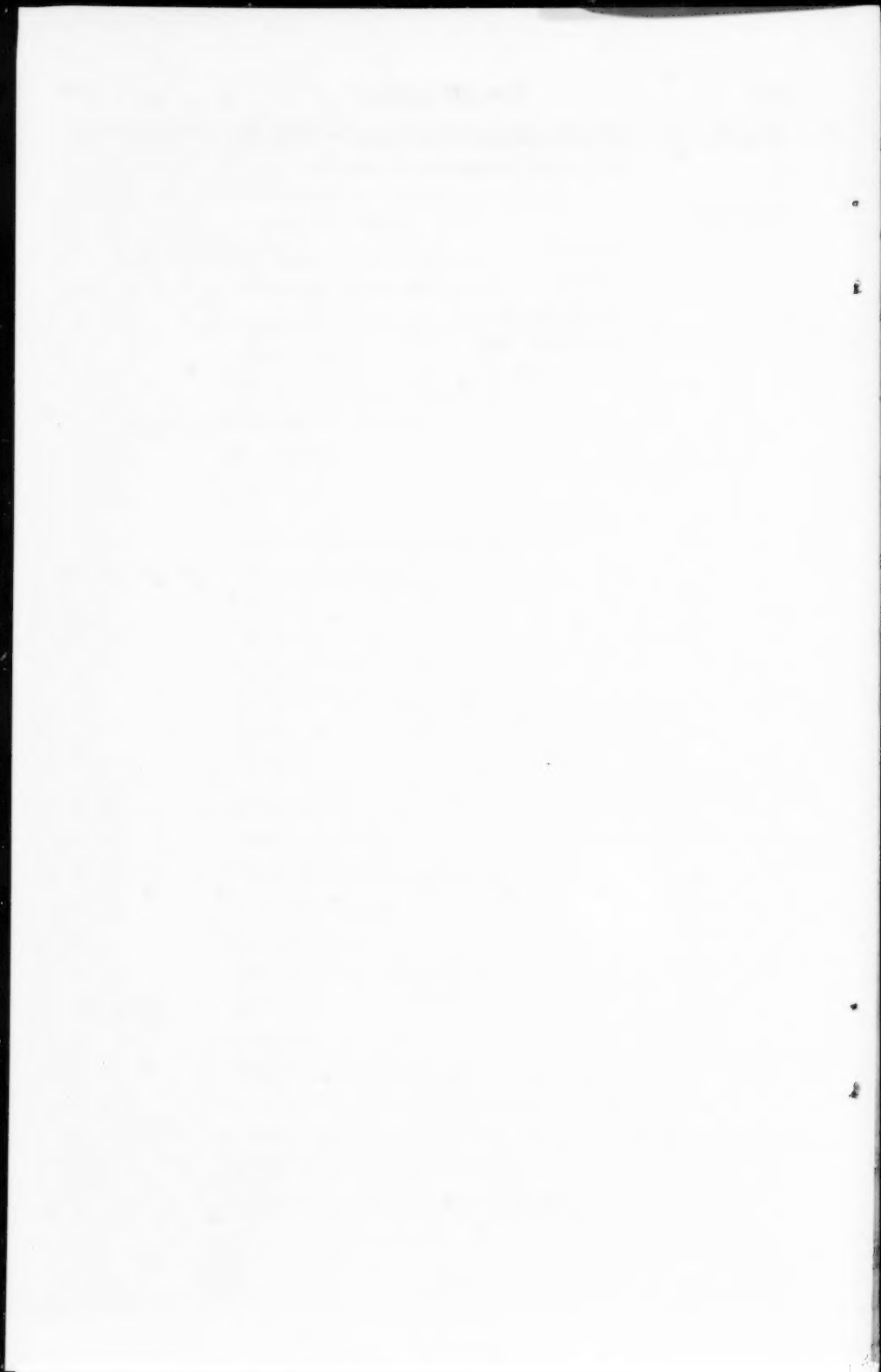
can Standards Association with Society representation, and approved by the Association in 1961:

$A_a, A_c, A_g, A_r$	= cross-sectional areas;
$a_i, a_n$	= Fourier constants;
$E, E_a, E_g, E_r$	= moduli of elasticity;
$F$	= horizontal force (external);
$H$	= horizontal components of arch thrust;
$h$	= rise at crown;
$h_i$	= height of arch at $i^{\text{th}}$ suspension rod;
$I, I_a, I_c, I_g$	= moments of inertia;
$K$	= a constant;
$k$	= $\frac{x}{L}$ ;
$L$	= span length between supports;
$M, M', M_a, M_g$	= bending moments;
$m_g$	= $\frac{A_g E_g}{A_c E_a}$ ;
$m_I$	= $\frac{I_g E_g}{I_c E_a}$ ;
$m_r$	= $\frac{A_r E_r}{A_c E_a}$ ;
$N, N'$	= axial forces;
$P, P_1$	= loads (external);
$q$	= membrane force along the span length;
$r_c, r_g$	= radii of gyration;
$U$	= strain energy;
$X_1, X_i$	= unknown forces or moments (internal);
$\alpha_F, \alpha_G, \alpha_P$	= constants;
$\beta_F$	= constant;
$\delta_H, \delta_{OH}$	= horizontal movements of arch at support;
$\Delta, \Delta_G$	= initial horizontal gaps between arch and girder;
$\Delta_q$	= vertical deflection of arch due to membrane force $q$ ;
$\Delta s$	= length along centerline of arch;
$\Delta x$	= length along girder or horizontal projection of;

$\Delta X_1, \Delta X_i$  = relative deflections or rotations at  $X_1, X_i$ ; and  
 $\phi$  = slope along centerline of arch rib.

Subscripts

a = arch rib;  
c = crown;  
g = tie girder; and  
r = suspension rod.



---

Journal of the  
STRUCTURAL DIVISION  
Proceedings of the American Society of Civil Engineers

---

DYNAMIC RESPONSE OF HIGHWAY BRIDGES

By John F. Fleming<sup>1</sup> and James P. Romualdi,<sup>2</sup> Associate Members, ASCE

---

SYNOPSIS

An analysis of the dynamic response of single span and three span continuous highway bridges to transient loads is presented. An analogous mathematical model is considered and the appropriate equations of motion are solved on a digital computer. The results of more than one thousand specific cases are analyzed to evaluate the effect of load characteristics and bridge geometry on highway bridge impact.

It is concluded that springing of the vehicle is one of the most important factors affecting the dynamic response of a highway bridge and that present (1961) specifications do not adequately provide for the dynamic response of bridges to standard design loads. Furthermore, the existence of a shallow area of settlement in the approach roadway, considering normally sprung loads, leads to impact factors appreciably greater than those usually considered in bridge impact.

---

INTRODUCTION

The dynamic effect of transient loads on bridges can be conveniently expressed in terms of an impact factor. This factor is usually defined as the ratio of the maximum dynamic stress produced in a bridge during passage of a load to the maximum stress that would occur if the load were acting stati-

---

Note.—Discussion open until March 1, 1962. To extend the closing date one month, a written request must be filed with the Executive Secretary, ASCE. This paper is part of the copyrighted Journal Structural Division, Proceedings of the American Society of Civil Engineers, Vol. 87, No. ST 7, October, 1961.

<sup>1</sup> Asst. Prof., Dept. of Civ. Engrg., Northwestern Univ., Evanston, Ill.

<sup>2</sup> Assoc. Prof., Dept. of Civ. Engrg., Carnegie Inst. of Tech., Pittsburgh, Pa.

cally, or moving at crawl velocity. However, the impact factor may also refer to deflection, shear, or reaction. Design formulas for dynamic impact usually indicate a percentage by which the static design loads should be increased to compensate for the dynamic effects of the moving load.

The problem of bridge impact has been recognized, at least with regard to railway bridges, from approximately the 1890's, but it is only since about 1930 that a major effort has been directed toward the problem of highway bridge impact. The first important report on this subject was published in 1931 by a special committee of the American Society of Civil Engineers.<sup>3</sup> The recommendations of this committee were the first widely accepted specifications for highway bridge impact and form the basis for most specifications in use today (1961). The information presented in the report was based on data obtained from a series of field tests. The loads used were 3-1/2 ton Liberty trucks traveling at a maximum velocity of 15 mph.

Since the publication of the report, few additional field tests were performed until 1952 when N. Von Eenam<sup>4</sup> obtained impact factors as high as 1.5 on a 110-ft pony truss. An H20-44 load traveling at 30 mph to 50 mph was used. In 1953, J. A. Wise,<sup>5</sup> M. ASCE, proposed a new impact formula based on tests performed on a seven span continuous girder bridge. However, it was not widely accepted.

One of the most recent series of field tests performed on highway bridges are those reported by J. M. Biggs.<sup>6,7,8</sup> The dynamic response of five single span girder bridges was observed in these tests under various loading conditions. The test results showed that springing of the vehicle is one of the major factors in highway bridge impact. Impact factors as high as 1.5 were measured under normal highway loading conditions.

One of the first persons to work on an analytical approach to the problem was Willis, who derived the differential equation for the deflection under a moving mass load for a beam of negligible mass. This equation was later solved by G. G. Stokes<sup>9</sup> (in 1896) by means of a power series. The equation as derived is of some use in the case of railway bridges because of the high ratio of the loads to the weight of the bridge. However, the assumption of negligible beam mass renders it inapplicable to problems of highway bridge impact.

The next important contribution to the problem was made by A. N. Krylov<sup>10</sup> in 1905 when he obtained a solution for the case of the mass of the load being

---

3 "Impact on Highway Bridges," Final Report of the Special Committee on Highway Bridges, *Transactions*, ASCE, Vol. 95, 1931.

4 "Live Load Stress Measurements of Fort London Bridge," by N. Von Eenam, *Proceedings*, Highway Research Bd., Vol. 32, 1935.

5 "Dynamics of Highway Bridges," by J. A. Wise *Proceedings*, Highway Research Bd., Vol. 32, 1935.

6 "Vibrations of Simple Span Highway Bridges," by J. M. Biggs, *Transactions*, ASCE, Vol. 124, 1959.

7 "Structural Design for Dynamic Loads," by Norris, Hansen, Holley, Biggs, Manyet, and Minami, McGraw-Hill Book Co., New York, 1959, p. 416.

8 "Vibration Measurements of Simple Span Bridges," by J. M. Biggs, *Highway Research Bd.*, Bulletin 124, 1956.

9 "Discussions of a Differential Equation Relating to the Breaking of Railway Bridges," by G. G. Stokes, *Transactions*, Cambridge Philosophical Soc., 1896.

10 "Über der erswungenen Schwingungen von gleichformigen elastischen staben," by A. N. Kryloff, *Mathematische Annalen*, Vol. 61, 1905, p. 211.



negligible compared to the mass of the bridge. This is equivalent to a constant force moving across the span. This solution is also not applicable to the problem of highway loadings.

Finally, in 1937, A. Schallenkamp<sup>11</sup> presented a rigorous solution for the case of a smoothly rolling load which considered both the mass of the load and the mass of the bridge. Although this solution does include most of the important variables involved, it is not in a form which is convenient for computation. Notable contributions have also been made by C. E. Inglis<sup>12</sup> and S. Timoshenko.<sup>13</sup>

Two of the most recently published papers on this subject are those by C. T. G. Looney,<sup>14,15</sup> F. ASCE, and Biggs.<sup>6,7</sup> The basic assumptions made in the numerical procedures presented by both Looney and Biggs are that the bridge can be represented by a simple beam, of which only the first or fundamental mode of vibration is considered, and that the deflected shape of the bridge can be approximated by a half sine wave. The methods used by Looney and Biggs are essentially the same, that is, the differential equation is written for the fundamental mode of the bridge and solved numerically. The equations included the mass of the load and the mass of the bridge. The main difference between the two procedures is that Looney assumes a smoothly rolling load whereas Biggs includes the effect of vehicle springing. The equations of motion derived by these investigators are for simply supported single span highway bridges and cannot be applied to determine the dynamic response of continuous highway bridges because of the assumption of a specific deflected shape of the bridge.

A comprehensive research program is being conducted at the University of Illinois, Urbana, Ill. This program has consisted of both an experimental and analytical phase.<sup>16</sup> There have been a number of other investigators who have made significant contributions to an understanding of the problem of highway bridge impact. A fairly complete bibliography is given in a report by the Committee on Deflection Limitations of Bridges of the Structural Division of ASCE.<sup>17</sup>

In this paper a method is used for determining the dynamic response of highway bridges to transient loads, which is applicable to both single span and multi-span continuous bridges. The several factors that have an effect on impact such as the mass of the load, the mass of the bridge, the springing of the vehicle and damping in the bridge and in the vehicle are included. The method is applied to a systematic analysis of the separate and combined effects of these variables. The results of more than one thousand specific solutions are

---

11 "Schwingungen von Trägern bei bewegten Lasten," by A. Schallenkamp, Vol. 8, No. 3, 1937, p. 187.

12 "Mathematical Treatise on Vibrations of Railway Bridges," by C. E. Inglis, Cambridge Univ. Press, London, 1934.

13 "Vibrations of Bridges," by S. Timoshenko, *Transactions*, ASME, Vol. 53, 1928.

14 "Impact on Railway Bridges," by C. T. G. Looney, Bulletin 352, Univ. of Illinois, Urbana, Ill.

15 "High-Speed Computer Applied to Bridge Impact," by C. T. G. Looney, *Proceedings*, ASCE, Vol. 84, No. ST5, September, 1958.

16 "Highway-Bridge Impact Problems," by Tung, Goodman, Chen, and Newmark, Highway Research Bd., Bulletin 124, 1956.

17 "Deflection Limitations of Bridges," Progress Report of the Committee on Deflection Limitations of Bridges of the Structural Division, *Proceedings*, ASCE, Vol. 84, No. ST3, May, 1958.

grouped in terms of four dimensionless parameters. The effect of the individual variables is considered and results for combinations of realistic values of the parameters are compared to existing impact specifications.

*Notation.*—The letter symbols adopted for use in this paper are defined where they first appear, in the illustrations or in the text, and are arranged alphabetically for convenience of reference in Appendix.

### ANALYTICAL PROCEDURE

There are certain conditions that must be satisfied by an analytical procedure. First, it should be applicable to any bridge geometry such as single

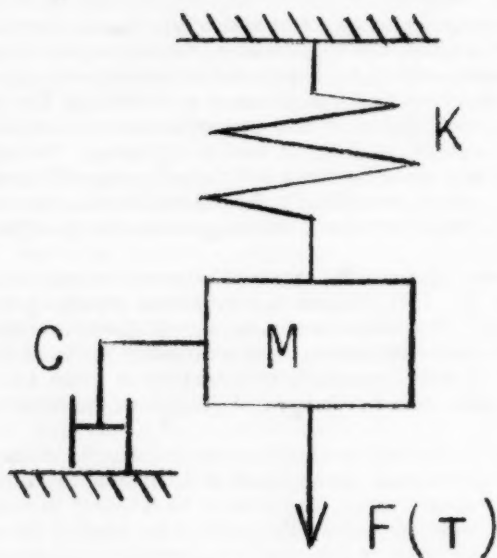


FIG. 1.—SINGLE MASS OSCILLATOR

span or multi-span continuous bridges with either constant or variable section over the length. Second, it should consider more than the fundamental mode of vibration of the bridge. Third, it should include the effect of all important variables such as the mass of the load and the bridge, springing of the vehicle, damping in the vehicle and in the bridge, and the effect of multiple axle loads. Finally, it should be in a form that lends itself to a convenient method of solution.

As a first step in the development of such a procedure consider the single mass oscillator shown in Fig. 1, in which  $M$  is the mass,  $K$  denotes the spring constant,  $C$  refers to the viscous damping coefficient and  $F(t)$  is an applied load that varies with time in a known manner. The equation of dynamic equi-

librium for this system is

$$F(t) - K y - C v = M a \dots\dots\dots (1)$$

in which  $y$ ,  $v$ , and  $a$  are the displacement, velocity, and acceleration of the mass, respectively. Although the exact solution for this particular system is simple to obtain, it will serve to demonstrate the numerical procedure which shall be applied to the bridge impact problem.

The numerical procedure is based on an integration process over finite intervals as shown in Fig. 2. The expression for the change in velocity over a time period  $\Delta t = t_2 - t_1$  is

$$\Delta v = v_2 - v_1 = \int_{t_1}^{t_2} a \, dt \dots\dots\dots (2)$$

in which the subscripts 1 and 2 refer to the beginning and end of the time interval, respectively. An approximation to this integral, as indicated in Fig. 2(a), is

$$v_2 - v_1 = \left[ \frac{a_2 + a_1}{2} \right] (\Delta t) \dots\dots\dots (3)$$

The error involved is the small unshaded area directly under the curve between  $t_1$  and  $t_2$ . This error is negligible if  $\Delta t$  is sufficiently small.

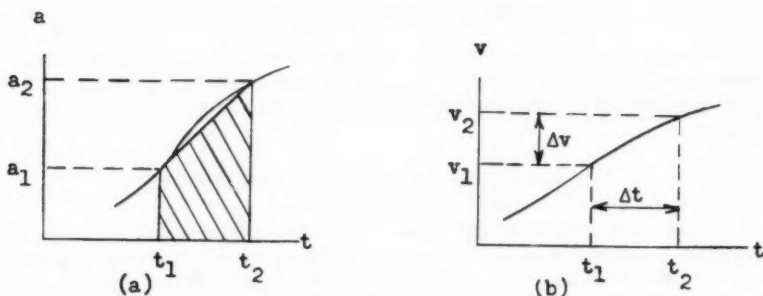


FIG. 2.—INTEGRATION PROCESS

A similar expression for the change in displacement in terms of the velocities at times  $t_2$  and  $t_1$  can be obtained with reference to Fig. 2(b), from which

$$y_2 - y_1 = \left[ \frac{v_2 + v_1}{2} \right] (\Delta t) \dots\dots\dots (4)$$

The equation of motion at the end of the time interval is

$$K y_2 = F(t_2) - C v_2 - M a_2 \dots\dots\dots (5)$$

This equation cannot be used directly in its present form to solve for  $y_2$  until the velocity and acceleration at time  $t_2$  are established. However, expressions

for  $v_2$  and  $a_2$ , obtained from Eqs. 3 and 4, are

$$a_2 = \frac{2}{(\Delta t)} (v_2 - v_1) - a_1 \dots\dots\dots (6)$$

and

$$v_2 = \frac{2}{(\Delta t)} (y_2 - y_1) - v_1 \dots\dots\dots (7)$$

Substituting these expressions into Eq. 5 an expression for the displacement at time  $t_2$  is found in terms of the displacement, velocity, and acceleration at time  $t_1$ . The resulting expression, after rearranging terms, is

$$\left[ \frac{4M}{(\Delta t)^2} + \frac{2C}{(\Delta t)} + K \right] y_2 = \left[ \frac{4M}{(\Delta t)^2} + \frac{2C}{(\Delta t)} \right] y_1 + \left[ \frac{4M}{(\Delta t)^2} + \frac{C}{(\Delta t)} \right] v_1(\Delta t) + \left[ \frac{M}{(\Delta t)^2} \right] a_1(\Delta t)^2 + F(t_2) \dots\dots\dots (8)$$

This expression can be used to determine the displacements of the system by a stepwise process where the acceleration, velocity, and displacement at the end of a time interval are used as initial conditions for the next time interval. The velocity and acceleration at time  $t_2$  can be computed from the known displacement by using Eqs. 6 and 7, from which

$$v_2(\Delta t) = 2(y_2 - y_1) - v_1(\Delta t) \dots\dots\dots (9)$$

and

$$a_2(\Delta t)^2 = 2[v_2(\Delta t) - v_1(\Delta t)] - a_1(\Delta t)^2 \dots\dots\dots (10)$$

The length of the time interval affects the accuracy of the solution. Experience has indicated that a time interval of one tenth to one-twentieth of the fundamental period of vibration of the system is sufficiently accurate for most purposes.

#### APPLICATION TO SINGLE SPAN BRIDGES

A single span girder bridge can be suitably represented by a system of concentrated masses, and yet retaining the static force-displacement relationships of the actual structure. The number of concentrated masses used to represent the bridge will be equal to the order of the highest mode of vibration of the bridge considered. It will be shown later that a system of three concentrated masses, as shown in Fig. 3, is sufficiently accurate to represent a single span highway bridge for most purposes. For a uniform section the three masses will be equal to  $\frac{mL}{4}$ , in which  $m$  is the mass of the bridge per unit length and  $L$  is the span length. However, a bridge of variable section can also be considered if the concentrated masses are chosen accordingly.

The equations of motion for this system at time  $t_2$ , including all of the variables previously mentioned, are

$$M_1 a_{1-2} = [(W + K \Delta_2) - M_u \ddot{y}_x] \phi_{1-2} - b_{11} v_{1-2} - b_{12} y_{2-2} - b_{13} y_{3-2} - C_b v_{1-2} \dots\dots\dots (11a)$$

$$M_2 a_{2-2} = [(W + K \Delta_2) - M_u \ddot{y}_x] \phi_{2-2} - b_{21} v_{1-2} - b_{22} y_{2-2} - b_{23} y_{3-2} - C_b v_{2-2} \dots\dots\dots (11b)$$

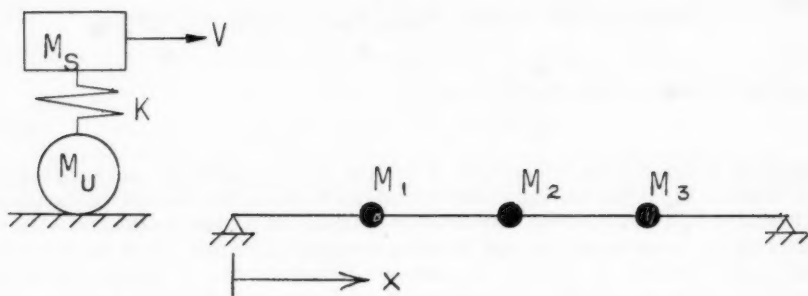


FIG. 3.—MATHEMATICAL MODEL OF SINGLE SPAN BRIDGE

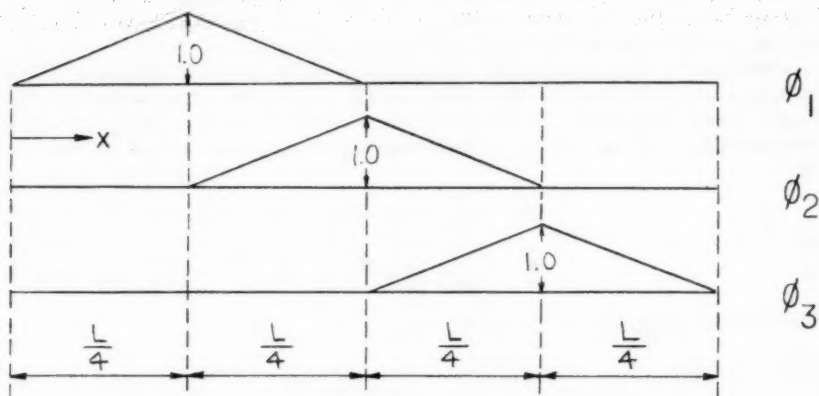


FIG. 4.—FORCING FUNCTIONS FOR SINGLE SPAN BRIDGE

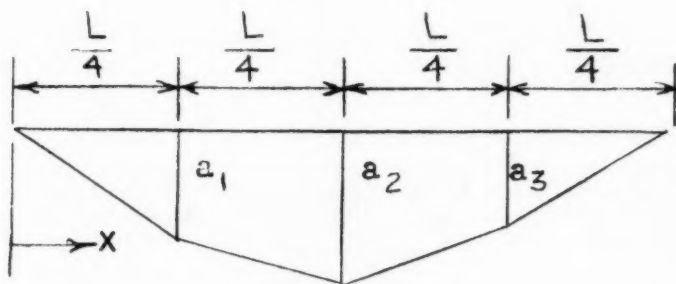


FIG. 5.—ACCELERATION DISTRIBUTION FOR SINGLE SPAN BRIDGE

and

$$M_3 a_{3-2} = [(W + K \Delta_2) - M_u \ddot{y}_x] \phi_{3-2} - b_{31} \dot{y}_{1-2} - b_{32} y_{2-2} - b_{33} y_{3-2} - C_b v_{3-2} \dots \dots \dots (11c)$$

and the equation of the sprung mass is

$$M_s (\ddot{\Delta}_2 + \ddot{y}_x) = -K \Delta_2 - C_v \dot{\Delta}_2 \dots \dots \dots (12)$$

in which  $W$  denotes the total weight of vehicle,  $M_u$  refers to the unsprung mass of vehicle,  $M_s$  is the sprung mass of vehicle,  $K$  describes the spring constant of vehicle,  $\ddot{y}_x$  is the vertical acceleration of bridge at a point a distance  $x$  from the end,  $C_b$  denotes the viscous damping constant of bridge,  $C_v$  is the viscous damping constant of vehicle,  $\Delta_2$  refers to the distortion of vehicle spring at time  $t_2$ ,  $\phi_i$  is the position function which determines the fractional part of the load to be considered acting on mass  $i$  and  $b_{ij}$  describes the stiffness influence coefficient. (The notation  $y_{i-2}$  signifies the displacement of mass  $M_i$  at time  $t_2$ ).

The  $\phi_i$  functions used for single span bridges are illustrated in Fig. 4. For example, when the load is at a point  $x = 0.375 L$ , the applied load on mass  $M_1$  and  $M_2$  is  $0.5 P$  and the applied load on mass  $M_3$  is zero.

Expressions for the stepwise computation of the dynamic response of this system can be derived in the same manner as previously described for the single mass oscillator. To simplify the derivation an expression for  $\Delta_2$  is obtained first by substituting the following expressions for  $\dot{\Delta}_2$  and  $\ddot{\Delta}_2$  into Eq. 12

$$\dot{\Delta}_2 = \frac{2}{(\Delta t)} (\Delta_2 - \Delta_1) - \dot{\Delta}_1 \dots \dots \dots (13)$$

and

$$\ddot{\Delta}_2 = \frac{2}{(\Delta t)} (\dot{\Delta}_2 - \dot{\Delta}_1) - \ddot{\Delta}_1 \dots \dots \dots (14)$$

The resulting expression for  $\Delta_2$  is

$$\Delta_2 = \frac{\left[ \frac{4 M_s}{(\Delta t)^2} + \frac{2 C_v}{(\Delta t)} \right] \Delta_1 + \left[ \frac{4 M_s}{(\Delta t)^2} + \frac{C_v}{(\Delta t)} \right] \dot{\Delta}_1 (\Delta t) + \left[ \frac{M_s}{(\Delta t)^2} \right] \ddot{\Delta}_1 (\Delta t)^2}{\left[ K + \frac{2 C_v}{(\Delta t)} + \frac{4 M_s}{(\Delta t)^2} \right]} - \frac{M_s}{\left[ K + \frac{2 C_v}{(\Delta t)} + \frac{4 M_s}{(\Delta t)^2} \right]} \ddot{y}_x \dots \dots \dots (15)$$

In this expression let

$$\beta = \frac{\left[ \frac{4 M_s}{(\Delta t)^2} + \frac{2 C_v}{(\Delta t)} \right] \Delta_1 + \left[ \frac{4 M_s}{(\Delta t)^2} + \frac{C_v}{(\Delta t)} \right] \dot{\Delta}_1 (\Delta t) + \left[ \frac{M_s}{(\Delta t)^2} \right] \ddot{\Delta}_1 (\Delta t)^2}{\left[ K + \frac{2 C_v}{(\Delta t)} + \frac{4 M_s}{(\Delta t)^2} \right]} \dots \dots (16)$$

and

$$\gamma = \frac{M_s}{\left[ K + \frac{2 C_v}{(\Delta t)} + \frac{4 M_s}{(\Delta t)^2} \right]} \dots \dots \dots (17)$$

Expressions for the velocities and accelerations of the masses at time  $t_2$  in terms of displacements, velocities and accelerations at time  $t_1$ , from Eqs. 6 and 7 are

$$v_{i-2} = \frac{2}{(\Delta t)} (y_{i-2} - y_{i-1}) - v_{i-1} \dots \dots \dots (18)$$

and

$$a_{i-2} = \frac{2}{(\Delta t)} (v_{i-2} - v_{i-1}) - a_{i-1} \dots \dots \dots (19)$$

Substituting Eqs. 18 and 19 into Eq. 11, the equations for the displacements of masses  $M_1$ ,  $M_2$ , and  $M_3$ , become

$$\begin{aligned} \left[ \frac{4 M_1}{(\Delta t)^2} + \frac{2 C_b}{(\Delta t)} + b_{11} \right] y_{1-2} &= b_{12} y_{2-2} + b_{13} y_{3-2} + (K \gamma + M_u) \ddot{y}_x \phi_{1-2} \\ &= \left[ \frac{4 M_1}{(\Delta t)^2} + \frac{2 C_b}{(\Delta t)} \right] y_{1-1} + \left[ \frac{4 M_1}{(\Delta t)^2} + \frac{C_b}{(\Delta t)} \right] v_{1-1}(\Delta t) + \left[ \frac{M_1}{(\Delta t)^2} \right] a_{1-1}(\Delta t)^2 \\ &\quad + (W + K \beta) \phi_{1-2} \dots \dots \dots (20a) \end{aligned}$$

$$\begin{aligned} b_{21} y_{1-2} + \left[ \frac{4 M_2}{(\Delta t)^2} + \frac{2 C_b}{(\Delta t)} + b_{22} \right] y_{2-2} &= b_{23} y_{3-2} + (K \gamma + M_u) \ddot{y}_x \phi_{2-2} \\ &= \left[ \frac{4 M_2}{(\Delta t)^2} + \frac{2 C_b}{(\Delta t)} \right] y_{2-1} + \left[ \frac{4 M_2}{(\Delta t)^2} + \frac{C_b}{(\Delta t)} \right] v_{2-1}(\Delta t) + \left[ \frac{M_2}{(\Delta t)^2} \right] a_{2-1}(\Delta t)^2 \\ &\quad + (W + K \beta) \phi_{2-2} \dots \dots \dots (20b) \end{aligned}$$

and

$$\begin{aligned} b_{31} y_{1-2} + b_{32} y_{2-2} + \left[ \frac{4 M_3}{(\Delta t)^2} + \frac{2 C_b}{(\Delta t)} + b_{33} \right] y_{3-2} &= (K \gamma + M_u) \ddot{y}_x \phi_{3-2} \\ &= \left[ \frac{4 M_3}{(\Delta t)^2} + \frac{2 C_b}{(\Delta t)} \right] y_{3-1} + \left[ \frac{4 M_3}{(\Delta t)^2} + \frac{C_b}{(\Delta t)} \right] v_{3-1}(\Delta t) + \left[ \frac{M_3}{(\Delta t)^2} \right] a_{3-1}(\Delta t)^2 \\ &\quad + (W + K \beta) \phi_{3-2} \dots \dots \dots (20c) \end{aligned}$$

As a final step in the derivation the vertical acceleration of the bridge at any point,  $\ddot{y}_x$ , must be expressed in terms of the accelerations of the discrete mass points. It is assumed that the values along the span vary linearly between these known points. Therefore, the assumed acceleration distribution along the length of the bridge is that shown in Fig. 5, for which  $a_1$ ,  $a_2$ , and  $a_3$  are the accelerations of the masses  $M_1$ ,  $M_2$ , and  $M_3$ , respectively. The acceleration at any point on the bridge is given by the following expressions for the indicated position ranges:

$$\ddot{y}_x = \frac{4x}{L} a_1 \quad \left( \text{for } 0 \leq x \leq \frac{L}{4} \right) \dots \dots \dots (21a)$$



$$\ddot{y}_x = \left(2 - \frac{4x}{L}\right) a_1 + \left(\frac{4x}{L} - 1\right) a_2 \quad \left(\text{for } \frac{L}{4} \leq x \leq \frac{L}{2}\right) \dots \dots \dots (21b)$$

$$\ddot{y}_x = \left(3 - \frac{4x}{L}\right) a_2 + \left(\frac{4x}{L} - 2\right) a_3 \quad \left(\text{for } \frac{L}{2} \leq x \leq \frac{3L}{4}\right) \dots \dots \dots (21c)$$

and

$$\ddot{y}_x = \left(4 - \frac{4x}{L}\right) a_3 \quad \left(\text{for } \frac{3L}{4} \leq x \leq L\right) \dots \dots \dots (21d)$$

Substituting Eqs. 18 and 19 into Eqs. 21, the final expressions for  $\ddot{y}_x$  are

$$\ddot{y}_x = \frac{16x}{L(\Delta t)^2} y_{1-2} - \frac{16x}{L(\Delta t)^2} \left[ y_{1-1} + v_{1-1}(\Delta t) + \frac{a_{1-1}(\Delta t)^2}{4} \right] \quad \left(\text{for } 0 \leq x \leq \frac{L}{4}\right) \dots \dots \dots (22a)$$

$$\begin{aligned} \ddot{y}_x = & \left[ \frac{8}{(\Delta t)^2} - \frac{16x}{L(\Delta t)^2} \right] y_{1-2} + \left[ \frac{16x}{L(\Delta t)^2} - \frac{4}{(\Delta t)^2} \right] y_{2-2} - \left[ \frac{8}{(\Delta t)^2} - \frac{16x}{L(\Delta t)^2} \right] \left[ y_{1-1} \right. \\ & \left. + v_{1-1}(\Delta t) + \frac{a_{1-1}(\Delta t)^2}{4} \right] - \left[ \frac{16x}{L(\Delta t)^2} - \frac{4}{(\Delta t)^2} \right] \left[ y_{2-1} + v_{2-1}(\Delta t) + \frac{a_{2-1}(\Delta t)^2}{4} \right] \\ & \left(\text{for } \frac{L}{4} \leq x \leq \frac{L}{2}\right) \dots \dots \dots (22b) \end{aligned}$$

$$\begin{aligned} \ddot{y}_x = & \left[ \frac{8}{(\Delta t)^2} - \frac{16(L-x)}{L(\Delta t)^2} \right] y_{3-2} + \left[ \frac{16(L-x)}{L(\Delta t)^2} - \frac{4}{(\Delta t)^2} \right] y_{2-2} - \left[ \frac{8}{(\Delta t)^2} - \frac{16(L-x)}{L(\Delta t)^2} \right] \left[ y_{3-1} \right. \\ & \left. + v_{3-1}(\Delta t) + \frac{a_{3-1}(\Delta t)^2}{4} \right] - \left[ \frac{16(L-x)}{L(\Delta t)^2} - \frac{4}{(\Delta t)^2} \right] \left[ y_{2-1} + v_{2-1}(\Delta t) + \frac{a_{2-1}(\Delta t)^2}{4} \right] \\ & \left(\text{for } \frac{L}{2} \leq x \leq \frac{3L}{4}\right) \dots \dots \dots (22c) \end{aligned}$$

and

$$\begin{aligned} \ddot{y}_x = & \frac{16(L-x)}{L(\Delta t)^2} y_{3-2} - \frac{16(L-x)}{L(\Delta t)^2} \left[ y_{3-1} + v_{3-1}(\Delta t) + \frac{a_{3-1}(\Delta t)^2}{4} \right] \\ & \left(\text{for } \frac{3L}{4} \leq x \leq L\right) \dots \dots \dots (22d) \end{aligned}$$

One of Eqs. 22 must be substituted into Eq. 20 for  $\ddot{y}_x$ . The one to be used depends on which section of the bridge is loaded. This process can easily be programmed for a high-speed digital computer. This will result in four sets of simultaneous algebraic equations for the displacements of the system. The additional equations required to compute the velocities and accelerations, once the displacements are known, are

$$v_{i-2}(\Delta t) = 2 [y_{i-2} - y_{i-1}] - v_{i-1}(\Delta t) \dots \dots \dots (23)$$

and

$$a_{i-2}(\Delta t)^2 = 2 [v_{i-2}(\Delta t) - v_{i-1}(\Delta t)] - a_{i-1}(\Delta t)^2 \dots \dots \dots (24)$$



The displacement of the sprung load relative to the bridge, in terms of displacements of the bridge, is

$$\Delta_2 = \beta - \gamma \ddot{y}_x \dots \dots \dots (25)$$

Eqs. 20 are now in a form suitable for the computation of the dynamic displacements of single span bridges by a stepwise process. For the case of multiple axle loads it is only necessary to consider the position of each load separately during each time step and use the corresponding values for  $\phi_1$  and  $\ddot{y}_x$ .

### CONTINUOUS BRIDGES

In the preceding procedure the deflected shape of the structure represents one of the results obtained rather than an assumption made in the derivation. Therefore, the same procedure can be used to derive expressions for the dynamic displacements of multi-span continuous bridges without violating conditions of continuity at the support. Expressions for the dynamic response of a three span continuous bridge will be derived. The same procedure may be applied to bridges continuous over any number of supports.

The continuous bridge is represented by one concentrated mass in each span as shown in Fig. 6. This mathematical model is used for simplicity in the derivation, although any number of concentrated masses may be used if desired. A more accurate representation of a true continuous highway bridge would probably be obtained by using three concentrated masses per span. Thus, higher modes of vibration would be included. The main purpose of this presentation is to demonstrate how the procedure used for single span bridges can be extended to the case of continuous bridges. The load is assumed to be unsprung, although vehicle springing can be considered in exactly the same manner as previously described. The remainder of the derivation is essentially the same as that described for single span bridges.

The equations of motion for the masses of the system shown in Fig. 6 at time  $t_2$ , are

$$M_1 a_{1-2} = [W - M_L \ddot{y}_x] \phi_{1-2} - b_{11} y_{1-2} - b_{12} y_{2-2} - b_{13} y_{3-2} - C_b v_{1-2} \dots (26a)$$

$$M_2 a_{2-2} = [W - M_L \ddot{y}_x] \phi_{2-2} - b_{21} y_{1-2} - b_{22} y_{2-2} - b_{23} y_{3-2} - C_b v_{2-2} \dots (26b)$$

and

$$M_3 a_{3-2} = [W - M_L \ddot{y}_x] \phi_{3-2} - b_{31} y_{1-2} - b_{32} y_{2-2} - b_{33} y_{3-2} - C_b v_{3-2} \dots (26c)$$

which can be reduced to a set of linear simultaneous equations for  $y_1$ ,  $y_2$ , and  $y_3$ . These equations are

$$\begin{aligned} \left[ \frac{4 M_1}{(\Delta t)^2} + \frac{2 C_b}{(\Delta t)} + b_{11} \right] y_{1-2} + b_{12} y_{2-2} + b_{13} y_{3-2} + M_L \ddot{y}_x \phi_{1-2} &= \left[ \frac{4 M_1}{(\Delta t)^2} + \frac{2 C_b}{(\Delta t)} \right] y_{1-1} \\ &+ \left[ \frac{4 M_1}{(\Delta t)^2} + \frac{C_b}{(\Delta t)} \right] v_{1-1}(\Delta t) + \left[ \frac{M_1}{(\Delta t)^2} \right] a_{1-1}(\Delta t)^2 + W \phi_{1-2} \dots \dots \dots (27a) \end{aligned}$$

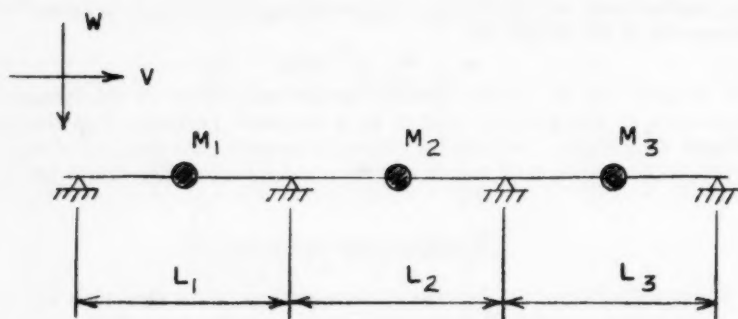


FIG. 6.—MATHEMATICAL MODEL OF CONTINUOUS BRIDGE

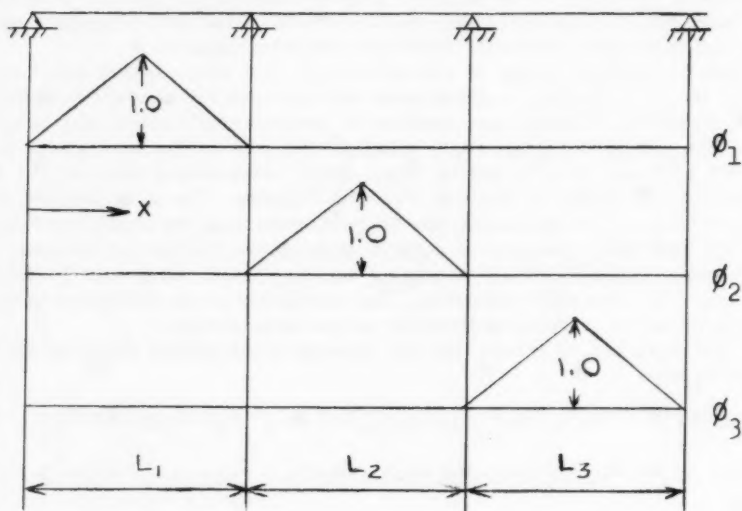


FIG. 7.—FORCING FUNCTIONS FOR CONTINUOUS BRIDGE

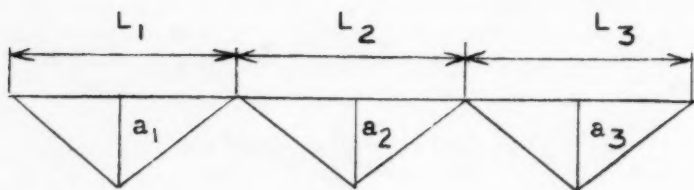


FIG. 8.—ACCELERATION DISTRIBUTION FOR CONTINUOUS BRIDGE

$$b_{21} y_{1-2} + \left[ \frac{4 M_2}{(\Delta t)^2} + \frac{2 C_b}{(\Delta t)} + b_{22} \right] y_{2-2} + b_{23} y_{3-2} + M_L \ddot{y}_x \phi_{2-2} = \left[ \frac{4 M_2}{(\Delta t)^2} + \frac{2 C_b}{(\Delta t)} \right] y_{2-1} \\ + \left[ \frac{4 M_2}{(\Delta t)^2} + \frac{C_b}{(\Delta t)} \right] v_{2-1}(\Delta t) + \left[ \frac{M_2}{(\Delta t)^2} \right] a_{2-1}(\Delta t)^2 + W \phi_{2-2} \dots \dots (27b)$$

and

$$b_{31} y_{1-2} + b_{32} y_{2-2} + \left[ \frac{4 M_3}{(\Delta t)^2} + \frac{2 C_b}{(\Delta t)} + b_{33} \right] y_{3-2} + M_L \ddot{y}_x \phi_{3-2} = \left[ \frac{4 M_3}{(\Delta t)^2} + \frac{2 C_b}{(\Delta t)} \right] y_{3-1} \\ + \left[ \frac{4 M_3}{(\Delta t)^2} + \frac{C_b}{(\Delta t)} \right] v_{3-1}(\Delta t) + \left[ \frac{M_3}{(\Delta t)^2} \right] a_{3-1}(\Delta t)^2 + W \phi_{3-2} \dots \dots (27c)$$

in which  $M_L$  is the mass of the load moving across the bridge.

The  $\phi_i$  functions used for continuous bridges are shown in Fig. 7 and the assumed acceleration distribution is shown in Fig. 8.

Due to the similarity between the  $\phi_i$  functions and the assumed acceleration distribution, a single expression for  $\ddot{y}_x$  can be written, as

$$\ddot{y}_x = a_1 \phi_1 + a_2 \phi_2 + a_3 \phi_3 \dots \dots \dots (28)$$

This expression is valid because, for any load, only one of the functions  $\phi_1$ ,  $\phi_2$ , or  $\phi_3$  will be non-zero. The expression for  $\ddot{y}_x$  can be substituted into Eq. 27 to obtain the final form of the expressions for  $y_1$ ,  $y_2$ , and  $y_3$ . When this substitution is made terms of the form  $\phi_1 \phi_2$ ,  $\phi_1 \phi_3$ , and  $\phi_2 \phi_3$  will occur. However, these terms will be equal to zero at all times because only one of the  $\phi_i$  terms will be non-zero for any given load. The final equations for the dynamic displacements of a three span continuous bridge, represented by one concentrated mass in each span, are

$$\left[ \frac{4 M_1}{(\Delta t)^2} + \frac{4 M_L}{(\Delta t)^2} (\phi_{1-2})^2 + \frac{2 C_b}{(\Delta t)} + b_{11} \right] y_{1-2} + b_{12} y_{2-2} + b_{13} y_{3-2} \\ = \left[ \frac{4 M_1}{(\Delta t)^2} + \frac{4 M_L}{(\Delta t)^2} (\phi_{1-2})^2 + \frac{2 C_b}{(\Delta t)} \right] y_{1-1} + \left[ \frac{4 M_1}{(\Delta t)^2} + \frac{4 M_L}{(\Delta t)^2} (\phi_{1-2})^2 \right. \\ \left. + \frac{C_b}{(\Delta t)} \right] v_{1-1}(\Delta t) + \left[ \frac{M_1}{(\Delta t)^2} + \frac{M_L}{(\Delta t)^2} (\phi_{1-2})^2 \right] a_{1-1}(\Delta t)^2 + W \phi_{1-2} \dots \dots (29a)$$

$$b_{21} y_{1-2} + \left[ \frac{4 M_2}{(\Delta t)^2} + \frac{4 M_L}{(\Delta t)^2} (\phi_{2-2})^2 + \frac{2 C_b}{(\Delta t)} + b_{22} \right] y_{2-2} + b_{23} y_{3-2} \\ = \left[ \frac{4 M_2}{(\Delta t)^2} + \frac{4 M_L}{(\Delta t)^2} (\phi_{2-2})^2 + \frac{2 C_b}{(\Delta t)} \right] y_{2-1} + \left[ \frac{4 M_2}{(\Delta t)^2} + \frac{4 M_L}{(\Delta t)^2} (\phi_{2-2})^2 \right. \\ \left. + \frac{C_b}{(\Delta t)} \right] v_{2-1}(\Delta t) + \left[ \frac{M_2}{(\Delta t)^2} + \frac{M_L}{(\Delta t)^2} (\phi_{2-2})^2 \right] a_{2-1}(\Delta t)^2 + W \phi_{2-2} \dots \dots (29b)$$

and

$$\begin{aligned}
 & b_{31} y_{1-2} + b_{32} y_{2-2} + \left[ \frac{4 M_3}{(\Delta t)^2} + \frac{4 M_L}{(\Delta t)^2} (\phi_{3-2})^2 + \frac{2 C_b}{(\Delta t)} + b_{33} \right] y_{3-2} \\
 & = \left[ \frac{4 M_3}{(\Delta t)^2} + \frac{4 M_L}{(\Delta t)^2} (\phi_{3-2})^2 + \frac{2 C_b}{(\Delta t)} \right] y_{3-1} + \left[ \frac{4 M_3}{(\Delta t)^2} + \frac{4 M_L}{(\Delta t)^2} (\phi_{3-2})^2 \right. \\
 & \quad \left. + \frac{C_b}{(\Delta t)} \right] v_{3-1}(\Delta t) + \left[ \frac{M_3}{(\Delta t)^2} + \frac{M_L}{(\Delta t)^2} (\phi_{3-2})^2 \right] a_{3-1}(\Delta t)^2 + W \phi_{3-2} \dots (29c)
 \end{aligned}$$

The only additional equations required are Eqs. 23 and 24 mentioned previously for computing the velocities and accelerations at time  $t_2$  once the displacements are known:

$$v_{i-2}(\Delta t) = 2 [y_{i-2} - y_{i-1}] - v_{i-1}(\Delta t) \dots \dots \dots (23)$$

and

$$a_{i-2}(\Delta t)^2 = 2 [v_{i-2}(\Delta t) - v_{i-1}(\Delta t)] - a_{i-1}(\Delta t)^2 \dots \dots \dots (24)$$

#### MODEL STUDIES

The procedure of representing a distributed mass structure by a series of discrete masses, but retaining the elastic properties of the distributed mass system, is widely accepted as a useful tool in structural dynamics. However, to demonstrate the validity of the mathematical model and the accuracy of the computational procedure in this application, experimental results from tests on a model beam are compared to computed results for several cases of moving loads. The results are excerpted from a test program being performed (in 1961) at Carnegie Institute of Technology, Pittsburgh, Pa., on the dynamic response of single and multi-span bridges.

Complete details of the apparatus will not be described herein, but the essential features are a test beam and a load that moves across the beam at a selected velocity. A schematic diagram of the apparatus is shown in Fig. 9. The test span is a steel beam 8 ft long, 3/4 in. wide-by-1/2 in. deep. The beam is cambered to provide a horizontal surface when deflected due to its own dead weight. Provisions were made in the design of the apparatus to apply either a mass load, consisting of a weight on a roller, or a pure force, consisting of a long stretched spring attached to a roller. A wide range of velocities, corresponding to any conceivable highway condition is obtainable. Both deflection and moment at the center of the beam are measured and continuously recorded on an oscillograph. The times at which the load enters and leaves the span are recorded by an event marker on the oscillograph. This permits an accurate determination of the velocity of the load.

For ease and clarity it is advantageous to present test and analytical data in terms of dimensionless parameters. These parameters should include the properties of the bridge and of the unsprung load. Two dimensionless parameters which satisfy these conditions are

$$\alpha = \frac{\text{time of crossing}}{\text{fundamental period of bridge}}$$

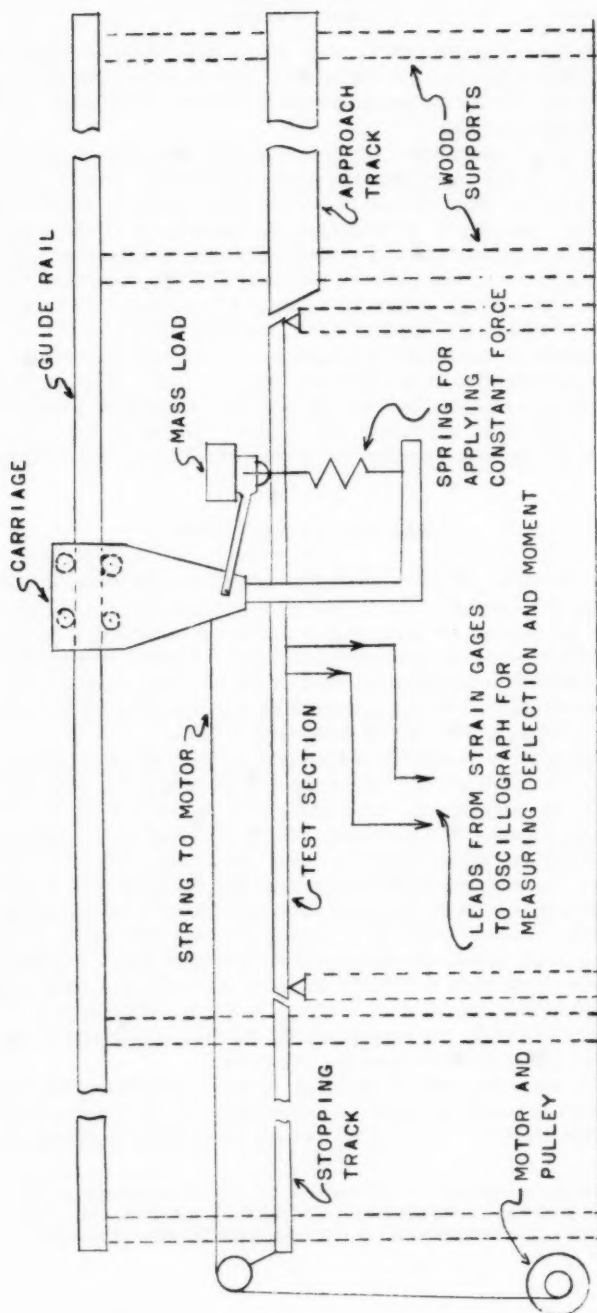


FIG. 9.—EXPERIMENTAL APPARATUS

and

$$R = \frac{\text{mass of load}}{\text{mass of bridge}}$$

An additional dimensionless parameter which describes the response of the bridge is the impact factor. For deflection, this is defined as the ratio of the dynamic deflection to the maximum static deflection which would occur if the load were applied statically.

In Figs. 10 and 11 the impact for deflection and moment, respectively, are shown for the case of a pure force traversing the beam. This corresponds to a value for  $R$  of zero. Figs. 12 and 13 are the results obtained for an arbitrary mass load. For both types of loading good agreement is observed between measured and computed impact for both deflection and moment. Many other comparisons have been made between the computed and measured response of the test beam for a large range of values of  $R$  and  $\alpha$  and in most cases the difference in the maximum impacts were less than 5%.<sup>18</sup>

The mathematical model for a single span bridge on which this method is based can be considered to be an adequate representation of the real structure. If greater accuracy is desired it can be obtained by using a larger number of concentrated masses to represent the bridge. The same procedure can be used to derive the expressions needed to compute the dynamic response of the bridge.

#### ANALYTICAL RESULTS

*Single Span Bridges.*—The expressions for dynamic response derived herein are ideally suited for solution on an electronic digital computer. Accordingly, the equations of motion as derived previously for both single span and three span continuous bridges were programmed for the IBM 650 digital computer. With these programs a complete picture of the dynamic response for various load characteristics and bridge geometries was obtained. The details of the computer programming will not be described herein.

Highway bridges vary widely in type and loading, and to properly investigate the dynamic response of bridges the bridge properties and load characteristics must be considered. The important properties of the bridge are weight, stiffness, length, and geometry. The properties of the loads are magnitude, axle spacing, velocity, and vehicle springing. All of the properties mentioned are self-explanatory except possibly the springing of the vehicle. Generally, the major part of a vehicle is supported on a spring and a smaller part is in direct contact with the roadway (wheels and parts of the undercarriage). Although the tires are flexible, the springing of balloon tires is neglected. There is also a further division for the case of sprung loads; (1) the case in which the load is initially in its equilibrium position when it enters the bridge, and (2) the case in which the load is initially vibrating with some definite amplitude when it enters the bridge.

*Unsprung Loads.*—The effect of many of the variables involved in bridge impact can be evaluated by first considering the case of an unsprung single axle load. This simplification is necessary for a clear understanding of the

<sup>18</sup> "An Experimental Study of a Mathematical Model for Investigating Highway Bridge Impact," thesis presented to the Carnegie Inst. of Tech., at Pittsburgh, Pa., in 1960, as partial fulfillment of the requirements for the degree of Master of Science.

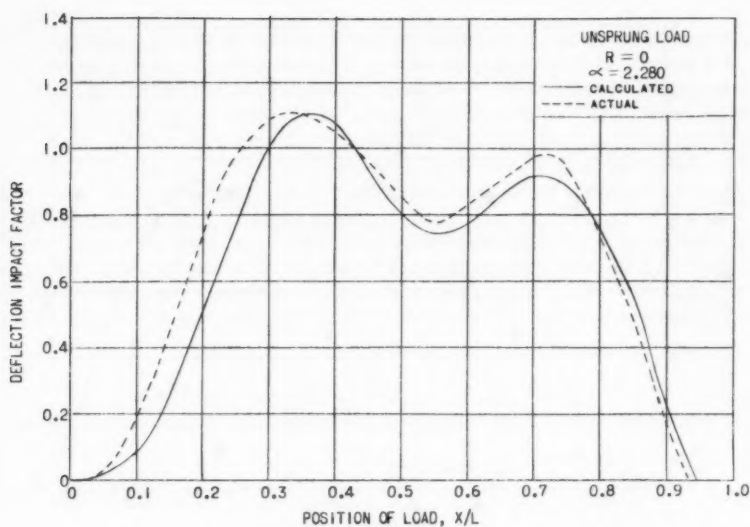


FIG. 10.—COMPARISON OF COMPUTED AND ACTUAL IMPACTS FOR DEFLECTION FOR PURE FORCE TRAVERSING BEAM

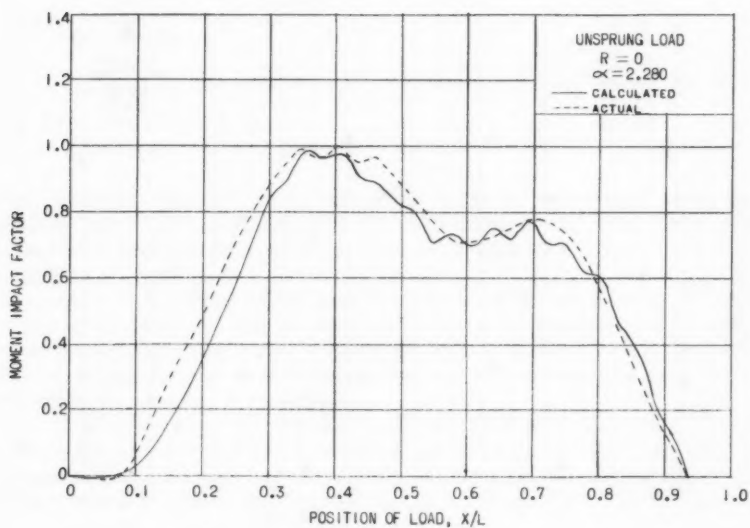


FIG. 11.—COMPARISON OF COMPUTED AND ACTUAL IMPACTS FOR MOMENT FOR PURE FORCE TRAVERSING THE BEAM

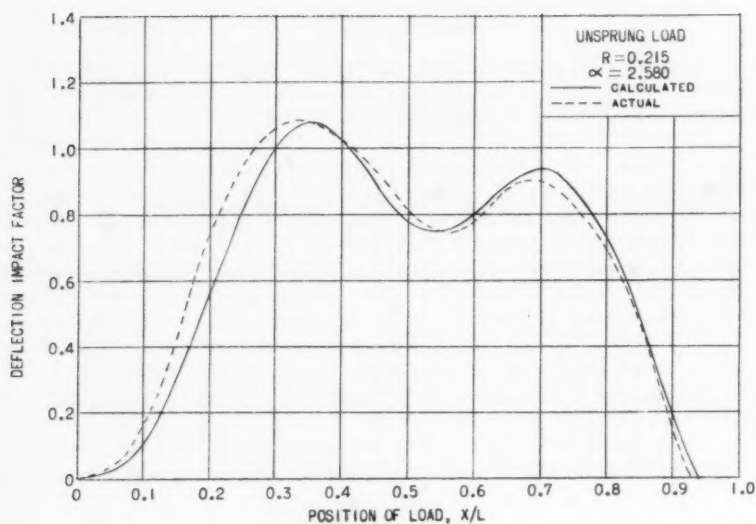


FIG. 12.—COMPARISON OF COMPUTED AND ACTUAL IMPACTS FOR DEFLECTION FOR AN ARBITRARY MASS LOAD

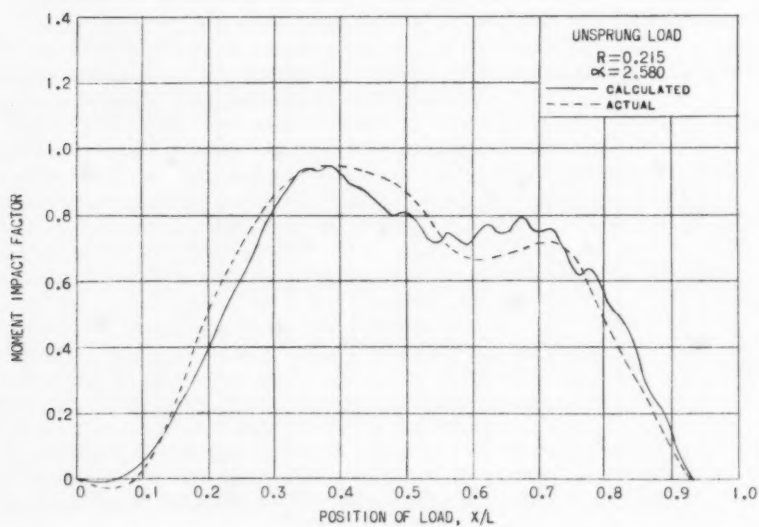


FIG. 13.—COMPARISON OF COMPUTED AND ACTUAL IMPACTS FOR MOMENT FOR AN ARBITRARY MASS LOAD



effects of variables such as the bridge characteristics, speed of the vehicle, and mass of the load.

The realistic range of values of the parameters  $R$  and  $\alpha$  which can be expected under highway loading conditions was determined by an analysis of the properties of a wide range of highway bridges. The standard bridge plans of the Bureau of Public Roads, U. S. Dept. of Commerce (BPR) were used.<sup>19</sup> Values from almost zero to approximately one can be expected for  $R$  and, assuming a maximum velocity of 80 mph, a value of approximately 1.5 or higher may be encountered for  $\alpha$ . Table 1 summarizes the properties of the standard bridges used in this study.

Figs. 14 and 15 show the relationships between maximum impact (for deflection and moment) and  $\alpha$  for values of  $R$  ranging from zero to 1.0. The case of  $R$  equal to zero represents a pure force crossing the span. The impacts for both deflection and moment are shown because they are not necessarily the

TABLE 1.—STANDARD SINGLE SPAN BRIDGES

Span, in feet	Weight, in pounds per foot	EI, ( $10^{11}$ lb-in <sup>2</sup> )	Fundamental Frequency, in cycles per second	Velocity to Cross Span in Natural Period, in miles per hour	Type
(1)	(2)	(3)	(4)	(5)	(6)
20	3422	1.07076	10.38	141.21	I-Beam
30	3401	2.51568	7.09	144.74	I-Beam
40	3425	4.12248	5.09	138.83	I-Beam
50	3574	8.03880	4.46	151.84	I-Beam
60	3633	11.2505	3.63	148.42	I-Beam
70	3881	14.7745	2.95	140.47	I-Beam
80	4019	20.6806	2.64	143.59	I-Beam
90	4142	59.6403	3.49	213.33	Girder
100	4240	77.1255	3.17	215.96	Girder
120	4490	134.244	2.81	229.31	Girder
140	5031	208.152	2.43	231.16	Girder

same. Moment depends on the deflected shape of the bridge which is not always the same under dynamic and static conditions. The difference between moment and deflection impact is further illustrated by a comparison of Figs. 10 and 11.

The effect of the mass of the load is apparent from the shift to the right of the curves in Figs. 14 and 15 as  $R$  is increased. Except for this shift the curves are almost identical for different values of  $R$ . There is an increase in the maximum impact as  $R$  is increased, but this increase is small considering the wide range of  $R$  investigated.

The general shape of the curves is logical. That is, a maximum at a value for  $\alpha$  of approximately 1.0 and decreasing as  $\alpha$  is increased beyond this point. Theoretically the curves are asymptotic to an impact factor of 1.0 as  $\alpha$  approaches infinity. Also, the curves should pass through the origin when  $\alpha$  is

<sup>19</sup> "Standard Plans for Highway Bridge Superstructures," U. S. Dept. of Commerce, Bur. of Pub. Rds., 1956.

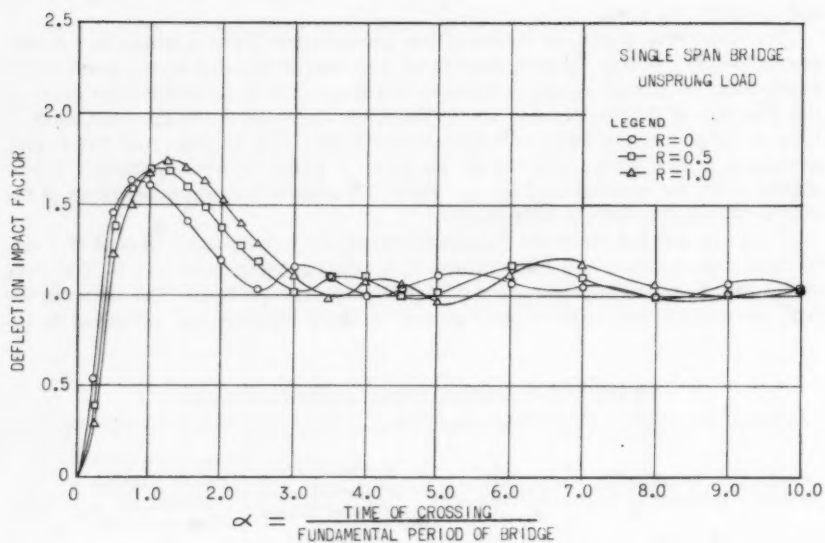


FIG. 14

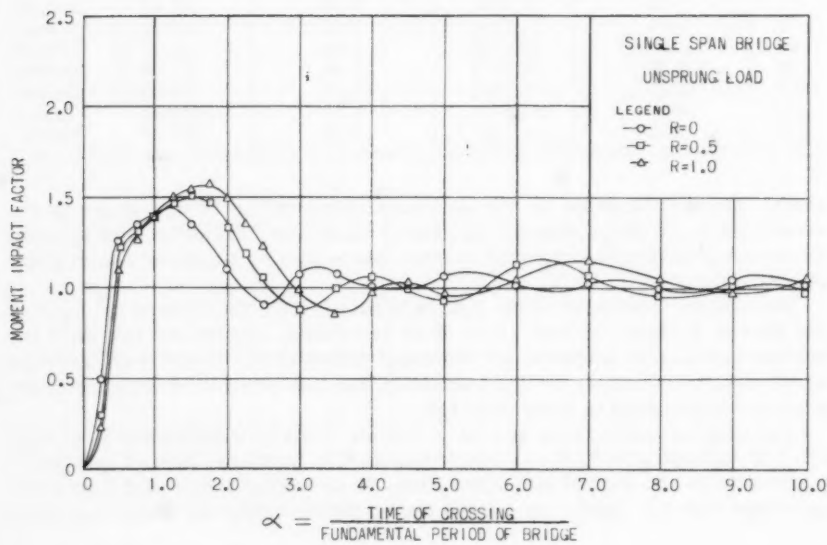


FIG. 15

zero. This corresponds to an infinite velocity, at which speed the bridge will not be affected by the load.

The curves presented to show the effect of  $R$  and  $\alpha$  are useful, but are inconvenient for predicting impact for given values of these parameters. It would be more advantageous to present data in a form such that they can be used to predict the impact that will be produced by a given set of conditions. Such presentations are shown in Figs. 16 and 17 which are plots of contours of equal impact as a function of  $R$  and  $\alpha$  for values of  $\alpha$  between zero and 5.0. A value for  $\alpha$  of 5.0 corresponds to a velocity of approximately 30 mph for typical girder bridges below 100 ft long.

The preceding assumption of a single axle load represents an oversimplification of the type of loading and a thorough study should include multiple axle loads. In this study the standard bridges were investigated for the effects of H20-44 and H20-S16-44 loadings [American Assn. of State Highway Officials

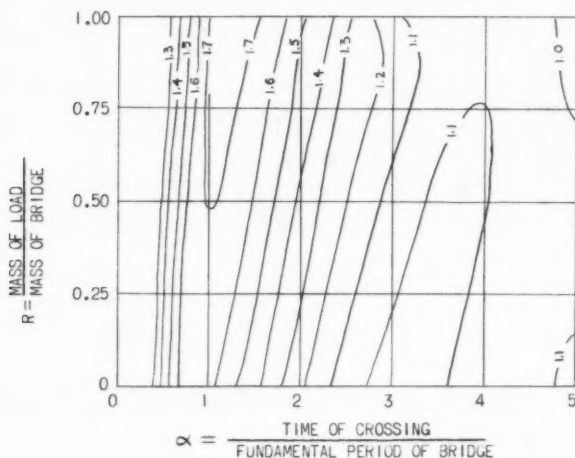


FIG. 16.—CONTOURS OF EQUAL DEFLECTION IMPACT FOR AN UNSPRUNG LOAD

[AASHO] Specifications]. The rear axle spacing of the H20-S16-44 load was varied between the allowable distances of 14 ft and 30 ft in order to obtain maximum impact. The data obtained from these loadings can be used to check values of impact predicted by the AASHO Specifications for single span bridges. These specifications state that the impact shall be computed from

$$I = \frac{50}{L + 125} \dots \dots \dots (30)$$

with a maximum of 30%.

Results of analyses of the effect of multiple axle loads on the standard bridges of the BPR are summarized in Figs. 18 and 19 in the form of plots of maximum impact as a function of span length. The impacts were found by first obtaining curves of impact as a function of  $\alpha$  similar to Figs. 14 and 15,

for each specific bridge and loading condition, and then choosing the maximum impact for velocities up to 80 mph. The maximum impact does not necessarily occur at the maximum velocity because of the effect of axle spacing. The velocity of 80 mph is chosen as a probable maximum velocity for design purposes. A comparison of maximum computed impacts to those specified by the present (1961) AASHO Specifications indicates that impacts higher than those predicted by the specifications can occur for short span bridges. For spans greater than 40 ft the present specifications are fairly accurate in predicting maximum impact for the case of an unsprung load.

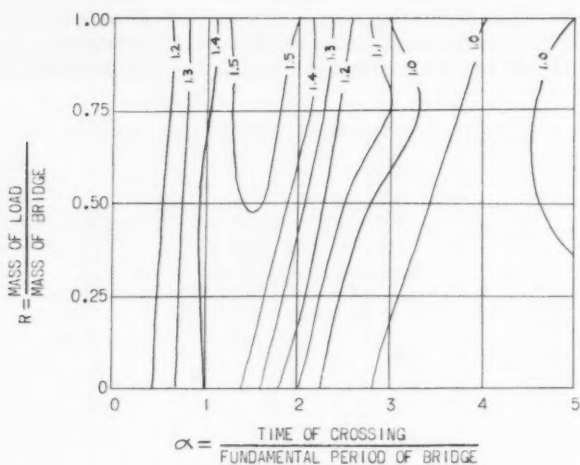


FIG. 17.—CONTOURS OF EQUAL MOMENT IMPACT FOR AN UNSPRUNG LOAD

**Sprung Loads.**—In evaluating the effect of vehicle springing it is useful to use another dimensionless parameter which embraces the springing characteristics of the vehicle. The parameter used in this analysis is

$$\rho = \frac{\text{Fundamental period of load}}{\text{Fundamental period of bridge}}$$

Considering that the natural frequencies of trucks vary from 60 to 180 cycles per min, realistic ranges of values for  $\rho$  are between approximately two and ten.

As mentioned previously, sprung loads can be grouped into two categories; loads without vertical amplitude when they enter the bridge and loads initially vibrating when they enter the bridge. Fig. 20 shows the general effect of  $\rho$  on impact for a load with no initial amplitude. The specific case treated is a 32,000-lb single axle load traveling at 80 mph on a typical 70-ft span. This corresponds to a value for  $\alpha$  of 1.75. The maximum impact occurs at a value for  $\rho$  of zero, or an unsprung load, and then decreases slightly until a value for  $\rho$  of approximately one is reached. Beyond this point the impact remains

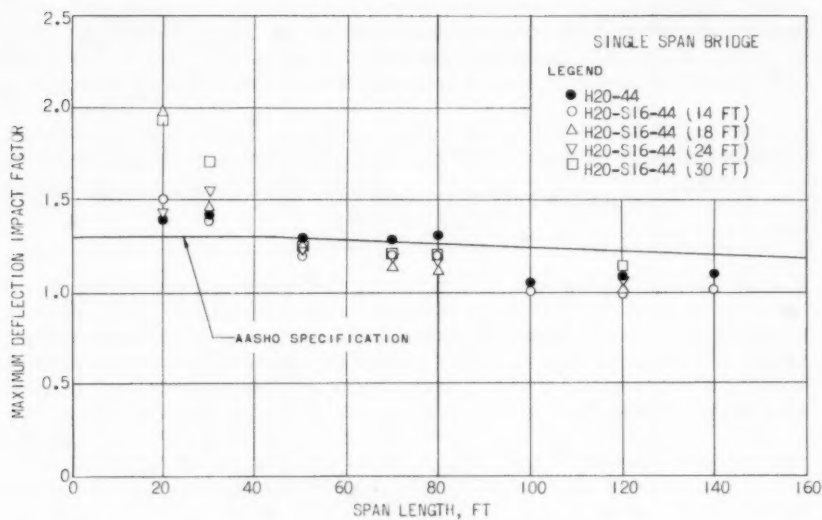


FIG. 18.—COMPARISON OF COMPUTED IMPACT WITH SPECIFICATIONS

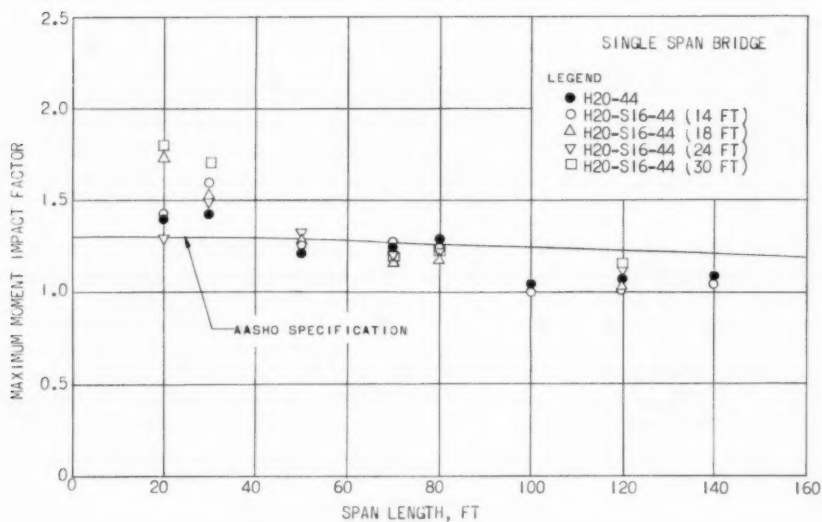


FIG. 19.—COMPARISON OF COMPUTED IMPACT WITH SPECIFICATIONS

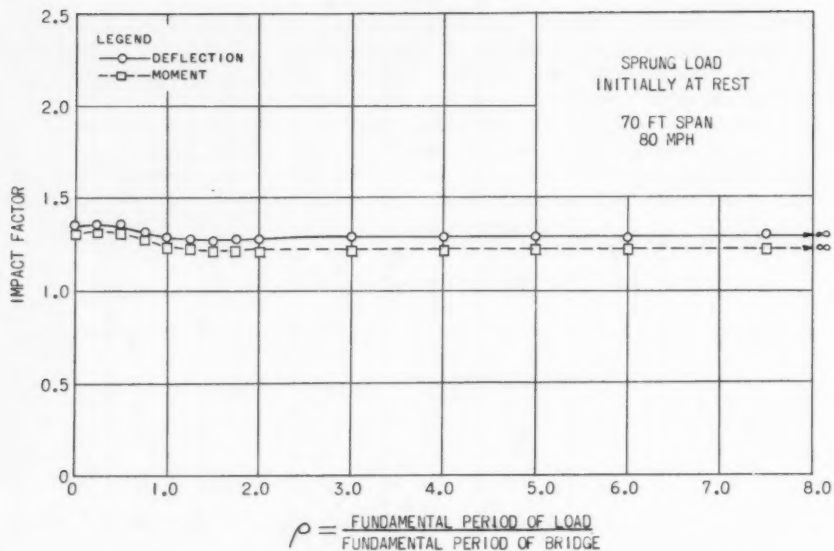


FIG. 20.—EFFECT OF VEHICLE SPRINGING, FOR SPRUNG LOAD INITIALLY AT REST

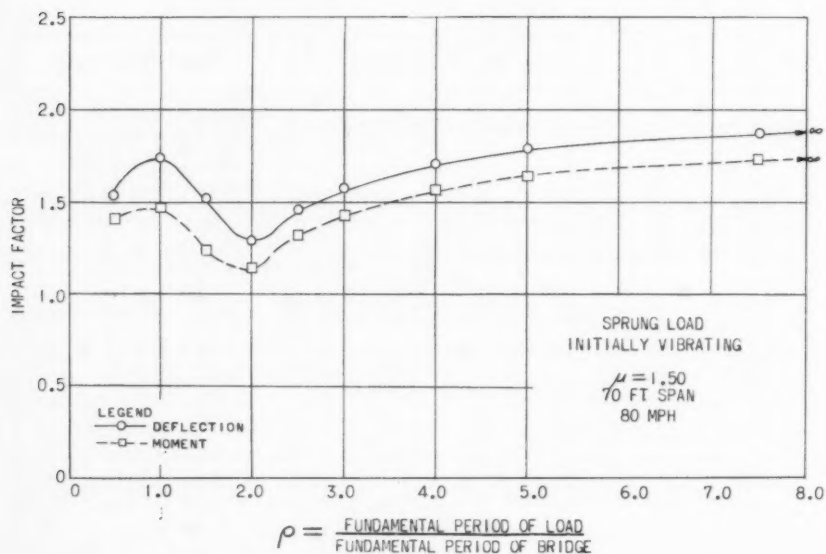


FIG. 21.—EFFECT OF VEHICLE SPRINGING, FOR SPRUNG LOAD INITIALLY VIBRATING

essentially constant up to an infinite value of  $\rho$  as shown to the right of the curve. The case for infinite  $\rho$  corresponds to a load on an infinitely flexible spring - or a pure force. Therefore, the effect of mounting a load on springs when it enters the bridge in its equilibrium position is to reduce the inertia of the load, thus reducing the impact. For all practical purposes, the load can be treated as a pure force.

A completely different situation occurs when the load is vibrating at some definite amplitude when it enters the bridge. In this case an important quantity is a parameter  $\mu$  which is defined as

$$\mu = \frac{(W + K \Delta_{\text{initial}})}{W} \dots\dots\dots (31)$$

Fig. 21 shows the general effect of  $\mu$  for a load initially vibrating when it enters the span. The specific case treated is again a 32,000 lb single axle load traveling at 80 mph on a typical 70 ft span. The value of  $\mu$  is 1.50, although the same general shape is obtained for any value of  $\mu$ . To eliminate one initial condition, it is assumed that the vehicle spring is in its maximum compressed position when the load enters the bridge (thus the vertical velocity of the load is zero).

The validity of the shape of the curve obtained can be demonstrated by considering the physical behavior of the load as it crosses the bridge. A value for  $\rho$  of 1.0 is a condition of resonance and, therefore, a point of maximum impact is expected. A value for  $\rho$  of 2.0 leads to interference, thus yielding a minimum impact factor. As the value of  $\rho$  is increased further the load vibrates fewer times as it crosses the bridge. Therefore, the effect becomes closer to that of a constant load ( $W + K \Delta_{\text{initial}}$ ). During the passage of the load the dynamic deflection and moment are caused by an equivalent load ( $W + K \Delta$ ), whereas the static values used in computing the impact factors are due only to the load  $W$ . The impact should therefore increase as  $\rho$  is increased. The limit point for an infinite value of  $\rho$  can be found by multiplying the impact for a pure force by the value of  $\mu$ . As shown previously a load on an infinitely flexible spring behaves as a pure force, and for infinite  $\rho$  the load on the bridge is a constant force ( $W + K \Delta_{\text{initial}}$ ) or  $\mu W$ . The limit points for both deflection and moment are shown to the right of the computed curve. The magnitude of the impact for the limiting value of  $\rho$  agrees with the shape of the computed curve.

From the magnitudes of impact obtained for a load initially vibrating it is obvious that springing of the vehicle is one of the most important considerations in determining the impact produced by moving loads. It is therefore important to establish expected values for  $\mu$ . The order of magnitude can be found by computing the amplitude of vibration produced by typical vehicles hitting a bump of realistic dimensions. To simplify the analysis the bump is assumed to have the shape of a half sine wave as shown in Fig. 22.

The differential equation of a sprung mass hitting the idealized bump is

$$M\ddot{y} + K y = K h \sin \frac{\pi V t}{L} \dots\dots\dots (32)$$

which can be solved to determine the response of the vehicle. For the case of a bump with a length equal to twice the height the maximum value of  $\mu$  obtained for typical vehicles is approximately 1.2 for a maximum height of 2.5 in. However, if a dip in the roadway is considered, for which the ratio of



length to depth may be as high as fifty, a value for  $\mu$  of 2.0 can be obtained. This is because a resonance condition can occur as the load traverses the dip at normal highway speeds in the case of a long dip, whereas the impulse produced by a short bump is fast compared to the natural period of the load.

The bumps and dips used in this analysis were idealized to a great degree but the important conclusion which can be reached is that large vehicle oscillations, and correspondingly high impacts, can occur if long shallow bumps or dips are encountered in the roadway as the load enters the bridge.

All of the preceding analyses for single span bridges neglect the effect of damping in the bridge. In the derivation of the equations of motion it is assumed that the damping in the bridge is viscous damping. Several investigators have shown, by means of field measurements, that this assumption is not entirely true but that it is sufficiently accurate for practical purposes.

To determine if damping has an important effect it is necessary to establish typical damping constants for girder bridges. These can be obtained from experimental data presented by Biggs.<sup>8</sup> Biggs showed that for free vibrations of typical girder bridges the tenth cycle has an amplitude of approximately 62%

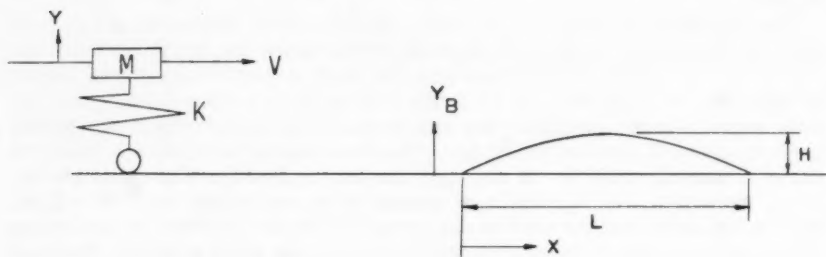


FIG. 22.—IDEALIZED BUMP

of the first cycle whereas the same quantity for stringer bridges is 25%. Using the value of 25% with the bridges shown in Table 1 the average computed viscous damping coefficient is 275 lb-sec per in.

This typical coefficient was used in computing impact factors for a series of loading conditions to check the effect of damping. A comparison of these impact values with those obtained for the same loading conditions without damping is shown in Fig. 23. The effect of damping is small and can be neglected. In fact, for design purposes it is safer to neglect damping, since it is not possible to rely on a definite damping coefficient for any specific bridge.

*Continuous Bridges.*—A study of three span continuous bridges using the assumed mathematical model of one concentrated mass per span is presented, although the study is not intended to be as extensive as that described for single span bridges. The standard three span continuous bridges analyzed are summarized in Table 2.

Figs. 24 to 26 show results obtained for a single axle load crossing a three span bridge, where the ratio between the center span and the equal end spans



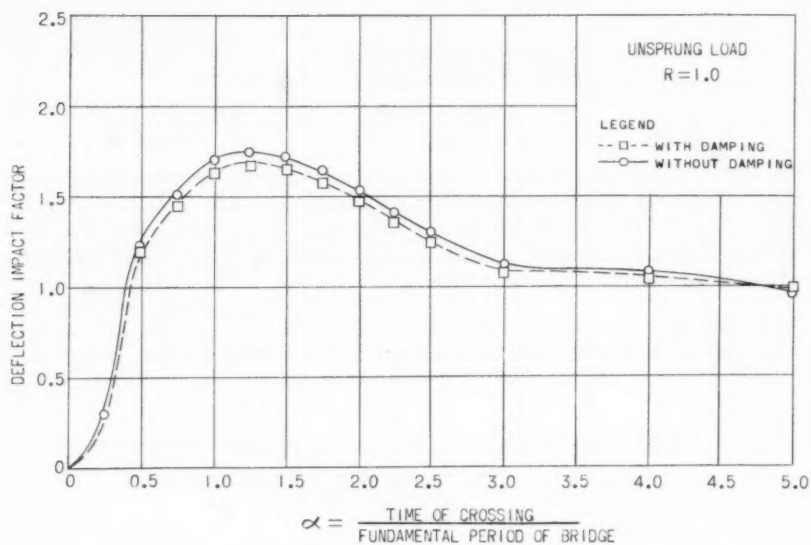


FIG. 23.—EFFECT OF VISCOUS DAMPING IN BRIDGE

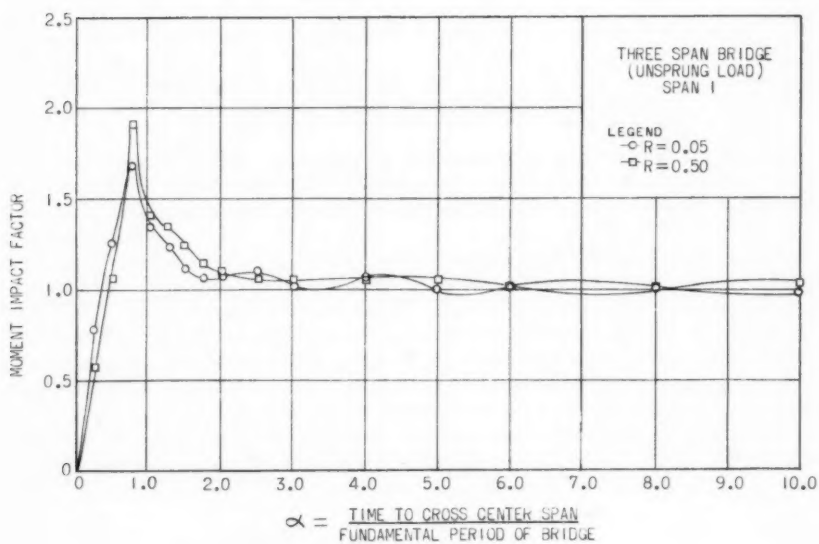


FIG. 24

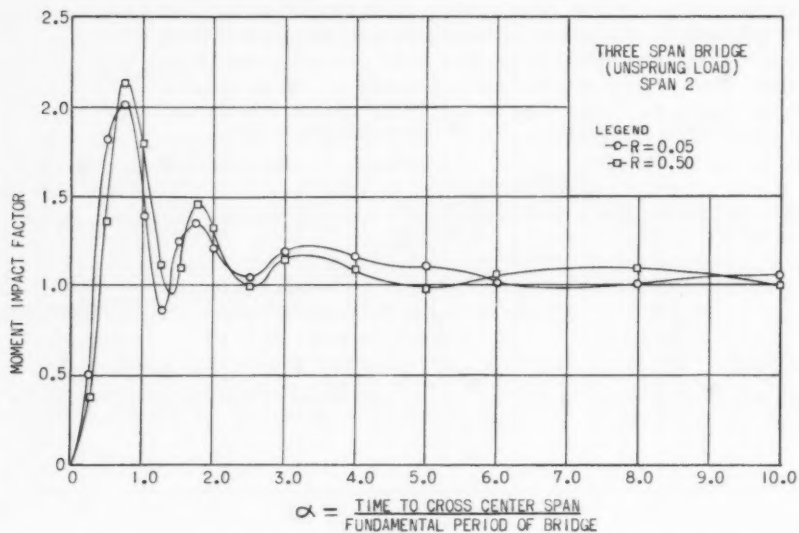


FIG. 25

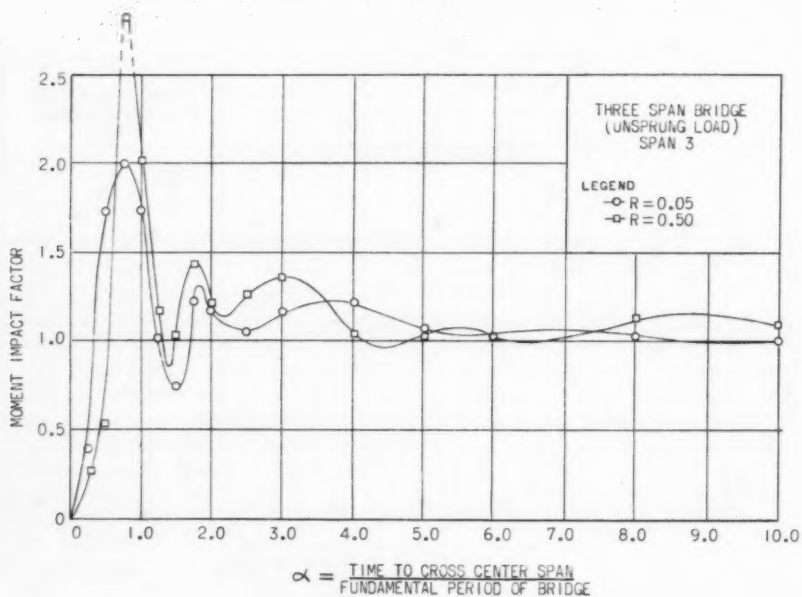


FIG. 26

is 0.8. The parameters  $R$  and  $\alpha$  are the same as those defined for single span bridges except that they refer to the center span only:

$$\alpha = \frac{\text{Time to cross center span}}{\text{Fundamental period of bridge}}$$

and

$$R = \frac{\text{Mass of load}}{\text{Mass of center span}}$$

From the shapes of the curves obtained it is seen that the general response characteristics of each individual span is not appreciably different from the response of a single span bridge. One main difference, however, is that the value of  $R$  has a much larger effect on maximum impact. For typical bridges, however, the velocity for a value of  $\alpha$  of approximately one, where this maximum impact occurs, is greater than 100 mph.

The complexities of continuous bridges, which may be of any number of spans of variable lengths, precludes the possibility of establishing generalizations in the form of contours of equal impact as shown in Figs. 16 and 17

TABLE 2.—STANDARD THREE SPAN CONTINUOUS BRIDGES

Span Lengths, in feet (1)	Weight, in pounds per foot (2)	EI, ( $10^{11}$ lb-in <sup>2</sup> ) (3)	Fundamental Frequency, in cycles per second (4)	Velocity to Cross Center Span in Natural Period, in miles per hour (5)	Type (6)
40- 50-40	3299	2,67642	2.99	101.70	I-Beam
48- 60-48	3363	3,92004	2.49	101.63	I-Beam
56- 70-56	3423	5,35320	2.12	100.95	I-Beam
64- 80-64	3560	6,66012	1.17	96.33	I-Beam
72- 90-72	3667	9,35388	1.63	99.80	I-Beam
80-100-80	3739	12,1253	1.49	101.36	I-Beam

for single span bridges. Considering the relatively high cost and size of such structures, it would be more advantageous and more in the interest of real economy to analyze each structure individually for its design load and design range of speed.

Two factors which were considered for single span bridges were neglected in the results shown for continuous bridges. These factors are damping in the bridge and springing of the vehicle. With regard to damping in the bridge, it was shown that for single span bridges the reduction in impact due to damping is small. For continuous bridges the reduction would be greater than in single span bridges because the load is on the bridge for a longer period of time. However, because it would be difficult to set a definite damping constant that can be relied on, the effect of damping was neglected. Springing of the vehicle was not included because there is no reason to believe that the results would be substantially different from those obtained for a single span bridge.

## CONCLUSIONS

Several conclusions have been reached in this investigation of the effects of the several variables on bridge impact. For unsprung loads the most im-

portant variable is the velocity of the load. The main effect of a change in the mass of the load is to change the velocity at which the maximum impact occurs. The change in the maximum impact produced due to changing the mass of the load is not large for single span bridges, but for continuous bridges the change can be appreciable.

From a comparison of maximum impacts obtained in this study with the AASHO Specifications it is observed that impacts higher than those predicted by the specifications can be obtained for short spans. For longer spans the maximum impacts obtained are about the same as those predicted by the specifications.

One of the most important considerations is the springing of the vehicle and the condition of the bridge approach. Extremely large impacts can be produced in the bridge due to the initial vibration of the load if an area of settlement occurs in the roadway in advance of the bridge. These impacts are much greater than those due to the several bridge and load variables normally considered in such investigations.

#### ACKNOWLEDGMENTS

The information presented herein was obtained by John F. Fleming, A.M. ASCE, as part of a thesis for the degree Doctor of Philosophy in Civil Engineering at Carnegie Institute of Technology. The experimental apparatus used in conjunction with this investigation was built by H. Wenzel, A.M. ASCE, a graduate student in the Department of Civil Engineering at Carnegie Institute of Technology.

---

#### APPENDIX.—NOTATION

---

The following symbols, adopted for use in the paper and for the guidance of discussers, conform essentially with "American Standard Letter Symbols for Structural Analysis" (ASA Z10.8-1949), prepared by a committee of the American Standards Association with Society representation, and approved by the Association in 1949:

- $a$  = vertical acceleration;
- $b_{ij}$  = stiffness influence coefficient;
- $C_b$  = coefficient of viscous damping of bridge;
- $C_v$  = coefficient of viscous damping of vehicle;
- $F(t)$  = applied load that varies with time;
- $I$  = impact factor;
- $K$  = spring constant;
- $L$  = span length;

- $M$  = equivalent concentrated mass;
- $M_L$  = mass of moving load;
- $M_s$  = sprung mass of vehicle;
- $M_u$  = unsprung mass of vehicle;
- $m$  = mass of bridge per unit length;
- $R$  = ratio of the mass of the load to the mass of the bridge;
- $t$  = time;
- $V$  = velocity of the load;
- $v$  = vertical velocity;
- $W$  = total weight of vehicle;
- $y$  = displacement;
- $\ddot{y}_x$  = vertical acceleration of bridge at a distance  $x$  from the end;
- $\alpha$  = ratio of time of crossing to the fundamental period of the bridge;
- $\Delta$  = distortion of vehicle spring;
- $\mu$  = ratio of total spring force to the weight of the load;
- $\rho$  = ratio of the fundamental period of the sprung load to the fundamental period of the bridge; and
- $\phi_i$  = a position function which determines the fractional part of the load to be considered acting on mass  $i$ .

1. The first part of the report is a general introduction to the subject of the study. It discusses the importance of the study and the objectives of the research.

2. The second part of the report is a detailed description of the methodology used in the study. It includes information about the sample size, the data collection methods, and the statistical analysis techniques.

---

Journal of the  
STRUCTURAL DIVISION  
Proceedings of the American Society of Civil Engineers

---

STRING POLYGON ANALYSIS OF FRAMES WITH STRAIGHT MEMBERS

By Jan J. Tuma,<sup>1</sup> F. ASCE and John T. Oden,<sup>2</sup> A. M. ASCE

---

SYNOPSIS

A general method for analyzing continuous, complex and multi-story frames with straight members is presented. The frame members may be of constant or variable section and their deformation may be caused by transverse loads, applied couples, change in volume or displacement of supports. The string polygon method is the extension of the conjugate frame method to multipanel structures. End-bending moments of each member of the panel are selected as unknowns. The moment matrix is written in terms of two sets of linear equations: (a) elasto-static equations, and (b) static equations; and solved simultaneously. The numerical procedure is illustrated by two examples.

---

INTRODUCTION

The representation of the elastic curve of a straight bar as a differential string polygon was introduced by O. Mohr<sup>3</sup> in connection with his concept of elastic weights and conjugate beams. H. F. B. Müller-Breslau developed the idea of joint load (knoten last) for straight members<sup>4</sup> and bent members<sup>5</sup> and

---

Note.—Discussion open until March 1, 1962. To extend the closing date one month, a written request must be filed with the Executive Secretary, ASCE. This paper is part of the copyrighted Journal of the Structural Division, Proceedings of the American Society of Civil Engineers, Vol. 87, No. ST 7, October, 1961.

<sup>1</sup> Prof. of Civ. Engrg., Oklahoma State Univ., Stillwater, Okla.

<sup>2</sup> Instr. in Civ. Engrg., Oklahoma State Univ., Stillwater, Okla.

<sup>3</sup> "Behandlung der Elastischen Linie Als Seillinie," by O. Mohr, *Zeitschr D. Architekt. u. Ing.*, Hannover, 1868.

<sup>4</sup> "Beitrag Zur Theorie Des Fachwerkes," by H. F. B. Müller-Breslau, *Zeitschr D. Architekt. u. Ing.*, Hannover, 1885, p. 31.

<sup>5</sup> "Die Graphische Statik Der Baukonstruktionen," by H. F. B. Müller-Breslau, A. Kroner-Verlag, Vol. 2, Part 2, 2nd Ed., Leipzig, 1925, p. 337.

applied these joint elastic weights to the computation of elastic curves of many important structures. The formulation of joint elastic weights may be found in works of J. Wanke,<sup>6</sup> F. Chmelka,<sup>7</sup> C. B. Biezeno,<sup>8</sup> W. Kaufman,<sup>9</sup> and others. The use of elemental and area elastic weights in connection with a two-dimensional conjugate structure was introduced by Hardy Cross<sup>10</sup> as "the column analogy method" and by J. S. Kinney<sup>11</sup> and S. L. Lee,<sup>12</sup> M. ASCE, as "the conjugate frame method." The application of the same elastic weights in connection with three-dimensional structures was reported by Frank Baron, F. ASCE,<sup>13,14</sup> and Jaan Kiusalaas.<sup>15</sup>

The extension of the conjugate frame method to the analysis of multipanel frames by means of joint elastic weights is presented herein. In the first part, the derivation of the analytical expression for the change of slope of a polygonal panel at a given joint is shown. The physical meaning of this change is explained and the joint elastic weight is introduced as a force-vector normal to the plane of the polygon in the second part of the paper. The formulation of the static equations, the deformation equations and the preparation of bending moment matrix is examined in the third part. The formation of multipanel conjugate structures, the formulation of the corresponding moment matrix, the numerical applications and conclusions follow in the last parts of the paper.

The study is restricted to coplanar systems with straight members. The customary assumptions of the rigid frame analysis are introduced and the sign convention of the three moment equation is adopted. The end-bending moments and end slopes are positive if they cause tension on the dotted side of the member. The elastic weights are positive if acting in the positive direction of the Z-axis.

*Notation.*—The letter symbols adopted for use in this paper are defined where they first appear, in the illustrations or in the text, and are arranged alphabetically, for convenience of reference, in the Appendix.

## ANGULAR FUNCTIONS

A bent bar  $ijk$  of variable cross section acted on by a general system of loads is considered (Fig. 1). The geometry of each segment is given by its length ( $d_j, d_k$ ), slope ( $\omega_j, \omega_k$ ) and variation of the cross section. The bending moments at  $i, j, k$  are assumed to be known and denoted by  $M_i, M_j, M_k$ , re-

6 "Zur Berechnung Der Formänderungen Vollwandiger Tragwerke," by J. Wanke, *Der Stahlbau*, 1939, No. 23, 24.

7 "Näherung Formeln," by F. Chmelka, *Der Stahlbau*, 1940, No. 23, 24.

8 "Elastic Problems of Single Machine Elements," by C. B. Biezeno and R. Grammel, *Engineering Dynamics*, Vol. 2, Blackie and Son, Ltd., Glasgow, 1956, p. 2.

9 "Statik Der Tragwerke," by W. Kaufmann, J. Springer-Verlag, 4th Ed., Berlin, 1957, p. 144.

10 "The Column Analogy," by Hardy Cross, *Engrg. Experiment Sta. Bulletin*, Univ. of Illinois, Urbana, No. 215, 1930.

11 "Analysis of Multi-Span-Frames," by J. S. Kinney, in "Steel Rigid Frames," by M. P. Korn, J. W. Edwards, Inc., Ann Arbor, Mich., 1953, p. 50.

12 "Conjugate Frame Method and Its Application in the Elastic and Plastic Theories of Structures," by S. L. Lee, *Journal, Franklin Inst.*, Vol. 266, 1958, p. 207.

13 "Laterally Loaded Plane Structures and Structures Curved in Space," by F. Baron and J. P. Michalos, *Transactions, ASCE*, Vol. 117, 1952, p. 279.

14 "A Circuit Analysis of Laterally Loaded Continuous Frames," by F. Baron, *Proceedings, ASCE*, Vol. 83, No. ST 1, January, 1957.

15 "Analysis of Rigid Space Frames by Conjugate Frame Method," by Jaan Kiusalaas, thesis presented to Northwestern Univ., at Evanston, Ill., in 1960, as a partial fulfillment of the requirements for the degree of Master of Science.



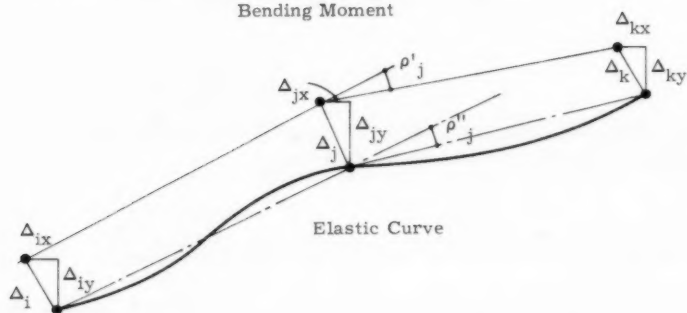
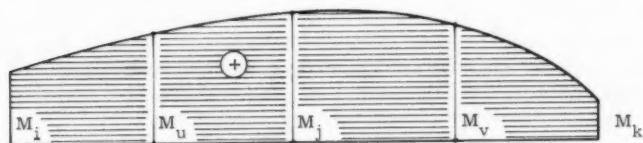
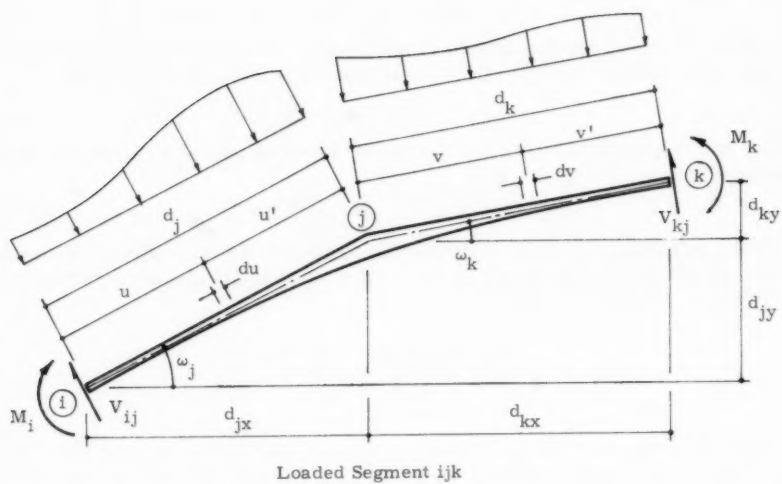


FIG. 1.—DEFORMATION OF SEGMENT IJK

spectively. The bending moment diagram and the elastic curve are shown in Fig. 1. The location of a cross section in the segment  $ij$  ( $jk$ ) is given by the ordinates  $u, u'$  ( $v, v'$ ), measured from the respective ends. The initial change in slope of bent line  $ijk$  (before deformation) at  $j$  is

$$\rho_j' = \omega_j - \omega_k \dots\dots\dots (1)$$

in which  $\omega_j$  and  $\omega_k$  are the angles of inclination of members  $ij$  and  $jk$  respectively. The change in slope of the same line after deformation at  $j$  is

$$\rho_j'' = \omega_j - \omega_k + \phi_j \dots\dots\dots (2)$$

Thus, the change of the change in slope of the same line at  $j$  caused by elastic deformation is

$$\rho_j''' - \rho_j' = \phi_j \dots\dots\dots (3)$$

If the influence of normal and shearing forces on the formation of the elastic curve is assumed to be small and is neglected, the change of change in slope in terms of bending moments is

$$\phi_j = \int_i^j \frac{M_u (M_u)}{E I_u} du + \int_j^k \frac{M_v (M_v)}{E I_v} dv \dots\dots\dots (4)$$

in which  $M_u, M_v$  are the real bending moments at  $u, v$ , respectively;  $(M_u), (M_v)$  denote the virtual bending moments at  $u, v$ , respectively;  $du, dv$  refer to the elemental lengths of segments  $ij, jk$ ;  $I_u, I_v$  are the moments of inertia of the cross sections at  $u, v$ ; and  $E$  is the modulus of elasticity. The real loading and the corresponding bending moment diagram are shown in Fig. 2. The virtual loading and the corresponding bending moment diagram are shown in the same figure.

From these diagrams, the real bending moments are

$$M_u = M_i \frac{u'}{d_j} + M_j \frac{u}{d_j} + BM_u \dots\dots\dots (5a)$$

and

$$M_v = M_j \frac{v'}{d_k} + M_k \frac{v}{d_k} + BM_v \dots\dots\dots (5b)$$

in which  $BM_u, BM_v$  are the bending moments due to loads.

Similarly, the virtual bending moments are

$$(M_u) = \frac{u}{d_j} \qquad (M_v) = \frac{v'}{d_k} \dots\dots\dots (6)$$

The deformation Eq. 4 in terms of Eqs. 5 and 6 becomes

$$\phi_j = \left\{ \begin{aligned} & M_i \int_i^j \frac{uu' du}{d_j^2 E I_u} + M_j \int_i^j \frac{u^2 du}{d_j^2 E I_u} + \int_i^j \frac{BM_u u du}{d_j E I_u} \\ & M_j \int_j^k \frac{v'^2 dv}{d_k^2 E I_v} + M_k \int_j^k \frac{v v' dv}{d_k^2 E I_v} + \int_j^k \frac{BM_v v' dv}{d_k E I_v} \end{aligned} \right\} \dots\dots (7)$$

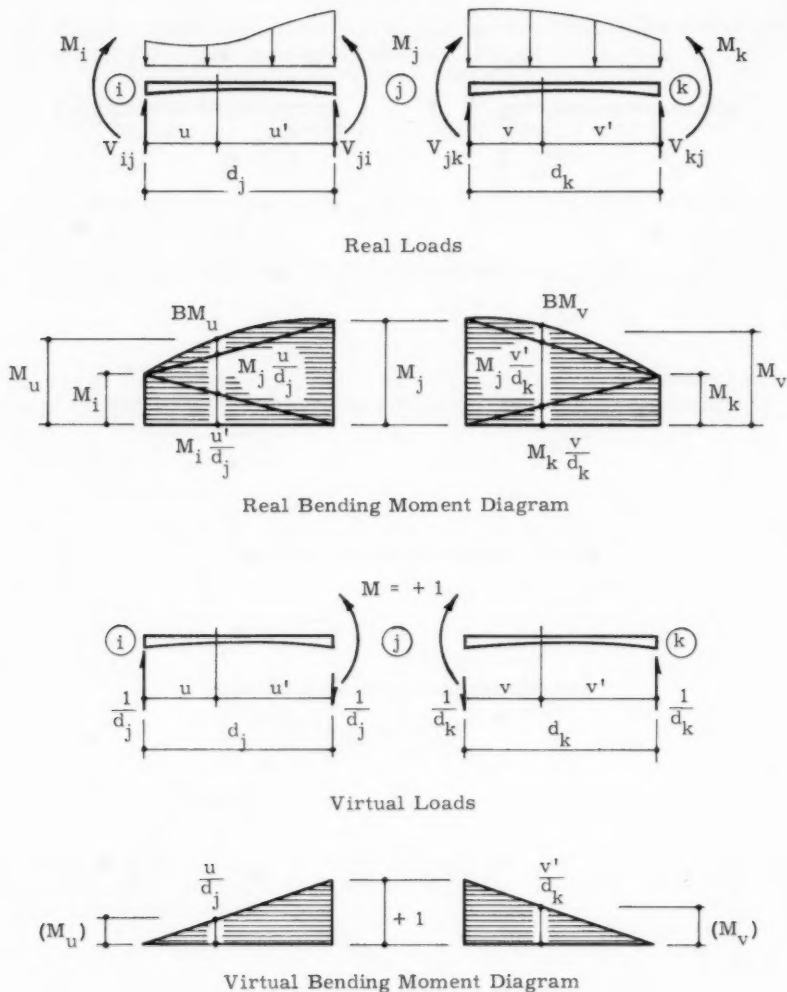


FIG. 2.—REAL AND VIRTUAL BENDING MOMENTS

The integral expressions in Eq. 7 may be interpreted as angular functions of the respective simple beams as will be shown.

(a) Angular flexibility  $F_{ji}$  ( $F_{jk}$ ) is the end of  $j$  of the simple beam  $ij$  ( $jk$ ) due to unit moment applied at  $j$  (Fig. 3)

$$F_{ji} = \int_i^j \frac{u^2 du}{d_j^2 E I_u} \quad \left| \quad F_{jk} = \int_j^k \frac{v'^2 dv}{d_k^2 E I_v} \dots\dots\dots (8)$$

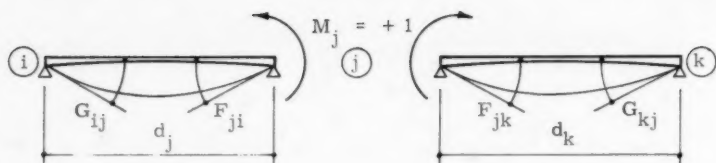


FIG. 3.—ANGULAR FLEXIBILITIES AND CARRY-OVER VALUES



FIG. 4.—ANGULAR LOAD FUNCTIONS

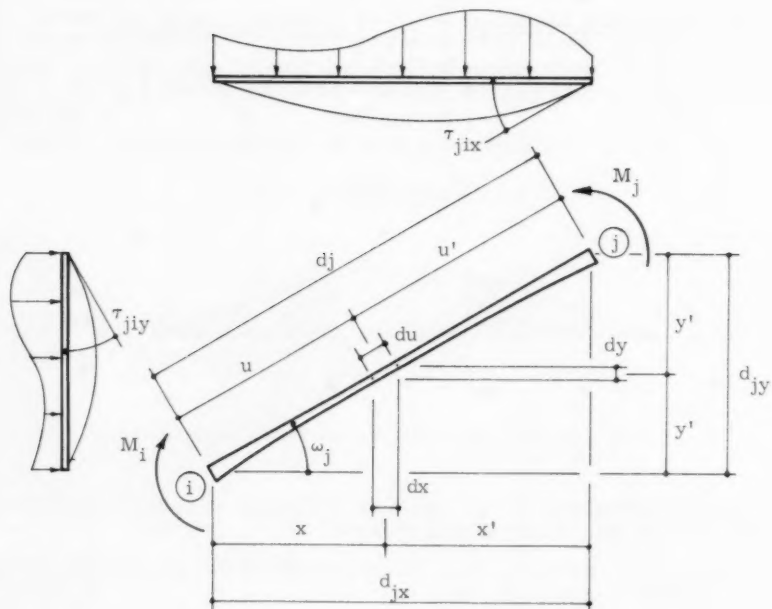


FIG. 5.—ANGULAR LOAD FUNCTION FOR HORIZONTAL AND VERTICAL LOADING

(b) Angular carry-over value  $G_{ij}$  ( $G_{kj}$ ) is the end slope of the simple beam  $ij$  ( $jk$ ) at  $i$  ( $k$ ) due to unit moment applied at  $j$  (Fig. 3)

$$G_{ij} = \int_i^j \frac{uu'}{d_j^2} \frac{du}{E I_u} \quad \left| \quad G_{kj} = \int_j^k \frac{vv'}{d_k^2} \frac{dv}{E I_v} \dots\dots\dots (9)$$

(c) Angular load function  $\tau_{ji}$  ( $\tau_{jk}$ ) is the end slope of the simple beams  $ij$  ( $jk$ ) at  $j$  due to loads (Fig. 4)

$$\tau_{ji} = \int_i^j \frac{BM_u u}{d_u} \frac{du}{E I_u} \quad \left| \quad \tau_{jk} = \int_j^k \frac{BM_v v'}{d_k} \frac{dv}{E I_v} \dots\dots\dots (10)$$

If instead of normal loads (Fig. 1), a system of vertical or horizontal loads is considered, the angular load functions of projected simple beams may be used (Fig. 5)

For vertical loading

$$\tau_{ji} = \int_i^j \frac{BM_u u}{d_j} \frac{du}{E I_u} = \frac{1}{\cos \omega_j} \underbrace{\int_i^j \frac{BM_u x}{d_{jx}} \frac{dx}{E I_u}}_{\tau_{jix}} \dots\dots\dots (11a)$$

and

$$\tau_{jk} = \int_j^k \frac{BM_v v'}{d_k} \frac{dv}{E I_v} = \frac{1}{\cos \omega_k} \underbrace{\int_j^k \frac{BM_v x'}{d_{kx}} \frac{dx}{E I_v}}_{\tau_{jkk}} \dots\dots\dots (11b)$$

All symbols of Eqs. 11 are defined by Fig. 5 and the last integral in each equation is defined as the end slope of the horizontal projection of the simple beam.

For horizontal loading

$$\tau_{ji} = \int_i^j \frac{BM_u u}{d_j} \frac{du}{E I_u} = \frac{1}{\sin \omega_j} \underbrace{\int_i^j \frac{BM_u y}{d_{jy}} \frac{dy}{E I_u}}_{\tau_{jiy}} \dots\dots\dots (12a)$$

and

$$\tau_{jk} = \int_j^k \frac{BM_v v'}{d_k} \frac{dv}{E I_v} = \frac{1}{\sin \omega_k} \underbrace{\int_j^k \frac{BM_v y'}{d_{jy}} \frac{dy}{E I_v}}_{\tau_{jky}} \dots\dots\dots (12b)$$

All symbols of Eqs. 12 are defined by Fig. 5 and the last integral in each equation is defined as the end slope of the vertical projection of the simple beam.

Substituting Eqs. 8 through 10 and Eq. 7 gives

$$\phi_j = M_i G_{ij} + M_j \Sigma F_j + M_k G_{kj} + \Sigma \tau_j \dots \dots \dots (13)$$

in which

$$\Sigma F_j = F_{ji} + F_{jk} \dots \dots \dots (14a)$$

and

$$\Sigma \tau_j = \tau_{ji} + \tau_{jk} \dots \dots \dots (14b)$$

Eq. 13 represents the change of the change in slope of the bent line  $ijk$  at  $j$  and may be (as any angle change due to elastic deformation) represented by an elastic weight. The similarity of the right side in Eq. 13 with the well known three moment equation is apparent<sup>16,17</sup> and it may be said that the three moment equation is a special case of the Eq. 13 with  $\phi_j$  equal to zero.

If the cross section of each member is different but constant between two joints, the following simplifications are possible (Eqs. 8 and 9)

$$\begin{array}{l|l} F_{ji} = \frac{L_j}{3 E I_j} & F_{jk} = \frac{L_k}{3 E I_k} \\ G_{ij} = \frac{L_j}{6 E I_j} & G_{kj} = \frac{L_k}{6 E I_j} \end{array} \dots \dots \dots (15)$$

The load functions  $\tau_{ji}$  and  $\tau_{jk}$  for the most common load conditions reduce to the expressions shown in Table 1.

#### SINGLE PANEL STRING POLYGON

*Elemental Elastic Weights.*—The change in slope of an element  $ds$  of a closed panel frame (Fig. 6) due to bending moment  $M_s$  may be treated as a force-vector and denoted as an elemental elastic weight

$$\bar{P}_s = \frac{M_s ds}{E I_s} \dots \dots \dots (16)$$

Then the deformation equations for this panel become

$$\int \frac{M_s ds}{E I_s} = \Sigma \bar{P}_s = 0 \dots \dots \dots (17a)$$

$$\int \frac{M_s x ds}{E I_s} = \Sigma \bar{P}_s x = 0 \dots \dots \dots (17b)$$

and

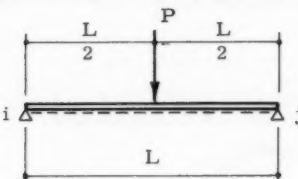
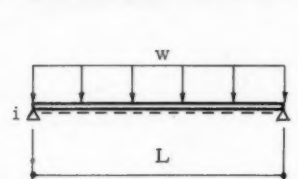
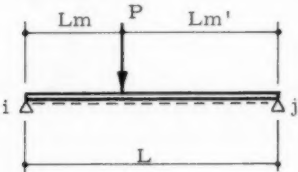
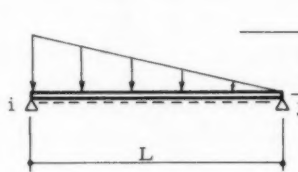
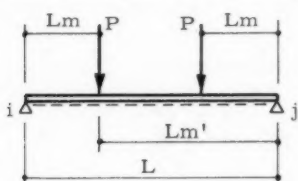
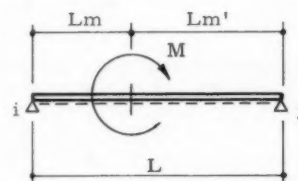
$$\int \frac{M_s y ds}{E I_s} = \Sigma \bar{P}_s y = 0 \dots \dots \dots (17c)$$

<sup>16</sup> "Calcul d'une Poutre Élastique Reposant Librement sur Desappuis Inégalement Espace's," by B. P. E. Clapeyron, Comptes Rendus, Paris, 1857.

<sup>17</sup> "Über Einige Aufgaben der Statik, Welche Auf Gleichungen der Clapeyronschen Art Führen," by H. Müller-Breslau, Zeitschrift für Bauwesen, Berlin, 1891.

Thus, the elemental changes in slope are represented by a set of elastic weights in a state of static equilibrium. The line of action of each elastic weight is normal to the plane of the frame and the sense of the elastic weight

TABLE 1.—LOAD FUNCTIONS

 $\tau_{ij} = \frac{PL^2}{16EI}$ $\tau_{ji} = \frac{PL^2}{16EI}$	 $\tau_{ij} = \frac{wL^3}{24EI}$ $\tau_{ji} = \frac{wL^3}{24EI}$
 $\tau_{ij} = \frac{PL^2}{6EI} \frac{m m' (1 + m')}{m}$ $\tau_{ji} = \frac{PL^2}{6EI} \frac{m m' (1 + m)}{m'}$	 $\tau_{ij} = \frac{pL^3}{45EI}$ $\tau_{ji} = \frac{7pL^3}{360EI}$
 $\tau_{ij} = \frac{PL^2}{2EI} \frac{m m'}{L - Lm - Lm'}$ $\tau_{ji} = \frac{PL^2}{2EI} \frac{m m'}{L - Lm - Lm'}$	 $\tau_{ij} = \frac{ML(1 - 3m'^2)}{6EI}$ $\tau_{ji} = \frac{ML(1 - 3m^2)}{6EI}$

is governed by the sign of the bending moment  $M_s$ . The sign convention for bending moments is stated in the introduction to this paper. The line connecting the points of application to all elastic weights is known as the conjugate

structure (Fig. 7). The application of the elemental elastic weights requires considerable labor. Bending moments and moments of inertia must be computed at the centroid of each strip and the elasto-static equations used are in terms of a large number of elastic weights.

*Segmental Elastic Weights.*—It is, however, always possible to remove individual members of the frames, consider them as separate conjugate beams, compute their reactions and apply these reactions as new loads on the initial

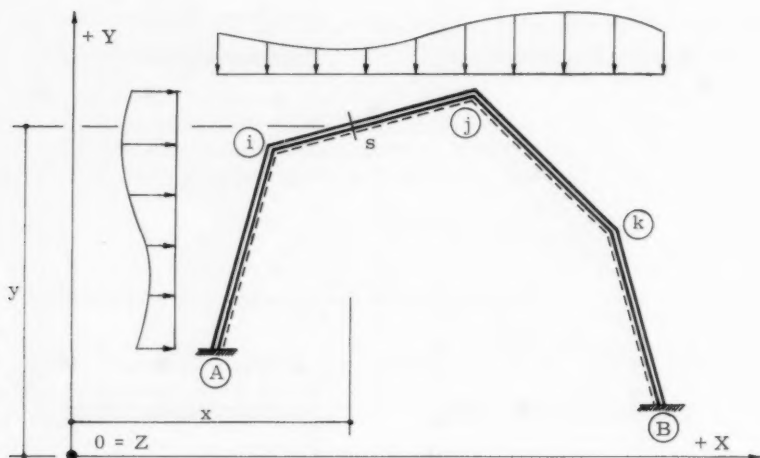


FIG. 6.—REAL STRUCTURE—REAL LOADS

conjugate structure (Figs. 8 and 9). The total elastic weight of segments  $ij$  and  $jk$  are

$$\bar{W}_j = \sum_i^j \bar{P}_s \quad \left| \quad \bar{W}_k = \sum_j^k \bar{P}_s \dots\dots\dots (18)\right.$$

The respective reactions of the separate beams are

$$\begin{array}{l} \bar{P}_{ij} = \sum_i^j \bar{P}_s \frac{u'}{d_j} \quad \left| \quad \bar{P}_{jk} = \sum_j^k \bar{P}_s \frac{v'}{d_k} \right. \\ \bar{P}_{ji} = \sum_i^j \bar{P}_s \frac{u}{d_j} \quad \left| \quad \bar{P}_{kj} = \sum_j^k \bar{P}_s \frac{v}{d_k} \right. \end{array} \dots\dots\dots (19)$$

The functions  $\bar{W}_j$  and  $\bar{W}_k$  are the segmental elastic weights defined as the changes in slope of the elastic curve between the respective ends of each segment.

*Joint Elastic Weights.*—The segmental reactions develop at the joints of the conjugate structure new elastic loads given by the general formula

$$\bar{P}_j = \bar{P}_{ji} + \bar{P}_{jk} \dots\dots\dots (20)$$



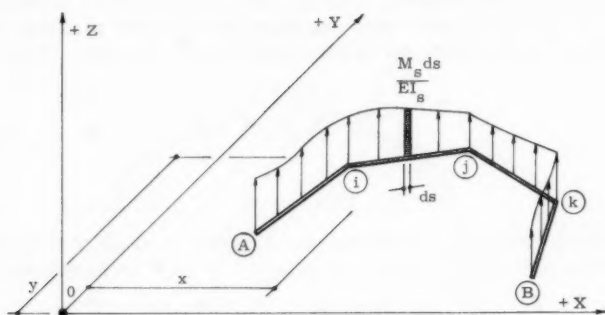


FIG. 7.—CONJUGATE STRUCTURE—ELEMENTAL ELASTIC WEIGHTS

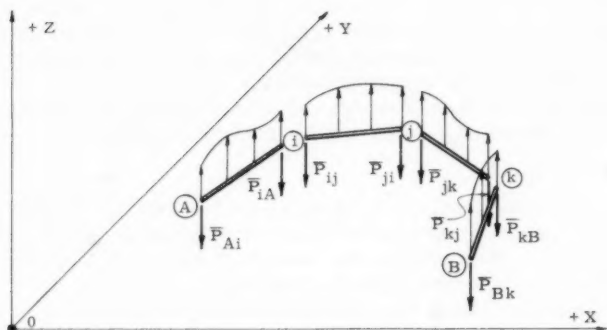


FIG. 8.—CONJUGATE BEAMS—ELEMENTAL ELASTIC WEIGHTS

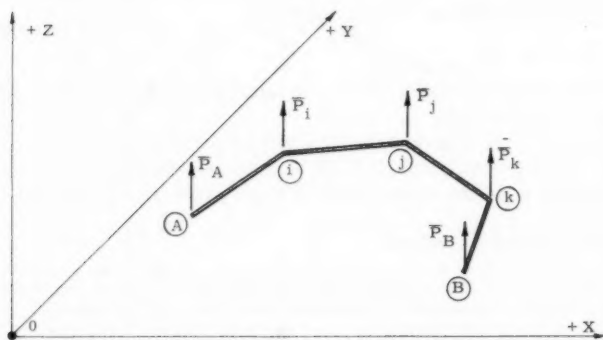


FIG. 9.—CONJUGATE FRAME—JOINT ELASTIC WEIGHTS

and denoted as the joint elastic weights. These joint elastic weights represent a new set of force-vectors again necessarily in a state of static equilibrium and equivalent to the initial set of elemental elastic weights. Thus

$$\sum \bar{P}_j = 0 \dots\dots\dots (21)$$

$$\sum \bar{P}_j x = 0 \dots\dots\dots (22)$$

and

$$\sum \bar{P}_j y = 0 \dots\dots\dots (23)$$

The joint elastic weight  $\bar{P}_j$  is the change of change in slope of the polygonal line  $ijk$  at  $j$ . Thus, the identity of Eq. 13 with Eq. 20 becomes apparent.

$$\bar{P}_j = \phi_j = M_i G_{ij} + M_j \sum F_j + M_k G_{kj} + \sum \tau_j \dots\dots\dots (24)$$

The joint elastic weight takes the form of the three moment equation and is a function of the angular parameters of segments  $ij$  and  $jk$ , and of the bending moments at the joints.

These elastic weights may be now used for two important purposes: (1) Computation of bending moments at joints, and (2) computation of joint displacements. Because all quantities are related to the joints of the polygon and the angular changes are defined as changes in slope of the polygon strings, the approach is called the string polygon method.

*Computation of Bending Moments.*—If a fixed end frame loaded as shown in Fig. 10 is considered, two types of solutions are possible.

Solution I (Fig. 11).

1. The cross-sectional elements  $N$ ,  $V$  and  $M$  (normal force, shear and bending moment) at a given fixed end or joint are selected as unknowns.
2. The bending moments at the remaining points of the polygon are expressed by statics in terms of these redundants.
3. Joint elastic weights are written by means of Eq. 24.
4. Elasto-static Eqs. 21, 22 and 23 are stated and solved simultaneously for  $N$ ,  $V$  and  $M$ .

The application of this solution in connection with the idea of the elastic center was recorded by Oden.<sup>18</sup> Solution of two hinged polygonal frames was presented by H. C. Boecker, A. M. ASCE.<sup>19</sup>

Solution II (Fig. 12).

1. Bending moments at the fixed ends and joints are selected as unknowns ( $m$  = number of unknowns).
2. Joint elastic weights are written by means of Eq. 24.
3. Three elasto-static Eqs. 21, 22, and 23 are stated.
4. Remaining conditions are stated from statics ( $m-3$  = number of required static equations).
5. Moment matrix is solved.

<sup>18</sup> "Analysis of Fixed End Frames with Bent Members by the String Polygon Method," by J. T. Oden, thesis, presented to Oklahoma State Univ., at Stillwater, in 1960, as partial fulfillment of the requirements for the degree of Master of Science.

<sup>19</sup> "Analysis of Pinned-End Frames with Bent Members by the String Polygon Method," by H. C. Boecker, thesis, presented to Oklahoma State Univ., at Stillwater, in 1960, as partial fulfillment of the requirements for the degree of Master of Science.

The application of the second procedure leads to a larger number of unknowns but it offers a more direct solution.

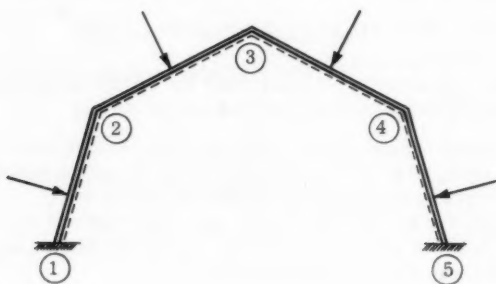


FIG. 10.—POLYGONAL FRAME

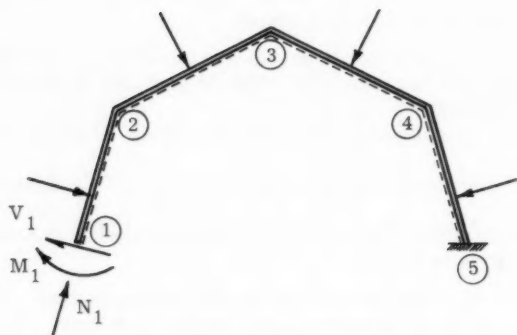


FIG. 11.—SOLUTION I

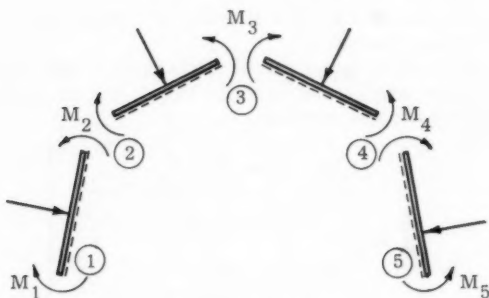


FIG. 12.—SOLUTION II

*Computation of Joint Displacements.*—Once the bending moments are known, the joint elastic weights are also known as numerical quantities and the displacement of a given joint along a given line is equal to the bending moment of the conjugate structure at that joint about that line.

It must be noted that all quantities are related to the joints. Displacements of intermediate points are not directly available.

### MULTIPANEL STRING POLYGON

The principles previously outlined may be easily extended to multipanel structures. The extension is based on two propositions:

(I) For an  $n$ -panel frame with  $m$  unknown end bending moments there exist  $3n$  elasto-static equations (three corresponding to each panel) and  $\mu$  static equations (each corresponding to one degree of freedom).

(II) Static equations are of two types: (a) Joint moment equations corresponding to the number of joints free to rotate, and (b) Shear equations corresponding to the number of translatory modes.

Thus there are as many equations as unknowns

$$m = 3n + \mu \quad \dots \dots \dots (25)$$

If the rigid frame shown in Fig. 13 is considered, the procedure of analysis may be summarized in the following steps:

1. End bending moments in all panels are selected as unknowns (Fig. 14). Directions of these bending moments must be selected in such a way that the compatibility is satisfied.
2. Joint elastic weights are computed for panels in terms of the assumed moments.
3. Conjugate structures are sketched (Fig. 15) and elasto-static equations stated.
4. Static equations for joint moments and panel shears are written.
5. Moment matrix is solved.

The frame shown requires solution of 16 unknowns from 9 elasto-static equations, 4 joint moment equations and 3 shear equations. The introduction of three redundants for each panel (Fig. 16) and the formulation of end moments in terms of these redundants reduces the number of unknowns to nine and the solution is simplified to nine elasto-static equations. The introduction of elastic center is also possible.

Because the end bending moments (at a joint of a closed panel in a continuous or complex frame) are not necessarily equal, the joint elastic weight expression (Eq. 24) takes a new form as

$$\bar{P}_j = \begin{bmatrix} \underbrace{M_{ij} G_{ij} + M_{ji} F_{ji} + \tau_{ji}}_{\bar{P}_{ji}} \\ \underbrace{M_{kj} G_{kj} + M_{jk} F_{jk} + \tau_{jk}}_{\bar{P}_{jk}} \end{bmatrix} \dots \dots \dots (26)$$

The upper quantity represents the influence of the member  $ij$ . The lower value represents the influence of the member  $jk$ . The signs of the force-vectors  $\bar{P}_{ji}$  and  $\bar{P}_{jk}$  are governed by the end bending moments. The values of  $\tau$ 's are positive if developed on the dotted side of the member. The similarity of the

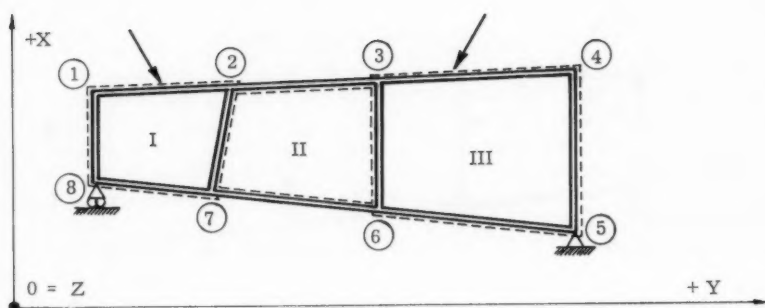


FIG. 13.—REAL FRAME

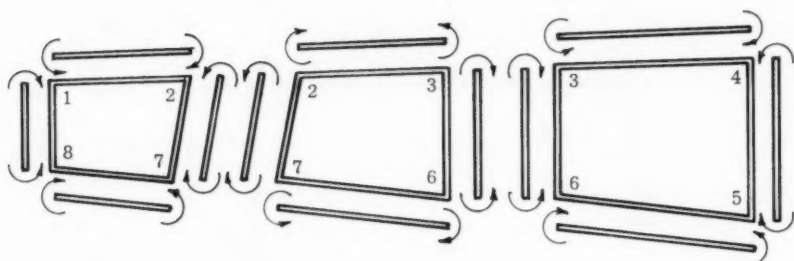


FIG. 14.—REAL PANELS

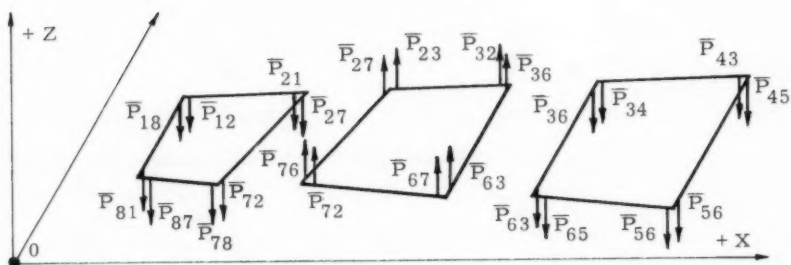


FIG. 15.—CONJUGATE PANELS

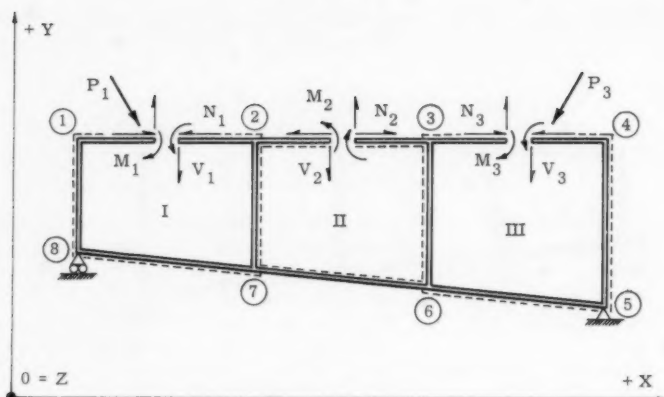


FIG. 16.—PANEL REDUNDANTS

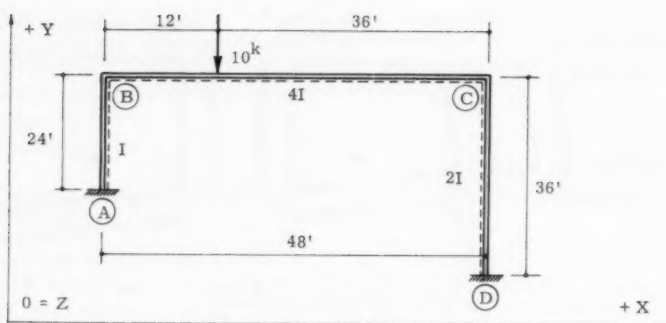


FIG. 17.—REAL FRAME

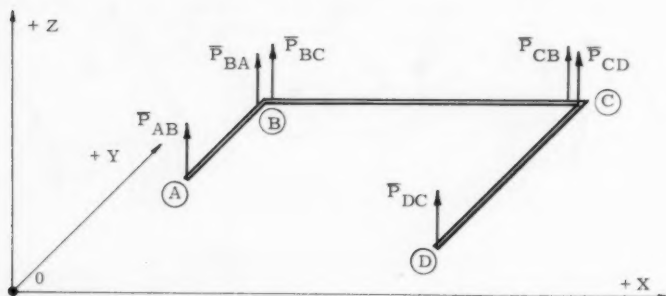


FIG. 18.—CONJUGATE BEAMS

right side expression in Eq. 26 with the less known four moment equation developed by Bleich<sup>20,21</sup> is well apparent.

### NUMERICAL EXAMPLES

The first numerical example will illustrate the application of the string polygon method to the solution of a one-story fixed-end frame (Fig. 17) while the second deals with the solution of a multi-panel frame (Fig. 18).

All values are given in kips, feet, or kip-feet, and moments of inertia are indicated on each member in the respective figure.

*Example 1.*—An unsymmetrical portal frame with bottom fixed and acted on by a single concentrated load is analyzed (Fig. 17). The end moments of all members are required.

(a) Angular Functions  $F$ 's,  $G$ 's and  $\tau$ 's must be computed for members AB, BC and CD. Because all members are of constant cross section, the simplified expressions given by Eqs. 15 and Table (1) are used.

Member AB

$$F_{AB} = F_{BA} = \frac{24}{3 EI} = \frac{8}{EI}$$

$$G_{AB} = G_{BA} = \frac{24}{6 EI} = \frac{4}{EI}$$

$$\tau_{AB} = \tau_{BA} = 0$$

Member CD

$$F_{CD} = F_{DC} = \frac{36}{3 E (2I)} = \frac{6}{EI}$$

$$G_{CD} = G_{DC} = \frac{36}{6 E (2I)} = \frac{3}{EI}$$

$$\tau_{CD} = \tau_{DC} = 0$$

Member BC

$$F_{BC} = F_{CB} = \frac{48}{3 E (4I)} = \frac{4}{EI}$$

$$G_{BC} = G_{CB} = \frac{48}{6 E (4I)} = \frac{2}{EI}$$

$$\tau_{BC} = \frac{(10)(12)(36)(84)}{6 E (48)(4I)} = \frac{315}{EI}$$

$$\tau_{CB} = \frac{(10)(12)(36)(60)}{6 E (48)(4I)} = \frac{225}{EI}$$

(b) Relative Elastic Weights (in terms of  $\frac{1}{EI}$ ) are obtained by means of Eq. 24 as functions of  $F$ 's,  $G$ 's,  $\tau$ 's and end moments  $M_A$ ,  $M_B$ ,  $M_C$ ,  $M_D$ .

$$\bar{P}_A = \bar{P}_{AB} = M_A (8) + M_B (4)$$

$$\bar{P}_B = \bar{P}_{BA} + \bar{P}_{BC} = M_A (4) + M_B (12) + M_C (2) + 315$$

$$\bar{P}_C = \bar{P}_{CB} + \bar{P}_{CD} = M_B (2) + M_C (10) + M_D (3) + 225$$

$$\bar{P}_D = \bar{P}_{DC} = M_C (3) + M_D (6)$$

<sup>20</sup> "Berechnung Statisch Unbestimmter Tragwerke Nach der Methode der Viermomentensatzes," by Fr. Bleich, 2nd Ed., J. Springer Verlag, Berlin, 1918.

<sup>21</sup> "Buckling Strength of Metal Structures," by Fr. Bleich, McGraw-Hill Book Co., New York, 1952, p. 200.

These elastic weights are now applied as force-vectors on the conjugate structure as shown in Fig. 18.

(c) Elasto-Static Equations may be written in many different forms. In this case, three moment equilibrium equations are utilized.

Static moment about AB

$$(48) (\bar{P}_D + \bar{P}_C) = 0$$

and

$$2 M_B + 13 M_C + 9 M_D + 225 = 0$$

Static moment about BC

$$(24) (\bar{P}_A) + (36) (\bar{P}_D) = 0$$

and

$$16 M_A + 8 M_B + 9 M_C + 18 M_D = 0$$

Static moment about CD

$$(48) (\bar{P}_A + \bar{P}_B) = 0$$

and

$$12 M_A + 16 M_B + 2 M_C + 315 = 0$$

These three deformation equations are in terms of four unknown moments; and for their solution one additional condition, based on the equilibrium of horizontal forces, must be introduced.



FIG. 19.—COLUMN SHEARS

(d) Shear equation derived from two free-body sketches shown in Fig. 19,

$$- V_{AB} + V_{DC} = 0$$

in terms of

$$V_{AB} = \frac{-M_A + M_B}{24} \quad \Bigg| \quad V_{DC} = \frac{-M_D + M_C}{36}$$



becomes

$$3 M_A - 3 M_B - 2 M_D + 2 M_C = 0$$

(e) Bending Moment Matrix formed by three elasto-static equations and one static equation follows.

$$\begin{bmatrix} 0 & + & 2 & + & 13 & + & 9 \\ + & 16 & + & 8 & + & 9 & + & 18 \\ + & 12 & + & 16 & + & 2 & & 0 \\ + & 3 & - & 3 & + & 2 & - & 2 \end{bmatrix} \begin{bmatrix} M_A \\ M_B \\ M_C \\ M_D \end{bmatrix} = \begin{bmatrix} -225 \\ 0 \\ -315 \\ 0 \end{bmatrix}$$

(f) Final Moments, obtained after finding the inverse of the bending moment matrix, are

$$\begin{array}{l|l} M_A = + 6.49 & M_B = - 21.38 \\ M_C = - 25.39 & M_D = + 16.43 \end{array}$$

*Example 2.*—An unsymmetrical, three panel, trapezoidal frame, with bottom fixed is analyzed (Fig. 20). Uniformly varying load is applied on columns 12

TABLE 2.—RELATIVE ANGULAR FUNCTIONS

Member	F	G	$\tau$
12	8.33	4.17	-4310
21	8.33	4.17	-4120
23	9.09	4.55	1500
32	9.09	4.55	1312
34 = 43	10.00	5.00	----
45 = 54	3.33	1.67	----
56 = 65	10.53	5.26	----
36 = 63	6.67	3.33	----
67 = 76	9.58	4.79	----
72 = 27	10.00	5.00	----
78 = 87	10.02	5.01	----

and 23. The cross section of each member is constant for its length. The end bending moments are assumed to be unknown. Again the dotted line indicates the tension side of the member. All angular functions are in terms of  $\frac{1}{EI}$  and this factor is omitted in all computations.

(a) Relative angular functions are computed similarly as in the preceding example and recorded in Table 2.

(b) Relative elastic weights for the ends of each member are computed with help of Eqs. 26 in Table 3 and applied on the conjugate structure as shown in Fig. 21.

(c) Elasto-Static Equations are written for each panel of Fig. 21:

TABLE 3.—RELATIVE ELASTIC WEIGHTS

12	$\bar{P}_{12}$	$8.33 M_{12} + 4.17 M_{21} - 4310$
	$\bar{P}_{21}$	$8.33 M_{21} + 4.17 M_{12} - 4120$
27	$\bar{P}_{27}$	$10.00 M_{27} + 5.00 M_{72}$
	$\bar{P}_{72}$	$10.00 M_{72} + 5.00 M_{27}$
78	$\bar{P}_{78}$	$10.02 M_{78} + 5.01 M_{87}$
	$\bar{P}_{87}$	$10.02 M_{87} + 5.01 M_{78}$
23	$\bar{P}_{23}$	$9.09 M_{23} + 4.55 M_{32} + 1500$
	$\bar{P}_{32}$	$9.09 M_{32} + 4.55 M_{23} + 1312$
36	$\bar{P}_{36}$	$6.67 M_{36} + 3.33 M_{63}$
	$\bar{P}_{63}$	$6.67 M_{63} + 3.33 M_{36}$
67	$\bar{P}_{67}$	$9.58 M_{67} + 4.79 M_{76}$
	$\bar{P}_{76}$	$9.58 M_{76} + 4.79 M_{67}$
34	$\bar{P}_{34}$	$10.00 M_{34} + 5.00 M_{43}$
	$\bar{P}_{43}$	$10.00 M_{43} + 5.00 M_{34}$
45	$\bar{P}_{45}$	$3.33 M_{45} + 1.67 M_{54}$
	$\bar{P}_{54}$	$3.33 M_{54} + 1.67 M_{45}$
56	$\bar{P}_{56}$	$10.53 M_{56} + 5.26 M_{65}$
	$\bar{P}_{65}$	$10.53 M_{65} + 5.26 M_{56}$

Panel 1;

$$\Sigma M_{12} = 0 \rightsquigarrow 30 (\bar{P}_{72} + \bar{P}_{78}) + 50 \bar{P}_{87} = 0$$

$$1. \quad 11.02 M_{78} + 6.00 M_{72} + 3.00 M_{27} + 13.03 M_{87} = 0$$

$$\Sigma M_{27} = 0 \rightsquigarrow 30 (\bar{P}_{12} + \bar{P}_{87}) = 0$$

$$2. \quad 8.33 M_{12} + 4.17 M_{21} + 10.02 M_{87} + 5.01 M_{78} - 4310 = 0$$

$$\Sigma M_{18} = 0 \rightsquigarrow 30 (\bar{P}_{21} + \bar{P}_{27} + \bar{P}_{72} + \bar{P}_{78}) = 0$$

$$3. \quad 8.33 M_{21} + 4.17 M_{12} + 15.00 M_{27} + 15.00 M_{72} + 10.02 M_{78} \\ + 5.01 M_{87} - 4120 = 0$$



Panel 2;

$$\Sigma M_{23} = 0 \curvearrowright 20 (\bar{P}_{63} + \bar{P}_{67}) + 30 (\bar{P}_{72} + \bar{P}_{76}) = 0$$

$$4. \quad 6.67 M_{63} + 3.33 M_{36} + 16.77 M_{67} + 19.17 M_{76} + 15.00 M_{72} + 7.5 M_{27} = 0$$

$$\Sigma M_{36} = 0 \curvearrowright 30 (\bar{P}_{23} + \bar{P}_{27} + \bar{P}_{72} + \bar{P}_{76}) = 0$$

$$5. \quad 9.09 M_{23} + 4.55 M_{32} + 15.00 M_{27} + 15.00 M_{72} + 9.58 M_{76} + 4.79 M_{67} + 1500 = 0$$

$$\Sigma M_{27} = 0 \curvearrowright 30 (\bar{P}_{32} + \bar{P}_{36} + \bar{P}_{63} + \bar{P}_{67}) = 0$$

$$6. \quad 9.09 M_{32} + 4.55 M_{23} + 10.00 M_{36} + 10.00 M_{63} + 9.58 M_{67} + 4.79 M_{76} + 1312 = 0$$

Panel 3;

$$\Sigma M_{34} = 0 \curvearrowright 10 (\bar{P}_{54} + \bar{P}_{56}) + 20 (\bar{P}_{63} + \bar{P}_{65}) = 0$$

$$7. \quad 1.67 M_{45} + 24.39 M_{56} + 26.32 M_{65} + 13.33 M_{63} + 6.67 M_{36} = 0$$

$$\Sigma M_{45} = 0 \curvearrowright 30 (\bar{P}_{34} + \bar{P}_{36} + \bar{P}_{63} + \bar{P}_{65}) = 0$$

$$8. \quad 5 M_{45} + 10 M_{36} + 10 M_{63} + 10 M_{34} + 10.53 M_{65} + 5.26 M_{56} = 0$$

$$\Sigma M_{36} = 0 \curvearrowright 30 (\bar{P}_{45} + \bar{P}_{43} + \bar{P}_{54} + \bar{P}_{56}) = 0$$

$$9. \quad 15.00 M_{45} + 15.53 M_{56} + 5.00 M_{34} + 5.26 M_{65} = 0$$

(d) Equations of statics offer seven additional conditions:  
the shear equations are

$$\Sigma M_0 = 0 \text{ (section mm)}$$

$$10. \quad 2 (M_{43} - M_{34}) + 2 (M_{65} - M_{56}) + M_{34} - M_{65} = 0$$

$$\Sigma M_0 = 0 \text{ (section nn)}$$

$$11. \quad 2 (M_{23} - M_{76}) + 3 (M_{67} - M_{32}) + 900 = 0$$

$$\Sigma M_0 = 0 \text{ (entire structure)}$$

$$12. \quad 3 (M_{87} - M_{12}) + 5 (M_{21} - M_{78}) + 8,560 = 0$$

TABLE 4.—BENDING MOMENT MATRIX

M <sub>34</sub>	M <sub>45</sub>	M <sub>54</sub>	M <sub>65</sub>	M <sub>63</sub>	M <sub>36</sub>	M <sub>23</sub>	M <sub>32</sub>	M <sub>67</sub>	M <sub>76</sub>	M <sub>72</sub>	M <sub>27</sub>	M <sub>12</sub>	M <sub>21</sub>	M <sub>78</sub>	M <sub>87</sub>	Const.
10.00	5.00	5.26	10.53	10.00	10.00											
5.00	15.00	15.53	5.26													
- 1.00	2.00	- 2.00	1.00													
1.00					- 1.00	1.00										
	1.67	24.39	26.32	13.33	6.67			1.00								- 1312
			1.00	- 1.00				9.58	4.79							
				10.00	10.00	4.55	9.09	10.77	19.17	15.00	7.50					- 1500
				6.67	3.33			4.79	9.58	15.00	15.00					- 900
								3.00	- 2.00							
											- 1.00		1.00			
									1.00	- 1.00				1.00		
										15.00	15.00	4.17	8.33	10.02	5.01	4120
										6.00	3.00			11.02	13.03	
												8.33	4.17	5.01	10.02	4310
												- 3.00	5.00	- 5.00	3.00	- 8560

and the joint equations are

$$13. \Sigma M_2 = 0 \curvearrowright M_{21} + M_{23} - M_{27} = 0$$

$$14. \Sigma M_3 = 0 \curvearrowright M_{32} + M_{34} - M_{36} = 0$$

$$15. \Sigma M_6 = 0 \curvearrowright M_{65} + M_{67} - M_{63} = 0$$

$$16. \Sigma M_7 = 0 \curvearrowright M_{76} + M_{78} - M_{72} = 0$$

(e) Bending moment matrix given by nine elasto-static equations, three shear equations and four joint moment equations in terms of sixteen unknown end moments is represented by Table 4.

TABLE 5.—FINAL MOMENTS

End	Moment	End	Moment	End	Moment
43	- 12.60	45	- 12.60	56	5.81
34	- 9.26	54	5.81	65	27.56
32	103.26	36	93.98	67	- 138.06
23	- 126.80	63	- 110.50	76	- 38.77
21	- 306.80	27	- 435.60	78	488.74
12	1003.85	72	- 449.97	87	- 520.30

(f) Final Moments obtained from the bending moment matrix are listed in Table 5.

### CONCLUSIONS

It has been shown that the string polygon method may be used in analyzing plane polygonal frames. The resulting bending moment matrix formed by the static and the elasto-static equations yield final design values, the bending moments at the ends of each member. Three visual concepts are utilized:

(a) The joint elastic weight is identical in form to the three or four moment equation.

(b) The deformation conditions are obtained from the conditions of elasto-static equilibrium.

(c) The continuity is obtained from the conditions of static equilibrium.

The extension of this procedure to the analysis of frames with nonprismatic members,<sup>22,23</sup> bent members,<sup>24</sup> wedged members,<sup>25</sup> truss-frames,<sup>26</sup> column-beams<sup>27</sup> and structures in space<sup>28</sup> is possible. The application of this procedure to the elasto-plastic analysis of coplanar frames is also possible.<sup>29</sup> The influence of axial and shearing deformations may be included.<sup>30</sup>

#### ACKNOWLEDGMENTS

The general theory of the string polygon for straight and bent members was presented by Tuma in his lectures at the Oklahoma State University, Stillwater, Okla.,<sup>31,32</sup> and by Tuma and Oden at the joint meeting of the Texas-Oklahoma Society of Civil Engineers in September, 1960. The application of the string polygon in connection with the elastic center was recorded by Oden in a Master of Science Thesis submitted to the Graduate School of the Oklahoma State University, Stillwater, Okla. In preparing the numerical examples the writers were assisted by D. C. McKee, M. ASCE, Assistant Professor of Civil Engineering, Louisiana State University, Baton Rouge, La. G. D. Houser, Graduate Assistant in the School of Civil Engineering, prepared the drawings.

---

22 "Beam Constants by the String Polygon Method," by S. L. Chu, thesis presented to Oklahoma State Univ., at Stillwater, in 1959, as partial fulfillment of the requirements for the degree of Master of Science.

23 "String Polygon Constants for Members with Sudden Change in Section," by J. W. Exline, thesis, presented to Oklahoma State Univ., at Stillwater, in 1961, as partial fulfillment of the requirements for the degree of Master of Science.

24 "Slope Deflection Equations for Symmetrical Bent Members by the String Polygon Method," by G. D. Houser, thesis presented to Oklahoma State Univ., at Stillwater, in 1961, as partial fulfillment of the requirements for the degree of Master of Science.

25 "Analysis of Wedged Frames with Bent Members by the String Polygon Method," by H. S. Yu, thesis presented to Oklahoma State Univ., at Stillwater, in 1961, as partial fulfillment of the requirements for the degree of Master of Science.

26 "Analysis of Rigid Truss-Frames by the String Polygon Method," by Y. I. Gonulson, thesis presented to Oklahoma State Univ., at Stillwater, in 1961, as partial fulfillment of the requirements for the degree of Master of Science.

27 "Column-Beams by the String Polygon and Carry-Over Method," by J. W. Harvey, thesis presented to Oklahoma State Univ., at Stillwater, in 1960, as partial fulfillment of the requirements for the degree of Master of Science.

28 "Theory of Space Structures," by Jan J. Tuma, Part K "String Polygon in Space," Lecture Notes, Oklahoma State Univ., Stillwater, 1961.

29 "Plastic Deformation Analysis of Frames at Ultimate Load by the String Polygon Method," by F. G. Gauger, thesis presented to Oklahoma State Univ., at Stillwater, in 1961, as partial fulfillment of the requirements for the degree of Master of Science.

30 "The General String Polygon," by C. M. Wu, thesis presented to Oklahoma State Univ., at Stillwater, in 1960, as partial fulfillment of the requirements for the degree of Master of Science.

31 "Numerical Methods in Structural Analysis," Lecture Notes, by Jan J. Tuma, Oklahoma State Univ., Stillwater, 1959.

32 "NSF Summer Institute for College Teachers of Structures and Soil Mechanics," Lecture Notes, by Jan J. Tuma, Oklahoma State Univ., Stillwater, 1960.

---

 APPENDIX.—NOTATION
 

---

The following symbols, adopted for use in the paper and for the guidance of discussers, conform essentially with "American Standard Letter Symbols for Structural Analysis" (ASA Z10.8-1949), prepared by a committee of the American Standards Association with Society representation, and approved by the Association in 1949:

$BM_u, BM_v$	= bending moments due to loads;
$d_j, d_k$	= lengths of segments $ij$ and $jk$ ;
$d_{jx}, d_{jy}, (d_{kx}, d_{ky})$	= horizontal and vertical projections of $d_j$ ( $d_k$ );
$du, dv$	= elemental length of segment $ij, jk$ ;
$E$	= modulus of elasticity;
$F_{ji}, F_{jk}$	= angular flexibilities;
$G_{ij}, G_{kj}$	= angular carry-over values;
$I$	= moment of inertia of the cross section;
$i, j, k$	= arbitrary points on the elastic curve;
$L$	= length of member;
$m$	= number of unknowns;
$M_i, M_j, M_k$	= moments at $i, j$ , and $k$ ;
$m, m'$	= length coefficients for computation of load functions;
$M_u, M_v$	= real bending moment at $u, v$ ;
$(M_u), (M_v)$	= virtual bending moment at $u, v$ ;
$N$	= normal force;
$n$	= number of panels;
$P$	= applied load;
$\bar{P}_s$	= elemental elastic weight;
$\bar{P}_{ji}$	= end shear of segment $ij$ at $j$ of the conjugate structure;
$\bar{P}_j$	= joint elastic weight;
$u, u' (v, v')$	= coordinates of cross sections of member $ij$ ( $jk$ );
$\bar{W}_j$	= segmental elastic weight of segment $ij$ ;
$x, y, z$	= orthogonal coordinates of a point in the structure;
$\Delta$	= end displacement;
$\mu$	= number of static equations;



$\omega_j, \omega_k$	= angle of inclination of members $ij$ and $jk$ ;
$\phi_j$	= change in the change of slope at $j$ ;
$\rho_j'$	= change in slope of line $ijk$ at $j$ after deformation; and
$\tau_{ji}, \tau_{jk}$	= angular load functions.

1. The first part of the paper is devoted to a discussion of the general principles of the theory of the structure of the atom.

2. The second part of the paper is devoted to a discussion of the general principles of the theory of the structure of the atom.

3. The third part of the paper is devoted to a discussion of the general principles of the theory of the structure of the atom.

---

Journal of the  
STRUCTURAL DIVISION  
Proceedings of the American Society of Civil Engineers

---

STRESSES AT A RE-ENTRANT CORNER OF A PLATE

By Mario G. Salvadori,<sup>1</sup> F. ASCE

---

SYNOPSIS

The floors of some modern buildings are simply supported on an inner rectangular core and external walls parallel to the sides of the core. Such floors are unsupported by intermediate columns and present re-entrant corners. The stresses at the corners of such plates are theoretically infinite, but become finite in the immediate neighborhood of the corner. Thus practical design stresses can be obtained by substituting for the actual plate a circular sector simply supported on its circular boundary and built-in on its straight sides. Such stresses are derived for the case of a circular sector with a right angle cutout and are good approximations of the stresses in the actual corner of the floor a distance from the corner of the order of two or three times the thickness of the plate.

---

INTRODUCTION

In many modern structures plates with one or more re-entrant corners are used to support uniform loads. Typical of such plates is a floor slab supported on a rectangular outer boundary and an inner core (Fig. 1). The stress in such plates may be easily evaluated with sufficient accuracy by numerical methods<sup>2</sup> everywhere except in the neighborhood of re-entrant corners.

---

Note.—Discussion open until March 1, 1962. To extend the closing date one month, a written request must be filed with the Executive Secretary, ASCE. This paper is part of the copyrighted Journal of the Structural Division, Proceedings of the American Society of Civil Engineers, Vol. 87, No. ST 7, October, 1961.

<sup>1</sup> Prof. of Civ. Engrg. and Architecture, Columbia Univ., N. Y., and Assoc., Paul Weidlinger, Cons. Engr., New York, N. Y.

<sup>2</sup> "Simply Supported Corner Plate," by Mario G. Salvadori and H. C. Reggini, *Proceedings, ASCE*, Vol. 86, No. ST 11, November, 1960.

Since the support conditions away from a re-entrant corner do not substantially influence the stresses at the corner, these can be approximated by considering a circular sector with the same re-entrant corner (Fig. 2). The stresses in such a sector are evaluated for conditions of simple support along the straight sides and of fixity along the circular boundary.

### DIFFERENTIAL EQUATION OF CIRCULAR SECTOR

A circular sector with a re-entrant corner  $\theta_0 = \alpha_1 \pi$ , ( $1 < \alpha_1 < 2$ ), is cut out of an annulus of outer radius  $a$  and inner radius  $b$  (Fig. 3). The sector is fixed along  $r = a$  and  $r = b$ , is simply supported along  $\theta = 0$  and  $\theta = \theta_0$ , and loaded with a uniform load  $q$ . The deflections of the sector  $w(r, \theta)$  are governed by the following boundary problem in which subscripts indicate differentiation:<sup>3</sup>

$$\nabla^4 w = \frac{q}{D} \dots \dots \dots (1)$$

$$w(a, \theta) = w(b, \theta) = w_r(a, \theta) = w_r(b, \theta) = 0 \dots \dots (2a)$$

and

$$w(r, 0) = w(r, \theta_0) = r^{-1} w_r + r^{-2} w_{\theta\theta} + \nu w_{rr} \Big]_{\substack{\theta=0 \\ \theta=\theta_0}} = 0 \dots (2b)$$

Letting:

$$\theta = \alpha_1 \theta \left( \alpha_1 = \frac{\theta_0}{\pi} \right), \alpha_m = m \alpha_1 \dots \dots \dots (3)$$

and

$$q = \sum_{m=1,3,5,\dots} q_m \sin(m\phi), q_m = \frac{4}{\pi} \frac{q}{m} \dots \dots \dots (4)$$

a solution of Eq. 1 satisfying Eqs. 2b may be written in the form:

$$\begin{aligned} w(r, \theta) &= \sum_{m=1,3,5,\dots} W_m(r) \sin(\alpha_m \theta) \\ &= \sum_{m=1,3,5,\dots} W_m(r) \sin(m\phi) \dots \dots \dots (5) \end{aligned}$$

Substitution of Eqs. 3 and 4 into Eq. 1 and the conditions of Eqs. 2a leads to the equation and boundary conditions for the  $W_m$ :

$$\begin{aligned} r^4 W_m^{iv} + 2r^3 W_m''' - (1 + 2\alpha_m^2) r^2 W_m'' + (1 + 2\alpha_m^2) r W_m' \\ - \alpha_m^2 (4 - \alpha_m^2) W_m = \frac{q_m r^4}{D} \dots \dots \dots (6) \end{aligned}$$

<sup>3</sup> "Theory of Plates and Shells," by S. Timoshenko and S. Workowsky-Kriech, McGraw-Hill Book Co., New York, 1959, p. 283.

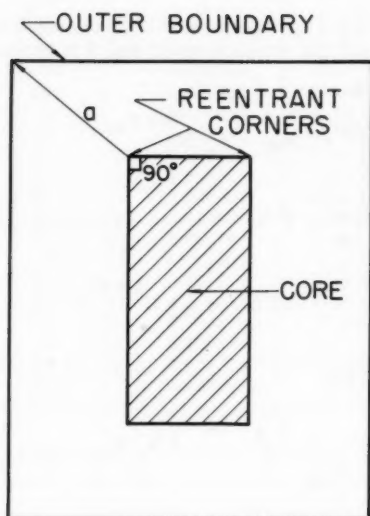


FIG. 1.—RECTANGULAR FLOOR SLAB

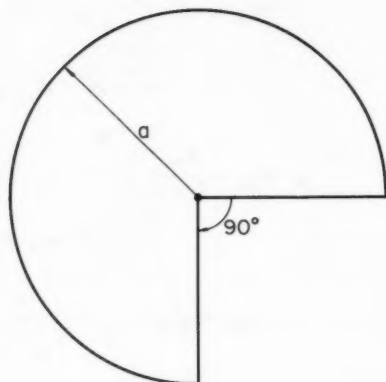


FIG. 2.—CIRCULAR SECTOR

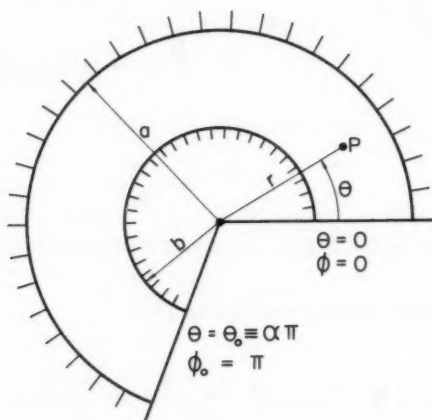


FIG. 3.—CIRCULAR ANNULUS SECTOR

and

$$W_m(a) = W_m'(a) = W_m(b) = W_m'(b) = 0 \dots\dots\dots (7)$$

The change of variable  $r = e^t$  reduces Eq. 6 to an equation with constant coefficients. From its general solution and the conditions of Eq. 7 it is found that for  $b = 0$ :

$$W_m = \frac{A_m}{2} \left[ -(\alpha_m - 2) R^{\alpha_m} + (\alpha_m - 4) R^{2+\alpha_m} + 2 R^4 \right] \alpha_m \geq 1, \alpha_m \neq 2, 4 \dots\dots\dots (8a)$$

$$W_m = \frac{A_m}{2 \alpha_m} \left[ (2 - \alpha_m) R^{2-\alpha_m} - (2 + \alpha_m) R^{2+\alpha_m} + 2 \alpha_m R^4 \right] \alpha_m < 1 \dots\dots\dots (8b)$$

$$A_m = \frac{4}{\pi m} \frac{1}{(16 - \alpha_m^2)(4 - \alpha_m^2)} \frac{q a^4}{D} \alpha_m \neq 2, 4 \dots\dots\dots (8c)$$

and

$$W_m = \frac{A_m'}{2} \left( R^{\alpha_m} - R^{2+\alpha_m} + 2 R^4 \ln R \right) \begin{cases} A_m' = \frac{1}{12 \pi m} \frac{q a^4}{D}; \alpha_m = 2 \\ A_m' = -\frac{1}{24 \pi m} \frac{q a^4}{D}; \alpha_m = 4 \end{cases} \dots\dots\dots (8d)$$

where

$$R = \frac{r}{a} \dots\dots\dots (9)$$

RIGHT ANGLE RE-ENTRANT CORNER:  $\theta_0 = \frac{3\pi}{2}$

For  $\theta_0 = 3\pi/2$  the previous equations give:

$$w(r, \theta) = A_1 \left( R^{4/3} - 2 R^{8/3} + R^4 \right) \sin\left(\frac{2}{3}\theta\right) + \frac{A_3'}{2} (R^2 - R^4 + 2 R^4 \ln R) \sin(2\theta) + \frac{1}{2} \sum_{m=5,7,9,\dots} A_m \left[ -(\alpha_m - 2) R^{\alpha_m} + (\alpha_m - 4) R^{2+\alpha_m} + 2 R^4 \right] \sin\left(\frac{2m}{3}\theta\right) \dots\dots\dots (10)$$

$$(R = r/a)$$

TABLE 1

R	$\alpha$	$\beta$	$\beta_1$	$\gamma$
0.0°	0.000000	$\infty$	$\infty$	$-\infty$
0.05	0.000398	0.040716	0.162710	-3.5136
0.10	0.000927	+0.000606	0.072528	-1.2908
0.15	0.001396	-0.018827	0.068135	-0.7308
0.20	0.001940	-0.030181	0.048879	-0.4768
0.25	0.002335	-0.037348	0.035012	-0.3262
0.30	0.002643	-0.041403	0.024298	-0.2218
0.40	0.002927	-0.042954	+0.00815	-0.0763
0.50	0.002790	-0.037579	-0.001196	+0.0303
0.60	0.002307	-0.026395	-0.007123	0.1192
0.70	0.001607	-0.010148	-0.009636	0.1990
0.75	0.001227	+0.000287	-0.009738	0.2370
0.80	0.000856	0.011750	-0.009123	0.2740
0.85	0.000529	0.024505	-0.007808	0.3106
0.90	0.000248	0.038558	-0.005849	0.3469
0.95	0.000064	0.053941	-0.003324	0.3829
1.00	0.000000	0.070674	0.000000	0.4151

Table 1 gives coefficients  $\alpha$ ,  $\beta$ ,  $\beta_1$  and  $\gamma$  for the displacement  $w$ , the moments  $M_R$  and  $M_t$  and the shear  $Q_R$ :

$$w = \sum_{m=1,3,5,\dots} (-1)^{\frac{m-1}{2}} W_m = \alpha \frac{q a^4}{D} \dots \dots \dots (11a)$$

$$M_R = -D \sum_{m=1,3,5,\dots} (-1)^{\frac{m-1}{2}} \left[ W_m'' + \nu \left( r^{-1} W_m' - \alpha_m^2 r^{-2} W_m \right) \right] \\ = (\beta + \nu \beta_1) q a^2 \dots \dots \dots (11b)$$

$$M_t = -D \sum_{m=1,3,5,\dots} (-1)^{\frac{m-1}{2}} \left[ r^{-1} W_m' - \alpha_m^2 r^{-2} W_m + \nu W_m'' \right] \\ = (\beta_1 + \nu \beta) q a^2 \dots \dots \dots (11c)$$

and

$$Q_R = -D \sum_{m=1,3,5,\dots} (-1)^{\frac{m-1}{2}} \left[ W_m''' + r^{-1} W_m'' - \left( 1 + \alpha_m^2 \right) r^{-2} W_m' \right. \\ \left. + 2 \alpha_m^2 r^{-3} W_m \right] = \gamma q a \dots \dots \dots (11d)$$

along the radius  $\theta = 3\pi/4$  for  $R = 0$  (0.05) 0.3,  $R = 0.3$  (0.1) 0.7, and  $R = 0.7$  (0.5) 1.0.

The moments and the shear become infinite at the corner. Their values a small distance from the corner may be used to approximate the design values of these quantities.

#### CONCLUSIONS

The formulas derived can be safely used to design a plate in the immediate neighborhood of a re-entrant corner under the assumption of simple support on the external walls. The stresses for the re-entrant corner of a plate built-in into the external walls cannot differ substantially from those derived, except in the neighborhood of the outer plate corner.



---

Journal of the  
STRUCTURAL DIVISION  
Proceedings of the American Society of Civil Engineers

---

VIBRATION ANALYSIS FOR STRUCTURAL FLOOR SYSTEMS

By Lawrence R. Burkhardt,<sup>1</sup> M. ASCE

---

SYNOPSIS

Structural supports of heavy industrial vibrating machinery often prove inadequate because of excessive vibration during machinery operation. In the majority of cases, this vibration is due to harmonic resonance causing vibration amplification.

The purpose of this paper is to present the designer with a means of eliminating this harmonic resonance by determining rapidly and easily the approximate basic floor beam frequencies by nomographs.

Two extreme conditions have been presented: that of single degree of freedom, and that of infinite degree of freedom on the basis that sufficient accuracy can be obtained by reducing all beam loadings to one or the other extreme.

---

INTRODUCTION

Beam vibration in structural floor systems that support heavy industrial equipment has long been a disturbing problem to engineers. Excessive vibration is difficult to eliminate in the design state, and it frequently causes inefficiency of both machinery and operating personnel, and can cause fatigue failure of structural members.

By use of vibration absorbers and damping devices, machinery may be made dynamically independent of its supporting structure, and virtually complete vi-

---

Note.—Discussion open until March 1, 1962. To extend the closing date one month, a written request must be filed with the Executive Secretary, ASCE. This paper is part of the copyrighted Journal of the Structural Division, Proceedings of the American Society of Civil Engineers, Vol. 87, No. ST 7, October, 1961.

<sup>1</sup> Structural Engr., Meissner Engineers, Inc., Chicago, Ill.

bration elimination attained. This elaborate and costly vibration isolation method is often impractical and uneconomical.

The goal, in general, is not the complete elimination of vibration, but the elimination of excessive vibration. Therefore, the time-consuming, complex methods of exact frequency analysis are not normally required in average in-

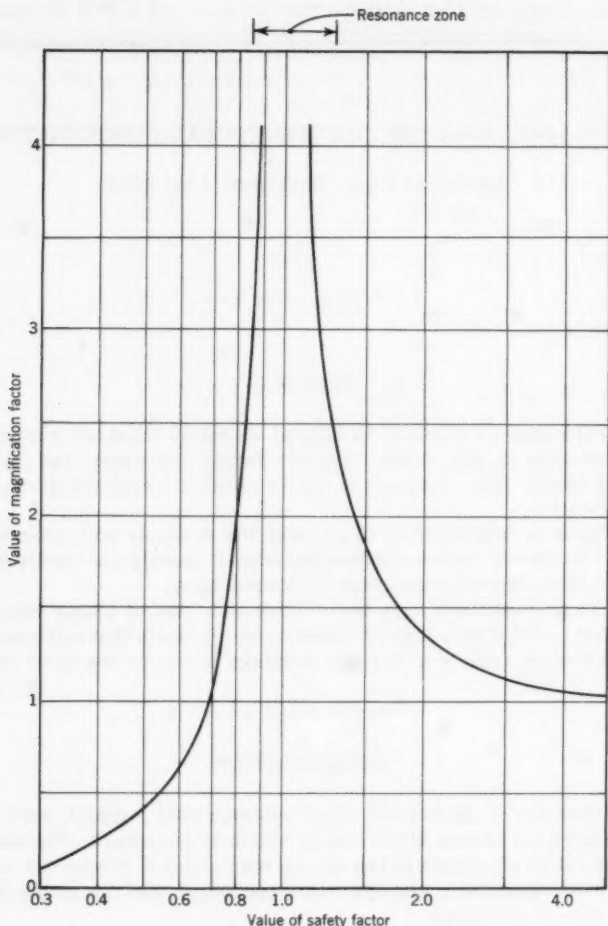


FIG. 1

dustrial installations. However, a simple, thoroughly practical method of analysis is available.

Formulas used to determine undamped, prismatic beam frequencies are basic, and a great deal has already been written about their application. This paper outlines a simplified, quick method of analysis—sufficiently accurate for

general use in a design office—for the elimination of excessive vibration caused by structural members being in resonance with vibrating or unbalanced machinery, for example, screens, fans, vibrating pan conveyors, presses, and so on.

The charts presented herein, which have proven invaluable design aids, are based on an undamped system and give accurate values of fundamental beam frequencies. Their application is limited to individual prismatic beams. It is assumed, if each beam in a confined floor system is adjusted to be out of phase with respect to its natural frequency in relation to an impressed vibrating force, that the floor system as a whole will not resonate.

It must be understood that, even though it is possible to adjust beam frequencies to eliminate excessive vibration caused by resonance, it is extremely difficult to completely eliminate the vibration. Any elastic body can be made to vibrate at any frequency by the application of a continuous vibrating force, but by beam frequency adjustment the amplitudes caused by impressed vibrations can be held to normal static deflections.

### FREQUENCY CHART EXPLANATION

Beam frequencies are a function of stiffness and of mass. A very rigid or stiff beam, having a high natural frequency, can be made to resonate at a low frequency by the attachment of sufficient dead load. This dead load need not be part of the beam itself, but must be securely attached to the beam, so that both will vibrate at the same frequency. The deflection caused by the attached or applied dead load is used to determine the load frequency of the beam. The mass of the beam itself is treated separately and is used to determine the natural beam frequency.

These two frequencies are then combined as a compound spring system in series. The combined, or resultant, frequency is then compared to the impressed vibrating force and, if necessary, the beam frequency is adjusted to eliminate resonance, through beam selection or span alteration.

As shown in Fig. 1, the resonance zone occurs when the impressed vibration is approximately equal to the resultant frequency. Infinite amplitudes can be obtained with lightweight machinery under conditions of perfect resonance. Actually, these infinite amplitudes are impossible to obtain because of damping factors in the connections and the materials themselves. It is possible, however, to obtain large amplitudes for the resonance condition previously mentioned. Safety factors, based on empirical data for various spans and type of support are given in Table 1.

Fig. 1

$$\text{Safety Factor} = \frac{\text{Resultant beam frequency}}{\text{Impressed Vibration}} \dots\dots\dots (1)$$

and

$$\text{Magnification Factor} = \frac{1}{\left[ 1 - \frac{(\text{impressed frequency})^2}{(\text{beam frequency})^2} \right]} \dots\dots\dots (2)$$

Safety factor values lower than one result in less amplitude than higher values because of a self-canceling effect. This is the case of concrete decks or beams on which large mass is supported. This is very desirable, but the beam vibration being considered is in first mode harmonics. Second or third mode frequencies which are four and nine times the first mode may fall in the resonance zone. Therefore, it is safer to keep the first mode vibration above the resonance zone. Economy may dictate the use of concrete decks or mass and safety factors less than one to reduce beam size for long spans.

Specifically, the charts are established for direct use of simple span steel beams, in which the full range of rolled sections is covered. Analysis of other support conditions and common structural materials may be obtained by the use of proper coefficients listed on the charts.

Material correction factors are also included for correction of natural steel beam frequencies, to that of materials having different elastic and mass properties. In addition, all frequencies used in the charts are expressed in vibrations per minute, to give a designer a "feel" of the beam frequency, because most impressed vibrations are stated in the same frequency units.

TABLE 1.—SAFETY FACTORS

Type of end support (framed to) (1)	Span (2)	Ratio of beam frequency to impressed vibration (safety factor) (3)
Column	Less than 20 feet	Greater than 1.5 or less than 0.80
Column	Greater than 20 ft.	Greater than 2.0 or less than 0.75
Beam	Less than 20 feet	Greater than 2.0 or less than 0.75
Beam	Greater than 20 ft.	Greater than 2.0 or less than 0.75

The following steps are to be followed in analyzing and designing a system for resonance elimination:

1. Perform complete structural analysis, using up to 100% impact.
2. Check individual beam frequencies and adjust beam size to conform to Table 1 using the following steps.

(a) Obtain dead load frequency. The dead load in this case is the load which is securely attached to the beam and which will, therefore, vibrate with the beam. The vibrating machinery is to be considered as live load. If the applied dead load is uniform, the weight of the beam may be included with the applied dead load to eliminate steps b and c. Note that Fig. 2 is for concentrated loads and Fig. 3 is for uniform loads. For Fig. 2

$$F = \frac{187.5}{D^{1/2}} \dots \dots \dots (3)$$

and

$$D = \frac{0.00124 \ P \ L^3}{I} \ C \ M \dots \dots \dots (4)$$

in which  $P$  is the concentrated load, in kips;  $D$  denotes the deflection, in inches;  $I$  refers to the moment of inertia;  $L$  is the span, in feet; and  $F$  defines the frequency, in vibrations per minute. For Fig. 3

$$F = \frac{211.5}{D^{1/2}} \dots\dots\dots (5)$$

and

$$D = \frac{0.000775 W L^4}{I} C M \dots\dots\dots (6)$$

in which  $W$  is the uniform load in kips per foot.

(b) Find the natural beam frequency, using Fig. 4. (This is necessary only when the applied dead load is concentrated or when it is nonexistent.) For Fig. 4

$$F = \frac{129,500 R}{L^2} C M \dots\dots\dots (7)$$

and

$$M = 0.00503 \left[ \frac{E_M}{Z_M} \right]^{1/2} \dots\dots\dots (8)$$

in which  $R$  is the radius of gyration, in inches;  $E_M$  denotes the modulus of elasticity of the material, in kips per square inch; and  $Z_M$  defines the mass density of the material, in kips seconds squared per inch to the fourth power.

(c) Combine the separate frequencies (if two or more were necessary to determine), and obtain a resultant frequency by use of Fig. 5. For Fig. 5

$$F = \frac{1}{\left[ \frac{1}{F_1^2} + \frac{1}{F_2^2} \right]^{1/2}} \dots\dots\dots (9)$$

(d) Obtain the frequency safety factor. Recommended safety factors are listed in Table 1.

(e) The undamped dynamic amplitude or deflection can be obtained by multiplying the live load static deflection by the magnification factor shown on Fig. 1.

(f) Note that from the curve on Fig. 1, safety factors can be either above or below the resonance zone. They will usually be below if a concrete deck is used. Safety factors below 1.0, without use of a concrete deck, may result in excessive deflection and therefore are subject to a live deflection investigation. (The deflection obtained would have the same frequency as the vibrating machinery.)

(g) Coefficients for other materials and support conditions are listed on the charts for ease of application. Note that when Figs. 2 and 3 are used, it is necessary to multiply the deflection by the elasticity and support coefficients and then determine the frequency corresponding to the new deflection.

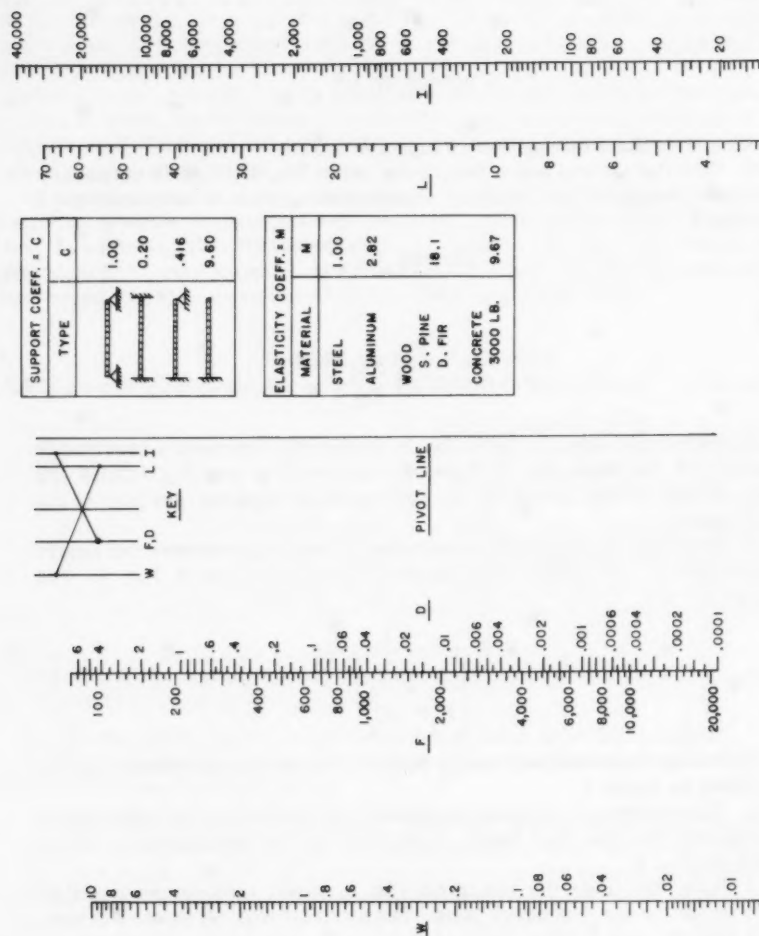


FIG. 2.—CONCENTRATED LOAD DEFLECTION AND FREQUENCY

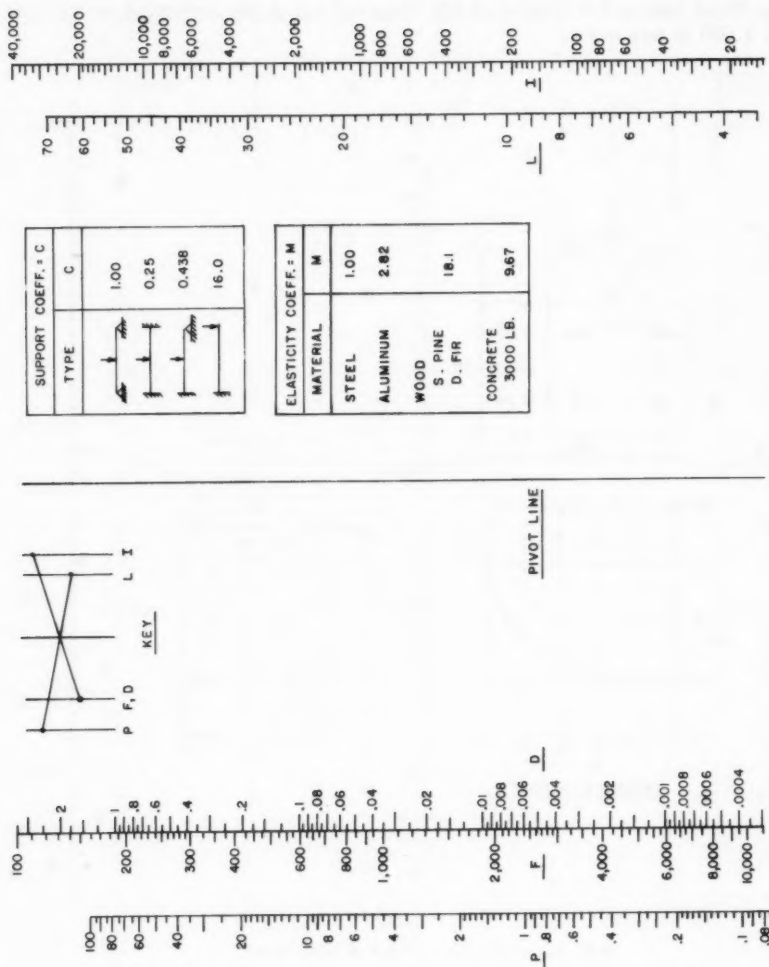


FIG. 3.—UNIFORM LOAD DEFLECTION AND FREQUENCY

**Example.**—A vibrating screen used for sifting materials and weighing 10,000 lb is operating at 800 rpm and is supported symmetrically on two 18 WF 50 beams spanning 18 ft. The beams are directly connected to columns. Screen supports are at 8 ft on center. Maintenance area around the screen gives a uniform dead load to the beams of 150 lb per ft and a concentrated centerline load of 1,000 lb per beam.

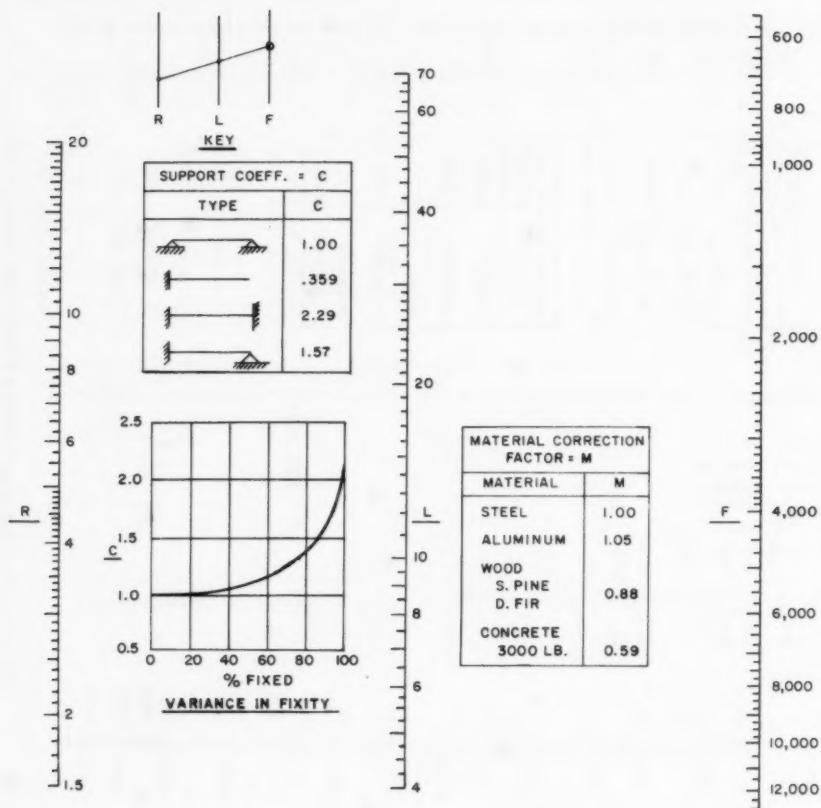


FIG. 4.—NATURAL BEAM FREQUENCY

The static analysis proves that the beams are more than adequate for the imposed dead load and live load of the screen. A dynamic analysis is as follows:

1. The uniform dead load (150 lb imposed and 50 lb for the beam itself) deflection is 0.019 in. and the corresponding beam frequency is 1,500 vibrations per min (Fig. 3).

2. The concentrated dead load deflection is 0.009 in. and the corresponding beam frequency is 1,950 vibrations per min (Fig. 2).



3. The combined or resultant beam frequency is 1,200 vibrations per min (Fig. 5).

4. The safety factor is  $1,200/800$  or 1.5. Beam resonance will not occur.

5. The approximate undamped dynamic deflection can be obtained from Fig. 1. The magnification factor corresponding to 1.5 is 1.85. Static deflec-

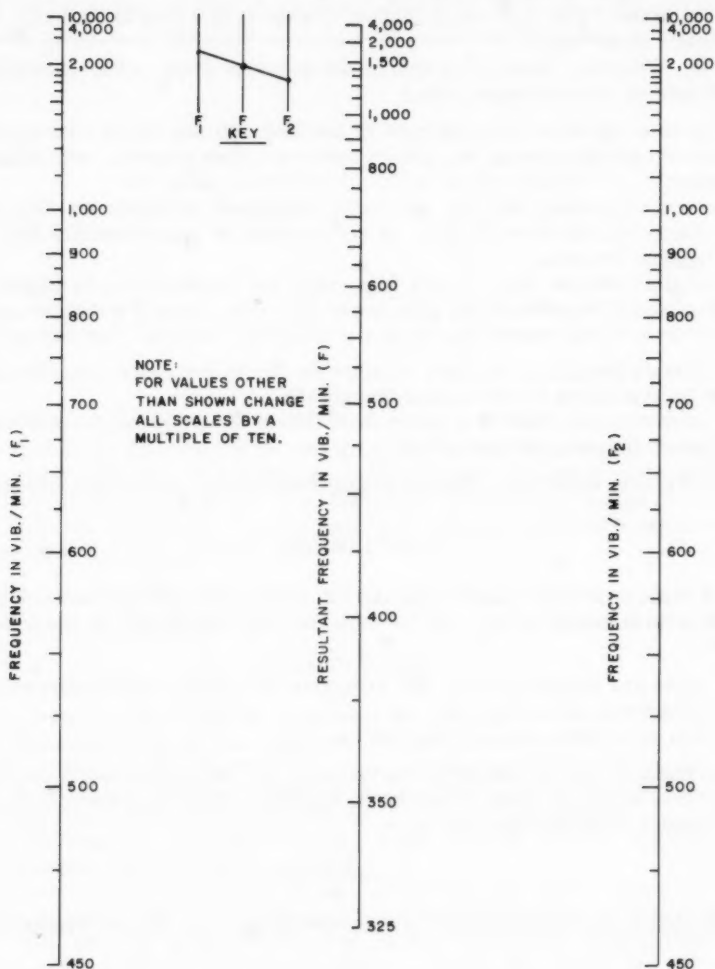


FIG. 5.—FREQUENCY RESULTANT

tion of the screen, assuming a centerline concentrated load, is 0.045 in. from Fig. 2. Dynamic deflection will be approximately  $0.045 \times 1.85$ , or 0.0832 in. The total oscillation of the beam would be twice the dynamic deflection or over  $5/32$  in. In this example, due to the large live load, a larger size beam should

be used. (A 21 WF 62 has a safety factor of 1.88, a dynamic deflection of 0.0383 in., and a total oscillation of less than  $3/32$  in.)

The applied frequency or pulsating force of various equipment has a frequency range as follows:

(a) Screens.—The rpm of the screen deck. (Range is usually 700 rpm to 1100 rpm or vibrations per min.)

(b) Fans.—The rpm of the blades. (Range is 400 rpm to 1000 rpm or vibrations per min.)

(c) Vibrating Pans.—The rpm of the conveyor deck. (Approximately 500 rpm or vibrations per min.)

Tolerable vibration is a function of the intended use of the structure—the comfort of operating personnel and its effect on other adjacent miscellaneous equipment.

It is recommended that the maximum undamped deflection as obtained by these charts be less than  $3/32$  in. at frequencies of approximately 1000 rpm for tolerable vibration.

The attached dead load is very important, for an excessive or higher than actual attached dead load will give lower than true beam frequencies, which will result in either unsafe design or uneconomical results. For example:

1. Unsafe design in the case of concrete floors for which beam frequency should be kept below the resonance range; and
2. uneconomical results in plate deck floors for which excessive dead load gives lower frequencies than actual.

Therefore, it is imperative that the initial dead load be as accurate as possible.

### CONCLUSIONS

The explanation and charts represent a "tool" that can find definite use in any structural design office. Its formulation has been based on the following needs:

1. Ease and rapidity of use, (No extensive calculations are required.);
2. directness of result; and
3. full structural range of application.

The basic formulas indicated in a reduced unit form are readily obtainable from the reference material noted in the Appendix. The steel modulus of elasticity used was 29,000 kips per sq in.

---

### APPENDIX.—REFERENCE MATERIAL ON PRISMATIC BEAM VIBRATIONS

---

1. "Mechanical Vibrations," by J. P. Den Hartog, McGraw-Hill Book Co., Inc., New York, 1956.
2. "Mechanical Engineers Handbook," by Lionel S. Marks, McGraw-Hill Book Co., Inc., New York, 1958.
3. "Vibration Problems in Engineering," by Stephen Timoshenko, D. Van Nostrand Co., Inc., New York, 1955.

---

Journal of the  
STRUCTURAL DIVISION  
Proceedings of the American Society of Civil Engineers

---

MULTIPLE RIBLESS SHELLS<sup>a</sup>

By Anton Tedesco,<sup>1</sup> F. ASCE and M. IABSE

---

SYNOPSIS

An analytical approach to the design of multiple ribless concrete shells is confirmed by the results of large scale model tests. Among the practical applications of the criteria that are described herein is the design of a major warehouse installation in Pennsylvania that utilizes modified ribless shells at a column spacing of 66 ft by 40 ft.

---

INTRODUCTION

The term "ribless shells" has become identified with a certain kind of shell structure. Conventional shells of the past had supporting and stiffening ribs that were distinctly separate in appearance and action from the shell itself. In an effort to simplify the construction of this shell and rib combination, the ribless shell was developed in which the rib or arch appears as a shallow band. Consequently, the term "ribless shell" is only relative and indicates that a conventional deep rib is not used.

Millions of square feet of multiple barrel concrete shell roofs have been built since about 1940 for warehousing and industrial purposes. Most of these roofs have smooth ceilings without projecting members. This is desirable from the standpoint of internal warehouse operations. Thus, the stiffening

---

Note.—Discussion open until March 1, 1962. To extend the closing date one month, a written request must be filed with the Executive Secretary, ASCE. This paper is part of the Structural Division, Proceedings of the American Society of Civil Engineers, Vol. 87, No. ST 7, October, 1961.

<sup>a</sup> Presented at the October, 1958 ASCE Convention in New York, N.Y.

<sup>1</sup> Vice Pres., Roberts and Schaefer Co., Inc., Engineers, Yew York, N.Y.

ribs have usually projected above the roof shell. This also has the advantage of allowing smooth travel and efficient reuse of the form centering. For spans of about 45 ft or 50 ft, stiffening ribs project 2 ft or more above the roof, thereby requiring flashing and provisions for drainage. The alternative solution, projecting the stiffening ribs below the roof slab, results in smooth, uninterrupted application of roofing and simple drainage. However, the advantages of easy form travel, smooth appearance, uninterrupted piping runs, and more uniform storage height are lost.

Designers have tried to combine the advantages of both solutions. The approach is similar to that used in the development of flat slab floors. A wide, thin rib-band is substituted for the deep, narrow rib. Penalties in the quantities of concrete and steel are accepted. These penalties, however, are compensated for by the savings in formwork, roofing, and drainage. The rib-band does not provide as effective a restraint for the shell as the conventional deep rib and, further, its thinness makes the structure more sensitive to non-uniform loads. The dimensions of the ribless shell roof, which can safely or economically be used without the danger of buckling, are therefore limited. To realize economy in this type of construction, it is necessary that the structural system consist of multiple spans in both directions. The advantage of "being ribless" increases with larger installations in which reuse of formwork and greater number of spans are possible.

#### FUNCTION OF RIBS

Fig. 1 illustrates the terminology used. The ribs serve as transverse stiffeners for the thin curved slab, thus permitting the transfer of shear forces from shell to rib. This in turn permits the shell to carry the applied loads longitudinally. The shell between ribs acts much as a deep beam of curved cross-section, and the ribs as arches transmitting the loads to the columns. Fig. 2 shows some typical cross-sections indicating the ribs above and below a shell.

Multiple barrel shells are statically indeterminate to a large degree and, therefore, can be made to carry applied loads in a variety of ways. This fact presents a challenge to the designer who has considerable latitude in proportioning the members in a shell system. (When all dimensions and properties of the structure have been fully established, there is only one way in which the structure can act). The structural behavior of a shell system is a function of the relative stiffness of the system's components. For example:

1. If the shell is restrained at the ribs and relatively free along its longitudinal edges, it will act as a beam spanning from rib to rib.
2. If the stiffness of the valley between shells is increased, or if additional support is provided along the valley where two shells intersect, increasing percentages of the load will be carried transversely.
3. If the curved shell element is rigidly supported along its longitudinal edges and shaped to the funicular line of the applied load, it will act as an arch, and there will be no moments under that load. If, for instance, a shell element of uniform thickness is shaped to a catenary, there will be no dead-load moments. Such a curved element could be treated structurally as made up of transverse strips, each acting independently as an arch, with no need for longitudinal shell action.

If arching action (with primarily compressive stresses) in the transverse direction can be accomplished with little deformation, this is the way the curved

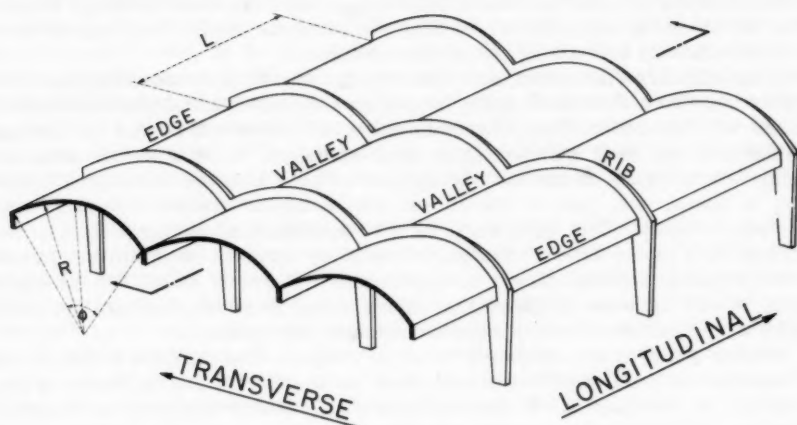


FIG. 1

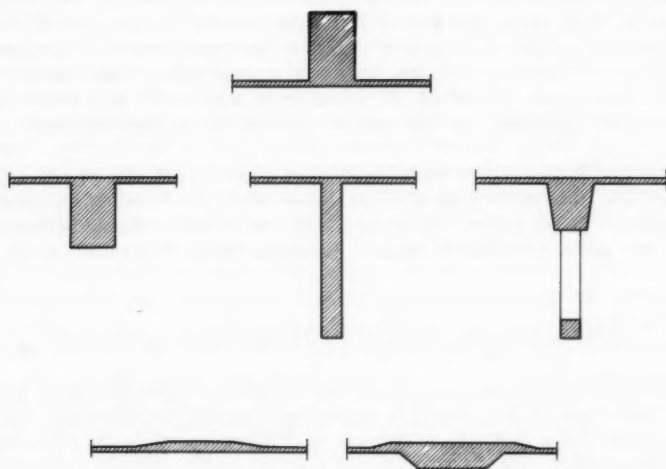


FIG. 2.—CROSS SECTIONS OF TRANSVERSE RIBS

shell element will attempt to act, in accordance with the law of least work. Where, on the other hand, due to slenderness, thin sections, shape of shell, or unsymmetrical loads, arch action would result in flexure contributing to a

substantial amount of work of deformation, this kind of behavior would be "vetoed" by the shell. Membrane stresses would then dominate, leading to a smaller total work of deformation.

Shell action will produce only nominal  $M_\phi$  moments in the transverse direction, which are of a smaller order than the moments necessary to carry non-uniform loads by a series of transverse arches.

If the ribs are eliminated, how would such a system be in equilibrium? The system may be stable under some, but perhaps not under all of the usual loads. There will be arch action if the cross-sectional curve will permit it. Certain portions of the shell will be highly over-stressed. If the structure does not buckle or collapse, there will develop something like the behavior of a flat slab in space, with part of the curved slab acting as a transverse arch band between columns. This arch band is the three-dimensional equivalent to the column strip of the flat slab design. The width of the arch band will be narrow at the supports and high stress concentrations will surely result. On the other hand, it will be wide at the crown, where a considerable portion of the shell will participate with the arch band in resisting deformation.

Without going to the extreme of "no ribs," inspect what happens to the action of the conventional multiple barrel shell as the size of the stiffeners is decreased. As the size of the ribs is decreased, a transverse strip of the shell over the columns will increasingly take over the supporting function of the rib. The thin shell strip or arch band has little stiffness and a small moment of inertia. Because of this, a thin arch band is less sensitive to footing movements or temperature variations than is a deep rib. Furthermore, bending moments  $M_\phi$  in such arch bands can be held relatively small, and the reduced stiffness of such an arch band is not objectionable as long as: (1) The loads are symmetrical; (2) the centroidal axis of the shell does not deviate greatly from the thrust line; and (3) the tops of the columns are prevented from appreciable horizontal movement. (Prevention of movement may either be due to great column stiffness or the uniform character of the loading of adjacent shells.)

Where the loads are predominantly unsymmetrical, or where horizontal loads as caused by earthquakes must be resisted, the bending moments in the arch bands can be large. For such loads, ribs with substantial moments of inertia are better suited to resist moments than a thin shell strip or arch band.

#### THEORETICAL VERSUS EXPERIMENTAL RESULTS

In 1948, the writer was involved in the design and construction of a multiple barrel shell roof of 50 ft by 50 ft spans for the Western Electric Company at Denver, Colo. The flashing problems in connection with the ribs above this roof reemphasized the desirability of having shells without projecting ribs. Calculations were made for an alternate design using heavier columns and a flexible roof, with arch bands taking the place of the ribs, and in which loading conditions identical to those in the original design were used. Insulation and roofing were required to extend over the arch bands. The calculations indicated that the design was structurally and economically feasible.

The feasibility of the ribless shell aroused considerable interest, however; it was felt that certain design assumptions would require verification before



the design could be considered successful. To obtain such verification, a series of laboratory and field tests of certain kinds of shell structures were conducted.

*Tests at Lehigh University.*—Tests were conducted at Lehigh Univ., Bethlehem, Pa., by Bruno Thürlimann, M. ASCE, M. IABSE and Bruce G. Johnston, F. ASCE.<sup>2</sup> The tests were conducted on a steel model of an actual cylindrical concrete shell roof, in the approximate ratio of 1 to 30. The steel model was equipped with conventional ribs, and their influence on the behavior of the shell was studied. A comparison of the experimental and theoretical results showed that a certain contributing width of the shell participated with the rib in resisting deformations. The comparison confirmed the validity of analytical expressions that had been used for the determination of an effective width of a cylindrical shell acting with the ribs.

*Tests at Harvey.*—Tests were conducted by Roberts and Schaefer Company of a concrete ribless shell structure, erected at Harvey, Ill., in 1950. The test structure basically was a 1:3 scale model of the Western Electric ribless shell prototype. It consisted of four barrel shells, continuous in the transverse direction and simply supported with an overhang in the longitudinal direction. Fig. 3 indicates the over-all dimensions of the structure. Each barrel has a span of 15 ft center to center of columns, and a length of 27 ft. The columns, of circular section, are spaced 18 ft in the longitudinal direction, providing a cantilever shell of 9 ft overhang. The overhang was provided to produce negative moments about a transverse axis comparable to those found along a line of interior columns in a continuous test structure. The height of the columns was increased disproportionately for the test structure so that the structure, after completion of the tests, could be used as a garage and storage building. Temporary tension ties were provided at the springing line at the columns to stabilize the structure during construction of successive bays. These ties also were used for the application of horizontal forces and lateral movements during the tests. Fig. 4 shows a view of the structure.

The cross-sections of the structure, at the column strip and at the midspan of the shell, are shown in Fig. 5. The shell thickness varies from 1 1/2 in. within the central region to 2 1/2 in. within the rib band. The rib band itself is a thickened strip of the shell extending across the barrels along the column lines; the width of the strip being 7 ft for the interior line of columns and 4 ft 6 in. for the exterior line of columns. Further, it was deemed advisable to increase the thickness of the shell in the region of the springing line.

During the tests, both horizontal and vertical movements were measured at various points of the shell and edge members of a test bay. These measurements were made by means of dial gages supported by a framework of 6 in. channels. The framework consisted of a series of longitudinal and transverse channels attached to a test bay. The framework was so articulated that relative as well as absolute movements could be determined for each point.

Strains were measured of the shell, columns, and edge members of a test bay. Type A-7 and A-12 SR-4 gages were used throughout to measure strains in the interiors of the various members. A few of the A-9 type (which has a 6 in. gage length) were placed on the surface of the shell to obtain the average strain in a long gage length. Dummy gages of each type were placed in unrestrained sections of concrete simulating in thickness the edge member and shell to compensate for the effects of temperature changes.

<sup>2</sup> "Analysis and Tests of a Cylindrical Shell Roof Model," by Bruno Thürlimann, and Bruce G. Johnston, *Proc.-Sep. No. 434*, ASCE, Vol. 80, April, 1954.

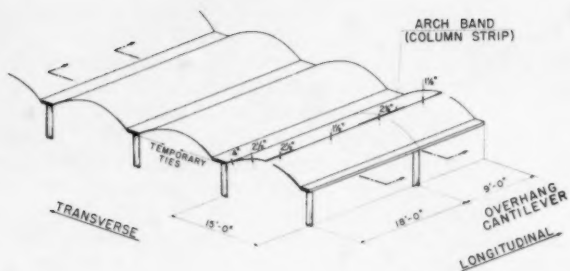


FIG. 3

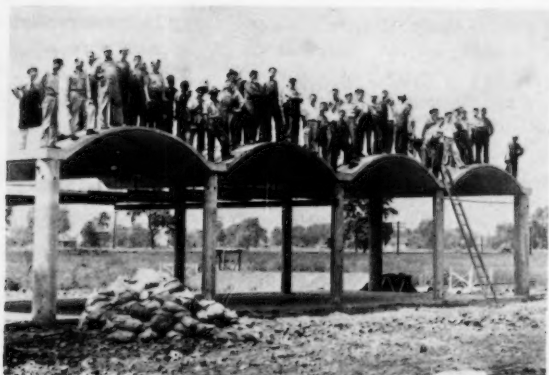


FIG. 4

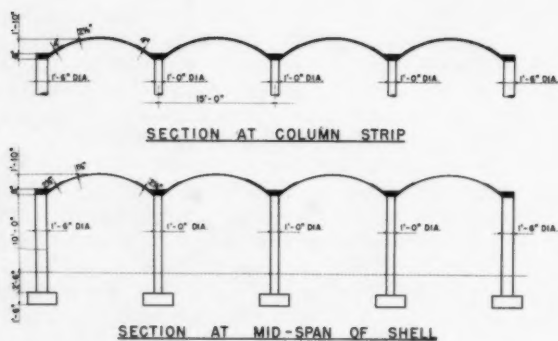


FIG. 5



Much care was observed in the preparation and placement of the gages. Particular mention only is made of the gages placed in the shell and edge member. These were prepared in advance and positioned before placing the concrete. Pencil rods of 3/16 in. square cold rolled steel were used. The rods were cut into 30 in. lengths and notched at approximately 2 in. intervals to insure adequate bonding with the concrete. The area of the rod to which the gage was to be attached was thoroughly cleaned with acetone and the gage cemented into place with Duco cement. This was allowed to dry for 24 hr with a slight pressure applied after the first 2 hr of drying. After a 24 hr drying period a coating of Petrolastic asphalt was applied. The asphalt was heated to a very fluid consistency and applied by pouring it over the gage with a spoon. The gage leads were then soldered to 15 in. lengths of moisture proof wire. The wire leads were then taped to the bar, and a second layer of asphalt was applied, covering the gage and lead wire connections. A hot knife blade was used to trim the bulb of asphalt and to seal any pin point openings. This bulb of asphalt was kept as small as possible.

The day prior to placing the concrete of the test shell, the pencil rods with gages attached were wired in place. Because these gages were intended to record only the normal forces present in the shell, care was taken to place them as near the center of the shell thickness as possible.

Several loading conditions were used during the tests. One of these was a load intensity of 50 psf placed over an interior test bay. The load was applied by means of ballast in 50 lb bags each. A test cycle consisted of placing and removing the entire load in six separate steps. All testing was done at night to reduce temperature effects to a minimum. The 50 lb test cycle was done on two consecutive nights. A load of 100 psf was applied and removed during one night in a three step cycle. Half loading was applied on the cantilever. Measurements were made for a concentrated load of 4500 lb (over a 16 sq ft area) placed at the crown and midway between rib bands, and for a concentrated load of 2900 lb (over an 8 sq ft area) placed at the crown at the free end of the cantilever.

Readings also were taken for an inward thrust applied at the tops of the interior columns by means of the tension ties. The load in the tension tie was determined by means of attached electrical gages. Test cylinders and beams were made during the various concrete placing operations and the modulus of elasticity and concrete strength were determined at the time of tests.

*Results of Harvey Tests.*—The results of the Harvey tests are summarized and compared to those of theory in Figs. 6 to 11. The symbols are those used in the ASCE publication dealing with shells.<sup>3</sup> The values of moments, indicated as measured, are based on deflection readings, whereas, those of the shell forces, indicated as measured, are based on strain gage readings. Solid lines indicate values obtained by theory, and small circles indicate values based on measurement.

Fig. 6 shows values of moments in the multiple frame formed by the columns and the column strip of the shell. The values are for a unit roof load on the second panel of the shell, with the panel fully loaded and one side loaded. The values of moments in the second panel are drawn to a larger scale in Fig. 7 and are for the same load distributions as in Fig. 6, except

<sup>3</sup> "Design of Cylindrical Concrete Shell Roofs," by the Committee on Masonry and Reinforced Concrete of the Structural Div., ASCE, Manual of Engineering Practice, No. 31, 1952.

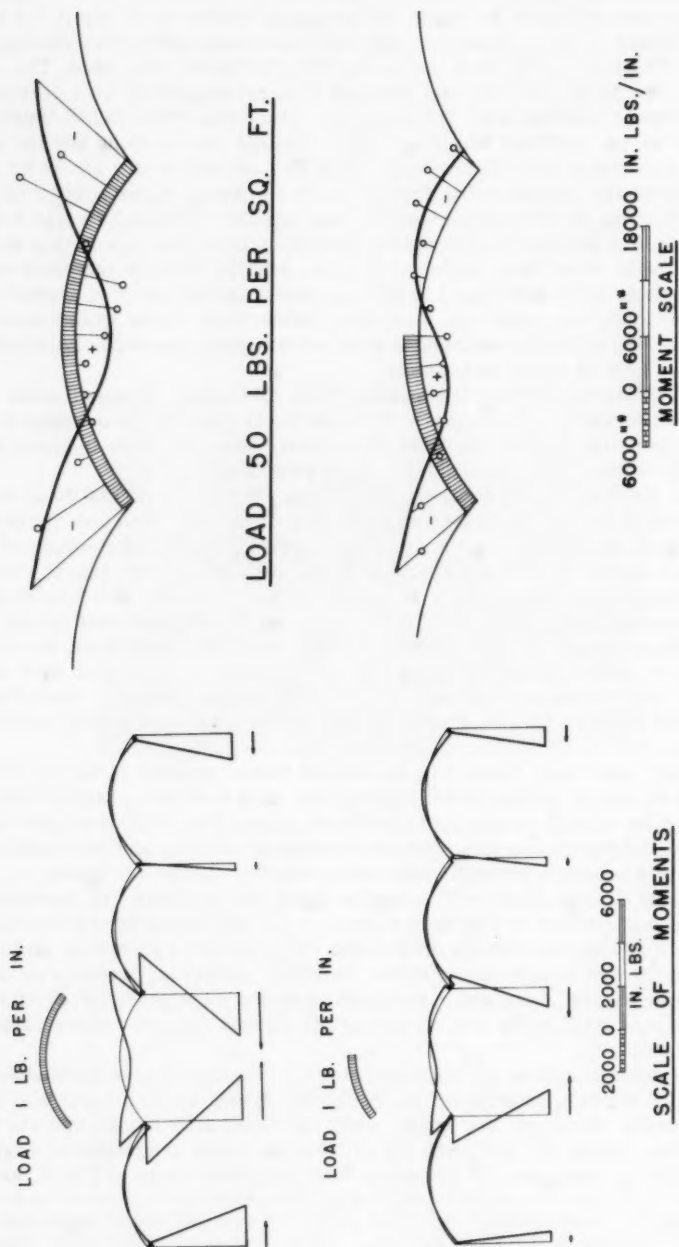


FIG. 6

FIG. 7.—THEORETICAL AND MEASURED MOMENTS — ARCH BAND

that the load is 50 psf. Fig. 7 shows the calculated and measured moments in the column strip of the shell. In Fig. 8, a comparison is given of the theoretical and measured vertical deflections of the arch band at the same locations, with the second panel fully loaded. The comparison shows good agreement between the two sets of values.

In Figs. 9 a summary is given of the character of the forces in the shell, as caused by shell action, when the second panel is fully loaded. Some of these forces were measured and checked well with the calculated values. In Fig. 9(a),  $T_x$  denotes the longitudinal force at mid span in pounds per inch of shell strip, and  $S$  is the shear force per unit of length at the column strip. The negative values of  $T_x$  denote compression in the shell, and the positive values denote tension at the valley edge members. In Fig. 9(b),  $T_\phi$  is the force in the ring direction in pounds per inch of shell width, and  $M_\phi$  is the transverse bending moment caused by shell action. The diagram for  $T_\phi$  indicates a large value of  $T_\phi$  at the crown of the loaded panel and a small value of the force at the springing line.

A comparison is given in Fig. 10 of the measured and calculated values of  $M_\phi$  when the second panel is loaded with 50 psf. The values of  $M_\phi$  are at the center of the loaded span and at the end of the cantilever. Note that the character of these curves is different from that shown for  $M_\phi$  in Fig. 9(b). The difference between the two sets of curves is caused mainly by the horizontal translation of the edge members when the second panel is fully loaded. The moments in the ring direction caused by the spreading of the edge members overshadow those caused by shell action.

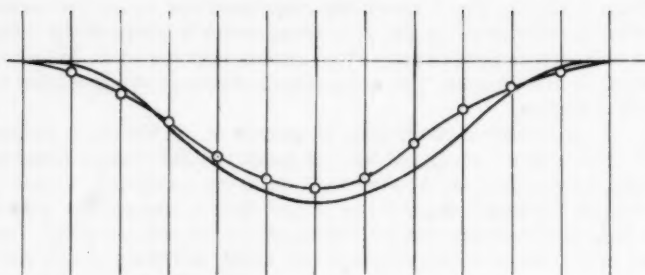
Fig. 11 shows values of longitudinal moments,  $M_x$ , along the crown of the shell when the entire shell, including the cantilever portion, is loaded. The dotted peaked line indicates the calculated values of  $M_x$  for a conventional shell restrained by a rib. The smooth curved line is drawn through some of the measured values and indicates the values of  $M_x$  which were actually developed in the vicinity of the shallow arch band. In Fig. 11, the diagrams for the forces  $T_x$  along the edge member are for the simple span fully loaded and the cantilever portion not loaded. The calculated values of  $T_x$  follow a parabolic distribution of moments.

*Analysis of Tests.*—The most valuable information was obtained by means of the deflection measurements. The information that was obtained by means of the electrical strain gages placed in the transverse direction was meager. This was because of the difficulty in placing and then holding these gages at the center of a very thin slab. The gages placed in the longitudinal direction were of greater value because, in this direction, the stresses in the shell are predominantly axial. The gages in the column gave valuable data that probably could not have been obtained by other means.

The test load of 50 psf produced stresses of such small values that in many instances the expected drift of the strain gage indicator was of the same magnitude as the reading produced by the strains. More significant results were obtained with the 100 psf load.

The results of the Harvey tests justified earlier design assumptions. The designers were reassured that the shell of the Western Electric prototype, in spite of the use of slab bands instead of ribs, had sufficient safety against buckling and should be satisfactory in all other respects.

It is recommended that arch bands of such structures be treated as arches. The magnitude of the forces that are calculated in this way will often determine



0 0.1" 0.2" 0.3" 0.4"

## VERTICAL DEFLECTION

FIG. 8.—THEORETICAL AND MEASURED ARCH DEFLECTION DUE TO FULL LOAD

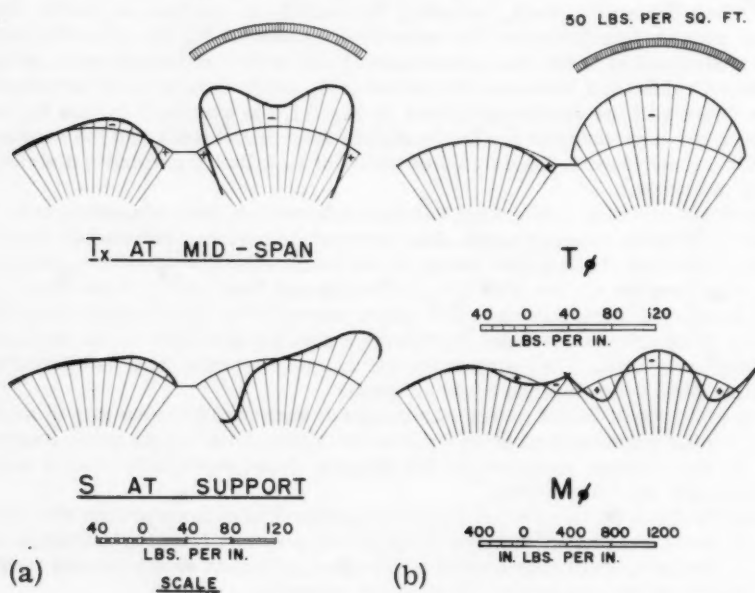
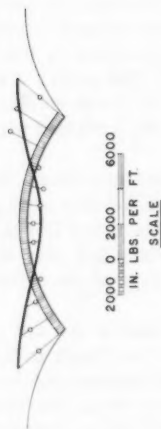
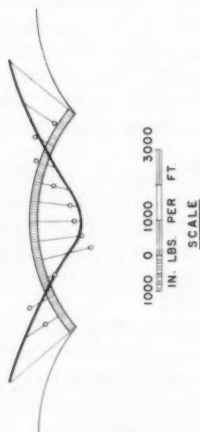


FIG. 9.—SHELL FORCES

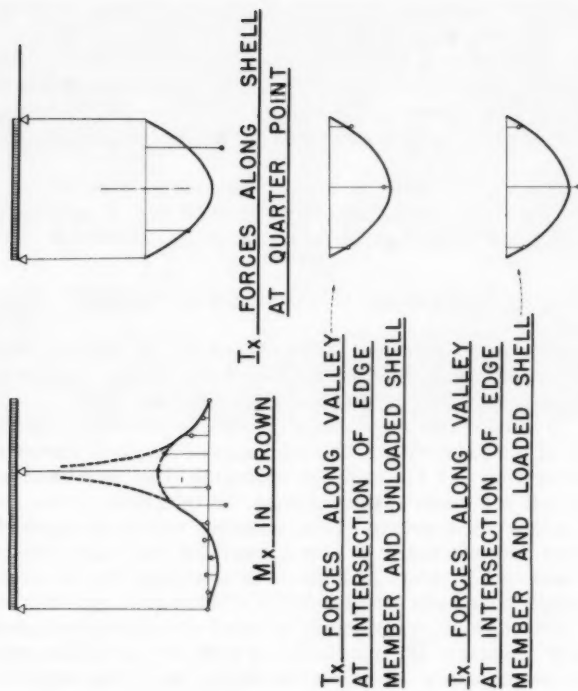
LOAD 50 LBS. PER SQ. FT.



AT THE CENTER OF THE LONGITUDINAL SPAN



AT THE END OF THE CANTILEVER

FIG. 10.—THEORETICAL AND MEASURED SHELL MOMENTS,  $M\phi$ 
 $I_x$  FORCES ALONG SHELL  
AT QUARTER POINT

 $M_x$  IN CROWN

 $I_x$  FORCES ALONG VALLEY  
AT INTERSECTION OF EDGE  
MEMBER AND UNLOADED SHELL

 $I_x$  FORCES ALONG VALLEY  
AT INTERSECTION OF EDGE  
MEMBER AND LOADED SHELL

FIG. 11.—THEORETICAL AND MEASURED VALUES

the actual width required for an arch band. It is suggested that the contributing width of the shell, including the slab band, be assumed as  $K\sqrt{Rt}$ , in which  $R$  is the radius and  $t$  the thickness of the shell. The value of  $K$  may be taken from the curves presented by Thürlimann and Johnston.<sup>2</sup> These curves are, however, based on a fully restrained shell. For a hinged condition, the value of  $K$  is one-half of that shown in the curves. Consequently, the proper value of  $K$  for a ribless shell is somewhere between one-half and one times that shown in the curves.

It is recommended that the actual longitudinal span (center line to center line of arch band) be used in the calculations of  $T_x$ . A reduction seems justified in the maximum theoretical values of the moments  $M_x$ .

### EXAMPLES OF ACTUAL STRUCTURES

*Western Electric Structure.*—Fig. 12 shows an interior view of the 50 ft span structure that was built for the Western Electric Company in 1948. This structure was built with conventional ribs above the roof.

In Fig. 13 dimensions are shown of the ribless prototype, taking into account the results of the Harvey tests. The thickness of the shell varies from 3 3/4 in. at the mid section to 5 1/2 in at the springing. The arch band is 17 ft wide at the crown and 9 ft wide at the columns. Its thickness varies from 7 in at the center to 10 in. at the supports. (This compares with a rib depth of 3 ft 3 in. for the structure that was built). A cost comparison was made between the ribless prototype and the structure as built. It is estimated that an over-all saving of about 5% might have been effected if the ribless prototype had been built.

*Shells Without Ribs.*—A number of shell structures designed for the Lone Star Cement Company are mentioned as examples of shells without arch ribs or thickened arch bands. The transverse spans of these structures vary from 25 ft to 77 ft, and the longitudinal spacings of columns vary from 16 ft to 21 ft. For these structures, arch action dominates and tension ties are used at the column lines. Concrete thicknesses vary from 3 in. to 5 in. for the smallest shell and from 6 in to 8 in. for the largest shell as determined by unsymmetrical loading considerations. This thickness was determined by the requirements of the arch band at the crown. At this location, the active width of the arch band is theoretically greater than the distance between tension ties, whereas the width narrows near the columns where the greatest stress concentrations occur.

*Air Force Installation.*—A 400 ft wide warehouse covering an area of 640,000 sq ft was constructed during 1958 at Olmsted Air Force Base in Pennsylvania. The structure, built under the direction of the Corps of Engineers, United States Army Engineer District, Baltimore, Md. was of a modified multiple ribless barrel shell design. The dimensions of the structure are shown in Figs. 14 and 15.

Note that the column spacing is 39 ft by 66 ft. The shells are not ribless in the sense of the Western Electric prototype. They are 3 in. thick in the central portion and increase in thickness near the arch band. However, the top surface of the roof has no sharp projections. The construction of the rib bands, protruding 9 in. below the ceiling, was not considered a serious interference to the movement of formwork. Because of the loads imposed by the 66 ft span, the depth of the rib-band was made 15 in. The rib-bands and columns were

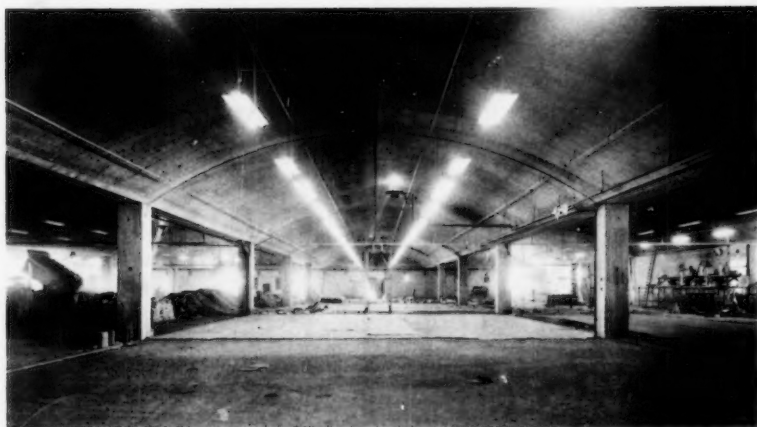


FIG. 12

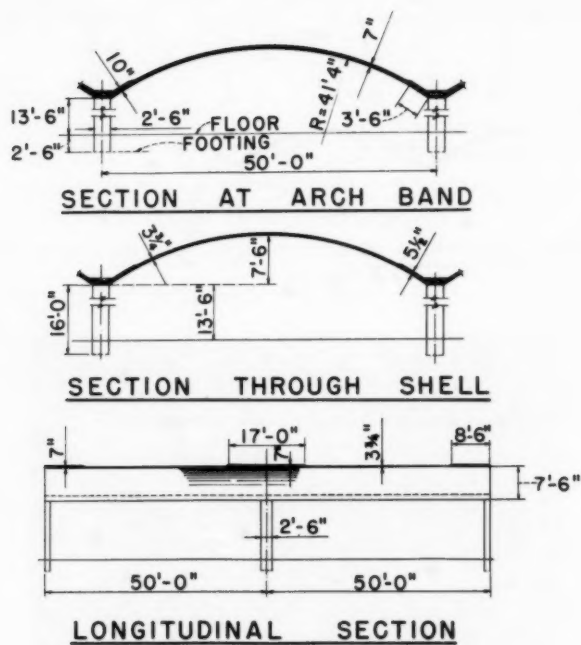


FIG. 13.—WESTERN ELECTRIC RIBLESS SHELL PROTOTYPE



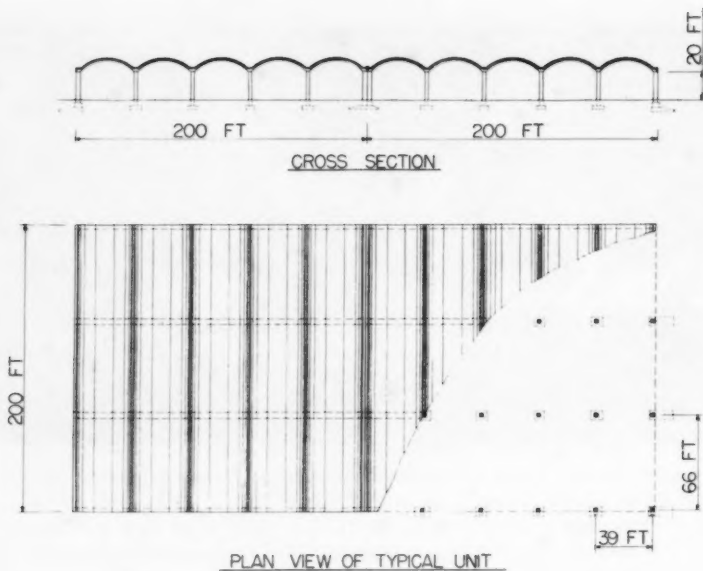


FIG. 14

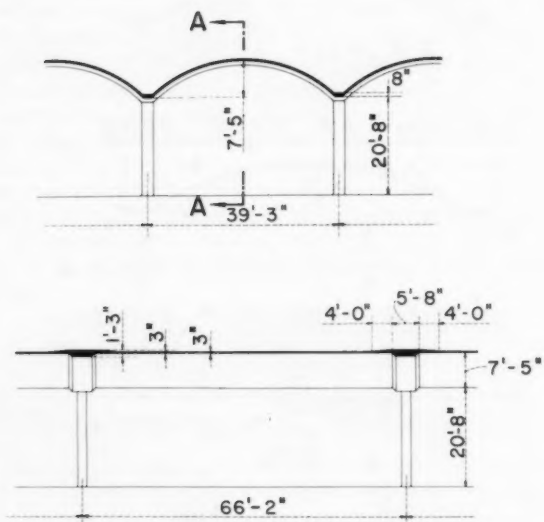


FIG. 15



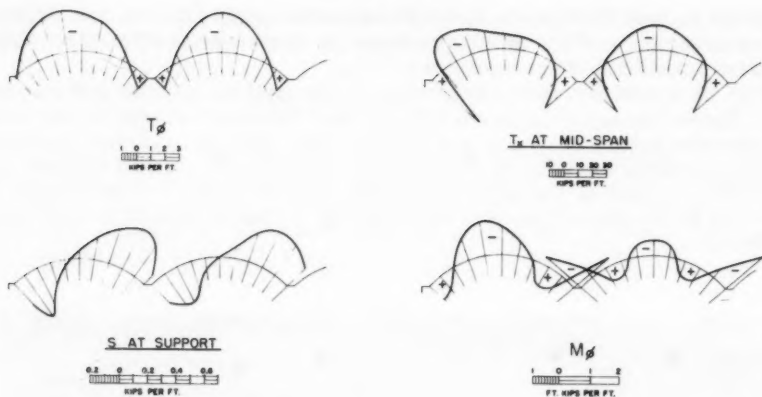


FIG. 16.—SHELL FORCES IN EXTERIOR AND INTERIOR BAYS OF 5-BAY WAREHOUSE STRUCTURE UNDER DEAD LOAD AND 30 PSF FULL LIVE LOAD

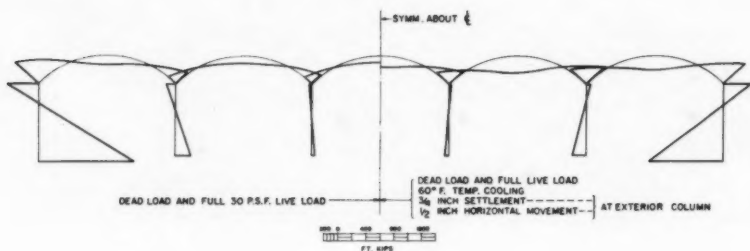


FIG. 17.—MOMENTS IN ELASTIC FRAME OF WAREHOUSE STRUCTURE

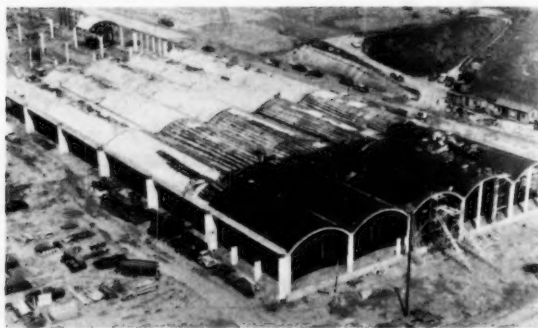


FIG. 18

analyzed as multiple frames. It should be mentioned that the interior footings are symmetrical and the exterior footings are shaped to take the thrust at the exterior boundaries of the warehouse.

Fig. 16 shows the calculated forces in the shell for interior and exterior bays. These forces are for the condition in which the exterior edge is supported by intermediate columns and the interior edge member is freely spanning. Note the positive values of  $T_\phi$  at the interior edge member. These indicate that the valley portion of the structure hangs from the shell. The distribution of moments in the elastic frame is shown in Fig. 17 and is similar to that shown in Fig. 6.

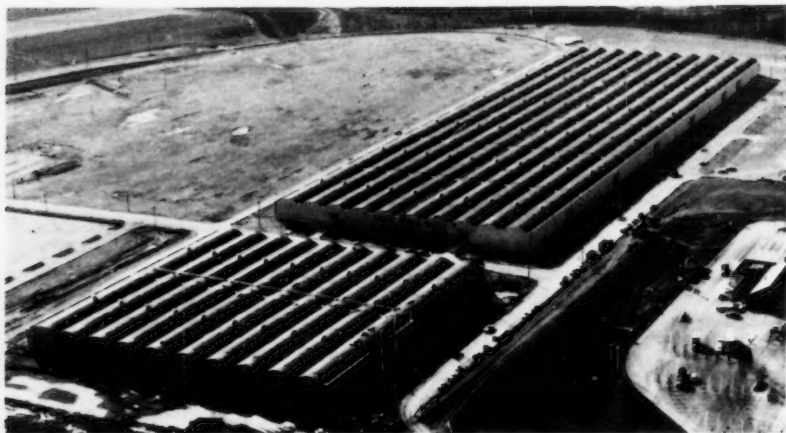


FIG. 19

Fig. 18 and Fig. 19 show other views of this modified multiple ribless shell. (For further details and the relative economy of this structure see the Appendix).

### CONCLUSIONS

It does not seem advisable, at this time, to construct multiple ribless shells with spans greater than 50 ft. For spans less than 50 ft, the arch bands and columns can be treated as multiple elastic frames. The loads to be taken on these frames are the actual loads and the shears transferred from the shell to the arch band. Stress concentrations in the vicinity of column tops require substantial concrete sections in these areas.

The horizontal deformations of intersecting edges may be quite considerable because of the flexibility of columns and arch bands, particularly when non uniform loads are on the structure. In such a case, the edges of a loaded shell may spread, producing large moments  $M_\phi$  in addition to those that usually exist. This can be especially important for the exterior shells of a multiple shell structure.

Based on tests and large scale installations, multiple ribless shells have proved to be feasible, practical, and economical.

#### ACKNOWLEDGMENT

The writer wishes to express his appreciation to Otto Gruenwald, who made the required design calculations, and to Walter A. Renner, M. ASCE, who planned and supervised the Harvey shell tests. This paper is based on a talk delivered by the writer at the June, 1956, Meeting of the American Society of Civil Engineers at Knoxville, Tenn.

---

#### APPENDIX.—ECONOMIES AND DETAILS OF AIR FORCE INSTALLATION

---

The design of the United States Air Force warehouse shown in Figs. 14, 15, 18, and 19 was the result of prolonged study and the research program de-

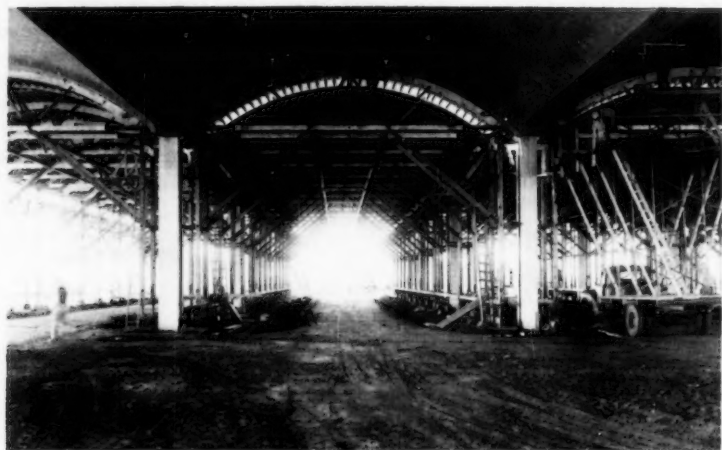


FIG. 20

scribed in this paper. This design replaced the standard Air Force warehouse which consisted of cast-in-place reinforced concrete rigid frames and a pre-cast roof deck. Both structures have comparable spans, clearances, and utilities.

In 1952, alternate bids on the 800,000 sq ft warehouse at Wilkins Air Force Base showed a saving for the modified ribless shell over the cast-in-place reinforced concrete rigid frame design. For administrative reasons, all bids were rejected at that time. In May, 1957, the bidding for 640,000 sq ft of warehouse area at Olmsted Air Force Base provided a comparison between the

cast-in-place shell design as described and a comparable precast concrete shell structure. All of the six bidders proposed to build the cast-in-place shell structure for less than the precast type. The accepted bid on the complete installation, as built, was \$5.80 per sq ft. (Included are heavy duty floor, waterproofed concrete block walls, cast-in-place fire walls, insulation, 5-ply roofing, aluminum flashing and joints, sprinklers, heating, lighting, ventilation, plumbing, drainage, and office space. Not included are grading and heating plant.) The cost of the precast alternate proved about 50¢ per sq ft higher. The unit cost of the cast-in-place barrel shell structural frame, above floor level, as shown in Fig. 15, was about \$1.85 per sq ft. Cast-in-place shell structures of this type, covering large floor areas, apparently are economical solutions, because it costs less to move a form centering with a built-in manufacturing plant along a building site than to move precast elements from a central plant over the same site and then pay additionally for their erection.

The contractor, Ritter Brothers of Harrisburg, Pa., found it economical to build an efficient job-site manufacturing plant. The contractor was the first to move form centering trusses for a shell roof with the use of a rubber-tired trailer with hydraulic raising and lowering devices, handling an entire forming unit of 39 ft by 33 ft plan area at one time.

Fig. 20 shows the form centering in place. Construction proceeded 5 bays wide with forms provided for a 200 ft by 200 ft area and used 16 times. After casting one half-width of the full length structure, the centering was rolled beyond the building area and moved sideways. Construction of the second half of the warehouse followed with forms travelling in opposite direction.

The engineers were concerned with the horizontal translation at the springing line of rib-bands, due to elastic deformation, footing rotation, and creep. The measured translations were below  $\frac{1}{4}$  in. This was in close agreement with predicted values. Masonry wall details provided for these movements.

---

Journal of the  
STRUCTURAL DIVISION  
Proceedings of the American Society of Civil Engineers

---

DEFLECTION THEORY OF ARCHES

By S. O. Asplund,<sup>1</sup> F. ASCE

---

SYNOPSIS

Influence coefficient expressions are developed in matrix form for all section forces of an arch. The influence coefficients include the effects of the vertical and horizontal displacements of the arch axis and, of course, the effects of bending and shear deformations and rib shortening. Temperature and inelasticity effects are referred to correction terms.

The practical usefulness of this method is based largely on the fact that total horizontal force is selected for "iteration parameter." Iterations often become superfluous because live load variations and arch displacements exert little influence on this parameter.

---

POLYGON ANGLES AND ANGLE BREAKS

The corner  $k$  of a polygon  $0, 1, \dots, j, k, l, \dots, m, n$ , Fig. 1, is located at  $x_k, z_k$  in a rectangular coordinate frame  $Cxz$ . The polygon side "angle"  $A_{jk}$  is defined by

$$A_{jk} = \frac{z_k - z_j}{x_k - x_j} = \frac{z_{jk}}{x_{jk}} \dots \dots \dots (1)$$

All these angles are given by the matrix formula (10)<sup>2</sup>

$$\Delta x^{-1} dz = X' z = A \dots \dots \dots (2)$$

---

Note.—Discussion open until March 1, 1962. To extend the closing date one month, a written request must be filed with the Executive Secretary, ASCE. This paper is part of the copyrighted Journal of the Structural Division, Proceedings of the American Society of Civil Engineers, Vol. 87, No. ST 7, October, 1961.

<sup>1</sup> Prof., Chalmers Inst. of Tech., Gothenburg, Sweden.

<sup>2</sup> Numerals in parentheses refer to corresponding items listed in Appendix.

in which

$$\Delta x = \begin{bmatrix} x_{01} & 0 & . & . \\ 0 & x_{12} & . & . \\ . & . & . & . \\ . & . & . & x_{mn} \end{bmatrix}, d = \begin{bmatrix} 1 & 0 & 0 & . \\ -1 & 1 & 0 & . \\ 0 & -1 & 1 & . \\ . & . & . & . \end{bmatrix}, z = \begin{bmatrix} z_1 \\ z_2 \\ . \\ z_m \end{bmatrix}, A = \begin{bmatrix} A_{01} \\ A_{12} \\ . \\ A_{mn} \end{bmatrix} \dots (3)$$

in which  $d$  is the first difference operator, and  $X$  denotes the first difference quotient operator.

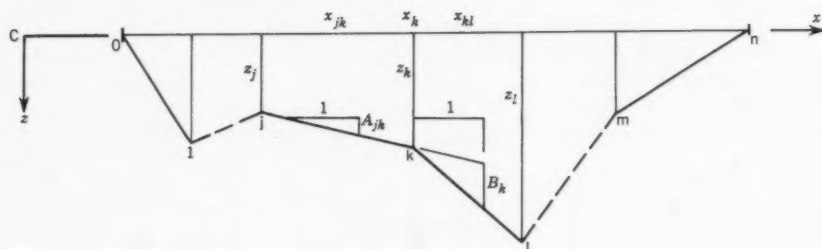


FIG. 1

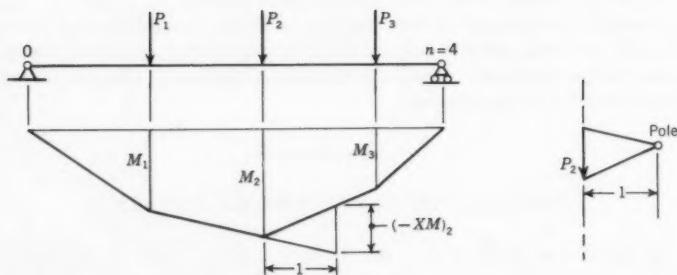


FIG. 2

The angle break  $B_k$  defined as in Fig. 1 is

$$B_k = A_{kl} - A_{jk} = \frac{z_l - z_k}{x_l - x_k} - \frac{z_k - z_j}{x_k - x_j} = \frac{z_{kl}}{x_{kl}} - \frac{z_{jk}}{x_{jk}} \dots (4)$$

All the angle breaks are in matrix form

$$B = -d^* A = -d^* \Delta x^{-1} dz = X z, X = -d^* \Delta x^{-1} d = -d^* X' \dots (5)$$

in which

$$X = \begin{bmatrix} -1/x_{01} & -1/x_{12} & 1/x_{12} & 0 & 0 \\ 1/x_{12} & -1/x_{12} & -1/x_{23} & 1/x_{23} & 0 \\ . & . & . & . & . \end{bmatrix}, B = \begin{bmatrix} B_1 \\ . \\ B_m \end{bmatrix} \dots (6)$$

The symbol  $X''$  could have been written instead of  $X$ , but this symbol is going to be used so frequently that the shorter notation  $X$  seems more practicable. The reader should verify the previous formulas carefully. Note that the boundary conditions  $z_0 = z_n = 0$  are included in the first and last of the equations  $B = Xz$ . Other linear boundary conditions can be handled. The first and second difference operator characters of  $X'$  and  $X$  in Eqs. 2 and 5 are revealed by (1) and (4).

### BEAM MOMENTS

The moment polygon for the simple beam, Fig. 2, may be obtained by drawing a string polygon with unit horizontal force on the vertical loads  $P$ . From Fig. 2 the negative angle break in the string polygon at  $k$  is seen to equal the load  $P_k$ . Therefore

$$-X M = P \dots (7)$$

Eq. 7 corresponds to the continuous differential equation

$$-M'' = p(x) \dots (8)$$

The term  $X$  is seen to be second difference operator. To solve  $-M'' = p$ , boundary conditions must be added whereas Eq. 7 can be solved directly, because  $X$  already contains the boundary conditions. Premultiplication by the negative inverse of  $X$  gives

$$M = -X^{-1} p \dots (9)$$

### BAND MATRIX INVERSION

The inversion of the three-diagonal band matrix  $X$  can be performed by a general band-matrix inversion method (11), (12). The writer has (12) inverted a band matrix of order  $n$  in approximately  $2n^2$  multiplications, whereas Gauss's inversion requires about  $5n^3/6$  multiplications. Because of the time-saving involved methods that call for the inversion of high order, full matrices should be avoided when methods calling for only band matrix inversions are possible.

### INFLUENCE COEFFICIENTS.—FORCE TRANSFORMATIONS

Eq. 9 is an influence coefficient formula, because each effect  $M$  is obtained by multiplying each load in the column  $P$  by the associated element in the row of  $-X^{-1}$  and adding the products, just as is done in all applications of the influence line method. Thus, in Eq. 9 the influence coefficients are  $M^i = -X^{-1}$ , so Eq. 9 can also be written as

$$M = M^1 P \dots\dots\dots (10)$$

In fact, the aforementioned band matrix inversion of  $X$  results in the well-known expressions for the influence line ordinates for a simple beam (11), (12)

$$X^{-1} = \begin{bmatrix} x_{01}x_{1n} & x_{01}x_{2n} & \cdot \\ x_{01}x_{2n} & x_{02}x_{2n} & \cdot \\ \cdot & \cdot & \cdot \end{bmatrix} \frac{1}{-x_{0n}} \dots\dots\dots (11)$$

From the point of view of the general matrix theory for indeterminate structures the matrix  $-X^{-1}$  in Eq. 9 can also be identified with the force transformation  $C$  that transforms, in the auxiliary, the (external) structure loads  $P$  into the member (segment) loads  $M$ .

#### TRANSVERSE FORCE

The transverse or vertical force  $V$  in a simple beam segment between two nearby loads equals the increment in moment divided by the segment length

$$\frac{(M_1 - M_k)}{x_{kl}} = V_{kl} \dots\dots\dots (12)$$

or by Eqs. 1 and 2

$$X' M = \Delta x^{-1} dM = V \dots\dots\dots (13)$$

The decrease in vertical force at a load  $k$  equals that load

$$V_{jk} - V_{kl} = P_k \dots\dots\dots (14)$$

or by Eqs. 4, 5, and 13

$$d^* V = d^* \Delta x^{-1} dM = -X M = P \dots\dots\dots (15)$$

#### BENDING DEFORMATIONS

The bending moments  $M$  in Fig. 2 deflect the beam by  $w$ , Fig. 3. The chords to the deflection curve are drawn in the segments  $x_{jk}$  and  $x_{kl}$ . The negative angle break at  $k$  between these chords is obviously  $(-X w)_k$ , which should be compared with Eq. 4. The slope deflection at  $k$  between the chord in  $x_{jk}$  and the tangent to the elastic line at  $k$  is  $f_{jk}^c M_j + f_{kj} M_k$  in which  $f_{kj}$  is the end flexibility at the end  $k$  of the beam  $jk$  and  $f_{jk}^c$  the cross flexibility of the same beam, Fig. 4. Variable flexibility of the beam segment is regarded by coefficients  $K$  and  $K^c$  and the influence of an axial force by factors  $\psi$  and  $\phi$  in

$$f_{kj} = \frac{s_{jk}}{3 E I} \frac{\psi_{kj}}{K_{kj}}, \quad f_{jk}^c = \frac{s_{jk}}{6 E I} \frac{\phi_{jk}}{K_{jk}^c} \dots\dots\dots (16)$$



in which  $K$  denotes the correction factors for variable  $E I$ ,  $E$  is the modulus of elasticity, and  $I$  refers to the moment of inertia. For a horizontal beam  $s_{ik} = x_{ik}$ . Further, the end angle between the deflection curve tangent at  $k$  and the

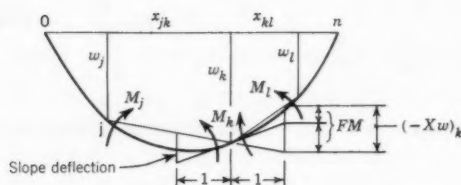


FIG. 3



FIG. 4

chord  $kl$  is  $f_{kl} M_k + f_{kl}^c M_l$ . The sum of this slope deflection  $kl$  and the slope deflection  $kj$  equals  $(-Xw)_k$

$$f_{jk}^c M_j + f_{kj} M_k + f_{kl} M_k + f_{kl}^c M_l = (-Xw)_k \quad \dots \dots \dots (17)$$

or for all segment boundaries

$$F^b M = -Xw \quad \dots \dots \dots (18)$$

with

$$F^b = \begin{bmatrix} f_{10} + f_{12} & f_{12}^c & 0 \\ f_{12}^c & f_{21} + f_{23} & f_{23}^c \\ f_{23}^c & f_{23}^c & f_{23}^c \end{bmatrix} \quad \dots \dots \dots (19)$$

in which  $F^b$  describes bending flexibility.

Mohr replaced the negative angle breaks between the segment chords of the deflection curve with elastic weights, often called angle weights. The angle weights  $-Xw$  caused by bending thus equal the slope deflection angle weights  $F^b M$ .

### SHEAR DEFORMATIONS

The transverse forces

$$T_{jk} = \frac{(M_k - M_j)}{s_{jk}} \quad \dots \dots \dots (20)$$

cause shear deformations

$$\gamma_{jk} = \left( \frac{\beta}{GA} \right)_{jk} T_{jk} \quad \dots \dots \dots (21)$$

in the beam segments, in which  $\beta$  is the shear shape factor. The difference  $\gamma_{jk} - \gamma_{kl}$ , Fig. 5, between the shear deformations of the two segments meeting at  $k$  forms additional shear angle weights  $F^S M$  in which

$$F^S = \begin{bmatrix} f_{10}^S + f_{12}^S & -f_{12}^S & 0 \\ -f_{12}^S & f_{21}^S + f_{23}^S - f_{23}^S \end{bmatrix}, \quad f_{jk}^S = \frac{\beta_{jk}}{(GA)_{jk}} \quad \dots (22)$$

in which  $F^S$  describes shear flexibility and  $G$  denotes the modulus of elasticity in shear.

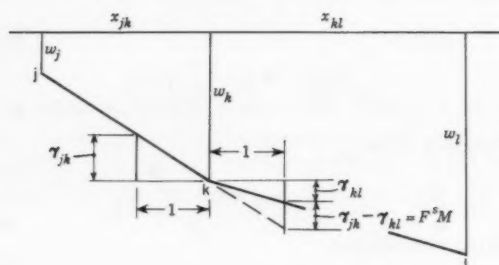


FIG. 5

### DEFLECTION CURVE CHORD POLYGON

From the preceding analysis

$$-X w = F^b M + F^S M \quad \dots (23)$$

or

$$F M = -X w \quad \dots (24a)$$

with

$$F = F^b + F^S \quad \dots (24b)$$

in which  $F$  denotes the beam and arch flexibility.

The moment of the vertical angle weights  $F M$  is, by Eq. 9,  $-X^{-1} F M$ . This value, by Eq. 24 equals the deflection  $w$  which motivates the method of elastic weights.

The same boundary conditions for  $M$  as in Eq. 7 are expressed in the first and last terms of Eq. 24, in this case  $M_0 = M_n = 0$ . On the right hand side of Eq. 24 (a) we express in  $X$  the boundary conditions for  $w$ . For a simple girder these boundary conditions are  $w_0 = w_n = 0$ . When the boundary conditions for  $M$  and  $w$  are different, different notations are used for  $X^n$  and  $X^W$ .

The continuous counterpart of

$$F^b M = - X w \dots\dots\dots (25)$$

is the bending differential equation

$$\frac{M}{E I} = - w'' \dots\dots\dots (26)$$

in which  $- w''$  corresponds to  $- X w$ . The sum of the elements in each row of  $F^b$ , or  $f_{jk}^c + f_{kj} + f_{kl} + f_{kl}^c$ , equals  $\frac{s_{jk}}{E I}$  when all  $s_{jk} = s_{kl}$ . In this way  $F^b$  corresponds to  $1/E I$ .

Boundary conditions must be added to solve the differential equation, but Eqs. 24 include the boundary conditions and can be solved directly

$$w = - X^{-1} F M \dots\dots\dots (27)$$

Here the band matrix inversion can be used again.

In the general matrix theory for indeterminate structures (14) it is also shown (Krohn's theorem) that the deformations  $F M$  are transformed by the transposed force transformation  $C^*$  into the structure displacement  $w$ . Thus

$$C^* F M = w \dots\dots\dots (28)$$

and it is again seen that

$$- X^{-1} F M = w \dots\dots\dots (29)$$

### THE ARCH

An elastic arch 1, 2, ..,  $m$  as in Fig. 6(a) is fixed at 1 and  $m$ . The locus of the centers of gravity of the arch sections is called the arch curve. For the analysis the arch curve is divided into  $m - 1$  segments of dead load length  $s_{jk}$  and horizontal and vertical projections  $x_{jk}$  and  $z_{jk}$ . It is practicable to locate the segment joints exactly where column or hangers carry the vertical loads into the arch. A rectangular coordinate frame  $C x z$  is used for defining the dead load coordinates  $x_k, z_k$  of every segment joint. The arch curve is simplified to straight lines between the joints. Proper corrections can subsequently be introduced.

**Auxiliary Structure.**—The arch will be analyzed by the force method by the help of a statically determinate auxiliary structure which is a simple beam  $0n$  made up of the arch 1, 2, .., with rigid extension  $10c$  and  $mnC$ , Fig. 6(b). At the joints 0 and  $n$  hinged supports are arranged and, at  $n$ , a horizontal roller track is placed. At the free ends  $C$  of the rigid arms, three pairs of self-equilibrating redundant forces  $R = [R_1 R_2 R_3]^*$  are applied. By means of these forces the condition of stress and deformation in the given arch  $1m$  is exactly simulated.

**Moments in the Deflected Arch.**—Dead load  $G$  will cause redundants  $R^G$ . When live load  $P$ , temperature and so on are added, the redundants change to

$$R^G + P = R^G + R \dots\dots\dots (30)$$

The arch joints displace from  $x$  to  $x + u$  horizontally and from  $z$  to  $z + w$  vertically  $x, u, z, w$  being column matrices containing  $m$  elements each. Abbreviating  $-X^{-1}$  by  $C$  the auxiliary beam, by means of Eq. 9, will obtain the moments  $C(G + P)$  at the segment joints in the dead load position.

However, what is actually sought is the beam moment at the joint after it is displaced to  $x + u$  and after the load  $G + P$  has also moved by  $u$  to the displaced joint, as the physical conditions of the problem require. Both corrections are included in a term  $M$ .

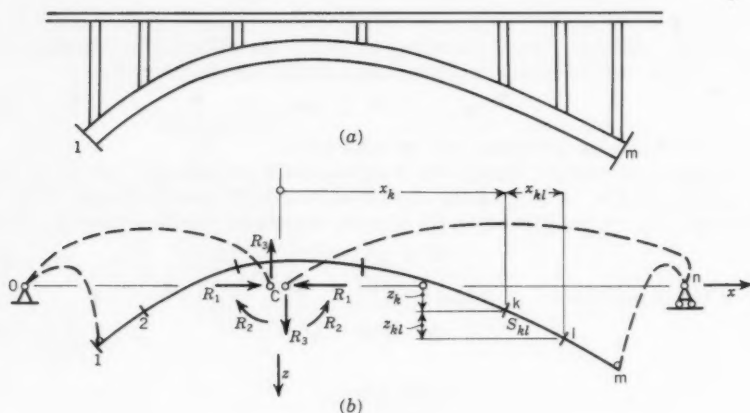


FIG. 6

When the beam moments caused by the redundants are added, Fig. 6 (b), the complete beam moments become

$$M = -X^{-1}(G + P) + \Delta M^0 + (z + w) R_1^{G+P} + i R_2^{G+P} + (x + u) R_3^{G+P} \dots \dots \dots (31)$$

The column matrix  $i$  has  $m$  elements, all ones. Eq. 31 can be written as

$$M = C(G + P) + R_1^{G+P} w + M^u + D R^{G+P} \dots \dots \dots (32)$$

in which

$$C = -X^{-1} \dots \dots \dots (33a)$$

$$D = [z \ i \ x] \dots \dots \dots (33b)$$

and

$$M^u = \Delta M^0 + R_3^{G+P} u \dots \dots \dots (33c)$$

in which  $D$  is the force transformation of redundants.

*Estimate of Horizontal Displacement Effects.*—The effects of the horizontal displacement are generally small in practical cases.

The simple beam moments  $M^0$  in the undeflected auxiliary beam are obtainable by Eq. 7 -  $X M^0 = G + P$ , or, using the form of Eq. 4 instead of Eq. 6 for  $Xz$ , by

$$(X M^0)_k = \frac{M_{kl}^0}{x_{kl}} - \frac{M_{jk}^0}{x_{jk}} = - (G + P)_k \dots \dots \dots (34)$$

When the abscissa intervals  $x_{kl}$  increase by small increments  $u_{kl}$ , the moments  $M_{kl}^0$  increase by small  $\Delta M_{kl}^0$  while the loads  $(G + P)_k$  remain unaltered. Conventional differentiation gives

$$\frac{\Delta M_{kl}^0}{x_{kl}} - \frac{M_{kl}^0 u_{kl}}{x_{kl}^2} - \left( \frac{\Delta M_{jk}^0}{x_{kl}} - \frac{M_{jk}^0 u_{jk}}{x_{jk}^2} \right) = 0 \dots \dots \dots (35)$$

The term  $M_{kl}^0/x_{kl}$  is replaced by the beam segment vertical force  $V_{kl}^0$  and Eqs. 4 and 5 are used for  $\Delta M^0$  to yield

$$(X \Delta M^0)_k = \frac{V_{kl}^0 u_{kl}}{x_{kl}} - \frac{V_{jk}^0 u_{jk}}{x_{jk}} \dots \dots \dots (36)$$

By Eq. 4,  $R_3 X u$  is added to Eq. 36 and it is noted that  $V_{kl}^0 + R_3$  equals the actual arch segment vertical force  $V_{kl}$ . The horizontal movement correction gives

$$(X \Delta M^0)_k + (R_3 X u)_k = (X M^u)_k = \frac{V_{kl} u_{kl}}{x_{kl}} - \frac{V_{jk} u_{jk}}{x_{jk}} \dots \dots (37)$$

The equilibrium of the arch segment  $kl$  requires (Fig. 7) that

$$H_{kl} z_{kl} + V_{kl} x_{kl} = M_l - M_k = M_{kl}, \quad H_{kl} = H^G + R_1 = H \dots (38)$$

in which  $H$  is the total horizontal force in the arch. When Eq. 38 is substituted in Eq. 37

$$(X M^u)_k = \frac{M_{kl} u_{kl}}{x_{kl}^2} - \frac{M_{jk} u_{jk}}{x_{jk}^2} - H \left( \frac{z_{kl} u_{kl}}{x_{kl}^2} - \frac{z_{jk} u_{jk}}{x_{jk}^2} \right) \dots \dots (39)$$

Under ordinary circumstances the live load is relatively small or fairly proportional to  $G$ . Then, in this small correction for  $u$ , the first two terms on the right hand side can be neglected, or it can subsequently be corrected by iteration. A three-diagonal band matrix  $X^z/x^2$  is formed in the same way as  $X$  in Eq. 6 but with every  $1/x_{kl}$  replaced by  $z_{kl}/x_{kl}^2$ . For all segment joints  $k$ , Eq. 39 then assumes the form

$$X M^u = - H X^z/x^2 u \dots \dots \dots (40)$$

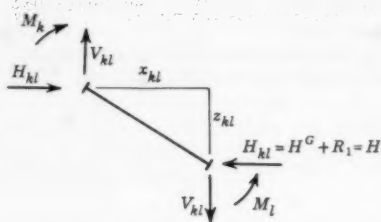


FIG. 7

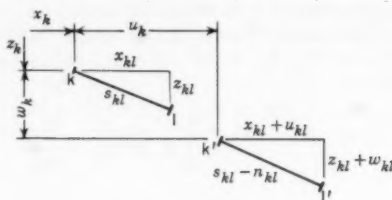


FIG. 8

Fig. 8 shows an undeflected arch segment  $s_{kl}$  and the same segment shortened by  $n_{kl}$  in its deflected position. It is seen that

$$s_{kl}^2 = x_{kl}^2 + z_{kl}^2, (s_{kl} - n_{kl})^2 = (x_{kl} + u_{kl})^2 + (z_{kl} + w_{kl})^2 \quad (41)$$

or, omitting powers of  $n$ ,  $u$ , and  $w$

$$- s_{kl} n_{kl} = x_{kl} u_{kl} + z_{kl} w_{kl} \quad (42)$$

or

$$\frac{-u_{kl}}{x_{kl}} = \frac{z_{kl} w_{kl}}{x_{kl}^2} + \frac{s_{kl} n_{kl}}{x_{kl}^2} \quad (43)$$

or, subtracting the corresponding expression for  $u_{jk}$ ,

$$-X u = X^2/x^2 w + X^2/x^2 n \quad (44)$$

Introducing Eq. 44 into Eq. 40 gives, neglecting  $n$ ,

$$X M^u = H X^2/x^2 X^{-1} X^2/x^2 w = H X^2/x^3 w \quad (45)$$

The last term was obtained by inserting Eq. 43 directly into the  $H$ -term in Eq. 39. Eq. 45 accounts for the horizontal displacements and the simultaneous load displacements and can be entered into Eq. 32

$$M = C (G + P) + H (I + X^{-1} X^2/x^3) w + D R^G + P \quad (46)$$

**Form Load Condition.**—Assume that the dead load  $G$  is also the “form load,” which, acting alone, induces only zero moments in the arch. This rule obviously prescribes the arch form when all  $G$  are given. The form condition must be fulfilled also at the joints 1 and  $m$ , by adding proper vertical loads  $G_1$  and  $G_m$  there. Any discrepancy in the real dead load from the form load  $G$  will be treated as a part of the live load  $P$ .

By these rules and definitions the dead load condition of the arch,  $P = 0$ , is characterized by zero displacements of the arch,  $u = w = 0$ , and by the form load redundants  $R = R^G$ . For this situation Eq. 32 becomes the form load condition

$$0 = C G + D R^G \quad (47)$$

with  $R_2^G = R_3^G = 0$ / Thus Eqs. 33 give

$$zR_1^G = X^{-1} G \dots\dots\dots (48a)$$

or

$$G = X z R_1^G \dots\dots\dots (48b)$$

*Moments in the Auxiliary.*—Eqs. 47, subtracted from Eq. 46 gives (denoting  $R^G + P - R^G$  by  $R$ )

$$M = H (I + X^{-1} X z^2 / x^3) w + C P + D R \dots\dots\dots (49)$$

Eq. 47 is multiplied by  $X$ . Note that  $X C = -I$  by Eq. 33a and use Eq. 27

$$(X + H F + H X z^2 / x^3 X^{-1} F) M = Q M = -P + X D R \dots\dots (50)$$

The  $Q$  term,  $(X + H F + H X z^2 / x^3 X^{-1} F)$ , contains a three-diagonal part  $X + H F = Q'$  that is easily inverted and a smaller part  $Q''$  caused by the horizontal movements. The inverse of  $Q$  is computed by the approximate formula

$$Q^{-1} = Q'^{-1} - Q'^{-1} Q'' Q'^{-1} \dots\dots\dots (51)$$

The solution for  $M$  is

$$M = -Q^{-1} P + Q^{-1} X D R = Q^{-1} X (C P + D R) \dots\dots (52)$$

*Axial Thrust in the Auxiliary.*—The equilibrium of the joint  $k$ , Fig. 7, requires that

$$N_{kl}^{G+P} = \frac{H x_{kl}}{s_{kl}} - \frac{V_{kl}^{G+P} z_{kl}}{s_{kl}} \dots\dots\dots (53)$$

in which  $N$  is the axial thrust in the arch. For form load only

$$V_{kl}^G = -\frac{H_{kl}^G z_{kl}}{x_{kl}} \dots\dots\dots (54)$$

and

$$N_{kl}^G = \frac{H_{kl}^G x_{kl}}{s_{kl}} - \frac{V_{kl}^G z_{kl}}{s_{kl}} = \frac{H_{kl}^G s_{kl}}{x_{kl}} \dots\dots\dots (55)$$

For live loads Eq. 53 reads

$$N_{kl} = \frac{R_1 x_{kl}}{s_{kl}} - \frac{V_{kl} z_{kl}}{s_{kl}} \dots\dots\dots (56)$$

Using

$$V_{kl} = V_{kl}^0 + R_3 \dots\dots\dots (57a)$$

and

$$V_{kl}^0 = \frac{M_{kl}^0}{x_{kl}} \dots \dots \dots (57b)$$

yields

$$N_{kl} = - \frac{M_{kl}^0 z_{kl}}{s_{kl} x_{kl}} + \frac{R_1 x_{kl}}{s_{kl}} - \frac{R_3 z_{kl}}{s_{kl}} \dots \dots \dots (58)$$

and

$$N^P = - D^{z/xs} M^0 + \left[ \frac{\Delta x}{\Delta s} \ 0 \ - \ \frac{\Delta z}{\Delta s} \right] \begin{bmatrix} R_1 \\ R_2 \\ R_3 \end{bmatrix} \dots \dots \dots (59)$$

in which  $D^{z/xs}$  is a diagonal matrix with the elements  $z_{kl}/x_{kl} s_{kl}$ . The elements  $x_{kl}/s_{kl}$  and  $z_{kl}/s_{kl}$  are arranged in the column matrices  $\Delta x/\Delta s$  and  $\Delta y/\Delta s$ .

By Eq. 4

$$- X M^0 P = P \dots \dots \dots (4)$$

Eqs. 58 and 59 can be written

$$N = C' P + D' R \dots \dots \dots (60)$$

and

$$C' = D^{z/xs} X^{-1}, \ D' = \left[ \frac{\Delta x}{\Delta s} \ 0 \ - \ \frac{\Delta z}{\Delta s} \right] \dots \dots \dots (61)$$

Finally Eqs. 52 and 60 can be combined into the segment force formula

$$\begin{bmatrix} M \\ N \end{bmatrix} = \begin{bmatrix} Q^{-1} X \ 0 \\ 0 \quad I \end{bmatrix} \begin{bmatrix} C \ D \\ C' \ D' \end{bmatrix} \begin{bmatrix} P \\ R \end{bmatrix} \dots \dots \dots (62)$$

*Arch Segment Deformations.*—The angle breaks and rib shortenings of the separate arch segments are deduced by

$$m = F M + m^t \dots \dots \dots (63)$$

$$n = F' N + n^t \dots \dots \dots (64)$$

or

$$\begin{bmatrix} m \\ n \end{bmatrix} = \begin{bmatrix} F \ 0 \\ 0 \ F' \end{bmatrix} \begin{bmatrix} M \\ N \end{bmatrix} + \begin{bmatrix} m^t \\ n^t \end{bmatrix} \dots \dots \dots (65)$$

in which  $F'$  is the axial load flexibility. Both  $m$  and  $n$  consist of an elastic part,  $FM$  and  $F'N$  and an inelastic part,  $m^t$  and  $n^t$ , caused by temperature



changes, inelastic settlements, misfits, shrinkage, and so on. The matrix  $F$  was developed in Eqs. 24 while  $F'$  obviously is a diagonal matrix with the elements  $\frac{s_{kl}}{E A_{kl}}$ . The dead load elastic rib-shortening  $F' N^G$  is assumed to be eliminated by jacking and so forth.

*Displacements Between Rigid Arm Ends.*—The movements  $r = [r_1 \ r_2 \ r_3]^*$  at  $C$  will be studied. They are caused by bending and shear of the arch represented by angle weights  $m_k$  at all joints  $j$  and caused by rib shortening  $n_{kl}$  of all segments  $k \ l$ . Fig. 9 (a) indicates that a sole angleweight  $m_k$  will move the right hand rigid arm end at  $C$  by  $r'_1 = -z_k m_k$  in the direction of  $R_1$ , rotate it by  $r'_2 = m_k$ , and move it by  $r'_3 = x_k m_k$  in the direction of  $R_3$ . Fig. 9 (b) indicates that a rib shortening  $n_{kl}$  produces an arm end displacement of  $r''_1$

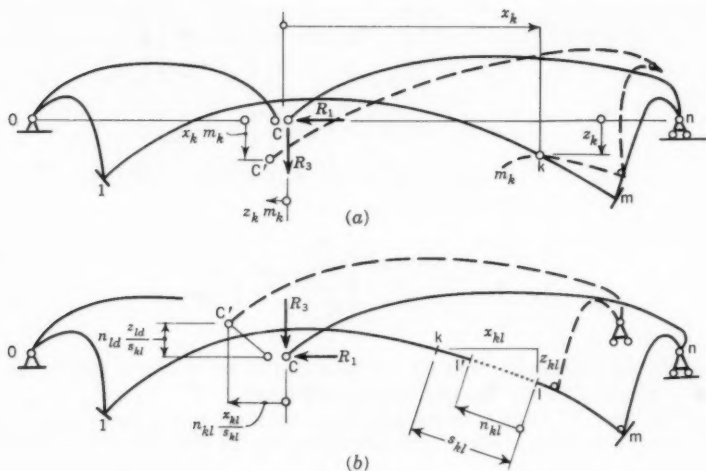


FIG. 9

$= n_{kl} x_{kl} / s_{kl}$  and  $r''_3 = -n_{kl} z_{kl} / s_{kl}$ . Thus, all the angle weights and rib-shortenings will produce an arm end movement of  $r = r' + r''$

$$\begin{bmatrix} r_1 \\ r_2 \\ r_3 \end{bmatrix} = \begin{bmatrix} z^* \\ i^* \\ x^* \end{bmatrix} m + \begin{bmatrix} \left( \frac{\Delta x}{\Delta s} \right)^* \\ 0 \\ - \left( \frac{\Delta z}{\Delta s} \right)^* \end{bmatrix} n \quad \dots \dots \dots (66)$$

With previous definitions of  $D$  and  $D'$  (Eqs. 33 and 61)

$$r = D^* m + D' n \quad \dots \dots \dots (67)$$

Similarly the displacements  $p$  of the loads  $P$  are found to be

$$p = C^* m + C'^* n \dots\dots\dots (68)$$

Eqs. 67 and 68 can be combined into

$$\begin{bmatrix} p \\ r \end{bmatrix} = \begin{bmatrix} C^* & C'^* \\ D^* & D'^* \end{bmatrix} \begin{bmatrix} m \\ n \end{bmatrix} = A^* \begin{bmatrix} m \\ n \end{bmatrix} \dots\dots\dots (69)$$

These tangible deductions of the formula for  $r$  are superfluous (14). Considering that  $P$ ,  $R$ ,  $M$ , and  $N$  are statically and  $p$ ,  $r$ ,  $m$ , and  $n$  kinematically compatible Krohn's theorem applied to Eq. 62 immediately results in Eq. 69.

*Force Method Equations.*—Eq. 62 is substituted into Eq. 65 and Eq. 65 into Eq. 69 to yield

$$\begin{bmatrix} p - p^t \\ r - r^t \end{bmatrix} = \begin{bmatrix} C^* & C'^* \\ D^* & D'^* \end{bmatrix} \begin{bmatrix} FQ^{-1} X & 0 \\ 0 & F' \end{bmatrix} \begin{bmatrix} C & D \\ C' & D' \end{bmatrix} \begin{bmatrix} P \\ R \end{bmatrix} \dots\dots\dots (70)$$

$$\begin{bmatrix} p - p^t \\ r - r^t \end{bmatrix} = A^* fA \begin{bmatrix} P \\ R \end{bmatrix} = \begin{bmatrix} c & d^* \\ d & k \end{bmatrix} \begin{bmatrix} P \\ R \end{bmatrix} = g \begin{bmatrix} P \\ R \end{bmatrix} \dots\dots\dots (71)$$

and

$$\begin{bmatrix} p^t \\ r^t \end{bmatrix} = \begin{bmatrix} C^* & C'^* \\ D^* & D'^* \end{bmatrix} \begin{bmatrix} m^t \\ n^t \end{bmatrix} = A^* \begin{bmatrix} m^t \\ n^t \end{bmatrix} \dots\dots\dots (72)$$

in which  $f$  is the member flexibility,  $g$  denotes the structure's flexibility, and  $c$ ,  $d$  and  $k$  refer to the partial flexibility matrices.

From Eq. 70 it is noted that the structure behaves like a first order theory (elastic theory) structure with a bending elasticity of  $FQ^{-1}X = F''$ , instead of  $F$ .

Secondly, it is noted that  $F''$  is symmetric, because its inverse

$$\begin{aligned} X^{-1} Q F^{-1} &= X^{-1} (X + HF + HX^{z2/x3} X^{-1} F) F^{-1} \\ &= F^{-1} + HX^{-1} + HX^{-1} X^{z2/x3} X^{-1} \dots\dots\dots (73) \end{aligned}$$

is symmetric.

Thirdly, it can be seen that all the elements of  $g$  in Eq. 71 can be obtained by performing the multiplications in  $A^* f A$

$$c = C^* F'' C + C'^* F' C \dots\dots\dots (74a)$$

$$d = D^* F'' C + D'^* F' C' \dots\dots\dots (74b)$$

and

$$k = D^* F'' D + D'^* F' D' \dots\dots\dots (74c)$$

Because  $XC = -I$ , it is possible to substitute  $-FQ^{-1}$  for  $F'' C$ .

By a "part inversion" (14) Eq. 71 can be written

$$\begin{bmatrix} p & -p^t \\ & -R \end{bmatrix} = h \begin{bmatrix} P \\ r & -r^t \end{bmatrix} \dots\dots\dots (75)$$

and

$$h = \begin{bmatrix} e & -d^*K \\ -Kd & K \end{bmatrix}, K = -k^{-1} \\ e = c + d^*Kd \dots\dots\dots (76)$$

in which  $h$  is the part-inverted flexibility and  $k$  denotes a partial-flexibility matrix.

*Arch Condition and Segment Forces.*—The auxiliary will function exactly as the given arch when the redundants  $R$  are given such magnitudes that the arm end movements  $r$  at  $C$  reduce to zero ( $r = 0$ ). This modifies Eq. 75 to

$$\begin{bmatrix} p & -p^t \\ & -R \end{bmatrix} = h \begin{bmatrix} P \\ -r^t \end{bmatrix} \dots\dots\dots (77)$$

Eqs. 77 and 76 contain the solution for the redundants

$$-R = -KdP - Kr^t \dots\dots\dots (78)$$

in which

$$R = R^i P + R^c r^t \dots\dots\dots (79a)$$

$$R^i = Kd \dots\dots\dots (79b)$$

and

$$R^c = K \dots\dots\dots (79c)$$

which are substituted into Eq. 62 for the segment forces

$$\begin{bmatrix} M \\ N \end{bmatrix} = \begin{bmatrix} Q^{-1} & X & 0 \\ 0 & I \end{bmatrix} \begin{bmatrix} C & D \\ C' & D' \end{bmatrix} \begin{bmatrix} P \\ KdP + Kr^t \end{bmatrix} \dots\dots\dots (80a)$$

or

$$\begin{bmatrix} M \\ N \end{bmatrix} = \begin{bmatrix} Q^{-1} & X & 0 \\ 0 & I \end{bmatrix} \begin{bmatrix} C + DKd & DK \\ C' + D'Kd & D'K \end{bmatrix} \begin{bmatrix} P \\ r^t \end{bmatrix} = \begin{bmatrix} M^i & M^c \\ N^i & N^c \end{bmatrix} \begin{bmatrix} P \\ r^t \end{bmatrix} \dots\dots (80b)$$

or explicitly

$$M^i = -Q^{-1} + Q^{-1} X D Kd, M^c = Q^{-1} X D K \dots\dots\dots (81)$$

and

$$N^i = C' + D' K d, N^c = D' K \dots\dots\dots (82)$$

These are the influence coefficient expressions for arch segment forces as previously explained. The influence coefficients are  $M^i$  and  $N^i$ , and the correction coefficients for inelastic "action"  $M^c$  and  $N^c$ .

The transverse force in each arch segment  $k$   $l$  equals the moment increase  $M_{kl} = (\Delta M)_{kl}$  divided by the segment length  $s_{kl} = (\Delta s_{kl})$

$$T = T^i P + T^c r^t, \quad T^i = \frac{\Delta M^i}{\Delta s}, \quad T^c = \frac{\Delta M^c}{\Delta s} \quad (83)$$

in which  $T$  is the arch shear.

*Displacements of the Arch.*—The deflections, or the displacements  $p$  associated to the vertical loads  $P$  are also obtained from Eqs. 77 and 76

$$p = p^t + e P + d^* K r^t \quad (84a)$$

or

$$p = p^t + p^i P + p^c r^t, \quad p^i = e, \quad p^c = d^* K \quad (84b)$$

Finally, the column of horizontal displacements  $U$  can be found by means of Eq. 44, or by addition of Eq. 43 starting from either abutment.

*Rib-Shortening Approximation.*—A quite satisfactory approximation of the rib-shortening effect can usually be obtained as in Eq. 55 by writing also for

the live load  $N_{kl}^P = \frac{H_{kl}^P s_{kl}}{x_{kl}}$ . This changes Eq. 61 to

$$C' = 0, \quad D' = \begin{bmatrix} \frac{\Delta s}{\Delta x} & 0 & 0 \end{bmatrix} \quad (85)$$

For equal temperature increase of  $t$  degrees in a symmetric arch

$$r^t = \begin{bmatrix} r_1^t & 0 & 0 \end{bmatrix} \quad (86)$$

and

$$r_1^t = -\omega t L \quad (87)$$

which agree with Eq. 61 should be applied. In Eq. 87  $L$  is the horizontal distance between the springs.

## PRACTICAL APPLICATION OF THE THEORY

The practical computation of some section forces in an arch is shown by the following example in which influence and correction coefficients produced by a computer are used.

In this method the total horizontal force  $H$  is selected for "iteration parameter" because special conditions, for instance the arch displacements, exert a small influence on this parameter. Having chosen a value for the total horizontal force  $H$  the value of  $Q$  can be computed and all the influence and correction coefficients previously deduced. One such set of coefficients is often fully satisfactory. To be quite meticulous two sets could be computed, one for a total  $H$  in the lower and one in the upper range of the loads used. When a com-

parison with the elastic theory results is desired one set of coefficients must be computed for  $H = 0$ . This eliminates the effect of  $w$  in  $Q$ .

To find, for example, a maximum moment  $M_x$  at  $x$ , the live load is critically positioned on the positive area of  $M_x^i$ . The same load is applied to  $H^P i$  which gives the correct value of  $H^P$ ; after addition of  $H^G$  an accurate value of  $H$  is obtained. Thereafter, an interpolation between the already computed sets of influence coefficients becomes practicable to single out almost exactly the influence line  $M_x^i$  that corresponds to the correct value of  $H$ . The critical loading is again applied to this value of  $H$ .

**Numerical Example.**—A symmetric fixed arch, Fig. 10, has a span  $L = 1000$  ft and a rise of 159 ft. It is subdivided into six segments with  $\Delta x = [146.5 \ 208.0 \ 145.5 \ 145.5 \ 208.0 \ 146.5]$  ft and  $\Delta z = [81.8 \ 64.9 \ 13.0 \ 13.0 \ 64.9 \ 81.8]$  ft. Each segment has a constant bending stiffness  $EI = [6.75 \ 4.61 \ 4.52 \ 4.52 \ 4.61 \ 6.75]$   $\times 10^8$  kip ft<sup>2</sup>, and a constant axial stiffness  $EA = [2.73 \ 1.93 \ 1.91 \ 1.91 \ 1.93 \ 2.73]$   $\times 10^7$  kip. Influence and correction coef-

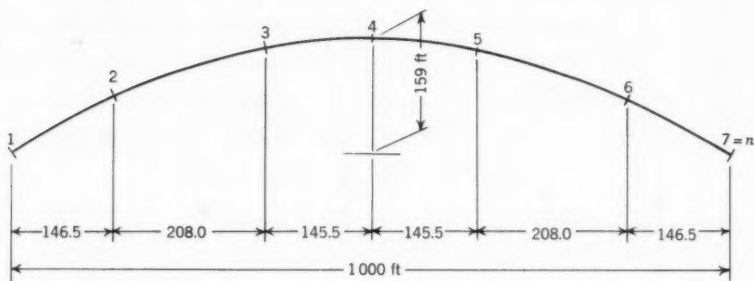


FIG. 10

ficients  $H^i$ ,  $M_4^i$ ,  $M_1^i$ ,  $v_3^i$ ,  $H^c$ , and so on are electronically computed for three total horizontal forces,  $H = 0$ , 7000 kips, and 8000 kips, and reproduced in Table 1.

The form load  $G = H^G X z = [-0.554, 0.242, 0.223, 0.178 \text{ sym}] \times H^G$  causes a horizontal force of  $H^G = 6990$  kips. The live load consists of one panel point load of 160 kips and other panel point loads of 80 kips or zero. A temperature increase or decrease of  $60^\circ\text{F}$  is considered  $\omega = 6.5 \cdot 10^{-6}$  per  $^\circ\text{F}$ .

A temperature increase of  $60^\circ\text{F}$  gives  $r_1^t = -\omega t L = 6.5 \cdot 10^{-6} (60) (1000) = 0.390$  ft.

**Positive Crown Moment.**—An inspection of Table 1 reveals that the 260 kip concentration should be placed at the crown and that no other panel point loads be applied. For an estimated  $H = 7500$  kips it is found that  $H^P = (1.53) (2.60) = 398$  kips. A temperature decrease gives

$$H^P = 155 (-0.390) = -60 \text{ kip}$$

TABLE 1.—PART OF COMPUTER RESULTS FOR ARCH ANALYSIS EXAMPLE

Load at joint		Horizontal force						
		1	2	3	4	5	6	7
$H = 0, H^i$		0	0.351	1.237	1.493	1.237	0.351	0
7000		0	0.334	1.250	1.527	1.250	0.334	0
8000		0	0.331	1.252	1.532	1.252	0.331	0
Load at joint		1	2	3	4	5	6	7
$H = 0, M^i$		0	- 9.04	- 5.78	42.70	- 5.78	- 9.04	0
7000		0	- 10.23	- 5.67	46.00	- 5.67	- 10.23	0
8000		0	- 10.42	- 5.65	46.51	- 5.65	- 10.42	0
Load at joint		1	2	3	4	5	6	7
$H = 0, 10^6 w^i_3$		0	- 73.61	- 23.46	+ 30.04	+ 50.71	+ 20.45	0
7000		0	- 79.77	- 29.19	+ 33.05	+ 58.43	+ 23.04	0
8000		0	- 80.77	- 30.20	+ 33.52	+ 59.74	+ 23.49	0
Load at joint		1	2	3	4	5	6	7
$H = 0, 10^6 w^i_3$		0	406	1277	171	- 915	- 578	0
7000		0	486	1475	181	- 1101	- 674	0
8000		0	500	1509	183	- 1133	- 690	0

Thus,  $H = 6990 + 398 - 60 = 7328$  kip. Iteration will not appreciably change this result. For this value of  $H$  we find

$$M_4 = [46.00 + (0.328)(0.51)] 260 = 12,000 \text{ kip ft}$$

caused by live load and

$$M_4 = H^C S = (-13145)(-0.390) = 5130 \text{ kip ft}$$

caused by temperature. The elastic first order theory ( $H = 0$ ) would have given

$$M_4 = (42.70)(260) - 11882(-0.390) = 11100 + 4630 \text{ kip ft.}$$

*Positive Spring Moment.*—Inspection of Table 1 indicates that 260 kip be placed at station 5 and 80 kip at station 4 and 6. For  $H = 7000$

$$H^P = 1.250(260) + (1.527) + 0.334(80) = 474 \text{ kip.}$$

A temperature rise gives  $H^P = 60$  kip. Thus,  $H = 7524$  kip. For this  $H$  the live load moment is

$$M_1 = (59.13)(260) + (33.30) + 23.28(80) = 19900 \text{ kip ft}$$

and the temperature moment  $M_1 = (22813)(390) = 8900 \text{ kip ft.}$

The corresponding elastic moment is obtained by setting  $H = 0$ :

$$M_1 = (50.71)(260) + (30.04 + 20.45)(80) = 17220 \text{ kip ft}$$

and for temperature

$$M_1 = (25054)(0.390) = 9770 \text{ kip ft.}$$

The total amplification for live load is  $19900 - 17220 = 2680$  kip ft or 16%, but the amplification for live load plus the temperature is  $28800 - 26990 = 1810$  kip ft or only 7%.

The maximum deflection at 3 is obtained when 260 kip is placed at 3, and 80 kip at 2 and 4, and when the temperature decreases. From this

$$H^P = (1.251)(260) + (0.333 + 1.529)(80) - 60 = 414 \text{ kip}$$

$$H = 7404 \text{ kip,}$$

$$10^6 v_3 = 1488(260) + (492 + 182)(80) = 441 \cdot 10^3,$$

$$v_3 = 0.441 \text{ ft}$$

caused by live load and  $-1.251(-0.390) = 0.488$  ft caused by the temperature decrease. By the elastic "first order" theory,  $H = 0$ , it is determined that

$$v_3 = [(1.277)(260) + (406 + 171)(80)] 10^{-6} + (-1.237)(-0.390)$$

$$= 0.378 + 0.482 \text{ ft}$$

The total amplification of the live load deflection is thus 0.063 ft or 17% in accordance with the deflection theory.

The horizontal displacement effect increased the maximum spring moment found previously by 2%.

The example illustrates a rather stiff arch. Steel arches have been built with much higher amplification of arch moments. In such cases the arch should perhaps be also checked for the condition that an increase of the dead and live loads by certain factors, for example, 1.2 and 2.0, will not reach the proportional limit of the arch material. This is, however, a design criterion that does not fall within the scope of this paper.

### CONCLUSIONS

Since the advent of electronic computers, the natural method of elastic arch design and analysis should be to select, first, a tentative stiffness variation and arch form, to compute the first order theory or "elastic" influence coefficients for all actual section forces, to apply the given loads for finding the critical section forces, and to design the sections. This yields new arch stiffnesses, weights, and so on, requiring a similar computation.

Traditionally, only the "elastic" influence coefficients, mostly taken from tables for special arch types, are applied in this analysis. Occasionally for large arches, an "amplification" computation is added.

By the theory presented herein, the second order theory final influence coefficients for moments and so forth are obtained with little more computer time than required for the first order theory coefficients. There seems to be a good reason for using only the deflection theory coefficients because they yield directly the actual moments and so on in the arch.

In this way an arch analysis will approach a standard suspension bridge analysis which is performed directly by the deflection theory rather than the first order theory. For bridges with girders of uniform stiffness, the moment, shear, and so on influence coefficients may be taken from published tables; for variable girder stiffness they can be easily obtained by a computer (11).

---

### APPENDIX I.—JOINT ACTION OF ARCH AND BRIDGE DECK

---

The loads are often transferred to the arch from a bridge deck supported on the arch by vertical hinged elastic columns or hangers. The composite structure of a continuous girder, elastic columns or hangers, and an arch can be analyzed by the second order deflection theory. The arch in Fig. 11 (d) supports a continuous girder, Fig. 11 (c), by means of elastic columns.

By a method already proven, (11) or (14) the continuous girder is first treated as if it were firmly supported at the columns, Fig. 11 (b) and analyzed according to the conventional theory for continuous beams loaded by the given distributed and concentrated loads  $g'$ ,  $p'$ , and  $P'$ . The firm girder moments  $M^f$ , shears  $T^f$ , deflections  $w^f$  and so on, are computed, saved, and finally added to the other results of the following analysis. The primed loads further cause firm girder support reactions  $P$  that will be used as joint loads  $G$  and  $P$ .



Both the deck and the arch will be divided into members or segments by joints at the columns. Magnitudes will be, as previously, noted, but superfixes

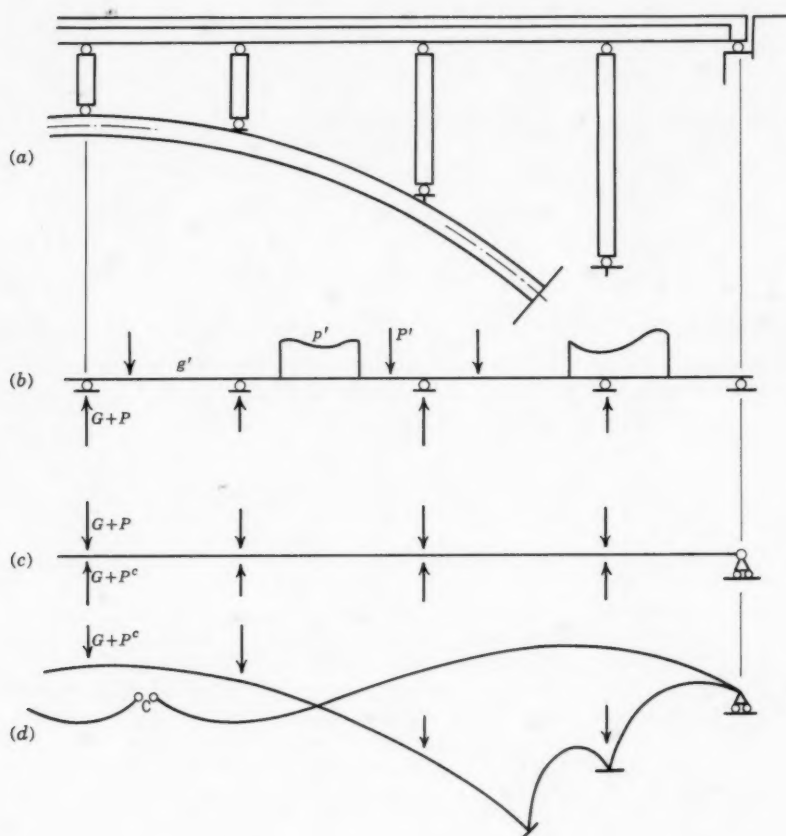


FIG. 11

a, c, and d will refer to the arch, columns, and deck. The deck, Fig. 11 (c), the arch, Fig. 11 (d), and the columns obey the equations

$$-X^d M^d = P - N^c, F^d M^d = -X^d w^d \dots\dots\dots (88)$$

and

$$F^a M^a = -X^a w^a, w^d - w^a = f^c N^c \dots\dots\dots (89)$$

by which

$$X^a, {}^{-1} F^a M^a + F^D (P - N^C) = f^C N^C, F^D = X^d, {}^{-1} F^d X^d, {}^{-1} \dots (90)$$

$$F^D, {}^{-1} X^a, {}^{-1} F^a M^a + P = B N^C, B = I + F^D, {}^{-1} f^C \dots (91)$$

and

$$N^C = B^{-1} P + A M^a, A = B^{-1} F^D, {}^{-1} X^a, {}^{-1} F^a \dots (92)$$

\* These column loads are entered into the arch moment Eqs. 50 and 45

$$(X^a + H F^a + H F^u) M^a = - B^{-1} P - A M^a + X^a D R \dots (93)$$

and

$$B (X^a + A + H F^a + H F^u) M^a = - P + B X^a D R \dots (94)$$

In Eq. 94  $B(X^a + A + H F^a + H F^u)$  is made to equal  $Q$  and  $B X^a = X$  after which the arch analysis is continued exactly as from Eq. 50. The entire analysis is readily programmed by an interpretive matrix program.

---

#### APPENDIX II.—READING REFERENCES ON DEFLECTION THEORY OF ARCHES

---

The deflection theory of arches was first formulated by Josef Melan (1), (3), (4) and by F. Engesser (2), and has afterwards been treated by a great number of writers as listed in the extensive bibliography presented by S. Bergstrom (7). Except for vertical arch deflections Aas-Jakobsen (6), Bergstrom (7), and Hirsch and Popov (8) considered horizontal arch movements also, but not horizontal load displacements. All papers mentioned treated the problem by differential equation, except for the paper by Hirsch and Popov (8), that analyzed a two hinged arch by a direct finite difference method. All previous treatments of the arch deflection theory were principally iterative, departing from the elastic theory and arriving at the results by means of successive "amplifications" of deflections and moments or by a formula

$$\nu/(\nu - 1)$$

Finite difference matrix methods were supplied to other structures in the fundamental papers of Hojlund-Rasmussen and Egervary, (9), (10). The writer attempted (11) to further develop such methods. The writer's contribution to the ASCE Second Conference on Electronic Computation (12) contains an algorithm for the inversion of band matrices, used in this paper and the more recent (1961) references (14) contain a general matrix method for indeterminate analysis of structures, partly followed in this paper.

1. "Zur Bestimmung der Spannungen in den durch einen geraden Balken mit Mittelgelenk versteiften Hangeträgen," by J. Melan, Zeitschrift Osterr. Ingenieur Architekten-Vereines 52, September, 1900, Vienna, p. 553.

2. "Einfluss der Formänderungen . . . der Dreigelenkbogen," by F. Engesser, *Z. Arch. und Ingwesen*, 1903, p. 178.
3. J. Melan *Handbuch Ingenieurwissensch.* II, Part 5, Chapter XII, 1906.
4. "Der biegsame eingespannte Bogen," by J. Melan, *Der Bauingenieur*, Springer, Berlin, 1925, p. 143.
5. "Untersuchungen über die knicksicherheit, die elastische verformung und das kriechen des betons bei bogen brücken," by F. Dischinger, *Der Bauingenieur*, No. 33-No. 36, Springer, Berlin, 1937.
6. "Increment of Moments in Arches," by A. Aas-Jakobsen, *Betong*, Stockholm, No. 1 and 3, 1943. In Norwegian.
7. "On Vertical Stability of Arches," by S. G. Bergstrom, *Diss.*, Stockholm, 1951. In Swedish.
8. "Analysis of Arches by Finite Differences," by E. G. Hirsch and E. P. Popov, *Proc. Paper No. 829*, ASCE, Vol. 81, 1955.
9. "Theorie der Hängebrücken mit Hilfe der Matrizenrechnung," by E. Egervary, *IABSE Publications* 1956, p. 149.
10. "Numerical Integration of the Differential Equation of the Column," by B. Hojlund-Rasmussen, *Diss.*, Copenhagen, 1957, presented in manuscript 1953. In Danish.
11. "Column-beams and Suspension Bridges Analyzed by Green's Matrix," by S. O. Asplund, *Transactions No. 204*, Chalmers Univ. of Tech., Gothenburg, Sweden, 1958.
12. "Inversion of Band Matrices," by S. O. Asplund, presented at the 1960 ASCE Second Conf. on Electronic Computation, at Pittsburgh, Pa., p. 513.
13. "Stability Problems of Compressed Steel Members and Arch Bridges," by G. Wastlund, *Proceedings*, ASCE, Vol. 86, No. ST 6, June, 1960, p. 60.
14. "A Unified Analysis of Indeterminate Structures," by S. O. Asplund, *Transactions No. 243*, Chalmers Univ. of Tech., Gothenburg, Sweden, 1961.

---

### APPENDIX III.—NOTATION

---

The letter symbols used in the paper are listed here for ease of reference and for the convenience of discussers:

- A = polygon side angle Fig. 1; cross-section area;
- A = force transformation;
- B = polygon angle break Fig. 1;
- C = force transformation of loads;

- $c$  = partial flexibility matrix;  
 $D$  = force transformation of redundants,  $D^Z/xs$ ;  
 $d$  = partial flexibility matrix;  
 $d$  = first difference operator;  
 $E$  = modulus of elasticity;  
 $F$  = beam and arch flexibility;  
 $F'$  = axial load flexibility;  
 $F''$  = arch second order theory flexibility;  
 $F^b$  = bending flexibility;  
 $F^s$  = shear flexibility;  
 $f$  = end flexibility, member flexibility;  
 $G$  = modulus of elasticity of rigidity in shear;  
 $g$  = structure flexibility;  
 $H$  = total horizontal force in arch;  
 $h$  = part-inverted flexibility;  
 $I$  = unit matrix, moment of inertia;  
 $i$  = column matrix of ones;  
 $K$  = correction factors for variable  $EI$ , inverted negative  $k$ ;  
 $k$  = partial flexibility matrix;  
 $M$  = moment,  $m$  associated deformation Fig. 9 (a);  
 $N$  = axial thrust in arch,  $n$  associated deformation Fig. 9 (b);  
 $n$  = order of matrix;  
 $P$  = given vertical loads,  $p$  associated displacements;  
 $R$  = redundant forces Fig. 6,  $r$  associated displacements;  
 $r$  = arm end movement;  
 $s$  = length of arch segment Fig. 6;  
 $T$  = arch shear,  $t$  associated deformation;  
 $u$  = horizontal arch displacement;  
 $V$  = arch segment vertical force;  
 $w$  = vertical displacement = deflection (or  $p$ );  
 $X$  = second difference quotient operator;  
 $X'$  = first difference quotient operator;  
 $x$  = abscissa,  $x_{jk}$  abscissa intervals;  
 $z$  = vertical coordinate; and

$\beta$  = shear shape factor.

Superscripts

c = cross flexibilities, correction coefficients;

i = influence coefficients;

G = dead load;

P = live load;

0 = simple beam magnitudes;

t = due to temperature and inelasticity;

u = due to horizontal displacements; and

\* = transposition.



---

Journal of the  
**STRUCTURAL DIVISION**  
Proceedings of the American Society of Civil Engineers

---

**STRENGTH OF PLATE GIRDERS IN SHEAR**

By Konrad Basler,<sup>1</sup> A.M. ASCE

---

**FOREWORD**

An investigation of welded plate girders was conducted at Lehigh University during the years 1957 to 1960. The objective of this project was to determine the static carrying capacity of transversely stiffened plate girders. The study was grouped into an experimental and a theoretical phase, and the results of the experiments were published as a Welding Research Council Bulletin.

The theoretical considerations are presented as a series of three papers, covering first the bending strength (Proc. Paper 2913, August 1961 Journal of the Structural Division), then the shear strength (this paper), and finally the interaction between bending and shear (Proc. Paper 2968, October 1961 Journal of the Structural Division).

---

Note.—Discussion open until March 1, 1962. Separate discussions should be submitted for the individual papers in this symposium. To extend the closing date one month, a written request must be filed with the Executive Secretary, ASCE. This paper is part of the copyrighted Journal of the Structural Division, Proceedings of the American Society of Civil Engineers, Vol. 87, No. ST 7, October, 1961.

<sup>1</sup> Consultant, Egg b. Zurich, Switzerland; formerly Res. Asst. Prof. at Lehigh Univ., Bethlehem, Pa.

---

### SYNOPSIS

A study of the shear strength of plate girders is presented. In utilizing the postbuckling strength offered by the transverse stiffening of girders, new design rules are proposed. The new approach is checked with ultimate load tests carried out at Fritz Engineering Laboratory.

---

### INTRODUCTION

In current (1961) civil engineering practice, the shearing stresses in webs of plate girders are analyzed according to the classical beam theory established by Navier and St. Venant. According to this theory the shear force is resisted by a state of shearing stresses as pictured in Fig. 1 (a). The principal stresses at the neutral axis are of the same magnitude as the shear stress and act at  $45^\circ$  with the longitudinal axis (Fig. 1 (b)). Such a shear carrying action may be called "beam action." To satisfy the condition of small deformations, on which this beam theory is based, transverse stiffeners must be spaced close enough so that instability due to shear is excluded.

Ever since plate girders came into use, it has been recognized that beam action alone is not the only way that shear can be carried. Extensive discussion of the problem of web stiffening was carried on just before the end of the last century (1), (2), (3), (4), (5).<sup>2</sup> Intuition led to the opinion that the action of a plate girder was similar to that of a Pratt truss (1). Turneaure (3) concluded from a girder test "that there is as much reason to suppose that the web stresses follow down the web and up the stiffeners, as in a Howe Truss, as to suppose that they follow the lines of a Pratt Truss." However, model studies (2), (5) and a girder test (4) clearly indicated the importance of the web as a tension element and the stiffeners as compression elements. The goal was, at

---

<sup>2</sup> Numerals in parentheses refer to corresponding items in Appendix III - References.



that time, to assess the nature of the stress flow in the web rather than to estimate the carrying capacity. Thus, more qualitative than quantitative results could emerge. At the beginning of this century it led to a rather liberal design of girder webs, with web depths greater than 170 times the web thickness. Meanwhile, a web buckling theory was developed to determine safe limits for the design of plate girders. A possible truss action was advanced merely to justify a somewhat lower factor of safety against web buckling than that required against other stability cases such as column failure. Later tests conducted in the United States (6), (7) were mainly concerned with the establishment of a slenderness limit for unstiffened webs.

In 1916, H. H. Rode wrote an outstanding dissertation (8) in which one chapter deals with webs of plate girders. It appears that he may have been the first to mathematically formulate the effect of a tension field or truss action which sets in after the web loses its rigidity due to buckling. He proposed to evaluate its influence by considering a tension diagonal of a width equal to 80 times the web thickness.

With the development of aeronautical science the shear-carrying capacity of membrane-like structures got new attention. The paramount requirement of aircraft design (to minimize the weight of the structure) led to extremely thin webs. Since such structures were built of aluminum alloys, the modulus of elasticity and hence the web buckling stress were correspondingly lower than for steel girders. By neglecting beam action completely in such structures and considering the web as a membrane resistant only to tension, Wagner formulated the "Theory of Pure Diagonal Tension" (9). While pure diagonal tension is one limiting case of the state of stress in a thin web, pure shear is the other, occurring only in stocky webs. Extensive experimental studies were undertaken by the National Advisory Committee for Aeronautics to cover the transition range, where "incomplete diagonal tension" occurs (10).

There are several reasons why the civil engineering profession has not applied the highly specialized practice of aeronautical engineering to the analysis of their structures. One reason is the reluctance to consider the flanges as transversely loaded by the tension field forces and acting as beams supported by the intermediate stiffeners. The flanges, utilized primarily in carrying the girder's bending moment, would have to be specially designed to serve this secondary purpose. With a continuous skin, such as around a fuselage or a wing of an aircraft, the boundary conditions are much more favorable for membrane action than in a welded plate girder where no angle sections between web and flange plate are used, which would provide a certain degree of rigidity.

The purpose of the subsequent study is to derive a simple but general formula for the ultimate shear strength of steel girders with flanges not resistant to membrane tension and with webs so slender that a certain tension action might develop. Utilizing some idealizations, a functional dependance of the shear strength on the principal parameters will be established.

*Notation.*—The letter symbols adopted for use in this paper are defined where they first appear and are arranged alphabetically, for convenience of reference, in Appendix II.

### THE ULTIMATE SHEAR FORCE

Assuming that the ultimate shear force,  $V_u$ , of a transversely stiffened plate girder could be expressed in a formula, it would certainly have to be a function

of the following dimensional variables: the stiffener spacing  $a$ , the girder depth  $b$ , the web thickness  $t$ , and the material properties  $\sigma_y$  and  $E$ , where  $\sigma_y$  is the yield stress and  $E$  the modulus of elasticity. The shear force for which unrestricted shearing occurs shall be termed "plastic shear force,"  $V_p$ , analogous to the term "plastic moment,"  $M_p$ , used in plastic analysis. Since  $V_p$  has the dimension of a force, it must be possible to express the ultimate shear force  $V_u$  in the form  $V_u = V_p f(a, b, t, \sigma_y, E)$ , where the function  $f$  is nondimensional. Therefore, whenever  $\sigma_y$  or  $E$  should occur, they can be brought in the form  $\epsilon_y = \sigma_y/E$ . The remaining variables  $a, b$  and  $t$ , with the length as their dimensions, can only occur in ratios; where  $\alpha = a/b$  and  $\beta = b/t$  are sufficient to express all possible relations between these three variables. Thus, a formula for the ultimate shear load must be of the form

$$V_u = V_p f(\alpha, \beta, \epsilon_y) \dots \dots \dots (1)$$

From Mises' yield condition for plane stress, which is illustrated in Fig. 1 (d), it is seen that the shear yield stress  $\tau_y$  equals  $\sigma_y/\sqrt{3}$ . The full plastic shear force is reached when yielding occurs throughout the web depth  $b$ , hence

$$V_p = \tau_y b t = \frac{1}{\sqrt{3}} \sigma_y b t \dots \dots \dots (2)$$

The shear contribution due to a possible tension field is considered next. Assuming that a field of uniform tension stresses  $\sigma_t$  flows through a web's cross section  $b t$  (Fig. 2 (a)), the resulting shear force  $V$  depends on the inclination  $\phi$  of the tension stresses. From Fig. 2 (b) it is seen that the maximum value is obtained when  $\phi$  is  $45^\circ$  and thus

$$V_{\max} = \frac{1}{2} \sigma_t b t \dots \dots \dots (3)$$

Whether a tension field, which is a membrane stress field, can develop depends on the boundaries of the plate. With regard to membrane stresses, a panel in a girder web has two very different pairs of boundaries, those along the flanges and those along the transverse stiffeners. A flange of a conventionally built welded plate girder has so little bending rigidity in the plane of the web that it cannot effectively resist vertical stresses at its junction with the web. Such flanges, therefore, do not serve as anchors for a tension stress field. The situation is different at the panel boundaries along the transverse stiffeners (Fig. 2 (c)). There the tension strips can transmit the stresses. Thus, only a part of the web contains a pronounced tension field which gives rise to a shear force  $\Delta V_\sigma = \sigma_t s t \sin \phi$ , where  $s$ , the field width, also depends on  $\phi$ .

When a thin-web plate girder panel is subjected to shear, it will reach a stage at which the compressive stress  $\sigma_2$  indicated in Fig. 1 (a) ceases to increase because the web deflects. For the stress in the tension diagonal direction, no such evading of duty exists. When the shear force is increased, yielding initiates along the tension diagonal. A further increase of the applied shear

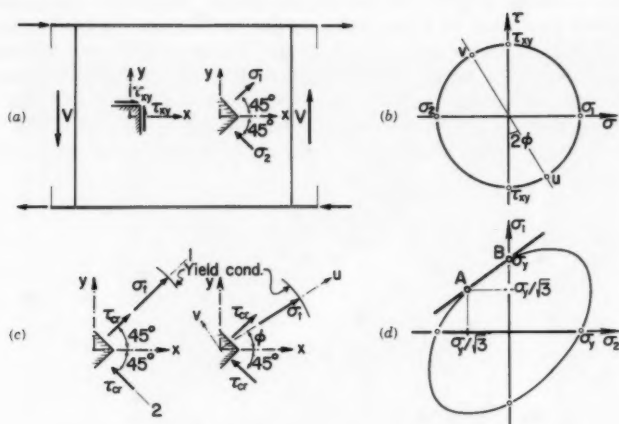


FIG. 1.—STATES OF STRESSES

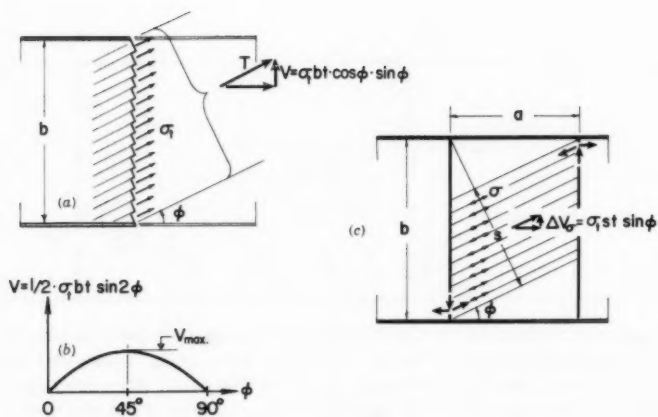


FIG. 2.—TENSION FIELD ACTION

force causes a wider portion of the web to yield. Since the increase in field width is gained by virtue of a decrease in the inclination of the tension stress with respect to the girder axis, an optimum value of the tension field contribution  $\Delta V_\sigma$  to the shear force  $V_\sigma$  is reached. It is reasonable to postulate that at ultimate shear load the inclination of the tension field is the one that furnishes the greatest total shear component  $\Delta V_\sigma$  of this tension field. With the notation as defined in Fig. 2 (c), this inclination is obtained from the condition

$$\frac{d}{d\phi} (\Delta V_\sigma) = \frac{d}{d\phi} (\sigma_y s t \sin \phi) = 0$$

or

$$\sigma_y t \left[ \frac{ds(\phi)}{d\phi} \sin \phi + s \cos \phi \right] = 0$$

With  $s(\phi) = b \cos \phi - a \sin \phi$ , it reduces to:

$$b \tan^2 \phi + 2 a \tan \phi - b = 0$$

which gives

$$\tan \phi = \frac{-a \left( \frac{+}{-} \right) \sqrt{a^2 + b^2}}{b} = \sqrt{1 + \alpha^2} - \alpha \dots \dots \dots (4a)$$

$$\sin \phi = \left[ \frac{1}{2} - \frac{\alpha}{2\sqrt{1 + \alpha^2}} \right]^{1/2} \dots \dots \dots (4b)$$

and

$$\cos \phi = \left[ 2\sqrt{1 + \alpha^2} \left( \sqrt{1 + \alpha^2} - \alpha \right) \right]^{-1/2} \dots \dots \dots (4c)$$

The strip corresponding to the optimum assumes a slope between  $45^\circ$  and  $0^\circ$ , when  $\alpha$  takes on values from 0 to  $\infty$ . It is also seen from Eqs. 4 that the tension strip inclination is less than the inclination of the panel diagonal, and the strip width a little wider than half the girder depth. In Fig. 3 the derived strip geometry is superimposed on a photograph of a thin-web girder panel subjected to shear (girder G7, Reference 11). The dark, yielded bands in the diagonally buckled zone, alternating with strips of unyielded or only slightly yielded metal, are due to the combined effect of bending and membrane stresses. The formation of the buckles produces plate bending stresses which are orthogonal to the diagonal tension (membrane) stresses and which are maximum at the surface of the web plate. Yielding is pronounced along the concave surfaces where

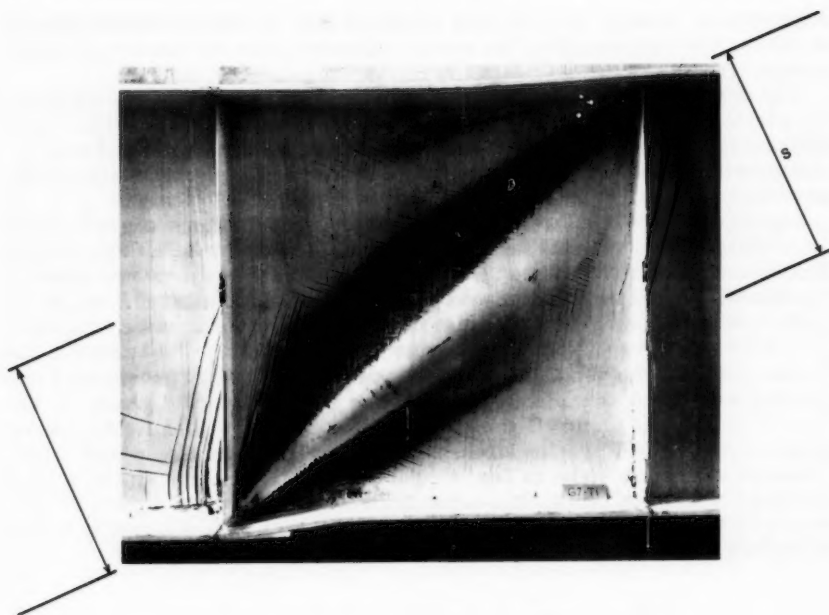


FIG. 3.—YIELDED SHEAR PANEL, 50 IN. BY 50 IN., 1/4 IN. WEB

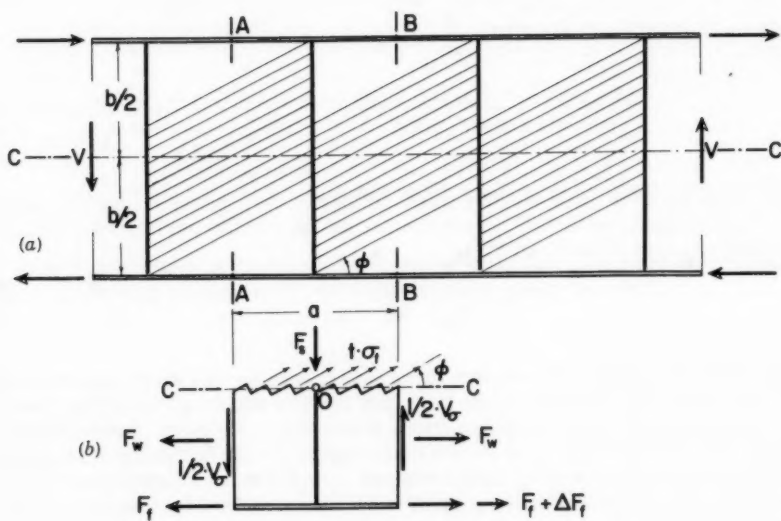


FIG. 4.—EQUILIBRIUM CONDITIONS APPLIED TO FREE BODY

compression bending stresses are superimposed on the membrane tension stresses, and retarded along the convex surfaces where the bending produces tension stresses, (Fig. 1 (c)).

Fig. 3 also illustrates the nature of the anchorage provided in the neighboring panels, where the horizontal tension component is transferred to the flange by shear. It indicates that the stiffeners must sustain axial forces. The magnitude of this shear and stiffener force can be derived using the idealized tension field, the inclination of which is fixed by Eqs. 4.

A succession of equal web panels all subjected to the same shear force is assumed as shown in Fig. 4 (a). Cutting along the sections A, B, and C, a free body is obtained as shown in Fig. 4 (b). At the face A in the web an unknown resultant is acting. It can be decomposed into a normal component  $F_w$  and a shear force component which, because of the symmetry of the chosen cut, must be  $V_\sigma/2$ . The force acting in the flanges is denoted as  $F_f$ . At section B the stress pattern in the web is the same as in section A, therefore the same components will occur as explained before. The flange force will change in the amount of  $\Delta F_f$ . At section C the stiffener force  $F_s$  and tension field stresses  $\sigma_t$  are acting. These tension stresses are under the inclination whose trigonometric values are given in Eqs. 4. Formulation of moments around point O and consideration of equilibrium in the horizontal and vertical directions furnishes three equations, from which the three unknowns  $\Delta F_f$ ,  $V_\sigma$ , and  $F_s$  can be computed:

$$\Delta F_f = -\sigma_t t a \sin \phi \cos \phi = -\sigma_t t b \frac{\alpha}{2\sqrt{1+\alpha^2}} \dots \dots (5a)$$

$$V_\sigma = -\frac{b}{a} \Delta F_f = \sigma_t t b \frac{1}{2\sqrt{1+\alpha^2}} \dots \dots \dots (5b)$$

and

$$F_s = +\sigma_t t a \sin \phi \sin \phi = \sigma_t t b \left( \frac{\alpha}{2} - \frac{\alpha^2}{2\sqrt{1+\alpha^2}} \right) \dots \dots (6)$$

In plate girders with slender webs neither a pure beam action ( $\tau$ ) nor a pure tension field action ( $\sigma$ ) occurs alone, but rather the sum of both. Therefore the ultimate shear load  $V_u$  is

$$V_u = V_\tau + V_\sigma \dots \dots \dots (7)$$

In order to compute these two shear contributions, two more assumptions are required. The first one is the postulate that the superposition of the stresses resulting from both carrying actions is limited by the state of stress which fulfills the yield condition, as shown in the sketch on the left-hand side of Fig. 1 (c). The second is the assumption that, up to  $\tau_{cr}$ , shear is carried in a beam-type manner, but that, from then on,  $V_\tau$  remains constant (an assumption reviewed in Appendix I). Any postbuckling benefit must be contributed by ten-

sion field action. Then,

$$V_{\tau} = V_{cr} = \tau_{cr} b t = V_p \frac{\tau_{cr}}{\tau_y} \dots\dots\dots (8)$$

According to the first assumption, the tension field stress  $\sigma_t$  can be expressed explicitly. It is defined as the stress which can be added to the state of shear stress at the point of bifurcation of equilibrium (where  $\tau_{xy}$  equals  $\tau_{cr}$ ) such that unrestricted yielding occurs in the tension field. For the following derivation, attention must be given to the subscripts used (Fig. 1 (c)). The fixed coordinates are  $x$  and  $y$ . The Cartesian coordinates  $u$  and  $v$  are generated out of  $x$  and  $y$  by counterclockwise rotation in the magnitude  $\phi$ . When  $\phi$  equals  $45^\circ$  these are called axis 1 and 2. By means of Mohr's circle, shown in Fig. 1 (b), it is seen that the state of shear stresses ( $\tau_{xy} = \tau_{cr}$ ) combined with the diagonal tension stress  $\sigma_t$  under the inclination  $\phi$  can be expressed as:

$$\sigma_u = \tau_{cr} \sin (2\phi) + \sigma_t \dots\dots\dots (9a)$$

$$\sigma_v = -\tau_{cr} \sin (2\phi) \dots\dots\dots (9b)$$

and

$$\tau_{uv} = \tau_{cr} \cos (2\phi) \dots\dots\dots (9c)$$

Introducing this set of stresses in Mises' yield condition

$$\sigma_u^2 + \sigma_v^2 - \sigma_u \sigma_v + 3 \tau_{uv}^2 - \sigma_y^2 = 0 \dots\dots\dots (10)$$

the following result for the tension field stress  $\sigma_t$  is obtained:

$$\frac{\sigma_t}{\sigma_y} = \sqrt{1 + \left(\frac{\tau_{cr}}{\sigma_y}\right)^2 \left\{ \left[ \frac{3}{2} \sin (2\phi) \right]^2 - 3 \right\}} - \frac{3}{2} \frac{\tau_{cr}}{\sigma_y} \sin (2\phi) \dots\dots (11)$$

With this expression the elements of the ultimate load computation are complete. According to Eqs. 5, 7, and 8 the ultimate shear load is:

$$V_u = V_p \left[ \frac{\tau_{cr}}{\tau_y} + \frac{\sqrt{3}}{2} \frac{\sigma_t}{\sigma_y} \sqrt{1 + \alpha^2} \right] \dots\dots\dots (12)$$

in which  $\sigma_t/\sigma_y$  is given by Eq. 11.

Two simplifications which will ease the numerical computation considerably are possible. The first one is an approximation of the yield condition which, for the case of plane stress, is pictured in Fig. 1 (d). It can be seen that states of stress anywhere between pure shear and pure tension only lead



to points on the ellipse between A and B. Hence the straight line  $\sigma_1 = \sigma_y + (\sqrt{3} - 1) \sigma_2$  passing through A and B is a fair approximation of the yield condition. For the limiting case of  $\phi$  equal to  $45^\circ$ ,  $\sigma_u$  and  $\sigma_v$  in Eqs. 9 become principal stresses,  $\sigma_1 = \tau_{cr} + \sigma_t$ , and  $\sigma_2 = -\tau_{cr}$ , respectively. If they are introduced in the approximate form of the yield condition, the following simple relation results:

$$\frac{\sigma_t}{\sigma_y} = 1 - \frac{\tau_{cr}}{\tau_y} \dots \dots \dots (13)$$

The second simplification is that the value for  $\sigma_t/\sigma_y$  be computed from Eq. 13 when  $\phi$  is not equal to  $45^\circ$ . This leads to a smaller tension field stress than Eq. 11 would give, and the underestimation increases the more  $\phi$  decreases from  $45^\circ$ , that is, as  $\alpha$  becomes larger. But, for panels with large  $\alpha$  ratios, larger shear displacements are required in order to develop a tension field. This second approximation should not, therefore, be considered merely as a simplification made on account of the economy but also as an allowance for compatibility conditions.

In order to check the influence of these two assumptions, the ultimate shear force, Eq. 12, was first computed using  $\sigma_t$  from Eq. 11 and termed  $V_u$  (11), then using Eq. 13 and termed  $V_u$  (13). The deviation would be defined as  $\delta\% = \frac{V_u(13) - V_u(11)}{V_u(11)} \cdot 100$ ; it is plotted in Fig. 5 against the variable  $\tau_{cr}/\tau_y$  for various values of  $\alpha$ . Combining the effects of both simplifications yields results which differ less than 10% from the shear load computation fulfilling Mises' yield condition exactly.

Thus, using Eqs. 12 and 13 the ultimate shear force can be computed as follows:

$$\frac{V_u}{V_p} = \frac{\tau_{cr}}{\tau_y} + \frac{\sqrt{3}}{2} \frac{1 - \frac{\tau_{cr}}{\tau_y}}{\sqrt{1 + \alpha^2}} \dots \dots \dots (14)$$

in which  $V_u$  represents the ultimate shear force;  $V_p$  is the plastic shear force  $= \tau_y b t$ ;  $\tau_y$  denotes the yield shear stress  $= \sigma_y/\sqrt{3}$ ;  $\alpha = a/b$ : aspect ratio, panel length to panel depth; and  $\tau_{cr}$  is the critical shear stress =

$$k(\alpha) \frac{\pi^2 E}{12(1 - \nu^2)} \left(\frac{t}{b}\right)^2.$$

When not otherwise stated,  $k(\alpha)$  is taken according to Reference 12 as  $k = 5.34 + \frac{4.00}{\alpha^2}$  for  $\alpha \geq 1$ , and  $k = 4.00 + \frac{5.34}{\alpha^2}$  for  $\alpha \leq 1$ . (This is the universally

accepted shear buckling coefficient for pin-ended rectangular plates. In European plate girder design, web buckling values are consistently given in relation to the parameter "web depth to web thickness," as is done previously. Thus, two different  $k$ -values must be stated to correspond to the cases when the panel length is greater than the web depth and when the panel length is less than the web depth. Since for a rectangular panel subjected to pure shear no distinction between loaded and unloaded edges is needed (all four edges are subjected to



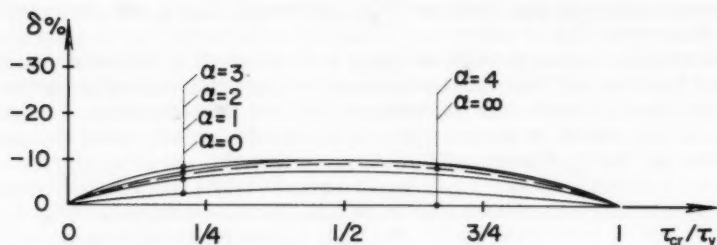
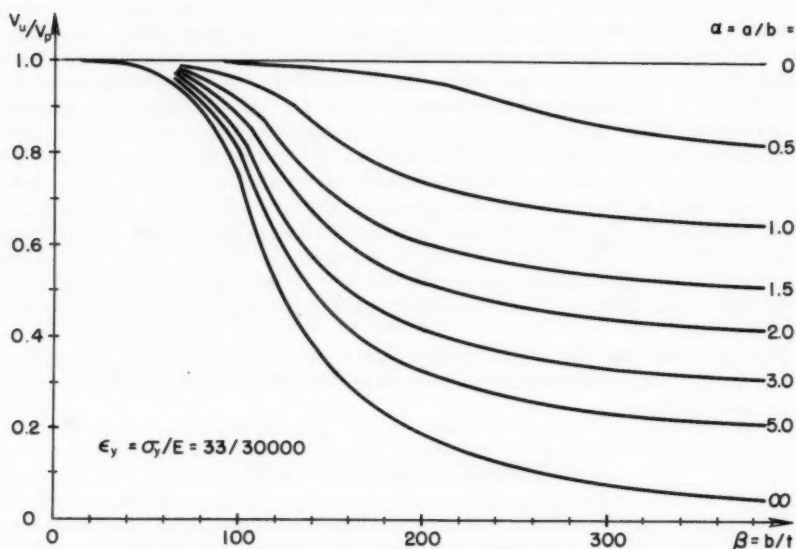


FIG. 5.—APPROXIMATION OF YIELD CONDITION

FIG. 6.—DEPENDENCE OF THE ULTIMATE SHEAR FORCE ON  $\alpha$  AND  $\beta$ 

the same shearing stress), an alternate way of stating the critical stress is the following:

$$\text{For } \alpha < 1.0, k = 5.34 + 4.00 \alpha^2, \tau_{cr} = \frac{k \pi^2 E}{12 (1-\nu^2)} \left( \frac{t}{a} \right)^2$$

$$\text{For } \alpha > 1.0, k = 5.34 + \frac{4.00}{\alpha^2}, \tau_{cr} = \frac{k \pi^2 E}{12 (1-\nu^2)} \left( \frac{t}{b} \right)^2$$

Neil Van Eenam pointed out that it is this second form which is more often used in American design practice.) Whenever the thus computed value  $\tau_{cr}$  exceeds the proportional limit, it has been considered only as an ideal value  $\tau_{cri}$  to be

reduced according to Eqs. 738 and 739 of Reference 12 in connection with Table 27 of Reference 12.

The reduction concept employed here does not allow a critical shear stress greater than  $\tau_y$  and thus does not account for any strain-hardening effect. It will, therefore, be too conservative for low web slenderness ratios. An estimate of this effect, based on experiments, is made subsequently under the heading "Influence of Strain-Hardening."

Using Poisson's ratio  $\nu = 0.3$ ,  $\tau_{cr}/\tau_y$  equals  $1.57 k(\alpha)/(\epsilon_y \beta^2)$ . Substituting this in Eq. 14 furnishes a function  $f$  on the right-hand side which depends on  $\alpha$ ,  $\beta$ , and  $\epsilon_y$  only. This function  $f(\alpha, \beta, \epsilon_y)$  is the one anticipated in Eq. 1, and it is seen that the requirement concerning the parameters is fulfilled.

The ultimate shear force according to Eq. 14 is plotted against the web slenderness parameter  $\beta$  in Fig. 6. With the nondimensional representation chosen, Fig. 6 gives the predicted ultimate force of a transversely stiffened thin-web plate girder as compared to the plastic shear force of the same girder. The influence of transverse stiffening is readily seen from Fig. 6. When stiffeners are not present, the value of  $\alpha = \infty$  applies. If the spacing were infinitely close, the girder could always develop its full strength, represented by the plastic shear load. The efficiency of transverse stiffeners depends very much on the slenderness ratio. The strength of a very slender web with a  $b/t$  ratio around 300 can be increased several times using stiffeners. This does not mean that a very close stiffener spacing, say  $\alpha = 0.5$ , should be chosen. It would be better to reduce the number of stiffeners and place additional material in the web. This would not only result in a lower slenderness ratio and hence permit a little higher allowable stress for any given value of  $\alpha$  but, because of the added web area, the computed shear stress for a given shear force would also diminish.

For the most efficient girder design it is necessary to specify the stiffener size required to achieve the derived tension field action. This will be discussed in the next section.

### INTERMEDIATE STIFFENERS

In contrast to loading stiffeners, intermediate stiffeners are transverse elements through which no external forces are introduced into the girder. Their function is two-fold: to preserve the shape of the girder's cross section and to insure postbuckling strength. Disregarding details at the flanges (which are thoroughly discussed elsewhere (13)), the first function will require a certain minimum stiffness. The second function demands a minimum strength, that is, a certain minimum cross-sectional area.

By dividing the girder's carrying capacity into two parts, simple beam action up to  $\tau = \tau_{cr}$  and tension field action up to yielding in the web, it is possible to determine stiffness and strength requirements for the transverse intermediate stiffeners separately. Because a state of shear stress corresponding to simple beam action (Fig. 1 (a)) causes no axial load in the stiffener whatsoever, the stiffener is only required to be rigid enough to force, at its location, a nodal line in the lateral deflection mode of the web. The stiffness requirements of the current design specifications are based on such considerations and ensure the required rigidity. In a tension field, however, the stiffener must take the vertical components of the diagonal stresses out of the web at one end and trans-

fer them to its other end. Therefore, this section will be devoted to the second requirement of an intermediate stiffener, the ability to sustain compression.

The stiffener force  $F_s$  is derived in Eq. 6. When the maximum shear force is reached, the value for  $\sigma_t$  can be taken from Eq. 13. The stiffener force to be expected at ultimate load is expressed by Eq. 15a. Depending on whether  $\alpha$  is greater or smaller than 1, and whether  $\tau_{cr}$  is beyond the proportional limit or in the elastic range, different analytical expressions for  $\tau_{cr}$  must be taken. An expression for the zone where  $\alpha \geq 1$  and  $\tau_{cri} = \tau_{cr}$  is given in Eq. 15b. It is seen that in nondimensional form the result is again only a function of the three independent variables  $\alpha$ ,  $\beta$ , and  $\epsilon_y$ :

$$F_s = b t \sigma_y \left( 1 - \frac{\tau_{cr}}{\tau_y} \right) \frac{\alpha}{2} \left( 1 - \frac{\alpha}{\sqrt{1 + \alpha^2}} \right) \dots \dots \dots (15a)$$

$$\left. \begin{aligned} \frac{F_s}{b^2 \sigma_y} &= \left[ \frac{1}{2\beta} - \left( 4.2 + \frac{3.1}{\alpha^2} \right) \frac{1}{\epsilon_y \beta^3} \right] \left( \alpha - \frac{\alpha^2}{\sqrt{1 + \alpha^2}} \right) \dots \dots \dots (15b) \\ &\text{where } \alpha \geq 1 \text{ and } \epsilon_y \beta^2 \geq 10.5 + \frac{7.8}{\alpha} \end{aligned} \right\}$$

Eq. 15a can be plotted against the two coordinates  $\alpha$  and  $\beta$ . This is done in Fig. 7 for  $\epsilon_y = 0.0011$ , by using the same  $k$ -values as shown following Eq. 14 and the reduction beyond the proportional limit as given in Eq. 18. There exists a maximum stiffener force which, surprisingly, is somewhere in the region where most girders are built. Its location can be found by partial differentiation of Eq. 15b with respect to the two variables  $\alpha$  and  $\beta$ . This will yield  $\alpha = 1.18$  and  $\beta = 6.22/\sqrt{\epsilon_y}$  with a maximum value of the stiffener force  $F_s = 0.015 \sqrt{\epsilon_y} \sigma_y b^2$ .

The physical explanation for this maximum is as follows. Comparing all plate girders with 50 in. web depth, the one with  $\alpha = 1.18$  and  $\beta = 187$  (corresponding to  $\epsilon_y = 33/30,000$ ) would require a stiffener strong enough to carry a 41 kip axial load in order to develop the maximum possible tension field. For all the other girders of the same depth the stiffener force corresponding to a full tension field could only be smaller, because:

- a. by increasing the stiffener spacing the tension field action becomes less and less effective and finally diminishes completely for  $\alpha = \infty$ ;
- b. by decreasing the stiffener spacing the stiffener density increases and therefore the share assigned to a single stiffener is reduced;
- c. by increasing the web slenderness the web area decreases and with it the ultimate shear force, which is an upper bound for the stiffener force; and
- d. by decreasing the web slenderness the web thickness increases and, although the web area becomes larger, more and more of the shear force will be carried in beam action leaving a diminished capacity for tension field action.

With this result, a simple expression for specifying the minimum required area of intermediate stiffeners can be derived as outlined next.

When the tension field has formed, part of the web is already at the stage of unrestricted yielding and no additional stresses can be assigned to it. Therefore, the stiffener force  $F_s$  can only be resisted by the actual area of the stiff-

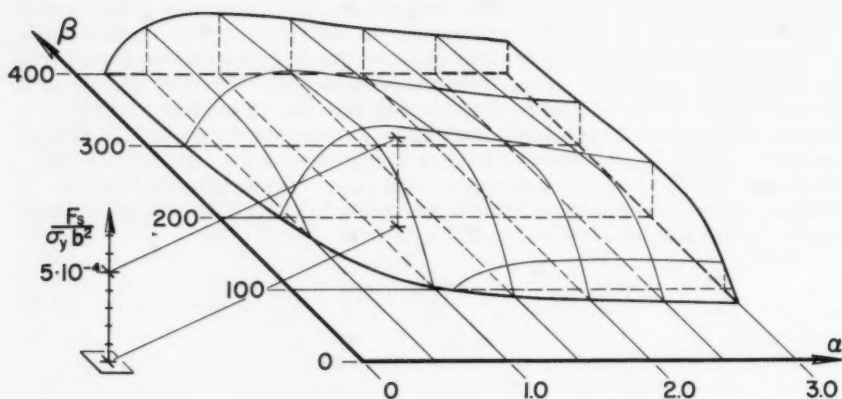
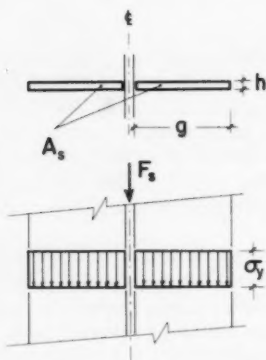
FIG. 7.—DEPENDENCE OF THE STIFFENER FORCE ON  $\alpha$  AND  $\beta$ 

FIG. 8.—STIFFENERS USED IN PAIRS

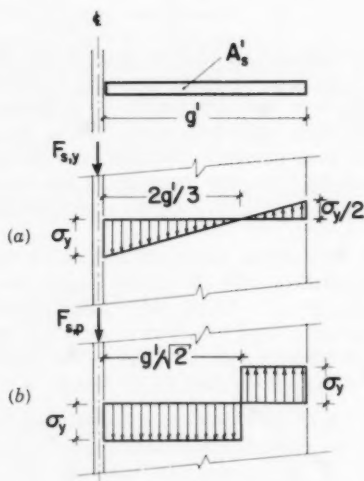


FIG. 9.—ONE-SIDED STIFFENERS

eners,  $A_s$ . ( $A_s$  is the sum of the areas of both stiffeners.) In this case the required area is simply  $F_s/\sigma_u$ , where  $\sigma_u$  is the ultimate axial stress in the stiffeners. If local buckling is avoided,  $\sigma_u$  is equal to the primary buckling stress of this stocky post, therefore practically equal to the stiffener's yield stress. If the latter is assumed to be the same as for the web, the following result is obtained:

$$\text{Required } A_s \geq 0.015 \sqrt{\epsilon_y} b^2 \dots \dots \dots (16a)$$

if not, this expression is to be multiplied by the ratio of web yield stress to stiffener yield stress.

In order to get a feeling for this area requirement, it is assumed that the stiffeners are built of rectangular plates with an outstanding leg width  $g$  which is 12 times the plate thickness  $h$  (Fig. 8). Assuming A7 steel, for which  $A_g \geq 0.0005 b^2$ , Eq. 16 then leads to  $g \geq b/18$ . That is, a 9 ft deep plate girder would require stiffeners of the size 2 plates - 6 in. by 1/2 in., while a girder with a web depth of only 4 ft 6 in. would require 2 plates - 3 in. by 1/4 in. A stiffener pair proportioned as just derived ( $g = b/18$ ,  $h = g/12$ ) exhibits a moment of inertia  $I_s \geq 53 \times 10^{-8} b^4$ , while  $I_g \geq 16 \times 10^{-8} b^4$  is the value required by Section 26 (e) of the AISC Specifications (14). Therefore, a stiffener size as derived here would simultaneously fulfill the minimum rigidity requirement for intermediate stiffeners.

Another stiffener arrangement, consisting of a single plate with cross-sectional area of  $A'_s$ , is presented in Fig. 9. It will be referred to as a one-sided stiffener. The plate is loaded along one of its edges. The state of stress in this plate, at the moment when yielding sets in, is shown in Fig. 9 (a). The axial load which causes this stress distribution is  $F_{sy} = 0.25 \sigma_y A'_s$ . If this load were increased and the stiffener plate proportioned such that unrestricted yielding is possible prior to plate buckling, the load would reach a limiting magnitude of  $F_{sp} = 0.414 \sigma_y A'_s$  and cause a stress distribution as shown in Fig. 9 (b). Equating each of the carrying capacities with the expected maximum value of  $F_s = 5.0 \times 10^{-4} \sigma_y b^2$  (derived for  $\epsilon_y = 0.0011$ ) gives:

$$\text{Yielding along the loading edge: } A'_s = 0.0020 b^2$$

$$\text{Yielding all over cross section: } A'_s = 0.0012 b^2$$

This is 2.4 to 4 times the area which a double-sided arrangement requires. It is interesting to note that an assumed participation of the web does not affect this relation. If participation would be assumed, equal effective web areas should be given to the one-sided and the double-sided arrangement. But then, by just deducting the amount which the web carries from  $F_s$ , the remainder of the force would cause the same relation between the one and the two-sides cases. In other words, no matter what minimum required area would be specified, a one-sided solution would use at least 2.4 times the sum of the areas of stiffeners made in pairs, provided the stiffeners are made of rectangular plates.

A one-sided stiffener plate may therefore have to be about five times as heavy as either of the plates in a two-sided arrangement when tension field action is the basis of design. This is more than would be expected. The reason for this is that stiffener sizes are generally determined using only a stiffness criterion. Taking moments of inertia about the axis at the interface between stiffener and web, it is readily seen that, if the outstanding leg of a one-sided stiffener is only 26% greater than the width of one of a pair, it would provide as much lateral stiffness. Therefore, with respect to stiffness, the one-sided stiffener would require only 63% of the total area of a two-sided arrangement, while 240% might be required to implement a tension field.

If an equal leg angle is used as a one-sided stiffener, the eccentricity would be less severe and a similar reasoning as given previously would lead to  $A'_s = 0.0009 b^2$  for A7 steel, or, generally expressed, 1.8 times the area of a stiffener pair.

In order to ensure an adequate shear transfer from the web plate into the stiffeners, the connectors (rivets or welds) will have to be sufficient in number and size. No matter whether the arrangement is one or two-sided, the connectors have to build up, over half the girder depth, a force that may be as much as  $F_s = 0.015 \sqrt{\epsilon_y} \sigma_y b^2$ . It is not expected that in actuality the shear transfer is exactly constant per unit length, such that a linear increase of the axial force over half the girder depth occurs. But a requirement that the stiffener force  $F_s$  be built up over a third of the depth should provide enough tolerance for nonuniformity in shear flow. The connectors then need to be proportioned so as to provide, at ultimate load, a shear flow  $v'$  per unit length of intermediate stiffener of  $3 F_s/b$ :

$$v' = 0.045 b \sqrt{\frac{\sigma_y^3}{E}} \dots \dots \dots (16b)$$

For A7 steel with a yield point of 33,000 psi and factors of safety of 1.65 or 1.83, the required shear flow for which rivets or welds must be designed at the commonly applied allowable stresses is  $30 b$  or  $27 b$ , respectively, where  $b$  is in inches and the shear flow is given in pounds per linear inch.

The area requirements of this section are derived under the assumption that the stiffener should not fail before the ultimate shear strength of the adjacent panels is reached. In girder sections predominantly subjected to bending, failure due to shear cannot occur and the required stiffener area may be reduced. Assuming the shear force  $V$  to be carried in beam action until the critical shear force  $V_{cr}$  is reached, only the excess  $V - V_{cr}$  carried in tension field manner causes axial forces in the transverse stiffeners. Hence the required value of stiffener area is obtained by reducing the previously specified values, which are obtained under the ultimate shear force  $V_u$ , in the ratio  $(V - V_{cr})/(V_u - V_{cr})$ . A simplification to the conservative side would be a reduction ratio  $V/V_u$ . In terms of allowable stresses this would be  $\tau/\tau_{all}$ ,  $\tau$  being the highest shear stress that can occur under any combination of live and dead load in one of the adjacent panels, and  $\tau_{all}$  the associated maximum permissible shear stress in that panel.

#### DETAILING OF GIRDER ENDS

For the end panel of a girder the boundary conditions are different than in an intermediate panel. When web yielding sets in, there is no neighboring plate serving as an anchor for a tension stress field. Bearing stiffeners at the end of a girder, together with an extended portion of the web, may offer partial restraint. Also, a more or less pronounced gusset plate action in the upper corner of the end of the web, as indicated in Fig. 14, may help to develop a partial tension action. But the degree of this contribution is uncertain. Since beam action does not depend on tension-resistant boundaries, the computed shear forces  $V_{cr}$  and  $V_u$  are the limits between which the ultimate shear strength of an end panel lies.

Premature failure of girders due to the failure of end posts was experienced and reported elsewhere (11). A picture of a failed girder end appears in Fig. 10. The web and end stiffener combination was not strong enough to resist the horizontal component of the tension field stress. An appreciation of





FIG. 10.—END POST FAILURE

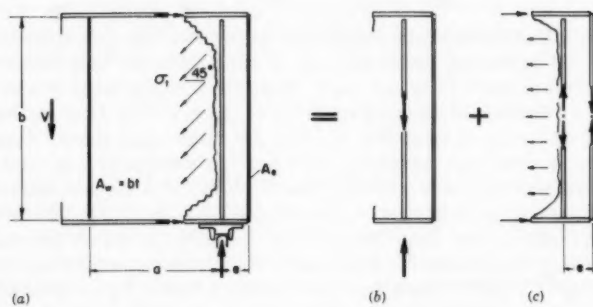


FIG. 11.—DETAIL AT GIRDER END

the curvature imposed on it is obtained by noting the plumb line hanging over the girder end and the compressive yielding at the outer edge of the stiffener flange and the web toe.

In order to exclude the possibility of a premature end panel failure in an unframed girder, as for example a bridge girder supported on masonry, there are two basically different approaches possible. The simplest and generally most economical solution (one which would have to be used on framed girders) is the choice of a stiffener spacing for the end panel such that the computed average shearing stress does not greatly exceed  $\tau_{cr}/N$ , where  $N$  is the factor of safety. A provision for such a limit has already been established (Reference 14, Sec. 26e and Reference 15, Art. 1.6.80).

To illustrate this, let it be assumed that the smaller dimension of the web plate be denoted as  $a$  and the larger as  $b$ . The limiting shear stress is then

$$\tau = \frac{\tau_{cr}}{N} = k \left( \frac{b}{a} \right) \frac{\pi^2}{N^{12} (1 - \nu^2)} E \left( \frac{t}{a} \right)^2$$

in which the value  $k (b/a)$  varies only between 9.34 (a square plate) and 5.34 (an infinitely long plate) (12). Assuming an average value of  $k = 7.34$  and a factor of safety  $N = 1.65$ , the previously given condition becomes

$$\tau \leq 4 E \left( \frac{t}{a} \right)^2 \dots \dots \dots (17a)$$

If the modulus of elasticity  $E$  and the shearing stress  $\tau$  are expressed in pounds per square inch and the inequality is solved for  $a$ , the well known expression (Sec. 26 (e), Reference (14)) is obtained

$$a > \frac{11,000}{\sqrt{\tau}} t \dots \dots \dots (17b)$$

While the first possibility of eliminating premature end panel failure exists in avoiding the development of a tension field in that panel, an alternate solution is to make the end post resistant to membrane tension. This could be done by bending down the top flange at the end of the girder or by welding an independent plate to the end. The required end post dimensions could be estimated as follows.

For simplification let it be assumed conservatively that the tension stress field would act under an inclination of  $45^\circ$  and be uniformly distributed over the entire girder depth (Fig. 11 (a)). Then the tension field would subject the end post to a vertical compressive force of  $V_\sigma = V - V_{cr}$  (the excess not taken by beam action) and a horizontal load of the same magnitude. Thus the maximum bending moment to which the end post is subjected amounts to  $V_\sigma b/8$ . That is, a compressive and a tensile force of  $V_\sigma b/(8e)$  are introduced in the end plate and bearing stiffener respectively (Fig. 11 (c)). The design of the bearing stiffener by the limitation of the bearing pressure is still adequate since the new force component induced is tensile and is superimposed on compression (Fig. 11 (b)). Equating the resisting force  $A_e \sigma_y$  offered by the end plate with the force component of the bending moment leads to  $A_e \sigma_y = (V - V_{cr}) b/(8e)$ . In terms of allowable stress and by substituting Eq. 17a for  $\tau_{cr}/N$ ,



the following expression for end post proportioning is obtained:

$$A_e = A_w \frac{b}{8e} \left( \frac{\tau}{\sigma_{all}} - \frac{4E}{\sigma_{all}} \frac{t^2}{a^2} \right) \dots \dots \dots (17c)$$

### INFLUENCE OF STRAIN-HARDENING

For all compression elements made of mild steel there exists a range of low slenderness ratios within which the actual failure stress exceeds the yield stress. This is explained by the fact that yielding is confined to slip bands. The steel next to these bands is only on the verge of yielding whereas that within the bands already has strain-hardened. Thus, the member never loses all its rigidity, and it is a mistake to assume that all buckling curves must end at the yield level as the slenderness ratio approaches zero. Haaijer and Thürlimann (16) have determined the range of slenderness ratios in which compact columns and plates subjected to edge compression will strain-harden before reaching their limiting buckling stress. So far there exists no similar theoretical treatment for the case of shear, although it appears to be of significance since the webs of all rolled sections are proportioned on the assumption that the limit of their shear carrying capacity lies in the strain-hardening range.

In order to obtain an estimate of the shear strength in this low web slenderness range, recourse can be made to experimental work. Fortunately, there exists a series of tests carried out by Inge Lyse and H. J. Godfrey (7) which cover the range of web depth-to-thickness ratios from 50 to 70. The tests included welded plate girders without intermediate transverse stiffeners, whose test data are summarized in the upper left quadrant of Table 1. How far the experimentally obtained ultimate shear force,  $V_u^{ex}$ , exceeded the plastic shear force  $V_p$  is seen from Fig. 12, which uses the same coordinates introduced before with Fig. 6.

It becomes apparent in comparing these test results with Fig. 6 that the conventionally applied reduction procedure as stated in connection with Eq. 14 is too conservative. Let it be assumed that a relationship of the simple form  $\tau_{cr} = C \tau_{cri}^n$  exists above the proportional limit with  $C$  and  $n$  to be determined. Since the ideal critical stress  $\tau_{cri}$  and the actual critical stress  $\tau_{cr}$  have to be equal at the proportional limit  $\tau_{pr}$ , the value  $C$  is determined as  $C = \tau_{pr}^{(1-n)}$ . Trials to fit the Lyse-Godfrey test data indicate that, for  $\tau_{pr}$  equal to  $0.8 \tau_y$ , 0.5 is the best choice for the exponent  $n$ . Thus, the reduction formula becomes

$$\tau_{cr} = \sqrt{\tau_{pr} \tau_{cri}} \dots \dots \dots (18)$$

which affords a much more realistic estimate of the shear strength in the inelastic and strain-hardening range.

Since the difference in shear strength given by Figs. 6 and 12 are based on the presence of local strain-hardening, which must be preceded by shear yielding, the shear resisting capacity of the web cannot be assumed as being significantly augmented by the development of a tension field when  $\tau_{cr} > \tau_y$ . Hence, when substituting Eq. 18 in Eq. 14, the second term in the righthand side must be omitted if  $\tau_{cr} > \tau_y$ .

TABLE 1.—SUMMARY OF SHEAR

Source	Girder No.	Experimental Values			
		$\alpha = \frac{a}{b}$	$\beta = \frac{b}{t}$	$A_w$ , in sq in.	$\sigma_y$ , in kips per sq in.
(1)	(2)	(3)	(4)	(5)	(6)
Group A Reference 7	WB - 1	3	56.5	3.47	43.3
	WB - 2	3	54.9	3.57	47.8
	WB - 3	3	58.9	4.36	49.6
Group B Reference 7	WB - 6	3	70.0	4.40	33.1
	WB - 7	3	60.6	3.88	33.7
	WB - 8	3	59.7	4.10	29.7
	WB - 9	3	50.0	3.12	30.3
	WB - 10	3	49.4	3.14	30.3
Part 3 Reference 11	G6 - T1	1.5	259	9.65	36.7
	G6 - T2	0.75	259	9.65	36.7
	G6 - T3	0.5	259	9.65	36.7
	G7 - T1	1.0	255	9.80	36.7
	G7 - T2	1.0	255	9.80	36.7
Part 4 Reference 11	E1 - T1	3.0	131	19.1	41.7
	E1 - T2	1.5	131	19.1	41.7
	G8 - T1	3.0	254	9.85	38.2
	G8 - T3	1.5	254	9.85	38.2
	G9 - T3	1.5	382	6.55	44.5

$$^a \tau_{cri} = k \frac{\pi^2 E}{12 (1 - \nu^2)} \left( \frac{t}{b} \right)^2 = k \frac{26750}{\beta^2} \text{ kips per sq in., with } k = 5.34 + \frac{4.00}{\alpha^2} \text{ for}$$

$$^b \tau_{cr} = \tau_{cri} \text{ when } \tau_{cri} \leq 0.8 \tau_y, \text{ and } \tau_{cr} = \sqrt{0.8 \tau_y \tau_{cri}} \text{ for } \tau_{cri} > 0.8 \tau_y.$$

$$^c \text{ Computed according to Eq. 14 when } \tau_{cr} \leq \tau_y; \text{ for } \tau_{cr} > \tau_y, \text{ simply } V_u/V_p =$$

$$^d \text{ Values under Column 11 multiplied by } \tau_y A_w.$$

Because Fig. 12 can accommodate only two parameters, namely the stiffener spacing  $\alpha$  and the webslenderness ratio  $\beta$ , the curves can be applicable for only one value of  $\sigma_y$ , in this case taken as 33 kips per sq in. Such a value for  $\sigma_y$  is approximately correct for the beams of Group B in Table 1. For comparison, the curve for Group A beams where  $\sigma_y$  equals 47 kips per sq in. is shown as a dashed line. For all other test results the ratio  $V_u/V_p$  was adjusted for a normal yield stress of 33 kips per sq in., thus showing graphically the deviation from the theoretical prediction.

Fig. 12 also gives a survey of all the predominantly shear-type tests ever carried out at Fritz Engineering Laboratory on welded plate girders. The necessary test information (Experimental Values) and the theoretical predic-

## TESTS ON WELDED PLATE GIRDERS

$V_u^{ex}$ , in kips	Theoretical Values					$\frac{V_u^{ex}}{V_u^{th}}$
	$\tau_y = \frac{\sigma_y}{\sqrt{3}}$ , in kips per sq in.	$\tau_{cr}^a$ , in kips per sq in.	$\frac{\tau_{cr}^b}{\tau_y}$	$\frac{V_u^c}{V_p}$	$V_u^{thd}$ , in kips	
(7)	(8)	(9)	(10)	(11)	(12)	(13)
109	25.0	48.6	1.25	1.25	108	1.01
128	27.6	51.3	1.22	1.22	120	1.07
139	28.6	44.6	1.12	1.12	139	1.00
96	19.1	31.6	1.15	1.15	97	0.99
95	19.5	42.3	1.32	1.32	100	0.95
100	17.2	43.5	1.43	1.43	101	0.99
92	17.5	62.0	1.69	1.69	92	1.00
94	17.5	63.6	1.71	1.71	94	1.00
116	21.2	2.85	0.134	0.550	112	1.04
150	21.2	5.40	0.254	0.771	157	0.95
177	21.2	10.1	0.477	0.882	180	0.98
140	21.2	3.85	0.182	0.682	142	0.98
145	21.2	3.85	0.182	0.682	142	1.02
278	24.1	9.00	0.374	0.545	250	1.11
290	24.1	11.1	0.460	0.719	330	0.88
85	22.0	2.30	0.105	0.350	76	1.12
117	22.0	2.95	0.134	0.550	119	0.98
79	25.7	1.31	0.050	0.506	85	0.93
Standard-deviation						0.06

$\alpha > 1$ , and  $k = 4.00 + \frac{5.34}{\alpha^2}$  for  $\alpha < 1$ .

$\tau_{cr}/\tau_y$ .

tions (Theoretical Values) are presented for each individual test in Table 1. Column 13 gives the correlation between theory and experiment.

## ALLOWABLE SHEAR STRESSES

With Eq. 14 and the modification for strain-hardening presented in the previous section, the function  $f(\alpha, \beta, \epsilon_y)$  anticipated in Eq. 1 is established and plotted in Fig. 12 for the special case of  $\epsilon_y = 0.0011$ . Using Eqs. 1 and 2, the ultimate shear force can be expressed as given in Eq. 19a. Dividing both sides by a factor of safety  $N_u$  against ultimate load, the allowable shear force,  $V_{all}$ ,

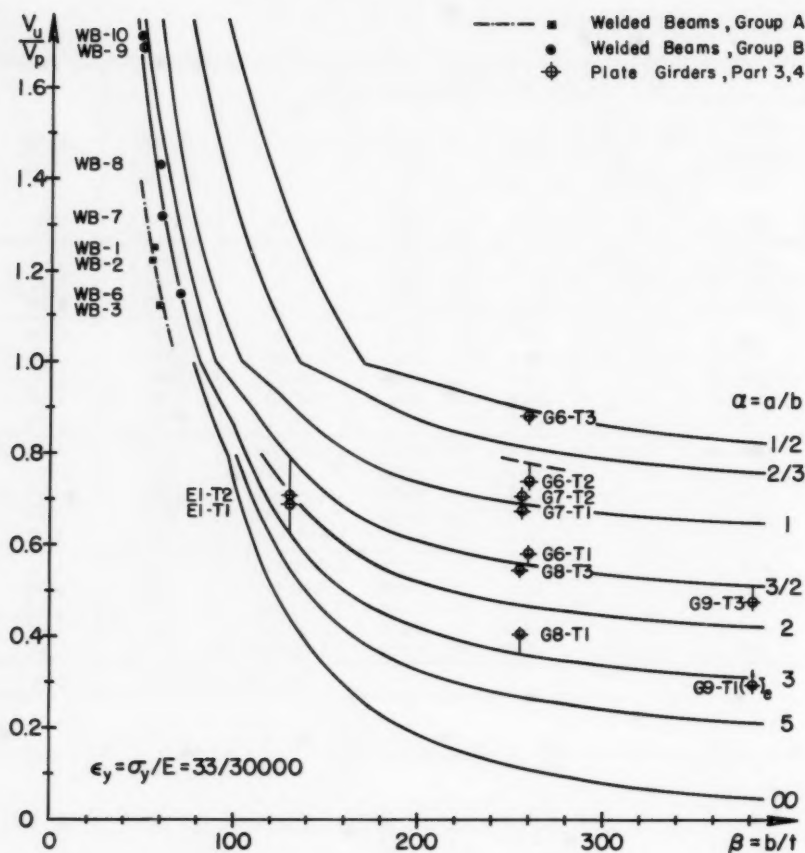


FIG. 12.—TEST RESULTS OF WELDED PLATE GIRDERS SUBJECTED TO SHEAR

appears in Eq. 19b. With the conventional shear stress computation (shear force divided by the web area) the allowable stress is expressed in Eq. 19c.

$$V_u = \frac{\sigma_y}{\sqrt{3}} b t f(\alpha, \beta, \epsilon_y) \dots \dots \dots (19a)$$

$$V_{all} = \frac{V_u}{N_u} = \frac{\sigma_y}{N_u \sqrt{3}} b t f(\alpha, \beta, \epsilon_y) \dots \dots \dots (19b)$$

and

$$\tau_{all} = \frac{V_{all}}{b t} = \frac{\sigma_y}{N_u \sqrt{3}} f(\alpha, \beta, \epsilon_y) \dots \dots \dots (19c)$$

In assuming a constant factor of safety  $N_u = 1.65$  and a yield stress of 33 kips per sq in., the allowable shear stresses for various values of  $\alpha$  and  $\beta$  are plotted in Fig. 13. Because the shear yield stress is  $\tau_y = 33/\sqrt{3} = 19$  kips per sq in., the nominal factor of safety against yielding is  $19/13 = 1.46$  in the presently used AISC Specifications (14). There appears no reason to change this margin which is merely a margin against deformations greater than those associated with elastic shear strain and not against catastrophic failure. Therefore, the maximum allowable shear stresses are limited to 13 kips per sq in. With the same reasoning the allowable shear stresses for the AASHTO Specifications could be fixed. The proposed factors of safety against ultimate load and yielding are  $N_u = 33/18 = 1.83$  and  $N_y = 19/11 = 1.73$ , respectively.

If it should be considered desirable to assign different factors of safety  $N_\tau$  and  $N_\sigma$  for beam and tension field action, respectively, this could readily be done due to the special nature of Eq. 14. Thus, the permissible shear stresses in the most general form would read:

$$\left. \begin{aligned} \tau_{all} &= \frac{\sigma_y}{N_\tau \sqrt{3}} \left( \frac{\tau_{cr}}{\tau_y} + \frac{1 - \frac{\tau_{cr}}{\tau_y}}{\frac{2 N_\sigma}{\sqrt{3} N_\tau} \sqrt{1 + \alpha^2}} \right) \text{ for } \frac{\tau_{cr}}{\tau_y} \leq 1 \\ \tau_{all} &= \frac{\sigma_y}{N_\tau \sqrt{3}} \frac{\tau_{cr}}{\tau_y} \text{ for } 1 < \frac{\tau_{cr}}{\tau_y} < \frac{N_\tau}{N_y} \\ \text{with } \frac{\tau_{cr}}{\tau_y} &= \frac{\pi^2 \sqrt{3} E}{12(1-\nu^2) \sigma_y} \frac{k}{\beta^2} \text{ for } \frac{\tau_{cr}}{\tau_y} \leq 0.8 \\ \frac{\tau_{cr}}{\tau_y} &= \sqrt{\frac{0.8 \pi^2 \sqrt{3} E}{12(1-\nu^2) \sigma_y} \frac{k}{\beta^2}} \text{ for } \frac{\tau_{cr}}{\tau_y} > 0.8 \end{aligned} \right\} \dots (19d)$$

In the range of high web slenderness ratios, the stiffener spacing should not be arbitrarily large. Although the web might still be sufficient to carry the shear, the distortions could be almost beyond control in fabrication and under load. In the past the AASHTO and the AISC Specifications limited the maximum stiffener distance to 6 ft and 7 ft, respectively. With a minimum web thickness of 5/16 in., and a stiffener spacing of 7 ft the distance between stiffeners would never exceed 270 times the web thickness. It is suggested that such a relative measure, rather than an absolute one, be used to specify the maximum stiffener spacing in the range of high web slenderness ratios. The rule, that the shorter panel dimension does not exceed 270 times the web thickness when  $\alpha < 1.0$ , was used to terminate the curves of Fig. 13. The justification for such a rule can be found in the fact that the resistance of a rectangular plate to transverse loading is essentially governed by the ratio of shorter span to plate thickness.

In the medium range of web depth-to-thickness ratios, the cut-off curve is arbitrarily taken as a straight line between the points  $\alpha = \infty$ ,  $\beta = 170$  and  $\alpha = 1$ ,  $\beta = 270$ . These limits may be too liberal for certain cases. The designer's judgement, however, is still needed to determine the density of transverse stiffeners when rigidity and stiffness criteria, or fabrication and erection aspects, are governing rather than mere strength considerations.

Finally, in the low range of web depth-to-thickness ratios, detail considerations generally determine the location of stiffeners. A direct application of load to the web can be made for webs which are proportioned to allow a certain degree of strain-hardening (that is, for webs whose allowable shear stress is

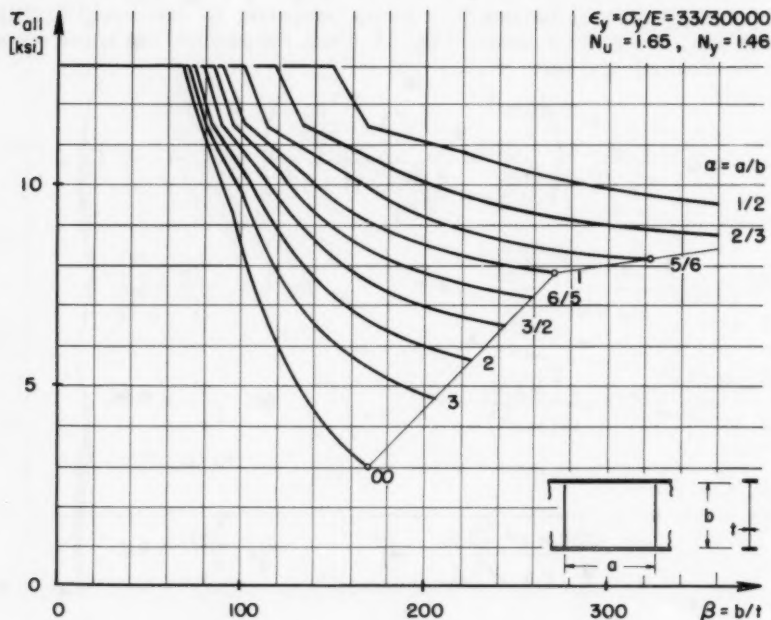


FIG. 13.—PROPOSED ALLOWABLE SHEAR STRESSES (AISC)

13 kips per sq in.), provided the compressive stress at the webtoe of the fillets is suitably limited in order to avoid web crippling. For all other cases the load application must be made by means of transverse stiffeners, unless it can be shown that the transverse pressure is small enough not to cause vertical buckling of the flange into the web.

## APPENDIX I.—REVIEW OF THE ULTIMATE SHEAR STRENGTH THEORY

In order to determine the shear strength of a girder it was assumed that the girder acts according to beam theory up to the critical load and thereafter in a tension field manner up to the point of web yielding. Considering initial web distortions and residual stresses due to welding, the probability of a clearly defined boundary between these two types of behavior appears questionable. The assumption should, therefore, be taken as an estimate for the amount of shear to be carried in compression rather than a phenomenon that can be actually observed.

If a plate subjected to shearing stresses is assumed to be built of two sets of strips orthogonal to each other and acting in compression and tension respectively, the compression strips are then elastically supported by the tension strips. This is the reason why the critical stress of a shear panel is much higher than that of an equivalent isolated compression strip extending from panel border to panel border. If more tension is superimposed on the tension strips, it is obvious that, until yielding occurs, the conditions for stresses in the compression strips are improved since the "spring constants" of the elastic supports increase. But when yielding sets in, the ratio of shear carried in beam and in tension field action changes again. From the recorded load deflection curves in Reference 11, which generally exhibit a pronounced yield plateau, it is seen that the reduction in beam action is about compensated by the gain in tension field action due to the increase in field width. After all, the derived ultimate shear force expression is not very sensitive to a slight error in this assumption. If the contribution  $V_T$  in Eq. 8 would be overestimated, the yield condition would allow less tension field action and vice versa.

Some remarks as to the geometry of the tension field are in order. The inclination of the tension field was obtained from a maximum value condition as they were assumed to exist on a model girder. The assumption was made that the edges of the effective field would run through the panel corners (Fig. 4), and the two web triangles not included in the tension strip were not thought to be idle. They were supposed to digest the membrane stresses caused by the neighboring panels' tension fields and ultimately transfer them to the flanges. The shear force thus created is given by Eq. 5 and the resulting stiffener force by Eq. 6. Let this derivation be called Approach A.

It can be shown that the established expression for  $V_G$  is not very strongly dependent on the above derived tension field geometry. Another approach, Approach B, would lead to the same result. Let it be assumed that the girder carries the load in a truss-type manner, that is, that a tension diagonal forms whose centerline coincides with the panel diagonal and whose effective width, so far unknown, is a certain fraction of the girder depth, say  $\kappa b$ . This would lead to a shear contribution  $V_G = \kappa b t \sigma_t \sin \phi$ , where  $\phi = \arccot \alpha$ . Hence,

$$V_G = \kappa b t \sigma_t \frac{1}{\sqrt{1 + \alpha^2}}$$



When  $\alpha$  approaches  $\infty$ ,  $V_G$  diminishes to zero. At the other limit,  $\alpha = 0$ , the highest possible tension field contribution as derived in Eq. 3 should result. This fixes the constant  $\kappa$  as equal to  $1/2$ , and it is observed that  $V_G$ , derived this way, is exactly the same as in Eq. 5 of Approach A.

Using this second approach, however, the stiffener force  $F_s$  would equal the shear force  $V_G$ . This would mean that even for very close stiffener spacing each stiffener would have to carry the full amount of  $V_G$ , which is obviously incorrect. The reason for this deficiency is the fact that, for small values of  $\alpha$ , this truss assumption violates the yield condition because the strips of neighboring panels overlap and use portions of the web twice. But the longer the panel, the closer is the agreement between the stiffener forces of the two approaches. For  $\alpha \gg 1$ , Eqs. 5 and 6 yield the same result. Indeed, it will be

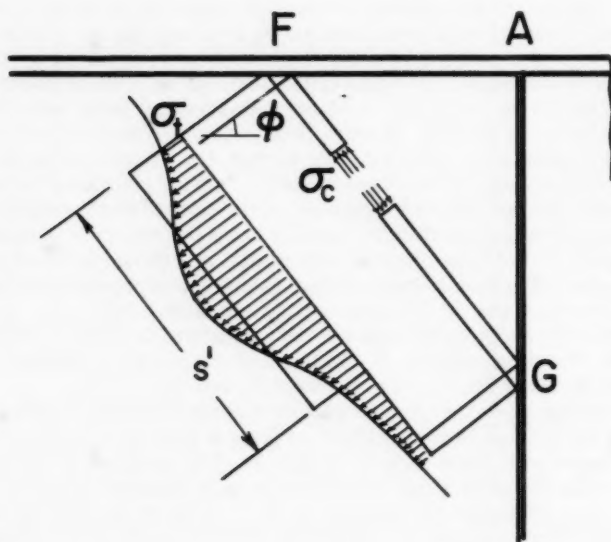


FIG. 14.—GUSSET PLATE ACTION

indicated next that for larger values of  $\alpha$  and lower slenderness ratios the tension diagonal of Approach B is not an impossible one, although its centerline, rather than its effective edge, is assumed to run through the panel corner.

For simplification, the plate corner may be considered to be built of two sets of orthogonal strips, one set under tension stresses  $\sigma_t$ , the other under compression stresses  $\sigma_c$ , as illustrated in Fig. 14. The postulate that no membrane stresses orthogonal to the plane of the top flange can occur leads to the relation  $\sigma_c = \sigma_t \tan^2 \phi$ . In approaching the corner the compression strips can pick up stress because the strip length shortens. According to the previously given relation this will be accompanied by a gradual increase of tension stresses as shown in Fig. 14. If this gradual increase of tensile stresses is ideal-



ized, the tension field may be thought to have an effective width intersecting the top flange at point F, some distance away from the corner A of the panel. It is seen that this distance increases with the web thickness and decreases to zero for an extremely thin web. Fig. 15 is a photograph of a panel with an aspect ratio  $\alpha = 1.5$ . It is taken from a girder with a sturdy web ( $\beta = 133$ ) and shows that the "edge" of the tension field is shifted away from the panel corners. Both the tension field (Approach A) and the tension diagonal (Approach B) are shown in outline. The tension field actually developed can, in this case, be considered to be between the predictions of the two approaches.

Finally, an Approach C might eliminate completely the idea of tension field inclination and effective width. This approach seeks merely for the simplest

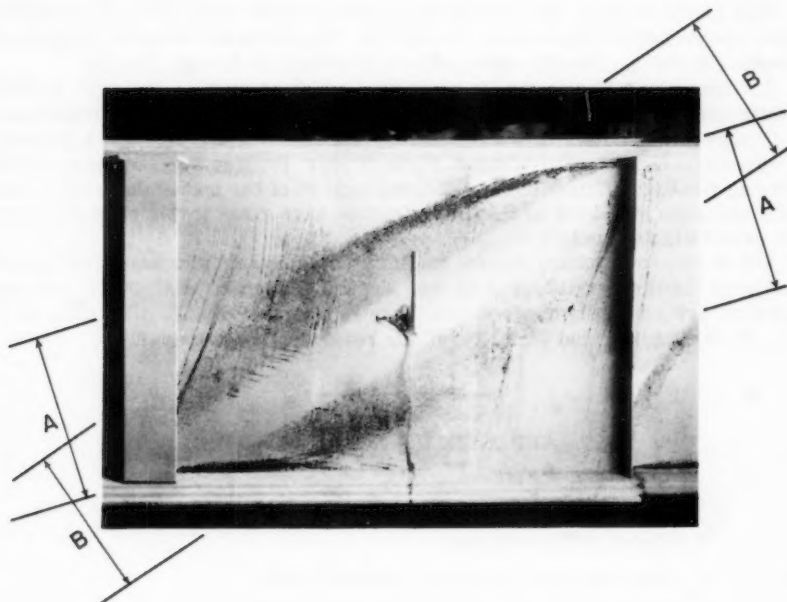


FIG. 15.—APPROACHES A AND B

set of coordinate functions which yield a result that might commonly be expected from a tension field type action. In order to free the functions from dimensions,  $V_\sigma$  is to be expressed as  $V_{\max} f(\alpha)$ , where  $V_{\max}$  is the highest possible shear force to be carried by tension stresses alone (Eq. 3) and is here considered to be the "amplitude." The pure coordinate function  $f(\alpha)$  must be normalized such that  $f(\alpha = 0) = 1$ . For large values of  $\alpha$ , it should approach zero with the power of  $1/\alpha$ . The most obvious choice for a simple function fulfilling these two limits is

$$f(\alpha) = (1 + \alpha^n)^{-\frac{1}{n}} \quad n > 1 \dots \dots \dots (20)$$

The result previously derived in Approaches A and B would be obtained for  $n = 2$ . Since no physical significance was noted in this approach, it does not give any detail information at all. For instance, since no stress flow is pictured, an equilibrium condition cannot be applied to get a stiffener force.

From this review it is seen that different interpretations of the state of web stress lead to about the same result with regard to the ultimate strength. This is rather comforting because the state of stress in a slender girder web at loads less than the static ultimate load cannot be obtained exactly from tension strips with constant effective width and inclination.

#### ACKNOWLEDGMENTS

This paper is based on a dissertation (17) carried out at Fritz Engineering Laboratory, Lehigh University, Bethlehem, Pennsylvania, of which William J. Eney is the Head. The Director of the Laboratory is Lynn S. Beedle.

The investigation was jointly sponsored by the American Institute of Steel Construction, the Pennsylvania Department of Highways, the U. S. Department of Commerce - Bureau of Public Roads, and the Welding Research Council. It was supervised by the Welded Plate Girder Project Subcommittee of the Welding Research Council. The financial support of the sponsors and the guidance which the members of the subcommittee have given to this research work are gratefully acknowledged.

The writer owes many thanks to Bruno Thürlimann who was professor in charge of the dissertation and former Project Director. His advice and suggestions are sincerely appreciated. Thanks are also due L. S. Beedle, B. T. Yen, T. R. Higgins, and W. A. Milek for reviewing the manuscript.

---

#### APPENDIX II.—NOTATIONS

---

A	= Area of cross section;
$A_s$	= cross sectional area of a stiffener pair;
$A'_s$	= cross sectional area of a one-sided stiffener;
a	= spacing of transverse stiffeners;
b	= depth of girder web;
E	= modulus of elasticity (30,000 kips per sq in.);
e	= distance, defined in Fig. 11;
F	= force;
k	= buckling coefficient;
s	= tension field width;
t	= thickness of web;
V	= shear force;

- $\alpha = a/b$  = aspect ratio, panel length to panel depth;  
 $\beta = b/t$  = slenderness ratio, web depth to web thickness;  
 $\epsilon$  = strain;  
 $\nu$  = Poisson's ratio (0.3);  
 $\sigma$  = normal stress;  
 $\tau$  = shear stress; and  
 $\phi$  = inclination of tension field;

Subscripts (or Superscripts):

- all = allowable;  
c = compression;  
cr = critical;  
ex = experimental;  
f = flange;  
p = plastic;  
pr = proportional;  
s = stiffener;  
t = tension;  
th = theoretical;  
u = ultimate;  
w = web;  
y = yielding;  
 $\sigma$  = as carried in tension; and  
 $\tau$  = as carried in shear.

---

APPENDIX III.—REFERENCES

---

1. "A Theory for Spacing Stiffeners in Plate Girders," by H. T. Beach, Engineering News, Vol. 39, No. 20, May, 1898, p. 322.  
Discussions:  
Engineering News, Vol. 39, No. 23, p. 370; Vol. 40, No. 1, p. 10; and Vol. 40, No. 6, p. 90.
2. "Spacing Stiffeners in Plate Girders," by Joseph M. Wilson, Engineering News, Vol. 40, No. 6, August, 1898, p. 89.  
Discussions:  
Engineering News, Vol. 40, No. 10, September, 1898, p. 154.

3. "Tests of the Stress in Plate Girder Stiffeners," by F. E. Turneaure, Engineering News, Vol. 40, No. 12, September, 1898, p. 186.
4. "Spacing Stiffeners in Plate Girders," by C. A. P. Turner & F. G. Shinner, Engineering News, Vol. 40, No. 25, December, 1898, p. 399.
5. "Spacing Stiffeners in Plate Girders," by H. T. Beach, Engineering News, Vol. 41, No. 7, February, 1899, p. 106.  
Discussion:  
Engineering News, Vol. 41, No. 15, 1899, p. 234.
6. "Strength of Webs of I-Beams and Girders," by H. F. Moore & W. M. Wilson, Bulletin 86, Univ. of Illinois, 1916.
7. "Investigation of Web Buckling in Steel Beams," by I. Lyse & H. J. Godfrey, Transactions, ASCE, Vol. 100, 1935, p. 675.
8. "Beitrag zur Theorie der Knickerscheinungen," by H. H. Rode, Wilhelm Engelmann Verlag, Leipzig, 1916, (Dissertation), and Eisenbau, Vol. 7, 1916, p. 121, 157, 210, 239, and 296.
9. "Ebene Blechwandträger mit sehr dünnem Stegblech," by H. Wagner, Zeitschrift für Flugtechnik und Motorluftschiffahrt, Vol. 20, 1929, p. 200, 227, 256, 279, and 306.
10. "A Summary of Diagonal Tension," by P. Kuhn, J. P. Peterson, & R. L. Levin, Tech. Note 2661, N.A.C.A., 1952.
11. "Web Buckling Tests on Welded Plate Girders," by K. Basler, B. T. Yen, J. A. Mueller, & B. Thürlimann, Bulletin No. 64, Welding Research Council, New York, September, 1960.
12. "Buckling Strength of Metal Structures," by F. Bleich, McGraw-Hill Book Co., New York, 1952.
13. "Plate Girder Research," by K. Basler & B. Thürlimann, Proceedings, A.I.S.C. Nat. Engrg. Conf., 1959.
14. "Steel Construction, Manual," A.I.S.C., New York, 1959.
15. "Standard Specifications for Highway Bridges," A.A.S.H.O., Washington, D. C., 1957.
16. "On Inelastic Buckling in Steel," by G. Haaijer, & B. Thürlimann, Proceedings, ASCE, Vol. 84, No. EM 2, April, 1958.
17. "Strength of Plate Girders," by K. Basler, Dissertation, Microfilm 59-6958, University Microfilms, Inc., Ann Arbor, Mich., 1959.

---

Journal of the  
**STRUCTURAL DIVISION**  
Proceedings of the American Society of Civil Engineers

---

**STRENGTH OF PLATE GIRDERS UNDER COMBINED BENDING AND SHEAR**

By Konrad Basler,<sup>1</sup> A. M. ASCE

---

**FOREWORD**

An investigation of welded plate girders was conducted at Lehigh University during the years 1957 to 1960. The objective of this project was to determine the static carrying capacity of transversely stiffened plate girders. The study was grouped into an experimental and a theoretical phase, and the results of the experiments were published as a Welding Research Council Bulletin.

The theoretical considerations are presented as a series of three papers, covering first the bending strength (Proc. Paper 2913, August 1961 Journal of the Structural Division), then the shear strength (Proc. Paper 2967, October 1961 Journal of the Structural Division), and finally the interaction between bending and shear (this paper).

---

Note.—Discussion open until March 1, 1962. Separate discussions should be submitted for the individual papers in this symposium. To extend the closing date one month, a written request must be filed with the Executive Secretary, ASCE. This paper is part of the copyrighted Journal of the Structural Division, Proceedings of the American Society of Civil Engineers, Vol. 87, No. ST 7, October, 1961.

<sup>1</sup> Consultant, Egg b. Zurich, Switzerland; formerly Res. Asst. Prof. at Lehigh Univ., Bethlehem, Pa.

---

### SYNOPSIS

A study of possible interaction between bending moments and shear forces on the carrying capacity of plate girders is presented. Based on theoretical considerations and experimental results, approximations suitable for design use are suggested.

---

### INTRODUCTION

Most plate girders are subjected to a combination of bending and shear. It is possible that a girder section can be subjected to bending moments alone, but not to shear alone. To postulate that no bending moments should occur over a girder panel would exclude shear forces likewise, since shear force is the rate of change of bending moment. Nevertheless, it is safe to disregard moments in the treatment of shear as long as they do not exceed a certain magnitude to be determined here.

Interaction will be concerned with a rearrangement of stress for two reasons. In very slender webs the stress rearrangement is predominantly due to web deflections; slight deflections of the web from a plane result in a transfer of the bending moment resistance from the web to the flange. This is achieved without a loss in shear carrying capacity which is essentially contributed by a tension field. In girders with stockier webs, however, the bending moment which cannot be carried by the web, because of high concurrent shear, is transferred to the flange through yielding.

For these reasons, compatibility conditions can be ignored to a great extent when the load carrying capacity of plate girders is determined. The procedure will thus be similar to plastic analysis, in which a lower bound of the carrying

capacity is obtained by considering a possible state of stress which is in equilibrium with the applied moment and shear yet nowhere violates the yield condition.

*Notation.*—The letter symbols adopted for use in this paper are defined where they first appear and are arranged alphabetically, for convenience of reference, in Appendix I.

### THE INTERACTION FORMULA

The flange moment,  $M_f$ , is defined as the moment carried by the flanges alone when the stresses over the entire flange are equal to the yield stress  $\sigma_y$ . The yield moment,  $M_y$ , is the moment initiating yielding at the centroid of the compression flange. The resisting moment of a fully yielded cross section is denoted as the plastic moment (1),<sup>2</sup>  $M_p$ . Approximating the distance between the flange centroids as equal to the web depth  $b$  and designating the area of a single flange as  $A_f$  and the web area as  $A_w$ , the three reference moments of a symmetrically proportioned girder cross section can be expressed as

$$M_f = \sigma_y b A_f \dots\dots\dots (1a)$$

$$M_y = \sigma_y b \left( A_f + \frac{1}{6} A_w \right) \dots\dots\dots (1b)$$

and

$$M_p = \sigma_y b \left( A_f + \frac{1}{4} A_w \right) \dots\dots\dots (1c)$$

The shear force  $V$  and the bending moment  $M$  give information as to their relative importance only if they are compared with girder properties. For this reason, and also to non-dimensionalize  $V$  and  $M$ , the shear force will be expressed in terms of the ultimate shear force  $V_u$  (2), and the moment in terms of the yield moment  $M_y$ . The shear force and the bending moment are not independent of each other. When the loading condition is fixed, the shear force and bending moment at any cross section of a particular girder depend on the common parameter  $P$  which denotes the load intensity. Therefore, the ratio  $M/V$  is independent of the load and characterizes the loading condition. If a Cartesian coordinate system has abscissa and ordinate of  $M/M_y$  and  $V/V_u$ , respectively, then there is an associated polar system whose length of radius vector is directly proportional to the load intensity  $P$ . The interaction curve  $C$  in such a coordinate system, Fig. 1, is defined as the boundary between points on the safe side and those which lead to failure. Because the vector length may be interpreted as the load intensity, the ultimate load  $P_u$  for a cross section subjected to bending and shear is by definition the intersection of its particular ray with the curve  $C$ . With this preparation the derivation of the interaction curve follows.

As pointed out in the "Introduction," the web can transfer its allotted moment to the flanges and retain its shear strength, provided that the moment

<sup>2</sup> Numerals in parentheses refer to corresponding items in Appendix II—References.

capacity of the flange is not exceeded. This means that, in the coordinate system explained previously, the failure curve is represented by a straight line

$$\frac{V}{V_u} = 1 \quad \dots \dots \dots (2)$$

as shown in Fig. 2.

Since a web which carries the ultimate shear force is utilized up to yielding, the flanges are the sole carriers of the bending moment. If it is assumed for the time being that these flanges are proportioned and laterally stiffened such that the yield stress can be reached, then the limiting moment which they can take is the flange moment  $M_f$ . If there were no shear present, the maximum moment that could be expected under the most favorable circumstances, disregarding strain-hardening, is the plastic moment  $M_p$ . The only portion on the moment scale where bending moments affect the shear carrying capacity

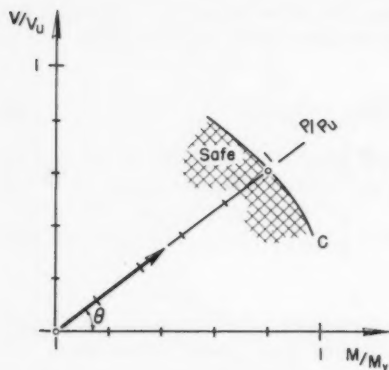


FIG. 1.—INTERACTION DIAGRAM

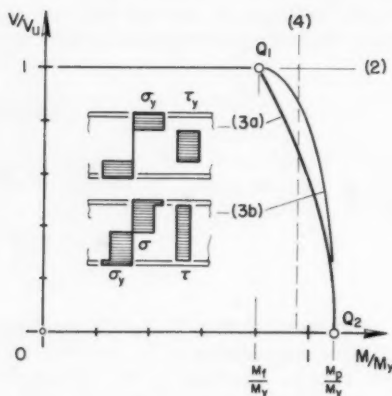


FIG. 2.—POSSIBLE INTERACTION CURVES

is therefore that between  $M_f$  and  $M_p$ . Thus, an interaction curve must pass through the points  $Q_1 (M_f/M_y, 1)$  and  $Q_2 (M_p/M_y, 0)$ . Since very small quantities of shear hardly affect the moment carrying capacity, the interaction curve should also start off at right angles to the abscissa at point  $Q_2$ .

The simplest set of interaction curves fulfilling these conditions is that given in Eq. 3a, with the exponent  $n$  greater than unity.

$$\left(\frac{V}{V_u}\right)^n + \frac{M - M_f}{M_p - M_f} = 1 \quad \dots \dots \dots (3a)$$

and

$$\left(\frac{V}{V_u}\right)^n + \left(\frac{M - M_f}{M_p - M_f}\right)^m = 1 \quad \dots \dots \dots (3b)$$



Should the curve also be tangent to the line  $V/V_u = 1$  at point  $Q_1$ , an interaction formula of the type of Eq. 3b would be required with  $m$  and  $n$  greater than unity.

For an exponent  $n = m = 2$ , possible states of stress leading to Eqs. 3a and 3b, respectively, are shown in Fig. 2. In approach (Eq. 3a) it is assumed that the portion of the web which participates with the flanges in resisting moment is unable to carry shear. In approach (Eq. 3b) normal stresses  $\sigma$  and shearing stresses  $\tau$  act over the entire web depth, but are interrelated with Mises' yield conditions:  $\sigma^2 + 3\tau^2 = \sigma_y^2$ .

In view of tension field action the more conservative approach (Eq. 3a), or (Eq. 3b) with  $m = 1$ , is preferred. The choice of an exponent  $n = 2$  for girders with very slender webs may be somewhat hypothetical. But in evaluating the strength of girders subjected to pure bending (3), it was shown that little more than the flange moment is preserved in slender web girders. Therefore, most of the interaction curve Eq. 3a is cut off by the requirement

$$\frac{M}{M_u} = 1 \quad \dots\dots\dots (4)$$

in which  $M_u$  is the ultimate bending moment evaluated from Eq. 18a of Reference 3. In Fig. 2, Eqs. 2, 3, and 4 are plotted for the case of  $M_f = 0.80 M_y$ ,  $M_u = 0.95 M_y$  and  $M_p = 1.10 M_y$ .

For its application to design, it is of advantage to express the interaction equations in terms of stress. Rewriting Eq. 3a with an exponent  $n = 2$  and solving it for the bending moment  $M$  leads to Eq. 5a.

$$M = M_f + (M_p - M_f) \left[ 1 - \left( \frac{V}{V_u} \right)^2 \right] \quad \dots\dots\dots (5a)$$

$$\frac{M}{S} \frac{S}{M_y} = \frac{M_f}{M_y} + \frac{M_p - M_f}{M_y} \left[ 1 - \left( \frac{V}{A_w} \frac{A_w}{V_u} \right)^2 \right] \quad \dots\dots\dots (5b)$$

$$\sigma = \sigma_y \frac{1 + \frac{1}{4} \frac{A_w}{A_f} \left[ 1 - \left( \frac{\tau}{\tau_u} \right)^2 \right]}{1 + \frac{1}{6} \frac{A_w}{A_f}} \quad \dots\dots\dots (5c)$$

and

$$\sigma = \frac{\sigma_y}{N} \frac{1 + \frac{1}{4} \frac{A_w}{A_f} \left[ 1 - \left( \frac{\tau}{\tau_{all}} \right)^2 \right]}{1 + \frac{1}{6} \frac{A_w}{A_f}} \quad \dots\dots\dots (5d)$$

Eq. 5b is obtained by dividing either side of Eq. 5a by the yield moment  $M_y$  and expanding certain fractions, where  $S$  denotes the section modulus and  $A_w$  the web area. The ratio  $M/S$  is the flange stress  $\sigma$  due to bending,  $M_y/S$  is the

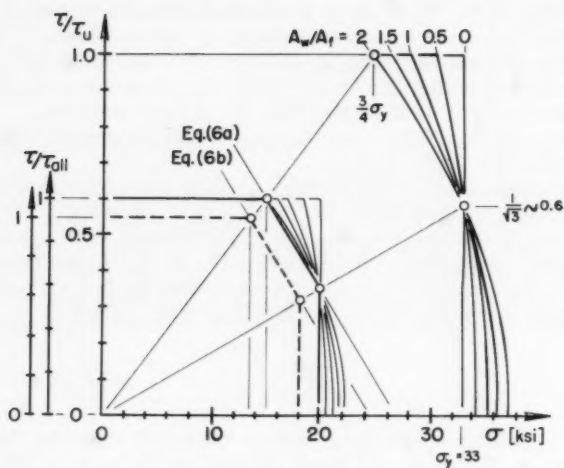


FIG. 3.—FAILURE ENVELOPES AND ALLOWABLE STRESSES

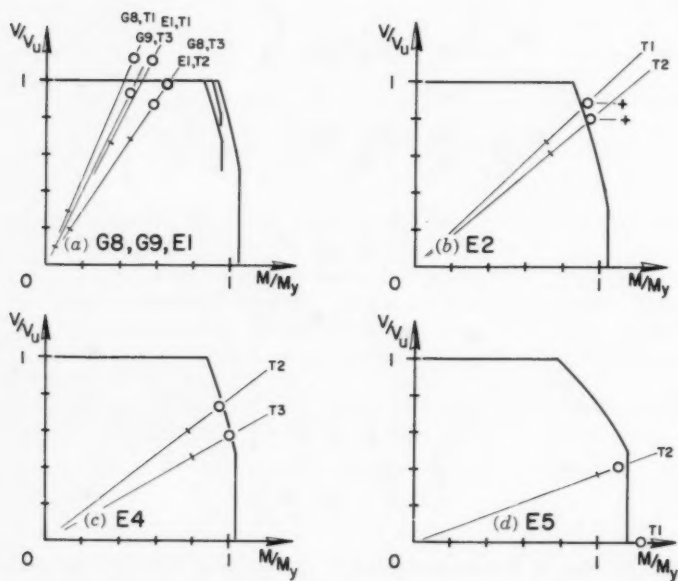


FIG. 4.—TEST RESULTS

yield stress  $\sigma_y$ ,  $V/A_w$  is the average shearing stress in the web, and  $V_u/A_w$  is the ultimate shear stress. If these values are substituted and the ratios  $M_f/M_y$  and  $(M_p - M_f)/M_y$  are expressed according to Eqs. 1, the result in Eq. 5c is obtained. Using this expression with various ratios of  $A_w/A_f$  and a yield stress  $\sigma_y = 33$  kips per sq in. (A7 steel) the failure envelopes are shown in Fig. 3.

If a constant factor of safety ( $N = 1.65$ , AISC) is applied, the coexistent allowable bending and shear stresses are as indicated in Fig. 3 by the thin lines determined from Eq. 5d. It is seen that, with the choice of an ultimate bending stress of 20 kips per sq in., an interaction check is required only if the shear stress exceeds about 60% of the allowable value. Also, an interaction limit in flange stress is not required below 15 kips per sq in. when  $A_w/A_f < 2$ . Since this ratio of web to flange area is about the upper limit of the generally used girder proportions, the possible interaction rules for girders made of A7 steel are:

$$\text{AISC: } \sigma < 27 - 12 \frac{\tau}{\tau_{\text{all}}} \quad \dots\dots\dots (6a)$$

and

$$\text{AASHO: } \sigma < 24.5 - 11 \frac{\tau}{\tau_{\text{all}}} \quad \dots\dots\dots (6b)$$

These two conditions are indicated in Fig. 3. The allowable stress range resulting from a factor of safety  $N = 1.83$  (AASHO) is plotted in broken lines.

Thus far, interaction has been treated solely as a stress problem. Conditions caused by local and overall instability of the compression flange must at least be mentioned. This will be done in the remaining part of this paper.

### CORRELATION WITH TEST RESULTS

In the course of this investigation some girders were tested with the purpose of obtaining information on the interaction between bending and shear. The girder properties, loading arrangement, and the test observations of these girders are presented elsewhere (4). With the help of the flange moment  $M_f$  and the plastic moment  $M_p$  (listed in Table 1.7 of Reference 4) as well as the ratios  $V_{u\text{ex}}/V_{u\text{th}}$  derived in Table 1 of Reference 2, the interaction diagrams of Fig. 4 are constructed. The reference moment values  $M_y$  which were used differ from those given in Table 1.7 of Reference 4 in that they are taken as the moment value which initiates yielding at the compression flange centroid, and not at the extreme fiber of the compression flange.

Girders G8, G9 and E1 are shear girders. Girders E2 and E4 furnished the most significant interaction data. Girder E5 is predominantly a bending girder. Since on each ray the distance of a point from the origin is directly proportional to the applied load, the relation between the conventionally computed web buckling load, the predicted ultimate load, and the experimentally obtained ultimate load can be easily visualized. The intersection of a ray with the failure envelope gives the predicted ultimate load, the circled points mark the observed ultimate loads, and the conventional buckling theory predicts web instability at a load (Table 1.9, Reference 4) indicated by a short transverse bar.

The choice of the cross section for which the moment values were computed is of significance because the bending moment varies throughout the length of the test girders and only the shear force stays constant (Fig. 1.3 of Reference 4). This section was chosen to be in the failed panel at a longitudinal distance one-half the web depth away from the high-moment end, or at the middle of the longitudinal panel dimensions when its length was less than its depth. The crosses shown in Fig. 4(b) would represent the test results if the sections with the maximum bending moment were used.

To justify the choice of a section other than at the moment peak, and also to illustrate the uncertainties unavoidably encountered when predicting ultimate loads in general and interaction in particular, the following paragraphs are presented. Of the various possibilities where small errors could occur, only those associated with the determination of the girder's yield strength and the choice and application of the yield condition will be examined.

The yield stress, on which all the test results discussed in this plate girder investigation are dependent to a great extent, is a material property whose determination depends on the shape of the coupon and the testing speed. To evaluate the accuracy with which the yield strength of a member can be predicted on the basis of coupon results, reference is made to tests conducted at Fritz Engineering Laboratory (5). It was found that for eighteen different wide flange shapes the static yield stresses of stub columns deviate between -8.2% and +4.7% from the yield strength predicted by the coupons. This indicates the uncertainty implicit in large scale experiments which should not be overlooked, even though coupon measurements are made on the very steel plates of which the test girder is built and even though both coupon and girder yield stress are obtained under static condition of zero strain rate.

The shear yield stress can only be computed from the tensile yield stress. Different values will be obtained depending on the assumed yield condition. The "yield condition of constant maximum shear stress," or "Tresca's yield condition," gives  $\tau_y = 0.50 \sigma_y$ . In this investigation Mises' yield condition was used for which  $\tau_y = 0.58 \sigma_y$ , this being 15% higher than predicted according to Tresca. The very fact that it is not known which of these two conditions is the more appropriate points up the much bigger uncertainties connected with yield level than with the steel properties  $E$  and  $\nu$  used in the theory of elasticity. Thus, the scatter of results seen in Fig. 4(a) is within the range that has to be expected when shear test results on built-up girders are compared with predictions based on coupon tests.

Mises' yield condition finds its application in most European specifications when interaction between bending and shear in plate girders is considered. Here the stress intensity

$$\sigma_g = \sqrt{\sigma_u^2 + \sigma_v^2 - \sigma_u \sigma_v + 3 \tau^2} \dots \dots \dots (7)$$

must not exceed a specified stress level at any point in the web. Thus, the same margin against incipient yielding is obtained as in a test coupon subjected to the normal stress  $\sigma_g$ . This method is, however, unsatisfactory for an interaction check of plate girders. Along the panel borders are residual stresses of unknown magnitude which are always neglected in the application of Eq. 7. Even if their magnitude were known, an estimate of the static carrying capacity could not be made, since the load producing yielding at one point is not in a

constant relationship with the load causing such exhaustion of ductility that failure of the structure occurs.

It would be better to accept as a criterion for carrying capacity that the yielding must spread over an entire girder cross section. Then it would be justified to disregard residual stresses due to fabrication since their resultant over an entire cross section vanishes. Still, a failure mechanism is only theoretically obtained by postulating an ideal elastic-plastic stress-strain relation. As soon as a pronounced moment gradient (shear force) is involved, test results are likely to exceed the predictions based on maximum moment. This has been observed with beams (Fig. 5.7, Reference 1) as well as with plate girders as pointed out before, and is due to the strain-hardening effect. Barring premature failure due to primary instability, failure of a statically determinate girder only occurs when yielding has progressed not only over the en-

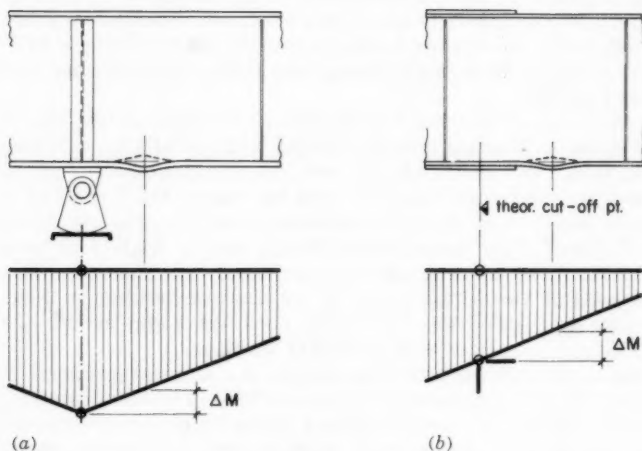


FIG. 5.—LOCAL TORSIONAL BUCKLING OF COMPRESSION FLANGE

tire cross section at peak moment but also over a certain length of the girder as well, after which failure is triggered by local inelastic buckling of a compression element. It must be noted that, due to the requirement of transverse stiffeners at places where concentrated loads are introduced, the maximum bending moment occurs always at the end of a panel. At this cross section, however, the web as well as the compression flange is restrained against local instability by the transverse stiffener which allows this yielded zone of limited length to strain-harden. Therefore, local torsional buckling of the flange occurs at cross sections where the moment value is smaller than that at the theoretical reaction line or cover plate end, as is illustrated in Fig. 5.

Consequently, in presenting the test results a "significant cross section" is chosen rather than the loading point at the end of a panel where the moment is

highest. This beneficial effect of a moment gradient will be considered again while discussing the influence of torsional buckling on interaction.

### INFLUENCE OF FLANGE INSTABILITY

So far it has been assumed that failure would occur by plain yielding, that is, the flanges could be strained up to the yield level without a premature instability failure due to lateral, torsional or vertical buckling of the compression flange. This requirement will now be dropped and the question raised as to how the results obtained by analyzing these three failure modes on girders subjected to pure bending (3) must be modified in the case of a combination of bending and shear.

The presence of shear has both a detrimental and a beneficial aspect. The beneficial aspect is due to the fact that shear forces always imply a moment gradient and, therefore, only a short girder portion is affected by the maximum moment. The adverse aspect is that a web which is exhausted by shear cannot simultaneously take its allotted bending moment and the flanges will have to compensate for it, resulting in a higher flange stress than computed by the section modulus concept.

*Lateral Buckling.*—From Fig. 7 of Reference 3 it is seen that the overturning moment (torsion) causing lateral buckling is made of a contribution by the compression flange and another by the web. A rearrangement of stresses between the web and the flange, however, does not change the overall or resulting overturning moment. And since the resisting moment, which is dependent on the lateral stiffness of the compression flange, is only slightly affected by the higher stress level, the adverse influence previously mentioned can be neglected in an analysis of lateral buckling. If the ultimate bending moment due to flange instability is called  $M_u$ , the failure condition given by Eq. 4, which is independent of shear, applies also to lateral buckling.

It remains to discuss the beneficial aspect of a moment gradient. This can be evaluated in the way proposed by Clark and Hill (6) and advocated in another publication (7), namely, by multiplying by a factor  $C_1$  the elastic critical stress which would result if the entire girder section were subjected to pure bending. Thus, the lateral buckling expression as represented in Eq. 11 of Reference 3 is generalized as follows:

$$\frac{\sigma_{cr}}{\sigma_y} = 1 - \frac{\lambda^2}{4 C_1} \quad 0 < \lambda < \sqrt{2 C_1} \quad \dots\dots\dots (8a)$$

and

$$\frac{\sigma_{cr}}{\sigma_y} = \frac{C_1}{\lambda^2} \quad \lambda > \sqrt{2 C_1} \quad \dots\dots\dots (8b)$$

in which

$$\lambda = \frac{1}{r} \sqrt{\frac{\epsilon_y}{\pi^2}} = 1 \sqrt{\frac{\epsilon_y}{\pi^2} \frac{A_f + \frac{1}{6} A_w}{I_f}}$$

Pursuant to the recommendation, Eq. 4.6, Reference 7, the effective inelastic buckling stress is obtained on the basis of an equivalent column slenderness,





and is reduced from Euler's curve in the same way as the basic column curve, Sec. 2.2, Reference 7. Eq. 8a fixes the thus derived critical stress in the inelastic range. This reduction in the inelastic range is graphically indicated in Fig. 6, where the buckling stress curves are plotted for various values of  $C_1$ .

As explained when discussing the case of pure bending (3), the standard slenderness abscissa  $\lambda$  in Fig. 6 can be supplemented by one for  $1/r$  and  $1/(2c)$ , the former being the slenderness ratio obtained by considering the compression flange together with  $1/6$  of the web as a column, while the latter is simply the ratio of buckling length to flange width, applicable only if the flange is a rectangle. Both of these abscissas are plotted for a yield strain  $\epsilon_y = 33/30,000$ ; the  $\lambda$  scale, however, is appropriate for any yield strain. Instead of the lateral bracing distance  $l$ , the "k-length"  $k l$ , an effective lateral buckling length, can be introduced to account for restraining influences offered by neighboring sections. Since St. Venant torsion is neglected, the value  $k$  is exactly

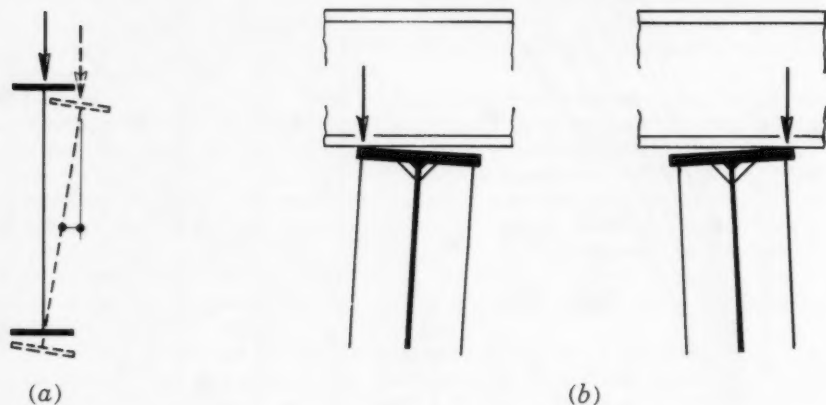


FIG. 7.—THE TIPPING EFFECT

the same as for columns subjected to identical axial stresses and end restraint as the compression flange, and also has the same physical significance (3).

Denoting as  $\kappa$  the ratio of the smaller end moments of a longitudinal girder segment free from interspan loads to the larger end moment, Eq. 4.13 of Reference 7 gives the following expression for the coefficient  $C_1$ :

$$C_1 = 1.75 - 1.05 \kappa + 0.3 \kappa^2 \quad (-0.5 < \kappa < +1) \quad \dots \quad (9)$$

This relationship between the stress raising coefficient  $C_1$  and the moment gradient is based on solutions obtained by Salvadori (8). With help of the sketches to the right of Fig. 6, the beneficial influence of a moment gradient can be readily studied.

A few cases of a girder with interspan loads are also inserted in Fig. 6. Here the critical stress is often further modified to include the effect of location of load application (top flange or bottom flange). If a load is suspended



from the bottom flange, the buckling stress curves presented are conservative; if loaded on top, a tipping effect could make the result unconservative. Although it makes a significant difference whether the load is acting through the shear center or not, it must be pointed out that, for the case of plate girders, the tipping effect is more an academic than a real problem. In most cases the points of load application are simultaneously points of lateral bracing. Even in the case where the loading beam is laterally unstayed the physical picture still does not correspond to the condition pictured in Fig. 7(a), since a cross beam offers torsional restraint to the girder. As seen from Fig. 7(b), the cross beam would exert a torsional restraint even if it were not tied to the girder by bolts. Transverse stiffeners are required under concentrated loads, hence theoretical knife edge load application at flange center is rather unlikely to occur. But when it does, as in the case of a crane girder, concurrent lateral forces are usually taken into account, and the analysis changes from an eigenvalue into a boundary value problem, i.e. stress limitations at the flange tips govern the design rather than lateral buckling stress. For these reasons no further provision against tipping seems required in plate girder specifications.

*Torsional Buckling.*—According to the analysis of girders subjected to pure bending given in Reference 3, torsional buckling is preceded by lateral buckling if the ratio of flange width to thickness is smaller than twelve plus the ratio of lateral buckling length to flange width. For larger flange width-thickness ratios, a critical stress can be obtained by entering Fig. 6 with the buckling length that fulfills this condition.

The beneficial effect of a moment gradient applies also to torsional buckling of a long, hinged plate under longitudinal edge compression, because its wave length extends also over the entire plate length. But the slight improvement in critical stress when the buckling length exceeds two or three times the plate width is less pronounced than in the case of lateral buckling; torsional buckling of the compression flange plate is of more local nature. Furthermore, the increase of flange stress, resulting from an exhausted web, should be accounted for. Rather than create further design provisions, the relation cited previously from Reference 3 might be used. The fact that, at the most stressed cross section of a panel, the compression flange is prevented from torsional buckling (Fig. 5) might be regarded as a compensation for any adverse influences.

This, of course, is only a step in the right direction. However, to compare numerically the mutually canceling effects would amount to an effort beyond the scope of this investigation. Not only would an exact analysis require knowledge of the combined failure mode of lateral and torsional buckling of the compression flange but strain-hardening and residual stresses would also have to be considered. Allowing lateral buckling alone, White attempted to include strain-hardening (9), while Galambos considered the influence of residual stresses in the absence of moment gradient (10). Torsional buckling of the flange plate in the inelastic range was studied by Haaijer and Thürlimann, disregarding possible interaction between lateral and torsional buckling (11).

*Vertical Buckling.*—To prevent a premature failure due to vertical buckling of the flange plate, a limit for the web's depth-to-thickness ratio was proposed in Reference 3. When the girder web is slender, a prerequisite for vertical buckling, the shear is carried principally in tension field manner. The question is whether or not the web's tension field would pull the flanges of a girder with I-shaped cross section into the web. In deriving expressions to predict the shear carrying capacity (2), no such intentional use of the flanges as supporting boundary members of a diagonal tension field was made. The inter-

action tests carried out on plate girders developed no detrimental effect prior to application of ultimate load. As an illustration, Fig. 8 shows a girder after tests which caused failure in different panels (4). It had a 50 in. by 3/16 in. web plate and 12 in. by 3/4 in. flanges. Of course, a straining beyond the ultimate load, that is, into the unloading range, would reach a point at which the compression flange plate suddenly buckles into the web. But this is not the primary cause of failure. Rather it is a factor limiting girder deformation capacity under bending after the ultimate loading has been reached. While certain girders exhibit a pronounced yield plateau in their load versus centerline deflection diagram, slender-web girders under a combination of bending and shear may lack this favorable property.

It is conceivable that shear stress might be a factor in initiating vertical buckling of compression flange in the plane of a girder web. This was not discernible in any of the tests reported in Reference 4, but these did not cover the entire interaction range with slender-web girders. However, precautionary measures have been taken in the derivation of Eqs. 6, from Eq. 5d, by the use



FIG. 8.—A THIN-WEB GIRDER AFTER TESTING

of a relatively large value for the ratio  $A_w/A_f$  as representative of all girders, whereas the derivation given in Reference 3 has indicated that girders prone to vertical buckling of compression flange have a low  $A_w/A_f$  ratio.

Interaction between bending and shear occurs only when both types of stresses simultaneously reach high values. Generally, this will only occur at interior supports of continuous girders. Due to the stress concentrated at these points, strain-hardening is possible, (Fig. 5). This favorable effect is not reflected in the conventional design rules which prescribe the same maximum bending stress limit, regardless of whether it occurs only at one cross section or over a certain length of the girder. As far as the compression flange is concerned, this effect was used to compensate for an unconservative provision for torsional buckling. In the tension flange, however, local torsional buckling cannot occur and the flanges can strain-harden. Also, the tension flange does not require provisions against vertical buckling, such as the relatively restrictive Eqs. 6 which, although derived for  $A_w/A_f = 2.0$ , would be applied to girders with a lower ratio of  $A_w/A_f$ , as pointed out above.

For these reasons it is suggested that the interaction Eqs. 6 be waived for the tension flange stress at interior reaction points of fully continuous girders. This may result in the choice of unsymmetrical cross sections having a smaller tension flange area than compression flange area, as advocated previously (12). Due to this measure, however, yielding in the tension flange would be initiated prior to instability of the compression flange, resulting in a beneficial redistribution of moments. Signs of imminent failure through tension yielding would be much better than a sudden collapse, triggered by compression flange instability.

#### ACKNOWLEDGMENTS

This report is based on research carried out at Fritz Engineering Laboratory, Lehigh University, Bethlehem, Pennsylvania, of which Wm. J. Eney is the Head. Director of the Laboratory is Lynn S. Beedle.

The American Institute of Steel Construction, the Pennsylvania Department of Highways, the U. S. Department of Commerce - Bureau of Public Roads, and the Welding Research Council jointly sponsored the research program. It was supervised by the Plate Girder Project Committee whose members are listed in the Acknowledgments to the first paper, Reference 3. The financial support of the sponsors and the guidance of the Committee are gratefully acknowledged.

Gratitude is expressed to Bruno Thürlimann, former Project Director and supervisor of the dissertation on which this work is based, for his support and effort contributed to this investigation. For the review of the manuscript the author is indebted to T. R. Higgins and Wm. A. Milek of the American Institute of Steel Construction, and Lynn S. Beedle and B. T. Yen of Lehigh University.

---

#### APPENDIX I.—NOTATION

---

$A_f$	= flange area;
$A_w$	= web area;
$b$	= depth of girder web;
$C_1$	= stress raising coefficient;
$c$	= half of flange width;
$I_f$	= moment of inertia corresponding to $r$ ;
$l$	= lateral buckling length;
$M$	= bending moment;
$M_f$	= flange moment;
$M_y$	= yield moment;
$M_p$	= plastic moment;
$M_u$	= ultimate moment;

- $N$  = factor of safety;  
 $r$  = radius of gyration (in lateral direction, by considering compression flange and one sixth of the web as column cross section);  
 $S$  = section modulus;  
 $V$  = shear force;  
 $V_u$  = ultimate shear force;  
 $\epsilon$  = strain;  
 $\kappa$  = ratio of smaller to higher end moment;  
 $\lambda$  = normalized slenderness ratio;  
 $\sigma$  = normal stress;  
 $\sigma_y$  = yield stress;  
 $\sigma_{cr}$  = critical stress, buckling stress of compression flange;  
 $\tau$  = shear stress;  
 $\tau_{all}$  = allowable shear stress; and  
 $\tau_y$  = shear yield stress.

---

#### APPENDIX II.—REFERENCES

---

1. "Commentary on Plastic Design in Steel," by WRC and ASCE, Proceedings, ASCE, Vol. 85, Nos. EM 3 & EM 4, 1959, Vol. 86, Nos. EM 1 & EM 2, 1960.
2. "Strength of Plate Girders in Shear," by K. Basler, Proceedings, ASCE, Vol. 87, No. ST 7, October, 1961.
3. "Strength of Plate Girders in Bending," by K. Basler, and B. Thürlimann, Proceedings, ASCE, Vol. 87, No. ST 6, August, 1961.
4. "Web Buckling Tests on Welded Plate Girders," by K. Basler, B. T. Yen, J. A. Mueller, and B. Thürlimann, Bulletin No. 64, Welding Research Council, New York, September, 1960.
5. "On the Yield Properties of Structural Steel Shapes," by L. Tall, and R. L. Ketter, Report 220A.33, Fritz Engrg. Lab. Lehigh Univ., Bethlehem, Pa., 1958.
6. "Lateral Buckling of Beams," by J. W. Clark, and H. N. Hill, Proceedings, ASCE, Vol. 86, No. ST 7, July, 1960.
7. "Guide to Design Criteria for Metal Compression Members," Column Research Council, Univ. of Michigan, Ann Arbor, Mich., 1960.
8. "Lateral Buckling of Eccentrically Loaded I-Columns," by M. G. Salvadori, Transactions, ASCE, Vol. 121, 1956, p. 1163.

9. "The Lateral-Torsional Buckling of Yielded Structural Steel Members," by M. W. White, Ph. D. Dissertation, Lehigh Univ., Bethlehem, Pa., 1956.
10. "Inelastic Lateral Buckling of Beams," by T. V. Galambos, Rep. No. 205 A.28, Fritz Engrg. Lab., Lehigh Univ., Bethlehem, Pa., 1960.
11. "On Inelastic Buckling in Steel," by G. Haaijer, and B. Thürlimann, Proceedings, ASCE, Vol. 84, No. EM 2, April, 1958.
12. "Further Tests on Welded Plate Girders," by K. Basler, Proceedings, A.I.S.C. Natl. Engrg. Conf., 1960.



---

---

Journal of the  
STRUCTURAL DIVISION  
Proceedings of the American Society of Civil Engineers

---

---

RECENT ADVANCES IN THE DESIGN AND  
BEHAVIOR OF CONCRETE BRIDGES<sup>a</sup>

By Hubert Rüsch,<sup>1</sup> M. IABSE

---

SYNOPSIS

The principal factors that influence recent advances in concrete bridge design are discussed. Among these factors are the use of high strength concretes and steels, the development of prestressing, the selection of structural types, and model statics. Construction features are also discussed.

---

INTRODUCTION

Because of war damage and an extension of the road system, an extraordinarily large number of bridges had to be built in Europe following World War II. Many of these bridges were of reinforced or prestressed concrete and were of a type which some decades ago would not have been believed to be possible. The development of these bridges has been so conspicuous that it is worth tracing the various factors contributing to this development.

FACTORS INFLUENCING THE DEVELOPMENT OF CONCRETE BRIDGES

*Use of High Strength Concrete.*—With increasing bridge spans, the ratios of dead load to live load are increasing and, therefore, becoming more and more unfavorable.

---

Note.—Discussion open until March 1, 1962. To extend the closing date one month, a written request must be filed with the Executive Secretary, ASCE. This paper is part of the copyrighted Journal of the Structural Division, Proceedings of the American Society of Civil Engineers, Vol. 87, No. ST 7, October, 1961.

<sup>a</sup> Presented at the October, 1958 ASCE Convention in New York, N.Y.

<sup>1</sup> Prof., Inst. of Tech., and Dir. of State Material Testing and Research Lab., Munich, Germany.

In extreme cases, these ratios can be as large as 10 to 1. This difficulty can be minimized by making the ratio  $f/\gamma$  between the strength and the specific gravity of the material as favorable as possible. The best way to achieve this is to increase the strength of the material since a raise in strength has nearly

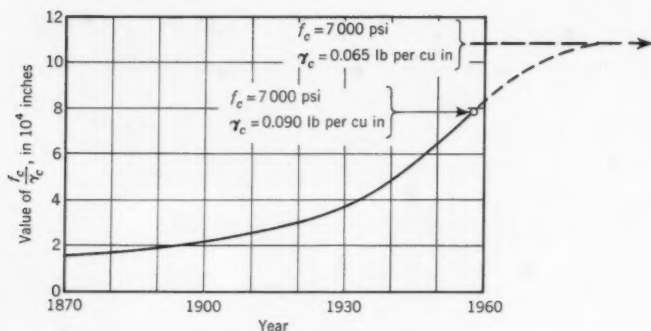


FIG. 1.—RATIO BETWEEN STRENGTH AND SPECIFIC GRAVITY OF CONCRETE AS A FUNCTION OF TIME

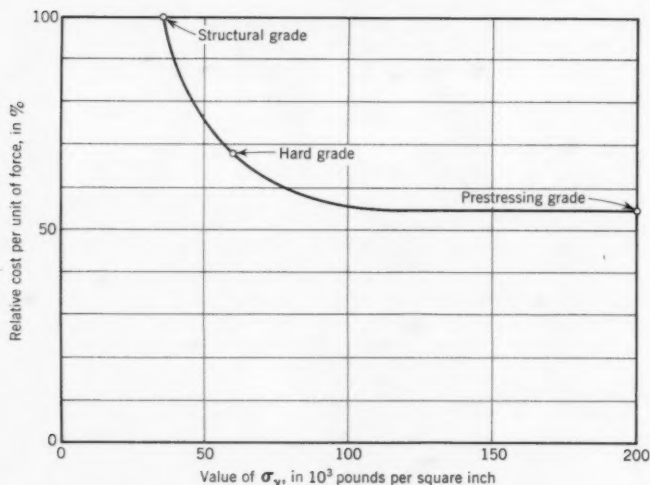


FIG. 2.—COSTS FOR STEEL IN REINFORCED CONCRETE STRUCTURES FOR VARIOUS GRADES OF STEEL

no influence on the specific gravity of either concrete or steel. Consequently, an increase in  $f/\gamma$  can produce the desired reduction of the dead load, provided that other circumstances allow the full utilization of the increased strength.

A full utilization of an increase in strength is not always possible for a given material. For example, in a steel bridge, the sizes of members are frequently



governed by limitations on thicknesses, slenderness ratios, considerations of buckling, and construction requirements. This example is given merely to indicate that other factors besides strength govern the selection of members. In concrete structures, the situation is more favorable, at least from the preceding viewpoint. The low permissible stresses of concrete lead, in general, to dimensions of cross sections that lie outside the buckling range. Also, from the point of view of construction, almost no obstacles exist to prevent the full utilization of the permissible stresses of high-strength concrete. Therefore, for a concrete bridge of some span, the use of a high-strength concrete almost always leads to a considerable saving of materials.

Fig. 1 shows the increase that has occurred in the ratio  $f/\gamma$  as a result of increases in concrete strength. The maximum value given in Fig. 1 corresponds to a concrete which has a strength of about 7,000 psi. This is the maximum strength used in Europe for concrete cast in place. Generally, this high strength is not obtained by an especially high cement content, but primarily by the proper choice of aggregates, the use of excellent cements, low water content, and by compacting the concrete with suitable vibrators. It is improbable that the  $f/\gamma$  ratio can further be raised by increases in strength to more than 8,500 psi for some time to come.

Another way to reduce the unfavorable influences of dead loads in concrete bridges is to use artificial aggregates, which combine high strength with low specific gravity. By baking clay, for example, hollow balls can be produced which possess a very high strength. By such means, the specific weight can be reduced about 25%, and a concrete strength of about 6,500 psi can be obtained.

The dotted line in Fig. 1 shows the further improvement of the ratio  $f/\gamma$  which the writer believes is still possible for a concrete produced at a construction site. Such an improvement would enable a designer to obtain concrete structures of nearly the same weight as steel structures. It should be mentioned that for long-span bridges of reinforced concrete a very small increase in  $f/\gamma$  can be very important. Such an increase leads to a reduction of the dead load by means of a decrease of the cross sectional dimensions. Consequently, the internal forces decrease, permitting a further reduction of the cross-sectional dimensions. Thus, a "chain reaction" is induced which enforces the influence of  $f/\gamma$ .

Finally, the increase of cost caused by the use of a concrete with a more advantageous ratio  $f/\gamma$  is small in most cases and does not have a great influence on total cost.

*Use of High-Strength Steels.*—High-strength steels can always be used with great advantage to resist the tensile forces in reinforced and prestressed concrete. Of course, in reinforced concrete the permissible steel stress is limited by the increased strain which can cause cracks of too great a width in the tension zone of the concrete. For this reason, the possibility of using steel with very high strength is limited to prestressed concrete.

In the production of high-strength steel, the price increases at a lesser rate than an increase in strength. Thus, the use of such steel can lead to considerable savings in cost. This is shown in Fig. 2, in which the total cost for one unit of force to be resisted by the tensile steel is drawn as a function of the yield point of the steel. The costs on which Fig. 2 is based apply to European practice and are for steel placed in a structure. In the case of prestressed concrete, the additional costs for anchoring and stressing of tendons, and for filling the tubes with mortar are included in the figure.

Fig. 2 shows that about 30% of the cost of steel can be saved in structures of reinforced concrete by the use of high-strength steel. For structures of prestressed concrete, the indicated saving is nearly 50%.

*Reduction of Dead Load by Choice of Appropriate Statical System.*—A maximum span, which cannot be exceeded, exists for every given statical system and for any value of the ratio  $f/\gamma$ . This is illustrated by an example in Fig. 3. The figure shows on the left side the dependence of the slenderness ratio  $L/d$  on the span length  $L$  for a simply supported T-beam. In this example, a value of  $f/\gamma$  equal to 40,000 in., corresponding to a normal concrete, is considered. For this system, the attainable maximum span approaches 520 ft. This however is only a hypothetical span because the depth of the beam would approach an infinite value. For a slenderness ratio of  $L/d$  equal to 10, the attainable maximum span is about 230 ft.

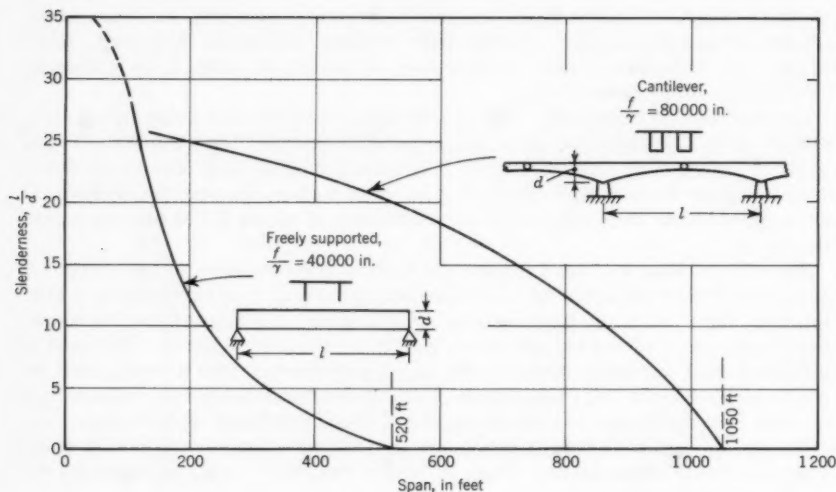


FIG. 3.—RELATIONSHIP BETWEEN SLENDERNESS AND SPAN

The maximum span can be increased considerably by choosing an appropriate statical system. The appropriate system is that in which large values of moments appear only close to the supports. At these places, the weight of the large cross sections that are required to resist the large moments has little influence on the internal forces because of the small eccentricity of the loads.

Fig. 4 shows the possible reduction in the unfavorable influence of dead load by the choice of an advantageous statical system. Four statical systems are compared: (a) a simply supported beam with constant depth, (b) a continuous beam with constant depth, (c) a continuous beam with varying depth, and (d) a cantilever beam with varying depth. For these four systems, the moments due to dead and live load were computed for a central span of 200 ft and a value of  $f/\gamma = 40,000$  in. The sum of the moments at a support and at the mid span can be taken as a measure of the material consumption. It should be noted that the

material consumption becomes smaller as the large moments are moved towards the supports. This advantageous effect is most obvious for the moments caused by dead loads. The cantilever beam is the most advantageous to resist the moments caused by live loads because, for a given section, the moments range between zero and a certain maximum value, which is caused by only one position of the load. Furthermore, the maximum moments appear at the supports.

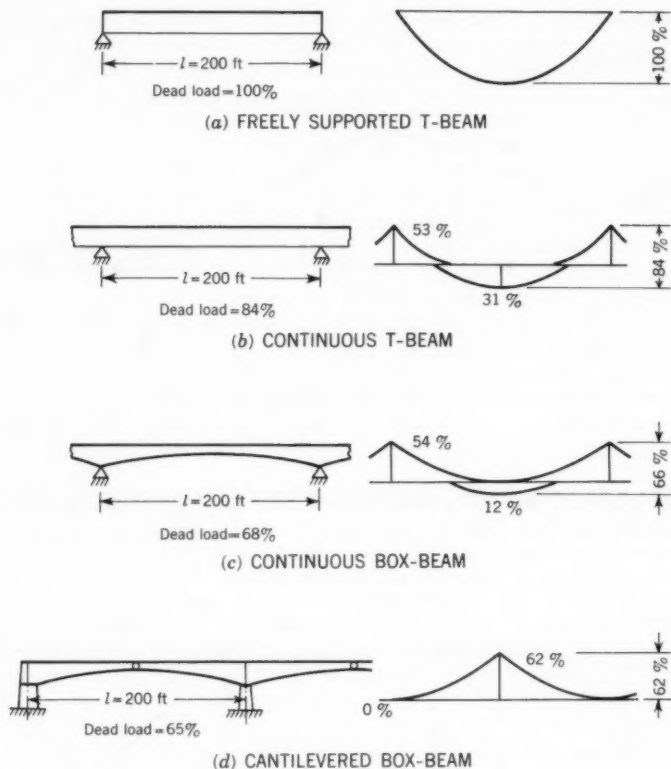


FIG. 4.—INFLUENCE OF STATIC SYSTEMS ON DEAD LOAD AND MOMENT VALUES

General use is made of this advantageous system in the construction of long-span bridges of reinforced or prestressed concrete. In most cases, however, this is not being done with the full realization of the important effects which the factor  $f/\gamma$  and the choice of the statical system have on the determinations of dead loads. Successful bridges of very long span will be built in concrete only when all technical possibilities are fully utilized. This is further illustrated in the right hand part of Fig. 3 by the curve showing the slenderness

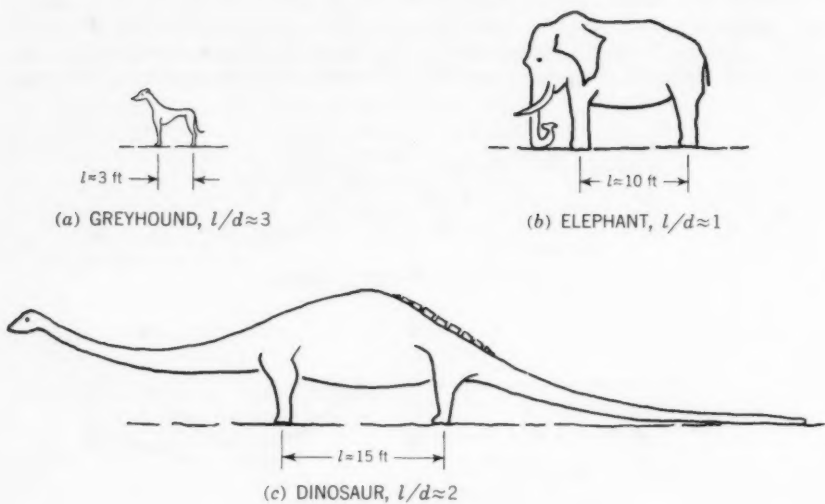


FIG. 5.—THE STATICS OF ANIMALS

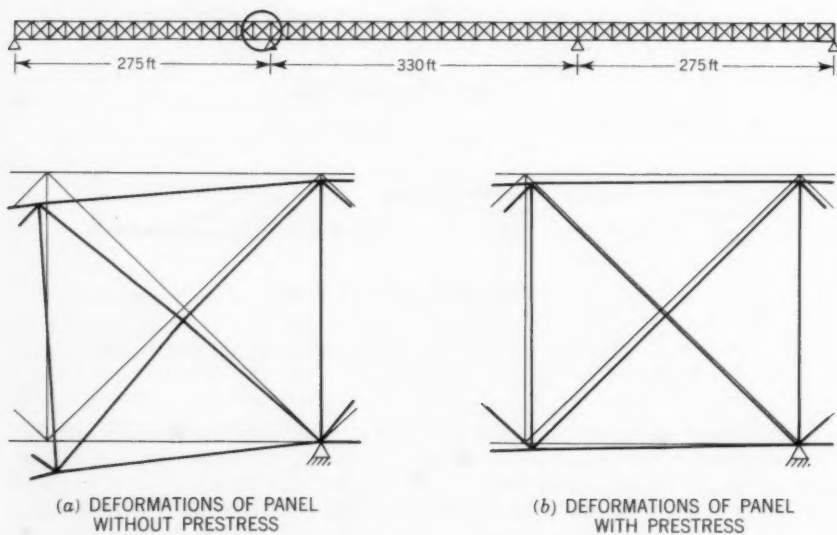


FIG. 6.—REDUCTION OF DEFORMATIONS BY PRESTRESS

ratio of a cantilever bridge for a value of  $f/\gamma = 80,000$  in. This knowledge is, strictly speaking, self-evident. It is nature, too, which demonstrates these facts. Small animals, that is animals with a small span of the body, are, in general, considerably more slender than big ones. The feasible limit for a simply supported beam is demonstrated by the elephant, which has a span of approximately 10 ft and a slenderness ratio of about 1 (Fig. 5(b)). If, in prehistoric times, larger animals existed this was only possible because of a more advantageous static system. This is demonstrated by the sketch of a dinosaur in Fig. 5(c). This animal developed a very pronounced neck and tail which act as cantilevers. Thus the total length of the animal has been enlarged, and the span, that is the distance between the feet, is increased.

However, in all these cases the attainable maximum spans are comparatively small, because the material being used has a very unfavorable  $f/\gamma$  ratio.

*Control of Internal Forces by Prestressing.*—One of the main advantages of prestressing is the possibility of changing the distribution of the internal forces of a structure in a favorable manner. The use of certain kinds of structures in bridge construction has only now become possible because of this fact.

This statement is illustrated by the example of a truss girder. In such a girder, the shape of the network is modified under the load due to the shortening of the compression members and the elongation of the tension members. If the joints of the truss are rigid, the primary deformations (Fig. 6) lead to secondary bending moments because angle changes at the joints cannot occur. The secondary stresses associated with these moments are dependent on the primary stresses and on the slenderness ratios of the members between joints. Even for concrete members of usual dimensions, the secondary stresses can be as large as 100% to 150% of the primary stresses. For this reason, structural-truss frames of concrete have not been successfully applied in bridge construction until now.

The preceding obstacle can be removed by the use of prestressing, which enables us to create compressive stresses in the concrete of the tension members. If the sum of external and prestressing forces causes equal compressive stresses in all members, independent of their being compression or tension members, the deformation of the truss girder leads only to a reduction of all dimensions of the network, and thus to an affine shape. In that case, the angles between the members do not change and secondary stresses do not appear.

In general, the same stress is not induced in all members of a truss for reasons of economy. Another reason is that the structure has to be dimensioned for various combinations of loads. Therefore, the secondary stresses do not fully vanish. However, experience has shown that for prestressed concrete the secondaries can be controlled to the extent that they do not exceed  $1/4$  of the primary stresses. It will be noted that these are of smaller magnitude than the limiting value of  $1/3$  that is frequently specified as the upper feasible limit.

In Fig. 7 a bridge is shown which was built in 1936 for the Autobahn in Germany. The superstructure was of steel with spans of 350 ft. This bridge was destroyed in World War II and subsequently was replaced by a temporary bridge. The latter was replaced by a prestressed concrete bridge, using trussed girders of the same spans (Fig. 8). The new design was based on the preceding reasoning and has the same slenderness ratio as the former steel bridge. Fig. 6 illustrates the extent to which the deformation of the concrete girder and the resulting angular displacements were reduced through the application of prestressing.

Many other examples could be given to show the ways in which prestressing in bridge construction can lead to improvements in the distribution of internal forces. It is sufficient to state that for continuous beams the distribution of moments can be changed to a great extent with the help of prestressing. This already is being done with success in bridge construction.

*High-Strength Steel in Reinforced Concrete Construction.*—The use of high-strength steel in ordinary reinforced concrete has focused attention on the need to control the width of cracks. At present (1961) most building codes are based on the assumption that wide cracks can be avoided solely by choosing a low permissible stress of the steel; this assumption is wrong. The width of the cracks depends to the same extent also on other factors. For this reason, cracks of non-permissible width can, at times, be observed in structures that have been designed for a very low steel stress.

Recently, extensive experiments and studies for the establishment of a basic theory regarding the formation of cracks have been performed in many coun-



FIG. 7.—MANGFALL BRIDGE, GERMANY, SUPERSTRUCTURE OF STEEL GIRDERS, BUILT IN 1936



FIG. 8.—MANGFALL BRIDGE, GERMANY, SUPERSTRUCTURE OF TRUSSED GIRDERS IN PRESTRESSED CONCRETE, BUILT IN 1958/1960

tries. These studies have shown that the width of the cracks depend primarily on the steel stress, the bond strength of the steel, the diameter of the bars, and on the ratio between the area of tensile reinforcement and the area of the tensile zone of concrete.

Some results of this investigation are presented in Fig. 9. In this figure, the maximum permissible diameters are drawn as a function of the ratio of tensile steel. For simplicity, the area of reinforcement has been given as a fraction of the total area  $b d$  of the web rather than of the area of the tensile zone, as would be more accurate. Permissible diameter was defined as that diameter for which the probability is 98% that the cracks will not be wider than  $1/85$  in. and will, in no case, exceed a width of  $1/70$  in.

Fig. 9 indicates that it is possible to use successfully in non-prestressed bridge construction a high-strength steel with a yield point of 60,000 psi. Of course, this steel will require a high bond strength and therefore bars with



small diameters will have to be used. In most cases, however, prestressed concrete is preferred in bridge construction, and conventionally reinforced concrete is primarily used for small spans and secondary members.

Doubt has been expressed at times that deformed bars of high-strength steel may not have the necessary fatigue resistance for use in bridge construction. To a certain degree this doubt is justified. Extensive tests on this question have been performed by the writer in the State Laboratory at Munich, Germany. These tests have shown that fatigue failures can be avoided by choosing an appropriate design of deformations for the bar surface and by improving production methods.

*Model Statics.*—An important feature of concrete is that there is no limit to the shape in which it can be used. In the past, this feature was not always utilized because of difficulties which, at times, arose in analysis. The develop-

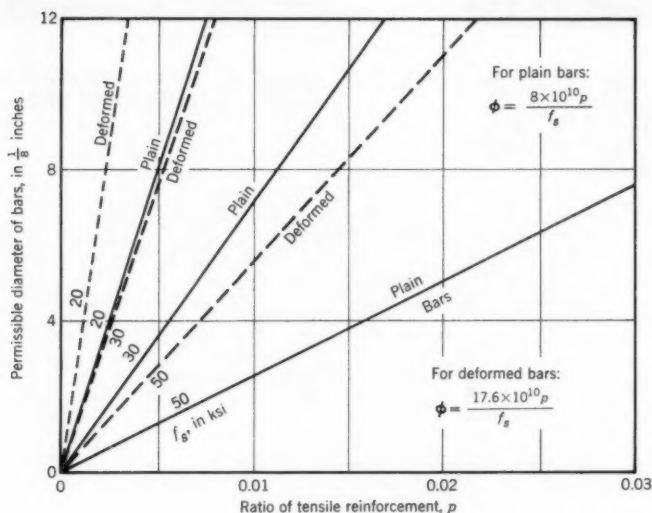


FIG. 9.—RELATIONSHIP BETWEEN MAXIMUM PERMISSIBLE DIAMETER AND RATIO OF TENSILE REINFORCEMENT

ment of the so-called "model analysis" has provided a means for the removal of these difficulties and for the greater utilization of this important feature of concrete. Where it is not possible to compute stresses analytically, the deformations of a model under load can be measured and the stresses therefrom deduced. The latter development is so promising that it should, by all means, be encouraged.

The results of analysis based on simplifying assumptions very often deviate markedly from the actual situation. The analytical results, however, may be exact in a mathematical sense. With model statics, simplifying assumptions are not necessary. In most cases it is possible to produce an exact scale model of materials which behave in a similar way to concrete and, thus, to determine the actual stress distribution. For example, model tests on bridges, con-



FIG. 10.—TEST SET-UP TO DETERMINE INFLUENCE SURFACES OF SKEW SLABS

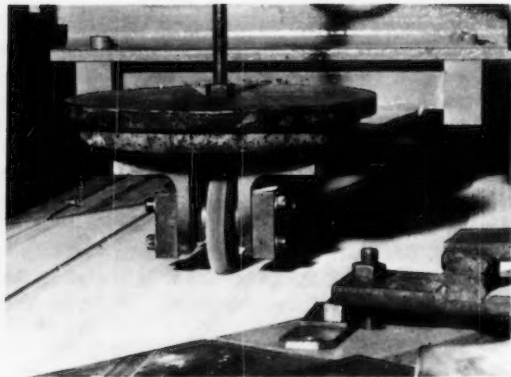


FIG. 11.—CLOSE-UP OF FIG. 10, SHOWING THE DEVICE TO LOAD THE MODEL

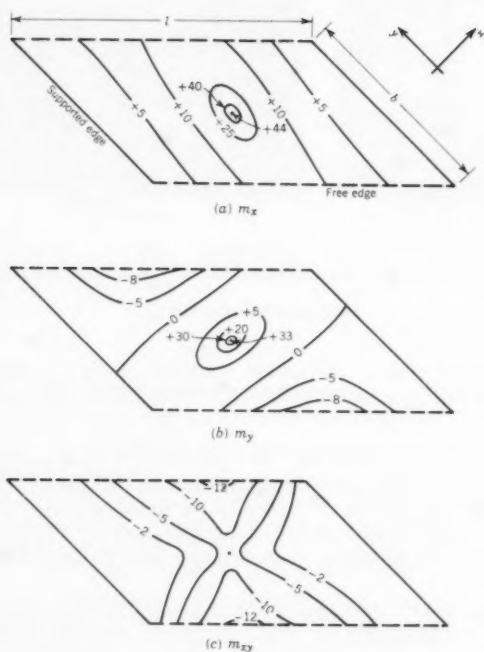


FIG. 12.—INFLUENCE SURFACES FOR THE MOMENTS IN THE MIDDLE PORTION OF A SKEW SLAB



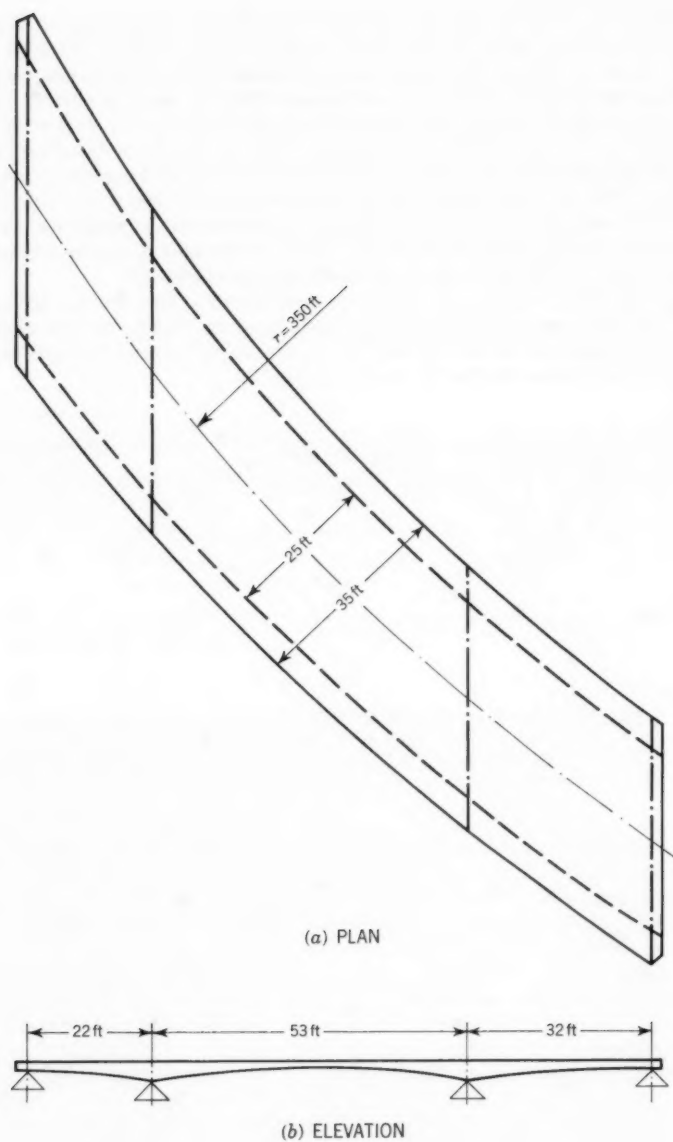


FIG. 13.—CURVED SKEW SLAB BRIDGE OF VARIABLE THICKNESS

ducted at the State Laboratory in Munich, showed that the stresses computed under simplifying assumptions can deviate as much as 50% from those deduced from measurements.

Modern roads very rarely cross an obstacle at a right angle. Therefore, most bridges are designed as skew bridges. Skew bridges of small span are usually built as slabs. However, the mathematical analysis of non-rectangular slabs and other skew bridges is extremely difficult. With a model, the distribution of stress in a skew slab can be determined with ease. It is even possible to measure, directly, influence surfaces. This is illustrated in Figs. 10 and 11 which show a device for moving a concentrated load with constant speed across the slab. The strains produced by this load at selected points are measured in three directions by electronic equipment and instantly graphed by a recorder. In this way, cross sections of the influence surfaces are produced from which contour lines of the surfaces are determined graphically.

An extensive investigation has been performed at the Munich Laboratory to study influence surfaces for various types of skew slabs; results of this project will be available in the future. A somewhat simplified example taken from the results of these studies is shown in Fig. 12.

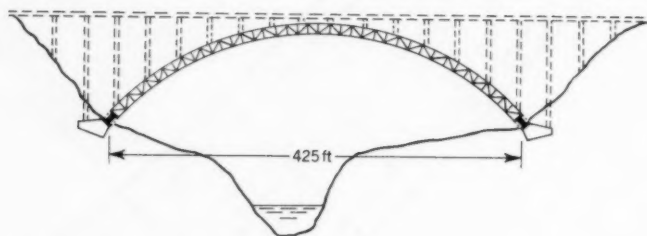


FIG. 14.—AMMER-BRIDGE AT ECHELSEBACH, GERMANY, APPLICATION OF THE MELAN-SYSTEM, THAT IS, THE REINFORCEMENT ACTS AS SELF-SUPPORTING SCAFFOLDING

In a similar way, difficult bridge designs are being investigated at the State Laboratory. These designs often cannot be analyzed mathematically because the structures are curved, oblique, or have a complicated cross-sectional shape (Fig. 13). At other times it is necessary to find the most advantageous shape of a structure by testing different models of a bridge.

*Reduction of Costs for Centering and Forms.*—A considerable proportion of the cost of concrete bridges goes into centering and forms. Therefore, for a considerable period of time attempts have been made to reduce these costs by new construction methods.

One of the first attempts in this direction was the so-called "Melan-method" which was developed around 1900. In this method (Fig. 14), the reinforcement bars of the structure are designed to be self-supporting and to serve as scaffolding for the rest of the structure. In Europe and Africa, several bridges, some of long span, have been built by this method. In time it became obvious that the self-supporting steel of the Melan type of structure needed more steel than was necessary for the reinforcement of the arch. Furthermore, the dead

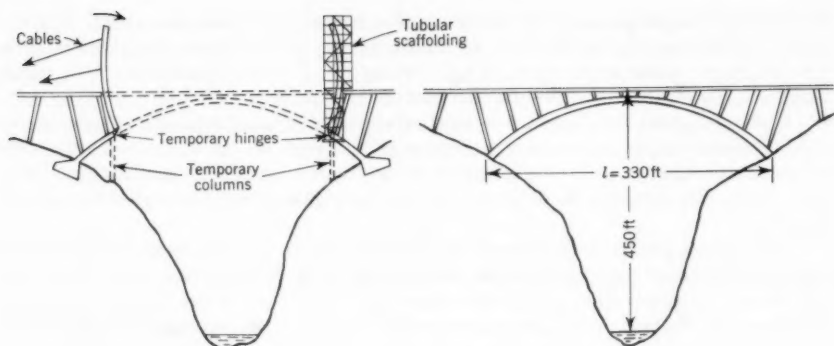


FIG. 15.—PAUL SAUER BRIDGE, DESIGNED BY MORANDI

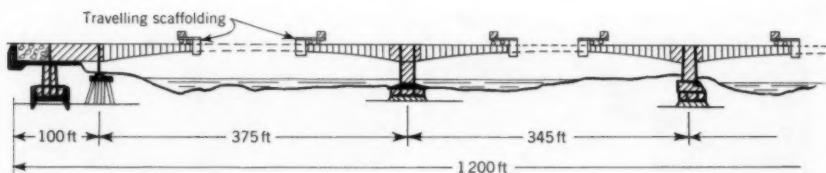


FIG. 16.—MOSEL-BRIDGE AT KOBLENZ, APPLICATION OF THE FREE CANTILEVER METHOD

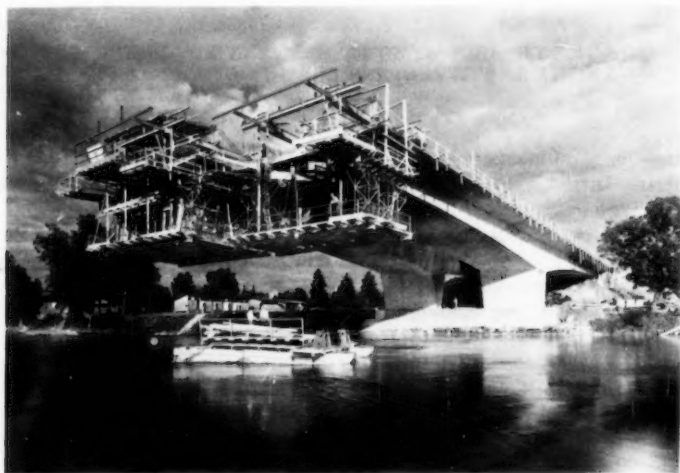


FIG. 17.—RING-BRIDGE AT ULM, GERMANY, APPLICATION OF THE FREE CANTILEVER METHOD

load of the structure is almost fully carried by the steel skeleton alone. Therefore, tensile cracks caused by the moments due to live load appear earlier in the concrete than with conventionally reinforced concrete arches. For these reasons, the Melan method of construction has been abandoned.

If steel beams are used for centering, it is more economical to arrange them outside the structure so that they can be reused. In bridge construction such beams are being used more and more for the set-up of scaffolding. They are being constructed in a way that permits them to be adapted to various lengths.

The use of prefabricated units is another way to save the high costs of centering. However, this method is economical only if many identical units can be produced and if the span is not too long. Where these conditions cannot be fulfilled, the saving in centering costs will be more than offset by the additional cost of erecting and connecting the units. In any case, it is believed that the use of prefabricated parts in bridge construction can be developed still further than at present.



FIG. 18.—CONCRETE ARCH AT SEMBRANCHER, SWITZERLAND



FIG. 19.—VIEW OF THE BOTTOM FACE OF THE LOMBARDS-BRIDGE AT HAMBURG, GERMANY

Another possible economy is to cast the structural parts in a position that will require little centering. A new and excellent example of this method is an arch bridge designed by Riccardo Morandi (Fig. 15).

An especially interesting method is the free cantilever method developed by Ulrich Finsterwalder. Symmetrical cantilever structures are the most appropriate for this method (Figs. 16 and 17). However, bridges with simply supported or continuous beams can be built in the same way if auxiliary supports are used. The bridge shown in Fig. 8 was built in this way, with temporary supports between the permanent columns.

Bridges using this method are built in sections of lengths of 10 ft to 20 ft. Every section is supported by a movable centering that cantilevers from the already hardened structure (Fig. 17). As soon as the concrete of the newly built section is sufficiently strong, the centering is moved forward a full section. In general, progress of 10 ft to 20 ft per week is accomplished. With two movable jigs, a bridge of 300 ft in length can be finished in about 2 months.

The Finsterwalder method, too, has only been made possible because of prestressing. If performed, for example, in conjunction with auxiliary supports, the stress-distribution changes during construction within a wide range. Temporarily, negative moments may appear at sections where, in the final state, only positive moments can arise. With the aid of prestressing, the concrete structure can be adjusted to meet the varying conditions; it is sufficient to increase or decrease the prestress temporarily in certain sections.

*Appearance and Maintenance.*—Concrete bridges of former decades often looked heavy because of their large dimensions. These dimensions have been obviated by the use of high-strength materials. A designer can now proportion a concrete bridge to be about as slender as a steel bridge. Furthermore, the concrete bridge can always be made aesthetically pleasing because of the possibility of shaping concrete to any desired form (Figs. 18 and 19).

Concerning maintenance, it is sufficient to state that a concrete bridge hardly requires any maintenance costs.

### CONCLUSIONS

There have been presented the essential reasons that influence recent advances in concrete bridge design. The use of materials of high strength, the introduction of prestressing, and the development of new structural shapes have freed the concrete bridge from its heavy dead weight. Thus, the present stage of development is characterized by the tendency toward lighter structures. This stage will continue because the concrete sections of modern bridge structures are still larger than necessary for stable construction and durability.



---

Journal of the  
STRUCTURAL DIVISION  
Proceedings of the American Society of Civil Engineers

---

FOLDED PLATE STRUCTURES OF LIGHT GAGE STEEL

By Arthur H. Nilson,<sup>1</sup> M. ASCE

---

SYNOPSIS

Newly-developed information relative to the performance of light gage steel shear diaphragms is coupled with the folded plate structural form to obtain a new type of structure suitable for long spans. A simple design theory is presented, and tests of a full-sized prototype structure are described.

---

INTRODUCTION

The problem of carrying roof loads over long spans has frequently occupied the attention of structural engineers and architects, and many structural forms have been developed. It is generally recognized that shell roofs provide an efficient solution. Characteristically, these structures translate applied loads into tensile and compressive forces and shears in the plane of their surface. These are termed membrane stresses, and the degree to which membrane stresses are dominant over the out-of-plane flexural stresses is a measure of the structural economy of the system.

Reinforced concrete is well adapted to shell construction. It can be formed into almost any desired shape, including the complex doubly-curved surfaces which offer the greatest structural advantage. However, while such roofs are highly economical of material, their cost may be high because of complications in forming, because of the elaborate falsework required, and due to the difficulty in placing concrete over the shell surface.

---

Note.—Discussion open until March 1, 1962. To extend the closing date one month, a written request must be filed with the Executive Secretary, ASCE. This paper is part of the copyrighted Journal of the Structural Division, Proceedings of the American Society of Civil Engineers, Vol. 87, No. ST 7, October, 1961.

<sup>1</sup> Assoc. Prof. of Civ. Engng., Cornell Univ., Ithaca, N. Y.

The folded plate roof has become popular in the United States. Sometimes called prismatic shells, these structures have a deep corrugated form somewhat similar to that of multiple-barrel cylindrical shells, except that plane elements are used, intersecting in "fold lines" in the direction parallel to the span.<sup>2,3</sup> They represent an attempt to simplify forming and still retain the advantages of shell construction. They are not ideal shells, because flexural action may have a considerable influence on their design. In spite of this, folded plates of reinforced or prestressed concrete have been built using thin elements, and spanning distances greater than 100 ft.

However, even for prismatic concrete shells, falsework and forming is an expensive item in the construction budget, particularly if schedules are such as to preclude the repetitive use of forms. In addition, concrete placement may be difficult due to the relatively steep slopes that are sometimes required. Precasting of the units on the site at ground level can reduce or eliminate the expensive falsework. Difficulty in handling the thin plates, which depend on the presence of adjacent plates for their strength and rigidity, and difficulty in restoring transverse and longitudinal continuity along the fold lines have restricted the use of this otherwise well-suited method of construction.

The use of light gage steel panels for folded plate roofs is proposed herein. The considerable capacity of welded panel assemblies to resist shear loads in their own plane has been demonstrated by extensive testing at Cornell University, Ithaca, N. Y. and elsewhere.<sup>4,5,6,7</sup> Such installations were originally conceived as a means for providing resistance to horizontal building loads due to wind, earthquake, and blast. Their high performance, combining strength, stiffness, and light weight, suggests that they may be used for primary structural purposes as well. Combining shear diaphragms with the folded plate form of construction, a three-dimensional roof system is created which offers many of the advantages of shell structures, and in addition is extremely light in weight and is easily erected in preassembled units. A prototype unit has been successfully tested on a 42 ft-6 in. span, and calculations indicate that spans up to 75 ft or more can be attained, using shallow panels of thin material.

## REVIEW OF FOLDED PLATE ACTION

The action of a folded plate structure in carrying loads is conveniently separated into two parts. In the transverse direction between fold lines, loads are carried by slab action, the loads applied to the surface being carried between fold lines by the bending strength of the surface. The ability of the

---

<sup>2</sup> "Hipped Plate Construction," by G. Winter and M. Pei, ACI Journal, January, 1947.

<sup>3</sup> "Design of Folded Plate Roofs," by H. Simpson, *Proceedings*, ASCE, Vol. 84, No. ST1, January, 1958.

<sup>4</sup> "Tests of Light Gage Steel Floor Panels Subject to Lateral Forces," by A. H. Nilson and G. Winter, Cornell Univ., January, 1956.

<sup>5</sup> "Report on Tests of Fenestra Type D Panels Used in Horizontally Loaded Diaphragms," by A. H. Nilson and G. Winter, Cornell Univ., March, 1959.

<sup>6</sup> "Shear Diaphragms of Light Gage Steel," by A. H. Nilson, *Proceedings*, ASCE, Vol. 86, No. ST11, November, 1960.

<sup>7</sup> "Diaphragm Action in Light Gage Steel Construction," by A. H. Nilson, *Journal of the Regional Tech. Meetings of AISI*, 1960.



fold lines to serve as lines of support for this transverse action will be demonstrated. In the longitudinal direction, the reaction of all such transverse beam strips is applied as a line loading along the fold lines. The action of the plate units in resisting this load may be likened to that of inclined deep girders, laterally braced by adjacent plates, and spanning between end walls of the structure. A simple folded plate building is shown in Fig. 1.

The key to the structural behavior of such buildings is in the capacity of the fold lines to serve as lines of support for the transverse beam strips. It will be shown that loads applied along these fold lines resolve themselves into components parallel to the two adjacent plates.

Referring to Fig. 2, the transverse slab strips will deliver reactions to the fold lines, the reactions from all such transverse strips contributing to cause

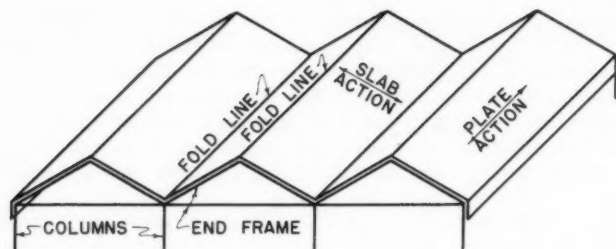


FIG. 1

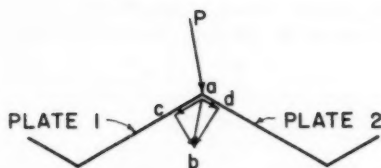


FIG. 2

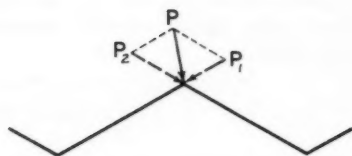


FIG. 3

a line loading along the entire length of the fold line. Let  $P$  be the resultant of all line loads acting at the fold line of plates 1 and 2. The direction of the fold line deflection,  $ab$ , will depend on the relative stiffness of the plates. The deflection of each plate can be resolved into components parallel and perpendicular to the plate, for example  $ac$  and  $cb$  parallel and perpendicular to plate 1, and  $ad$  and  $db$  parallel and perpendicular to plate 2. Each plate has negligible resistance to deflection normal to its plane, compared to its great stiffness in resisting deflection in its plane. It is seen that the fold line cannot deflect in any direction without causing in-plane deflection of one or both of the adjacent plates.

The manner in which the plates combine to resist applied line loading is apparent from the preceding examination. While any plate is extremely flexi-

ble out of its plane, it is extremely stiff in its plane, just as a deep beam is stiff. Consequently, a load in any direction is resolved into components parallel to the two adjacent plates. For satisfactory structural behavior, it is only necessary that the plates do not meet at too flat an angle. The resolution of the load  $P$  into loads  $P_1$  and  $P_2$  parallel to plates 1 and 2 is shown in Fig. 3. A similar situation is obtained at any other fold line. The reaction components at each edge of any plate are summed algebraically to obtain the net load acting transversely in the plane of any plate.

Reinforced concrete folded plates are designed transversely as continuous slabs, with top steel at the fold lines, and bottom steel between the fold lines. These transverse slabstrips deliver fold line loads which are resolved as described, into components in the plane of the two adjacent plates. The plates span as deep beams between end walls, with the principal tensile reinforcement at the lower fold line, or valley.

One design complication resulting from concrete folded plate roofs is that relatively slight differential displacements of the fold lines relative to one another can have a substantial influence on slab moments, and on the reactions delivered to the fold lines. This reaction difference requires a corrective deflection analysis, which will, in turn, change the slab reactions, and which will further change the plate deflections. The procedure becomes either a matter of successive approximation, or solution of a set of simultaneous equations.

A second characteristic design feature associated with concrete folded plate roofs is that the primary analysis may result in longitudinal plate stresses that differ on either side of a fold line. The resulting strain incompatibility cannot exist in the actual structure, because the stress and strain on one side of a fold line must be the same as on the other. The result is that longitudinal shears are caused along the fold line, acting equal and in opposite directions on the two adjacent plates, which restore compatibility. These edge shears modify longitudinal stresses across the entire width of each plate.

#### LIGHT GAGE STEEL FOLDED PLATES

In the proposed form of construction, light gage steel cellular panels such as the type shown in Fig. 4 are used to span in the transverse direction. Many varieties of cross section are suitable, but the essential feature is the provision of a continuous flat plate, connected to that of adjacent panels by intermittent seam welding, and which is welded directly to the longitudinal framing and end framing to be described. While other panel configurations might suffice to carry loads transversely between fold lines, the continuous flat plate is necessary in order to form the shear-carrying web of the longitudinal plate.

As shown in Fig. 5, these transverse panels are welded along the fold lines to light longitudinal bent plates, which will be referred to as fold line members, to distinguish them from the plates, by which is meant the entire inclined element. Each inclined element may then be thought of as an inclined plate girder, with the light gage steel panels forming the shear-carrying web, and the fold line members serving as flanges.

A few of the many possible roof cross sections are shown in Fig. 6. Fig. 6(a) shows the simple sawtooth section used also for the example in Fig. 1,

while Fig. 6(b) shows an unsymmetrical variation of this. The trapezoidal cross sections shown in Figs. 6(c) and 6(d) may find application, although it can be shown that the sawtooth section is more efficient structurally, and will require somewhat less welding. The only real limitation in the selection of the cross section is that any two adjacent plates must not meet at too flat an angle; otherwise large distortions may occur.

It will be noticed that, in each case, a vertical edge plate is shown. This will normally be required, because otherwise the outside inclined plate would have to cantilever from the fold line at its interior edge. While short canti-

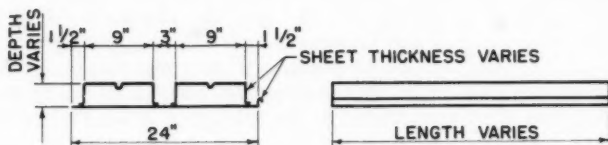


FIG. 4

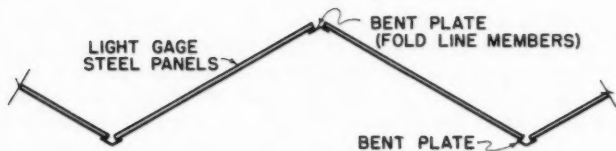


FIG. 5

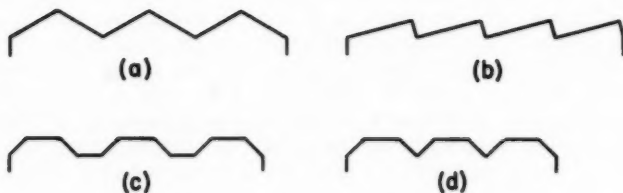


FIG. 6

vers can in fact be used (experimental unit), ordinarily this would not be advisable. As an alternate to the use of a vertical edge plate, light longitudinal framing with intermittent columns can be provided along these exterior edges. Such framing would carry only vertical loads, because the outward component of thrust would be taken by longitudinal action.

Because of the nature of the joint between adjacent panels, which permits bellows action, the light gage steel panels contribute relatively little to longitudinal flexural strength, and this contribution is conservatively neglected.

The longitudinal flange force applied to the fold line members can then be found by dividing the plate moment by the depth of the plate. This force, divided by the member area, will give the uniformly distributed compressive flange stress. For trapezoidal roof sections [Fig. 6(c)], only the inclined plates will contribute flange stress, since no bending is present in the horizontal plates. However, for triangular units [Fig. 6(a)], or for the member at the top of any vertical edge plate (Fig. 6), the uniform flange stress will be the algebraic sum of the contributions of each adjacent plate. It has been found in a number of trial designs that, because of the considerable width of the plates, the longitudinal stress in the fold line members is small, and in fact the size of these members will often be dictated by the minimum thickness for satisfactory welding (approximately 1/4 in.) and the minimum width for proper bearing and connection of the transverse panels (approximately 3 1/2 in.).

Several simplifying factors in design will be apparent for light gage steel plate roofs as compared with those of concrete. Since transverse beam strips can be considered simply supported at the fold lines, beam strip reactions and moments are unchanged by small differences in deflection of the fold lines. Consequently, no process of successive approximations relating deflections and reactions along the fold lines is required for light gage steel folded plates, and a direct solution is possible.

Secondly, while in concrete plates, the shear force along a longitudinal edge which ensures compatibility affects the magnitude of stress over the entire width of the plate, in the case of steel plates, the effect of such a shear force is confined to the fold line member along the loaded edge with little or no change in the stress level across the width of the plate, or at the opposite edge. This is because of the bellows effect at the seams between panels mentioned earlier. Consequently, the "stress distribution" procedure used in the analysis of concrete plates<sup>2,3</sup> is not required.

At the ends of the folded plate units, a bearing wall or steel frame must be provided to receive the end reaction of the inclined plates. This in-plane end reaction may be considered to be uniformly distributed through the depth of each of the plates. The situation is similar to that at the ends of a conventional plate girder, where bearing stiffeners are provided to take out the web shear, which is considered uniformly distributed throughout the depth.

If a masonry bearing wall is used at the span ends, a steel welding plate must be provided for attachment of the light gage panel web. This welding plate must be capable of resisting the tensile or compressive force along its axis due to folded plate action. If steel end frames are used, these must include a tie rod between valleys to take the unbalanced horizontal thrust that may result at an interior valley, and that will certainly result at the exterior edge. An alternative to this would be the use of rigid frames capable of resisting horizontal thrust applied at the top of the columns, but this solution would require heavy frames, as the thrust is substantial.

#### LIGHT GAGE STEEL SHEAR DIAPHRAGMS

The structural success of the type of light gage steel structure previously described is contingent on the capacity of welded light gage steel panel assemblies to resist shear loads in their own plane. This has been the subject of intensive investigation at Cornell University starting in 1955 and continuing to

1961, and reported as noted previously. More than fifty tests of full scale panel assemblies have been conducted, using members of varying span, depth, thickness, and configuration, and using a variety of welding methods and procedures. Thorough documentation has led to the wide acceptance of such assemblies for use as shear diaphragms to resist horizontal building loads due to wind and seismic forces.

During the installation and testing of panels used in the tests described, considerable information was gained relative to the most efficient and economical way to join light gage panels to one another and to the supporting steelwork. Special welding techniques were developed which have since become relatively standard.

In fastening panels to the supporting steel, a puddle weld is used. These are similar to the conventional plug weld except that no pre-punching of the thin steel sheet is involved. The hole is burned and the weld made in one continuous operation. Such welds are normally 1 in. in diameter.

Along the seams between the panels, if a standard hook joint (hook concave downward) is used, a linear puddle weld is used, in which an elongated hole is burned through the top of the hook, fusing the hook to the upper portion of the upstanding lip of the adjacent panel.

Other panel and joint configurations may dictate the use of welds or other fastenings differing from those described. Because the strength of any particular weld in light gage steel diaphragms will depend to a large extent on the configuration of the surrounding metal, it is held that the strength of any particular assembly is best established by full scale tests of that entire assembly. Such tests of panels of the type contemplated for use in folded plate structures have resulted in data of the type which is summarized in Fig. 7. Test results for two thicknesses of panel flat plate are shown, 16 gage and 18 gage, and two types of welding. Standard welding denotes 1-1/2 in. seam welds at 18 in. o.c., 1 in. puddle welds at exterior panel edges at 24 in. o.c., and three 1 in. puddle welds per panel end. Light welding denotes 1 in. seam welds 36 in. o.c., 1 in. puddle welds at exterior panel edges at 36 in. o.c., and three 1 in. puddle welds per panel end. Failure shear is shown as a function of panel span. For folded plate structures, the panel span would seldom be more than 10 ft, and the shear values for that span could be used for most installations. Trial designs of long span light gage steel folded plate roofs have indicated that assemblies with shear strength of approximately 5,000 lb per ft may be useful, and additional diaphragm tests of high strength systems are now (1961) in progress. The use of closely-spaced welds necessary for such strength would be confined to the outer regions of the folded plates near the end frames, and a graduation of welding could be used, with increasing weld spacing toward the center of the plate spans.

#### DEFLECTION

Deflection of long span structures is always a concern, from both the viewpoints of appearance and possible interference with the function of the building. The deflection of light gage steel folded plates is easily predicted using methods which show excellent agreement with the experimental observations, and in most cases will prove far below those values which are generally considered as acceptable upper limits. The method of calculation used is similar to that

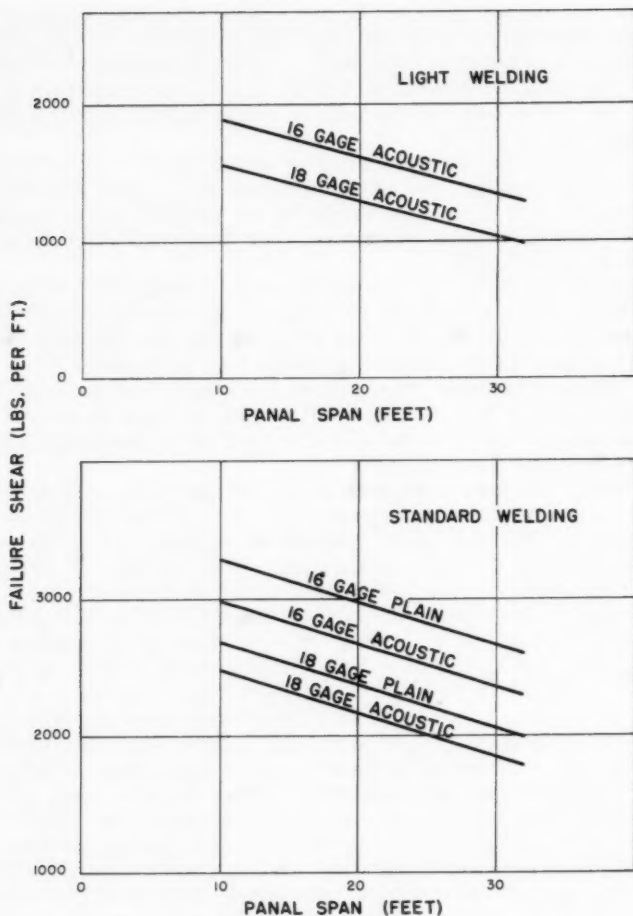


FIG. 7

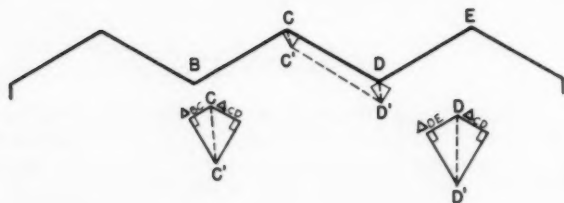


FIG. 8



used for determining truss deflections. The structure is temporarily separated at the fold lines, and the in-plane deflections of the individual plates are calculated separately. Then the fold lines are brought back into coincidence by means of a Williot displacement diagram, and the true movement of the fold line is determined graphically or analytically.

In Fig. 8, for example, suppose that the deflection of plate CD due to loads in its plane has been determined, using methods to be described. Likewise the deflection of plates BC and DE due to in-plane loads is known. The structure is temporarily disjointed, and these deflections are allowed to occur independently. Then at joint C, plates BC and CD are rotated about their far ends, the movement of the C end of each plate being essentially perpendicular to the plate surface. The two edges are brought back into coincidence at point C' as shown. A similar process establishes the location of point D', and any other joint movement can be found in a like manner.

The in-plane deflection of each plate is found as the sum of three parts: flexural deflection, shear deflection, and seam slip deflection.<sup>8</sup> Trial designs indicate that the flexural effect is dominant. The flexural deflection  $d_f$  is calculated as for any beam. For example, for a uniformly loaded simple span,

the midspan deflection will be  $\frac{5 w L^4}{384 E I}$  in which  $w$  is the in-plane unit load,  $L$

the plate span between end walls,  $E$  the elastic modulus for steel, and  $I$  the moment of inertia of the plate about its neutral axis. Consistent with the assumption made in flexural analysis, the longitudinal flexural contribution of the light gage panels is considered negligible, and the moment of inertia is based on the area of the fold line members only. It is evident that for trapezoidal roof cross sections [Fig. 6(c)] the entire area of both fold line members connected to any one inclined plate resists bending of that plate, since the horizontal plates have no bending stress, and so the entire area would be used in calculating moment of inertia. It is equally evident that for triangular cross sections [Fig. 6(a)] each fold line member is shared by the two adjacent plates, each contributing stress, and so it is convenient to consider half the area acting with each plate in computing moment of inertia. This last approach will be valid provided each of the two adjacent plates produces about the same stress in the fold line member. In the event that the stress contributions are substantially different, as for an unsymmetrical sawtooth cross section [Fig. 6(b)], or for the top of any of the vertical edge plates used (Fig. 6), the resulting stress will be the algebraic sum of the two stress contributions; accordingly the strain will be the algebraic sum of the strains. For such cases, it is well to return to fundamental deflection theory based on strains.

Plate deflection due to shear, considering the panel flat plate to provide one homogeneous web plate, can be found by well established methods. The midspan shear deflection can be expressed as

$$d_s = \frac{a M}{A G} \dots\dots\dots (1)$$

in which  $M$  is the bending moment in the plate at midspan,  $A$  is the area of the shear web (plate width times thickness of panel flat plate), and  $G$  is the shear

<sup>8</sup> "Deflection of Light Gage Steel Floor Systems Under the Action of Horizontal Loads," by A. H. Nilson, thesis presented to Cornell University at Ithaca, in 1956, as partial fulfillment for the requirements for the degree of Master of Science.

modulus of rigidity, all expressed in consistent units. The constant "a" has been well established from previous tests as equal to 1.3 for light gage steel diaphragms of the type described.

An additional shear-type deflection is present due to seam slip, or movement along the seams between adjacent panels, reflecting the fact that the web is not one homogeneous member. The amount of movement along any individual seam is closely found from the empirical expression

$$m = 4.1 \times 10^{-6} \left( \frac{V s}{h} \right) - 4.2 \times 10^{-3} \dots \dots \dots (2)$$

in which V is the external shear force at the section, s is the spacing of the seam welds, and h the width of the folded plate element. In using Eq. 2, negative results are to be set equal to zero.<sup>8</sup> It should not be applied to joints or welds substantially different from those described. The total midspan plate deflection due to seam slip,  $d_s'$ , can be found as the summation of seam slip values from support to midspan. Because V will normally decrease as the distance from the supports increases, and since the expression for m approximates a non-linear relation between V s/h and m the principal contribution will be near the supports.

#### DESIGN EXAMPLE

In order to clarify the special design aspects examined, an example has been prepared illustrating the design of a light gage steel folded plate roof of sawtooth configuration. The plate span between end frames is 50 ft and the unit width is 20 ft, providing a column-free interior area 50 ft-by-60 ft as shown in Fig. 9(a). Any number of units could be provided, joined along their longitudinal edges, so that a column-free space of any length and of width equal to the long dimension of the plates is easily obtained. The plate slope is to be 40°, and the design live load is 20 psf of horizontal roof projection.

Surface loads:	roofing	6 psf
	insulation	2
	panels	5
	suspended	2
		15 psf of surface

First designing the transverse beam strips:

$$M = 1/8 \times (20 \times 10) \times 10 + 1/8 \times (15 \times 13.08) \times 10 = 495 \text{ ft lb}$$

$$S = 495 \times 12/18000 = 0.330 \text{ in.}^3$$

A 1-1/2 in. deep panel of the type shown in Fig. 4, of 18 gage steel could be used to satisfy the vertical load requirements, but anticipating higher shear requirements, 1-1/2 in. deep 16 gage panels will be selected. For these panels, dead load is 5 psf of surface as assumed. Proceeding with the plate design:

Load per foot on fold lines =  $20 \times 10 + 15 \times 13.08 = 396 \text{ lb per linear ft}$  acting vertically downward. This load is resolved into components parallel to the two adjacent plates, as in Fig. 9(c), giving the plate load of 308 lb per linear ft per edge, or 616 lb per linear ft total. Then the plate moment:

$$M = 1/8 \times 616 \times 50^2 = 192,000 \text{ ft lb}$$



and the required flange area per plate:

$$A_f = 192,000 / (13.08 \times 20,000) = 0.735 \text{ sq in.}$$

The total area of a typical interior fold line member will be twice this, or 1.470 sq in. Bent plates  $3 \frac{1}{2} \times 1 \frac{1}{4} \times 3 \frac{1}{2}$  ft-0 in. are provided, giving an area of 1.690 sq in. Along the exterior edges, the marginal framing is increased in area slightly above that required for vertical loads to accommo-

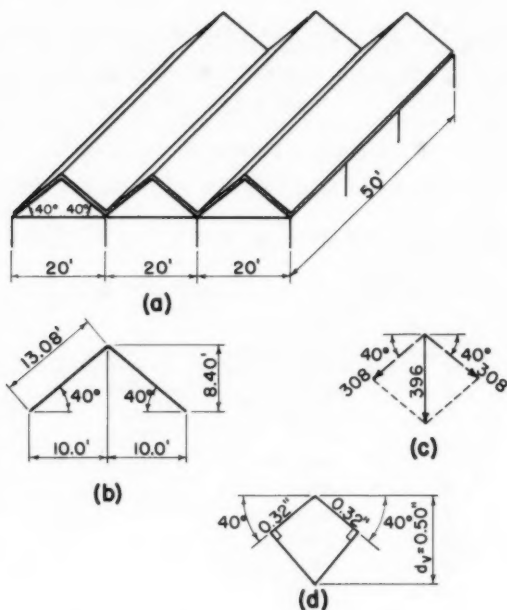


FIG. 9

date this axial stress. Precautions should be taken to insure full continuity across the joints at the columns. Designing for plate shear:

$$V = 616 \times 50 / 2 = 15,400 \text{ lb}$$

$$v = 15400 / 13.08 = 1,180 \text{ lb per ft}$$

From Fig. 7, for 16 gage panels with standard diaphragm welding, used on a 13 ft span, test failure shear is 3,200 lb per ft. Use of this system will provide a safety factor with respect to shear of 2.71, which is considered adequate. (There is no clear precedent for the selection of a proper safety factor for light gage steel folded plates. The AISI Specification calls for a safety factor of 2.50 with respect to welds, as compared with 1.65 to be used elsewhere in design. Considering that the strength of the proposed structural form is dependent on field welding, and in view of the lack of field experience with

structural welding of light gage steel, it is the writer's opinion that a safety factor between 2.50 and 3.00 would be appropriate.) Panels will be welded using 1-1/2 in. seam welds 18 in. o.c., three 1 in. puddle welds per panel end, and 1 in. puddle welds 24 in. o.c. along the end support frames. It is recognized that the seam welding could be reduced toward midspan, because the shear reduces linearly to zero at midspan, but for the sake of simplicity in this example, welding will be uniform throughout.

The question of deflection will be considered next. For the selected cross section:

$$I_{p1} = 2 A_f \times (h/2)^2 = 2 \times .845 \times (13.08 \times 12/2)^2 = 10,400 \text{ in.}^4$$

$$d_f = 5 WL^3/384EI = \frac{5 \times 616 \times 50 \times (50 \times 12)^3}{384 \times 30 \times 10^6 \times 10400} = 0.28 \text{ in.}$$

$$A_w = .0598 \times 13.08 \times 12 = 9.38 \text{ in.}^2$$

$$G = E/2(1 + \nu) = 30 \times 10^6/(2 \times 1.3) = 11.5 \times 10^6 \text{ psi}$$

$$d_s = \frac{a M}{A G} = 1.3 \times 192,000 \times 12/(9.38 \times 11.5 \times 10^6) = 0.03 \text{ in.}$$

$$m = 4.1 \times 10^{-6} (Vs/h) - 4.2 \times 10^{-3} \text{ with } s = 18 \text{ in. and } h = 157 \text{ in.}$$

Seam	V	m
1	14200	.00248
2	13000	.00198
3	11700	.00132
4	10500	.00075
5	9300	.00018
6	8000	-
7	6800	-
8	5600	-
9	4300	-
10	3100	-
11	1900	-
12	600	-

$$d_s' = .00671 = 0.01 \text{ in.}$$

Summing the three components of in-plane plate deflection, one obtains the total plate deflection:

$$d_t = 0.28 + 0.03 + 0.01 = 0.32 \text{ in.}$$

By means of the Williot diagram in Fig. 9(d), the total vertical deflection at midspan of an interior fold line is found to be 0.50 in. It is noticed that this is only 1/1200 of the 50 ft span. By a similar diagram, the outward spreading at the midpoint of the 50 ft building walls is found to be 0.42 in.

#### EXPERIMENTAL STUDY

Considering the new and untried nature of the proposed form of construction, it was considered desirable to initiate a program of testing of a prototype structure. A full-sized light gage steel folded plate unit was fabricated

in the structural testing laboratory at Cornell University, as shown in Figs. 10, 11, 12, and 13.

The cross section of the test structure was trapezoidal, similar to a single unit of the roof shown in Fig. 6(c). It consisted of five plates. The bottom plate, of 3 ft width, was joined to two 45° inclined plates of 5 ft-8 in. width, which were in turn connected to two 1 ft-6 in. horizontal top plates. Fenestra 1 1/2 D-16D-18 light gage steel panels were used for all plates. These panels have the configuration shown in Fig. 4, and have a 1-1/2 in. depth, a 16 gage flat bottom plate, and 18 gage double hat sections spot welded to the flat plate. All panels were galvanized steel. Fold line members used were 3 1/2 in.-by-1/4 in.-by-3 1/2 in. bent plates of structural grade steel, fabricated in 14 ft lengths and butt welded to form continuous members 42 ft long. At the exterior edge of the cantilevered top plates, a 2 in.-by-2 in.-by-1/4 in. structural steel angle was used. End frames used 6B12 inclined beams, butt welded to a 10 W 25 horizontal beam as shown in Fig. 13. The 10 in. beams rested

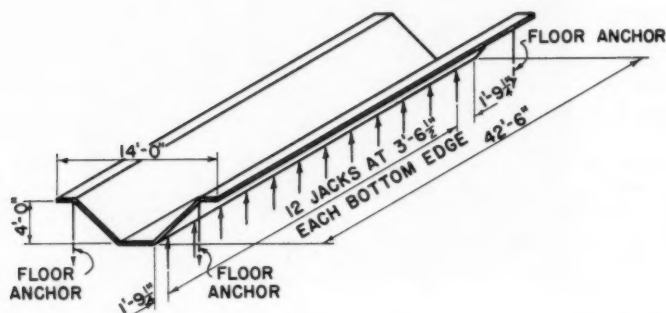


FIG. 10

on and were pinned to anchor bolt cap blocks. The 3-1/2 in. diameter alloy steel anchor bolts are carried below the laboratory floor into bedrock.<sup>9</sup>

**Welding and Assembly.**—The light gage steel panels were fastened to the fold line members and to the end frames using 1 in. diameter puddle welds, as described previously. Three such welds were used per panel end, located between the hat sections. Identical welds were used at the supporting end frames, spaced 18 in. o.c. The exact spacing of these welds was 4 in., 18 in., 18 in., 18 in., and 4 in., the outer welds being placed 2 in. from the ends of the 5 ft-6 in. inclined panel; a total of six such welds were thus placed along each sloping beam.

The hook-jointed seams between adjacent panels were fastened using linear puddle welds 1-1/2 in. long and 18 in. o.c., also previously described. Five such welds were used along each inclined seam, two across each top plate seam, and three across the bottom horizontal plate seam.

<sup>9</sup> "Light Gage Steel Folded Plate Roof," by K. Seetharamulu, thesis presented to Cornell Univ., at Ithaca, in 1961, as partial fulfillment of the requirements for the degree of Master of Science.

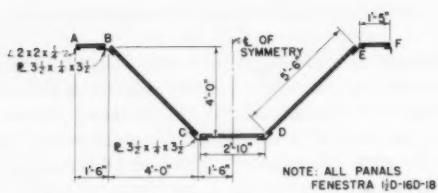


FIG. 11

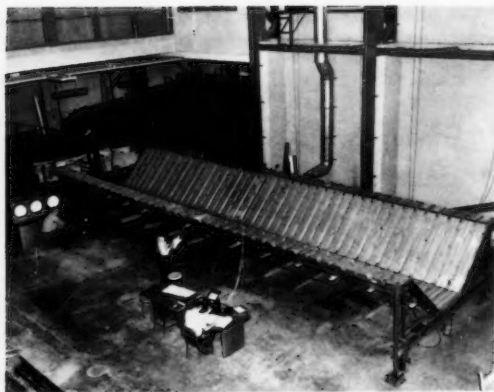


FIG. 12

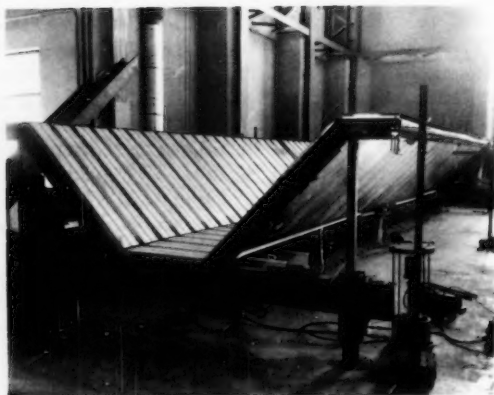


FIG. 13

All welds were made using 1/8 in. diameter E-6013 welding rod. A welding current of 210 amp at 45 v DC produced a burn-off rate of 14 in. per minute.

In order to facilitate assembly of the structure, it was convenient to fabricate the inclined plates in a horizontal position on the floor of the laboratory. All seam welding and end welding to fold line members was done in this horizontal downhand position. The inclined plates were then hoisted by one edge, using an overhead crane and distributing beam, and laid into position on shores at their desired location. The horizontal bottom plate panels were placed and welded, followed by the top cantilever panels, which were shored at their outer end until the assembly had been completed. All shoring was then removed.

*Method of Loading.*—The distributed surface loading which would be present for an actual structure could not conveniently be duplicated in the laboratory. However, since the flexural capacity of the transverse beam strips was well known from conventional theory and from extensive uniform load testing, this was not considered a serious handicap. Load was applied as a vertical line loading along the fold lines, as would be obtained from the end reactions of the uniformly loaded transverse beam strips. It was convenient to test the structure upside-down, that is, applying the loads upward by jacking against the floor. Line loading was applied along the two lower fold line members by this method, with hydraulic jacks spaced 3 ft-6 1/2 in. o.c. along these lines, and connected to a common manifold and pump shown in Fig. 12. The structure was pin-connected to the four floor anchors, providing the necessary downward vertical reactions.

As a result of the loading method selected, the first portion of the jack load applied served only to overcome the dead load of the structure. After the true zero load was obtained, an equal load increment was necessary to produce "dead load upward" conditions. Accordingly, -DL, zero load, and +DL jack pressures were 0 lb, 213 lb, and 426 lb, respectively. In plotting test results, these loads were plotted as -213 lb, 0 lb, and +213 lb, accounting for the negative load readings shown on the graphs. Accordingly, all dial gage readings and strain gage readings are corrected to read zero at the true zero load.

The test load was applied in cycles over a 5-day period. It was first carried to a point somewhat below service load conditions, dropped to zero, then returned to the previous load. After returning again to zero, the load was brought to full service value, then dropped to the +DL level, and then increased to its maximum value. Because the load attained without failure was higher than predicted on the basis of theory and previous experimental work with shear diaphragms, the load was removed entirely, and erection welds joining fold line members to end frames were cut loose, with the thought that they may have been contributing extra strength to the system. With these welds cut, the load was again applied, and failure was obtained at a load closer to but still higher than the predicted value.

*Instrumentation.*—Dial gages reading to 1/1000 in. were used to measure displacements throughout the assembly. These gages were limited to 1 in. travel, but were reset when necessary to obtain continuous data. Dial gage locations are indicated in Fig. 14(a), 14(b), and 14(c), and Fig. 16 shows a typical installation at midspan. At the midspan section, D2, D3, D6, D8, D10, and D11 measured vertical displacement of the fold lines, while D1, D7, and D12 recorded horizontal movement. At the south support frame, D13 and D15 measured longitudinal movement, D16 gave lateral displacement of the upper plate, and D14 was set to read the vertical displacement at the center of the

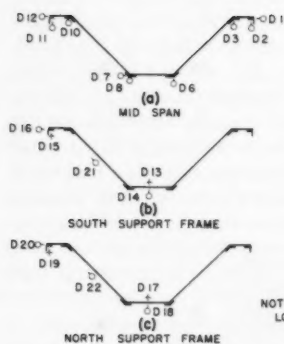


FIG. 14.—DIAL GAGE LOCATIONS

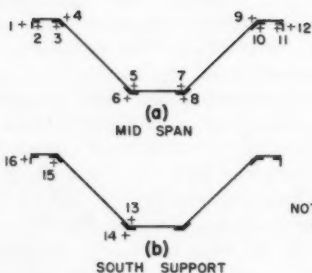
NOTE: ALL VIEWS  
LOOKING NORTH

FIG. 15.—STRAIN GAGE LOCATIONS

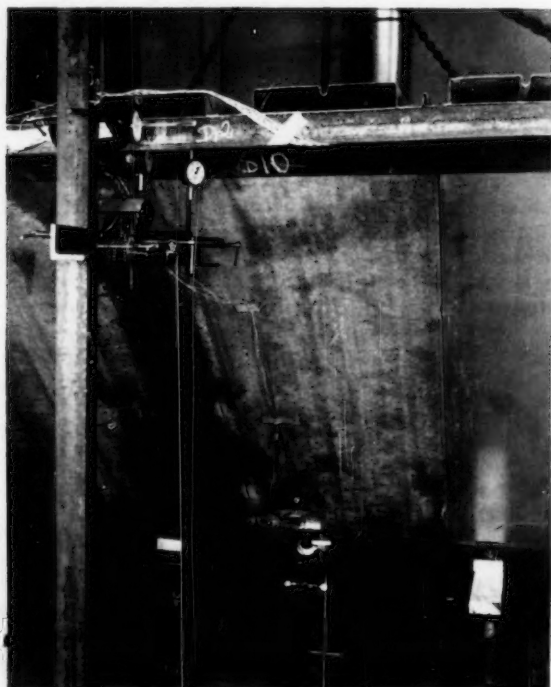


FIG. 16

support frame due to movement of the anchor assemblies and flexural distortion of the frame. Correspondingly, at the north support frame, D17 and D19 measured longitudinally, D20 laterally, and D18 vertically. Two additional dial gages were mounted along the first interior seams of the inclined plate at the south and north ends of the assembly. These gages, D21 and D22, were mounted to measure seam slip in the direction along the seam. A 36 in. base was used for both the dial gage and the facing plate in this case, to minimize the effect of local distortions.

Use was made of SR-4 electrical resistance strain gages in determining longitudinal strains in the fold line members. Six inch gage lengths were used in order to minimize errors due to local stress conditions near the welds, and due to imperfections in fold line member alignment. In addition, gages were installed in pairs, one on either side of the 1/4 in. thickness. At midspan, twelve SR-4 gages were mounted, two per fold line member as shown in Fig. 15(a). In addition, at a location close to the south support, four gages were mounted to read longitudinal stress due to restraint of the end frame as shown in Fig. 15(b). Ideally these would read zero; actually stress values at these end gages were small enough to be considered negligible. Temperature effect was compensated for by using an unstressed dummy gage of the same gage factor as that of the active gages.

The jack load was measured using a supplementary jack connected to the common manifold, acting in a frame containing a hydraulic load cell. This arrangement is shown in the lower right corner of Fig. 13. The load cell hydraulic system was in turn connected to bourdon tube gages, giving direct reading of load per jack in pounds.

*Test Results and Observations.*—The experimental structure performed in good agreement with predictions based on the methods of analysis previously suggested. Where departures were observed they were on the safe side. The failure load attained was somewhat higher than the predicted value. The deflections were almost exactly as predicted, and the flange stresses somewhat less than predicted by simple theory. These will be examined in more detail.

*Failure Load.*—The final failure load recorded was 2,340 lb per jack, which corresponds to a unit load of 94.5 lb per sq ft of horizontal projection and which produced failure of the puddle welds joining inclined plates to end frames. This is compared to a predicted failure load, based on the shear capacity of the inclined plates (as established by horizontal testing), of 2,090 lb per jack, or 84.5 lb per sq ft. As previously observed, a somewhat higher load of 2,610 lb per jack was attained during the test as a result of the contribution of erection welds joining the lower fold line members to the end frames. In theory, no welds are required at this point, since the flange stresses are zero at the supports. After unloading the structure and cutting loose these erection welds, the true failure load previously indicated was attained.

*Deflections.*—As seen in Fig. 17, the observed vertical deflection of the lower fold line members almost exactly coincides with the predicted values obtained using the methods proposed earlier. Included in the predicted values are the separate deflection contributions due to flexure, shear, and seam slip, which for this particular structure were about 85%, 11%, and 4% of the total deflection, respectively. The proportionate contributions would depend in other cases largely on the ratio of span to depth of inclined plate. It is also of interest to observe that, at an applied load of 50% of the failure load, the total observed vertical deflection was only 0.45 in., or 1/1130 of the 42 ft-6 in. span.



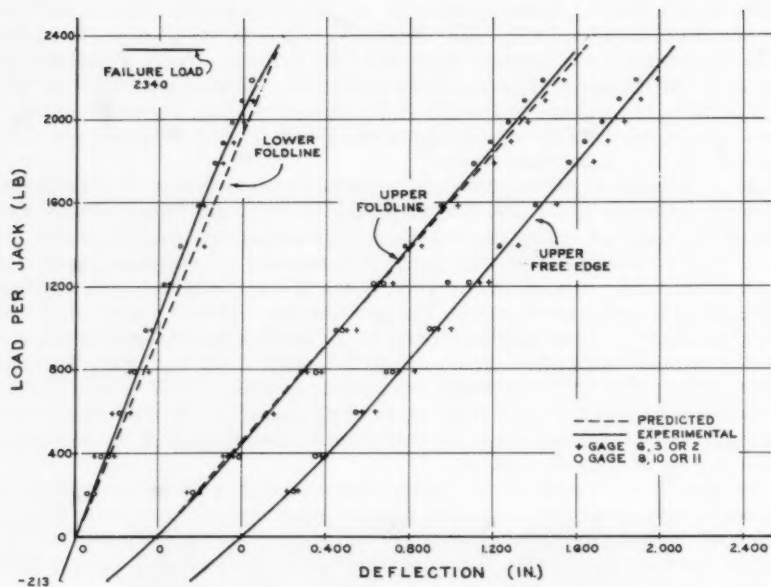


FIG. 17.—VERTICAL DEFLECTION AT MIDSPAN

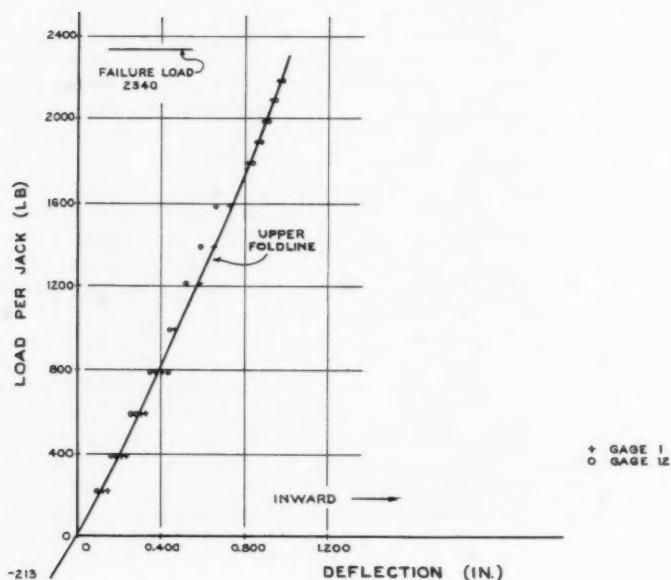


FIG. 18.—HORIZONTAL DEFLECTION AT MIDSPAN



For most installations, the vertical deflection of the upper fold line member would be the same as that of the lower fold line member. However, for the test structure, as is apparent from Fig. 17, the upper fold line member actually deflected about 2 1/2 times as much as did the lower fold line member. This difference is explained by the horizontal movement of the upper plate which was a characteristic of the test structure, but which would not be found in most installations. Referring to Fig. 11, the fold line member at B is under tension due to flexural action of plate BC, while the member at A is under little or no stress. Because of this difference, a concave-outward curvature in the horizontal plane is caused in plate AB. Because the ends of this plate are restrained against outward movement, the midspan section must move inward. This inward movement of the upper plates was clearly observed during the test, and is shown as a function of the load in Fig. 18. Because the in-plane deflection of both ends of plate BC are the same, and since the upper edge B has an additional inward component of movement, the Williot diagram for deflection at B will indicate a substantially larger vertical deflection than will the diagram for deflection at C. The predicted vertical deflection of the upper fold line, based on the in-plane deflection of BC and the horizontal deflection of AB is shown in Fig. 17 to coincide almost exactly with the observed movement.

Fig. 17 also shows the vertical deflection of the upper free edge member, which is seen to be virtually the same as that of the upper fold line. The slight differences observed are due to the rotation of plate BC resulting from the difference in edge movements described, which in turn causes rotation of the cantilever plate AB.

The relation between shear per seam weld,  $V_s/h$ , and resulting seam slip is shown in Fig. 19. The experimental curve is the average of values obtained at the north and the south ends of the test structure, at the first interior seam. Shown also in Fig. 19 is the load versus seam slip relation obtained from previous experimental work with horizontal diaphragms.<sup>8</sup> The agreement is seen to be good, particularly considering the great difference in span-depth ratio of the diaphragms, which was 2.50 for the original tests and 7.73 for the present test. The approximate bilinear relation

$$d_s' = 4.1 \text{ by } 10^{-6} (V_s/h) - 4.2 \text{ by } 10^{-3} \dots \dots \dots (3)$$

with negative results equal to zero, and which was proposed on the basis of the original diaphragm tests, is superimposed on Fig. 19. This is seen to give results which agree well and would be satisfactory for design purposes.

**Flange Stresses.**—Shown in Fig. 20 are the longitudinal stresses in the fold line members, obtained from electrical strain gage readings using a value for modulus of elasticity of  $30 \text{ by } 10^6$  psi. Gage locations are as shown in Fig. 15. Superimposed are the predicted stresses based on simplified theory. It is apparent that the load-stress relation for the top and bottom fold line members is nearly linear, and that in all cases the observed stress was less than that predicted by simple theory, the difference being of the order of 20%. This can be explained by the fact that the proposed theory does not consider the longitudinal flexural contribution of the light gage steel panels, predicted stress values being based on the area of the fold line members only. Because of the hook-shaped configuration of the joint between adjacent panels, a tensile or compressive load transverse to that joint will cause some accordioning of the joint, even at the seam welds, which are located close to the top of

the hook. It is for this reason that the flexural contribution of the panels is neglected. The fact that some resistance is provided, particularly where a seam weld is located close to the fold line member, is reflected by the differences between observed and predicted member stress. Since the size of fold line members would in many cases be dictated by practical considerations of welding and panel placement (as was the case for the experimental unit), this difference is probably not important.

The stress in the free edge member, which should be zero through the entire range of loads, is also shown in Fig. 20. Only slight stresses are noted, first compressive, then tensile as the applied load was increased toward

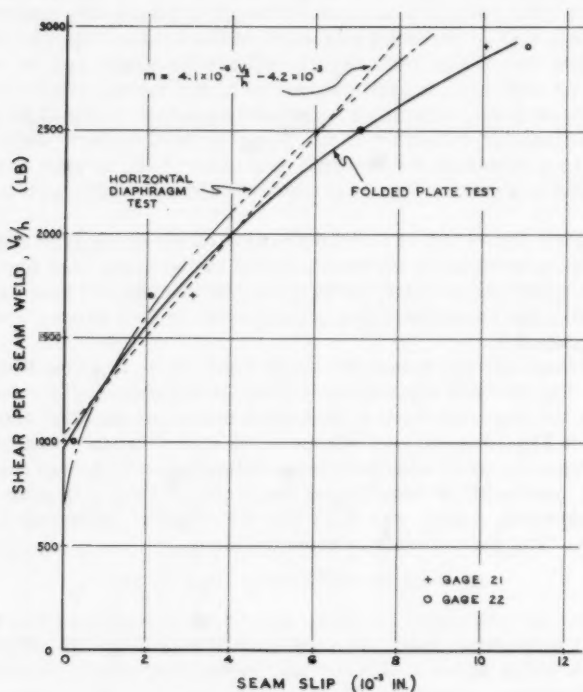


FIG. 19.—SEAM SLIP AT FIRST INTERIOR SEAM

failure. These stresses may be classified as secondary effects. Due to flexure of the inclined plate BC, fold line member B is in tension. The effect of this is to load the plate AB with shear outward from the span center, the effect being similar to an eccentrically loaded column, and producing small compressive stresses at the far edge due to bending of plate AB. Because of the accordioning at the hook joint, this stress is reduced to a small value. The reason for slight tensile stress in plate A at loads near failure is not clear, but may have to do with a shift in the effective neutral axis of the horizontal plate. For all practical purposes, this edge member stress can be considered to be zero.

**Distortion.**—Through the entire range of test loading, no detrimental distortion of the structure was observed. The shape of the cross section was

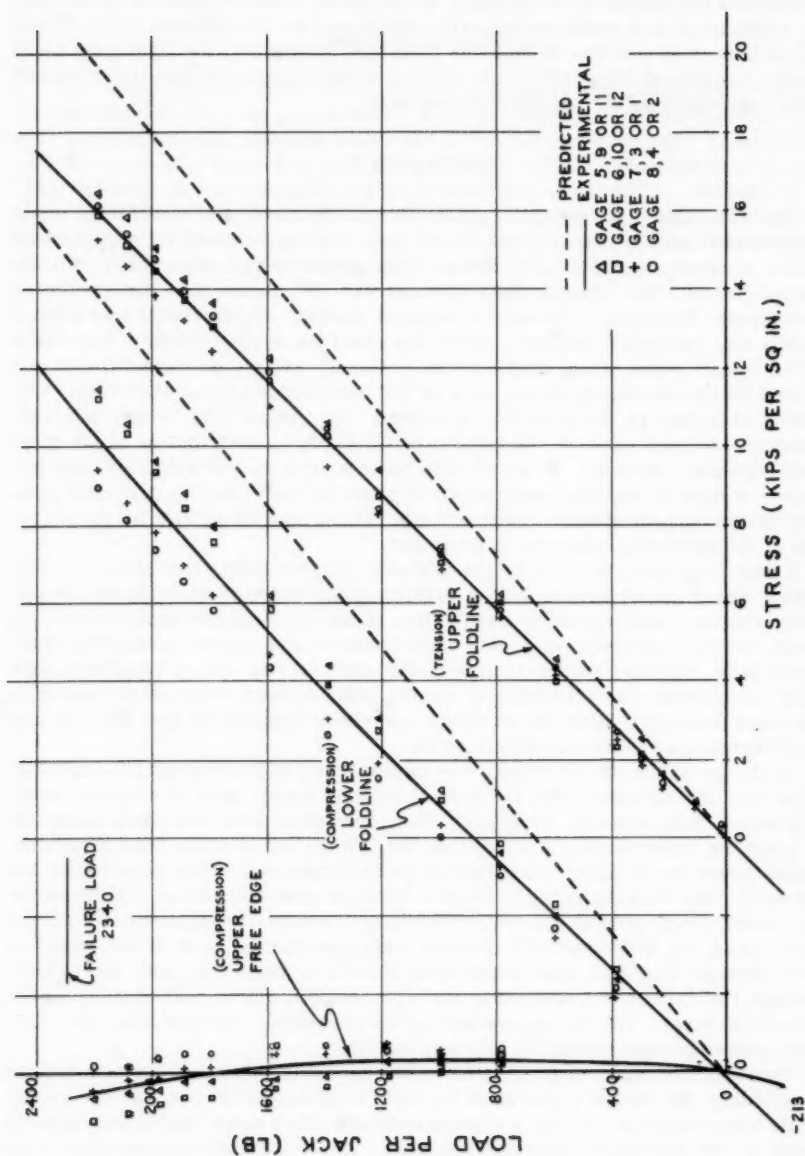


FIG. 20.—STRESSES IN FOLDLINE MEMBER AT MIDSPAN

retained, in spite of the rather severe conditions imposed by the use of relatively narrow top horizontal plates AB and EF. The slight horizontal displacements permitted by these plates would not be found in most installations, for which each unit would be laterally restrained by the adjacent unit. There was no observed rotation of fold line members relative to the light gage steel panels, in spite of the eccentricity of load application, each fold line member being restrained by the panels attached to it.

### CONCLUSIONS

The adaptation of design methods originally developed for folded plate structures of reinforced concrete to similar structures using light gage steel panels produces methods of analysis which give good agreement with experimental results. The ultimate load attained was 11% higher than that predicted by analysis. Throughout the entire range of loading, displacement was almost exactly that predicted, and well within the usually accepted limits. The shape of the folded plate cross section was retained, and no detrimental local or overall distortion was present, even at that load which produced failure. Observed stresses in the fold line members were about 20% lower than indicated by analysis, due to the neglect of the flexural contribution of the steel panel flat plate element. Because this difference is on the safe side, and because the size of fold line members will often be controlled by practical considerations and clearance requirements rather than by stress, no modification in the method of analysis is proposed.

It has been demonstrated by the experimental structure that the results of testing shear panel assemblies of relatively low span-depth ratio can be applied without modification to assemblies of the higher span-depth ratios that would be characteristic of folded plate construction, and to assemblies subjected to a variable rather than uniform shear. The use of relatively light flange members characteristic of folded plate construction, as compared to the much heavier rolled beam flange members common to horizontal shear diaphragms, was in no way detrimental.

While no particular difficulty was experienced in fabricating the test unit, it is well to emphasize that the type of welding required is of a special sort, of greater than average difficulty. Shop personnel doing the work made use of previous experience gained during the fabrication of more than fifty horizontal shear diaphragms using light gage steel panels. It has been found, for example, that welding using too high a heat, or done too slowly, will burn the thin steel sheet around the weld resulting in a defective connection. On the other hand, too little heat will produce improper fusion, as it is necessary to burn through the light gage steel panel locally to make the weld, and to burn through two layers of galvanizing, and frequently a prime coat of paint on the structural steel. The recommendations as to welding rod type and size, current, and amperage should be followed exactly.

The prefabrication of plate units in the horizontal position, as was done in assembling the test structure, is strongly recommended, because the puddle welds required at the seams and panel ends are much more easily and reliably made in the downhand horizontal position. This statement applies also to the puddle welds joining plate ends to supporting structure, and a fabrication de-

tail permitting pre-attachment of the inclined frame members to the folded plate by horizontal welding is desirable.

#### ACKNOWLEDGMENTS

The experimental work described in this paper was performed by Kaveti Seetharamulu, who was at the time a graduate student in Civil Engineering at Cornell University, working under the direction of the writer. The program was sponsored by Fenestra, Inc., manufacturers of the light gage steel panels. The substantial contributions of Gerald Sturman, A.M. ASCE, manager of the structural laboratory, and Ernest Pittman, mechanician, are gratefully acknowledged. The comments, advice, and suggestions of George Winter have been of great value in the course of the work.

1. The first part of the paper is a review of the literature on the topic of the paper.

2. The second part of the paper is a description of the methodology used in the study.

3. The third part of the paper is a discussion of the results of the study.

4. The fourth part of the paper is a conclusion and a list of references.

---

---

Journal of the  
STRUCTURAL DIVISION  
Proceedings of the American Society of Civil Engineers

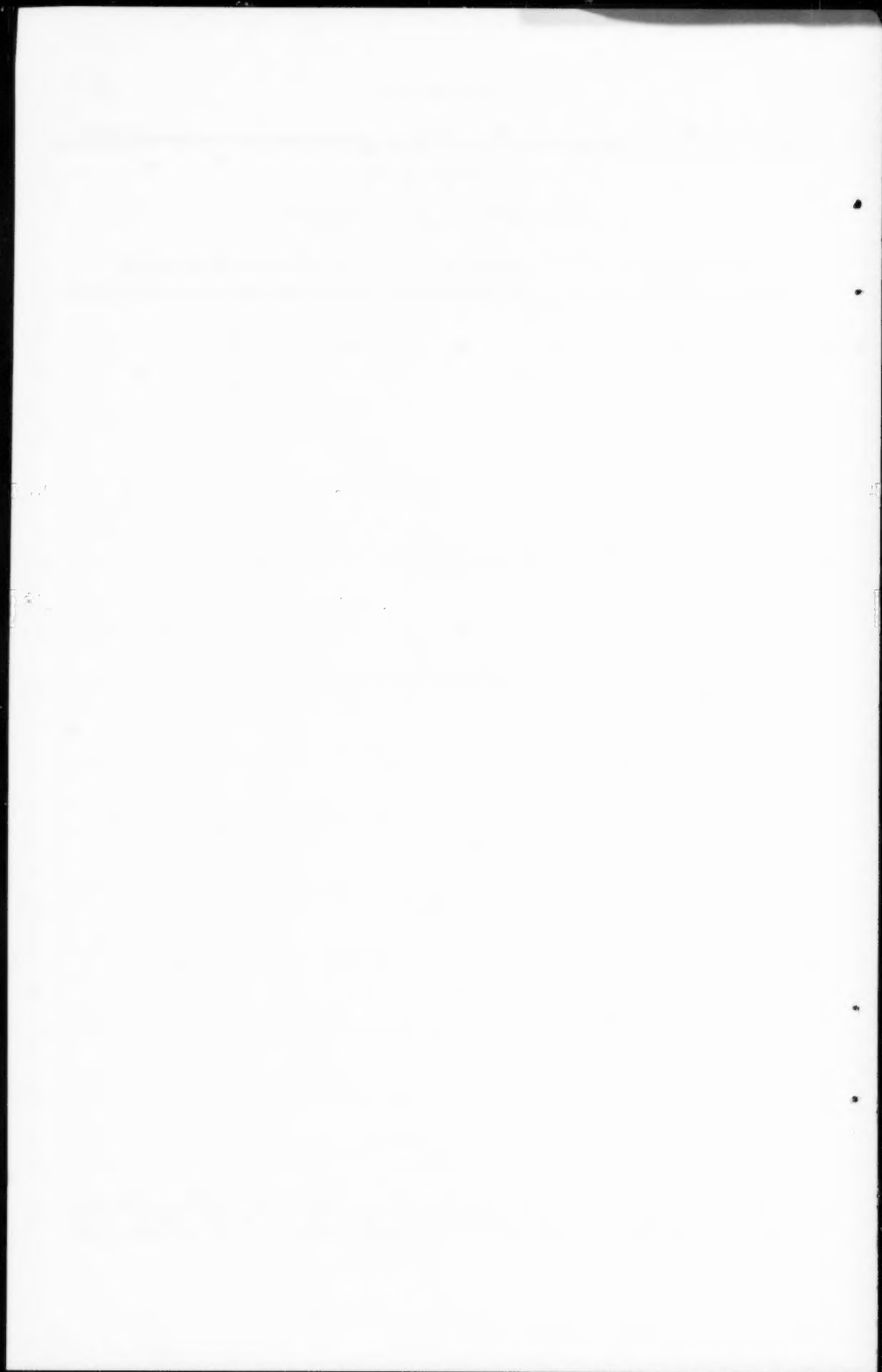
---

---

DISCUSSION

---

Note.—This paper is a part of the copyrighted Journal of the Structural Division, Proceeding of the American Society of Civil Engineers, Vol. 87, No. ST 7, October, 1961.





SECONDARY STRESSES IN PARALLEL WIRE SUSPENSION CABLES<sup>a</sup>

Closure by Thomas A. Wyatt

THOMAS A. WYATT.<sup>7</sup>—It is regretted that the behavior of the cable was described in general terms in order to reduce the length of the paper. The explanation of the effect of the cable bands given in the discussion is, of course, correct.

It is necessary to be careful when describing the string polygon formed by the cable. The lines of the actual resultant tension in each panel must intersect together with the suspender load. Fig. 3 was drawn as shown to avoid the difficulty of distinguishing between the various primary and secondary quantities, and it is formally correct that the component of suspender tension, normal to the cable, with the associated "primary" cable polygon angle, has no effect on the analysis. The two representations of the secondary influences are entirely equivalent, namely either addition of the moments indicated in Fig. 3 ( $M_{p,p-1}$ ) etc. to the force  $T$  along the cable axis, or alternatively displacement of the axis of the cable from the line of resultant tension. Considering the cable center lines measured at the middle of any two adjacent bays, the horizontal displacement of their intersection is most clearly shown by the second representation. The moment of the hanger tension (referred to as  $F_e$  in the discussion) balances the difference between the secondary moments in the two bays, being identical to the moment of force  $T$  at eccentricity  $l_c \theta_p$  in the writer's representation.

In the wrapped cable, there is a continuous redistribution of tension between the wires, and this corresponds to an angle between the cable axis and the string polygon or tension line. It is an important result of the analysis that the axial force is so large in relation to the wrapping tension that this angle is extremely small except for the localized bending close to the bands or saddles, and elsewhere the stresses involved in bending the wires (or groups of wires acting together without relative slip) are negligible. This is the basis of Eq. 17, and leads to Eq. 18 and 19 which, taken with Eq. 20, describe the fundamental behavior of the wrapped cable. In the opinion of the writer this represents the most important advance in analyzing the behavior of the cable in bending.

This is, unfortunately, different from the tests made in conjunction with the design of the Delaware River Bridge. The report mentioned in the discussion describes bending tests on a wrapped cable, both with and without clamping bands, but acting as a beam with no axial tension. The effect of the tension is to concentrate the bending at the ends, and thus to increase the stresses. The results for the beam action applied to the Delaware cable show stresses of 8,000 psi, whereas with the large tensile force added, the stress as computed

<sup>a</sup> July 1960, by Thomas A. Wyatt (Proc. Paper 2542).

<sup>7</sup> Asst. Engr., Freeman, Fox and Partners, Cons. Engrs., London, England.

by the writer is approximately 14,000 psi, plus a local bending stress depending on the saddle radius.

The data on friction are, however, most valuable. Although the low figures quoted for the coefficient of friction on pulling a single wire out of the experimental cable section may not fully show the effect of the constriction caused by the band on the resistance to movement of larger groups of wires, it is clear that the value should be much lower than first proposed. Since the more important secondary stresses increase with the coefficient of friction, the writer is inclined to use 25% for slip within the bands.

Whereas it is false to conclude (because there have been no failures or maintenance difficulties due to breakage of wires) that designers have in the past failed to achieve the greatest economy, it is certainly true that working stresses now proposed are generally higher than hitherto. With lighter deck construction, this increases the importance of the secondary stresses.

The theoretical approach made in the paper should serve as a logical basis for the interpretation and correlation of observed behavior. As a design recommendation, it can only be suggested that there is still a margin for the increase of "primary" stress, using the paper as a guide for detail design to keep the total stresses, including alternating stress effects, within the bounds accepted in present practice.

**Errata.**—In the original paper, on page 40, in Eq. 2 a square-root radical should be added to cover the terms  $f_T E$ . In line 2 below Eq. 2 change  $l_r$  to  $l_T$ . In line 2 of the second full paragraph change  $g = 1/9 r$  to  $g = 1/(9 r)$ .

On page 42, in the last ten lines, change  $\nu^1$  to  $\nu'$ . In the third line from the bottom change  $(1 - k)$  to  $(1 - K)$ .

On page 44 in the first six lines change  $\nu^1$  to  $\nu'$ . In the sixth line delete "or  $(1 - K) G \phi_0$ " and replace it with "represented by  $\gamma(1 - K) G \phi_0$ ."

On page 46, in line 6 under the heading "Multi-Wire Wrapped Cable" add the words "on both faces" just after "to the right of B."

On page 46, in line 4, change  $\psi_2 = s/3 f_T$  to  $\psi_2 = s/(3 f_T)$ .

On page 48, in the equation just prior to Eq. 19 add a square-root radical over the terms  $\frac{s E \psi_1}{j}$ . In addition, a closing brace should be added to the end of the equation.

On page 49, in lines 6 and 7 from the bottom, change the reference to Eqs. 15 and 16 to Eqs. 18 and 19.

On page 52, in line 6 of the first full paragraph change  $\psi_R$  to  $1\psi_R$  and then change the word "lower" to "tower."

On page 53, in line 7 change  $+ \log_e d_n$  to  $+ \log_e d_n q$ . In Eq. 31 change  $(1.0 \log_e q)$  to  $(1.0 + \log_e q)$ .

On page 54, in line 6 from the bottom, change  $1/g \div 9 r = 0.9 \text{ in.}$  to  $1/g = 9 r = 0.9 \text{ in.}$

On page 56 add to the definition of the term  $G$ ,  $= E I/1_h$ .

On page 59, in Appendix III, in the expression for  $s_A$  change  $\xi$  to  $\zeta$ . In the expression for  $s_B$  change  $\frac{4}{\sqrt{3}}$  to  $\frac{4}{3}$ .

METHOD FOR ANALYSIS OF MULTIBEAM BRIDGES<sup>a</sup>

Closure by John E. Duberg, Narbey Khachaturian, and Raul E. Fradinger

JOHN E. DUBERG,<sup>13</sup> NARBAY KHACHATURIAN,<sup>14</sup> M. ASCE, and RAUL E. FRADINGER,<sup>15</sup> A. M. ASCE.—It should be quite practical to evaluate the stiffness coefficient  $K$  as proposed by Ayra for any arrangement of moment-resisting correction. An exception may exist for a prestressing correction which carried transversely through all beams and, as such, its state of stress would depend on the motion of all beams. However, it is anticipated that for such a prestressing correction to be effective, it would maintain no relative motion of the sides of the beams and the analysis of the complete structure would more closely approach an orthotropic plate. For the structure envisaged by the writers, which included no lateral prestress, it is to be expected that the more significant hinge stiffness that was neglected was that of relative shearing deflections. This too could be added by assuming deflection springs at the hinges in a manner analogous to the torsions or spiral springs proposed by Arya.

The effect of thickness on the torsion bending constant  $C$ , or the second part of the torsion bending constant as it is known in aeronautical structures is of the same nature as the effect on the evaluation of the bending moment of inertia of a thick section if only the areas of the walls are considered acting at their centroids. That is, variations of strain through the sections are ignored and would only be significant for small ratios of thickness to cross sectional dimensions.

The concern of Robinson over the distortion of the cross section is unfounded as a contradiction to the basic torsion and flexure of beams since it has always been involved in the two-dimensional bending problem, that is, the plate of slab. Distortion of the cross section is more significant as a contribution to the relative rotation of the beams at the hinge and could be incorporated in the torsion spring as proposed by Ayra. However, few transverse-stiffening ribs or bulkheads will suffice to reduce this distortion to negligible amounts.

<sup>a</sup> July 1960, by John E. Duberg, Narbey Khachaturian, and Raul E. Fradinger (Proc. Paper 2552).

<sup>13</sup> Formerly Prof. of Civ. Engrg. Univ. of Illinois; now with Langley Research Center, Langley Field, Natl. Aeronautics and Space Admin., Va.

<sup>14</sup> Assoc. Prof. of Civ. Engrg., Univ. of Illinois, Urbana, Ill.

<sup>15</sup> Research Asst., Civ. Engrg., Univ. of Illinois, Urbana, Ill.

1. The first part of the paper is devoted to a discussion of the general principles of the theory of the structure of the atom. It is shown that the structure of the atom is determined by the laws of quantum mechanics, and that the structure of the atom is a function of the atomic number.

BASIC COLUMN STRENGTH<sup>a</sup>

---

Closure by Lynn S. Beedle and Lambert Tall

---

LYNN S. BEEDLE,<sup>21</sup> F. ASCE, and LAMBERT TALL,<sup>22</sup> A. M. ASCE.—From the results of test data<sup>10</sup> it has been shown that a tendency exists for thinner rolled shapes to exhibit a higher yield stress than do thicker rolled shapes. This test data, however, did not investigate any possible effect of temperature gradient. It is not possible, at present, to predict whether the temperature gradient during rolling influences the variation of yield stress in a structural shape. It is probable that higher yield stresses are a combined effect of more rapid cooling rate and increased working of the metal.

Due to this effect of rolling, coupons taken from the junction of flange and web usually exhibit a somewhat lower yield stress than coupons taken from the flange tips, for rolled I and H shapes. This effect is independent of the effect of residual stress. Residual stresses do not influence the yield stress level, as shown by the fact that yield stress levels taken from weighted coupons and from stub columns are the same (Fig. 11).<sup>10,11</sup> On the other hand, as noted in the paper, the effect of residual stress is to lower the proportional limit and to cause the stress-strain relationship of a stub column to be non-linear between that point and the yield stress level.

To overcome the variation of yield stress for different thicknesses, it is indeed possible to vary the carbon content of the steel. In fact, it is understood that this is common practice for the heavy shapes.

The writers are gratified to note that the results of the tests of Fisher and Viest agree favorably with those reported in the paper, particularly in comparing Figs. 13 and 35, and Tables 2 and 5.

The writers are aware that a large variation exists in structural shapes for residual stresses and yield stress. It is believed that the results presented, although not exhaustive, have indicated these variations, as well as providing information on mean values and scattering of data to be expected. For instance, Table 5 serves as an indication of the magnitude of residual stress to be expected in a rolled shape.

The mean values for residual stress given in Table 2 are not to be regarded as "generally applicable means." Since there is an apparent variation depending on shape and size, the experimental results were divided arbitrarily into "columns" and "beams." The maximum and minimum values shown are the results of experiments rather than the results of statistical computations involving a level of significance. Indeed, it is doubtful that the comparatively small populations involved in the tests should be used for a reliable statistical

---

<sup>a</sup> July, 1960, by Lynn S. Beedle and Lambert Tall (Proc. Paper 2555).

<sup>21</sup> Dir., Fritz Engrg. Lab., Lehigh Univ., Bethlehem, Pa.

<sup>22</sup> Research Asst. Prof., Lehigh Univ., Bethlehem, Pa.

analysis. It was for this reason that the suggested limits shown in Fig. 13 are the boundaries of test data, and not computed as a deviation from the mean. The test results presented by Fisher and Viest for one strain rate are within the suggested limits and may be regarded as a test of the validity of the suggested limits at that strain rate.

It is inevitable that a discussion will occur concerning the number of test data in a study. It becomes obvious that there is a practical, as well as an economical limit to the number of measurements that may be made, or of the variety of shapes that can be tested in any experimental study. Consequently, when the program was presented, a range of WF shapes were selected that would include a broad spectrum and in addition the extremes of weight, size, and width-thickness ratio. Also, duplicate specimens from two different mills were tested. It is recognized that the results of such a study may not satisfy a strict statistical requirement for reliability. Even if the deviation of an observation from a "generally applicable mean" is statistically significant, the deviation is not necessarily significant from a practical viewpoint.

This practical viewpoint reflects such factors as this: (a) residual stress is only one of the factors that influence column strength; (b) it varies from shape to shape, and for each shape there is a different column strength curve; (c) a single column curve for all shapes of necessity is an approximation to the curves for individual shapes; and (d) in design the factor of safety has traditionally included a percentage (undefined) for variation in properties. It is because of this that the writers consider that an adequate number of tests of rolled shapes were performed in order to provide a reasonable basis for an ultimate strength formula for A7 columns. Such a formula is now included in the CRC "Guide to Design Criteria for Metal Compression Members."<sup>17</sup>

*Errata.*—p. 141, line 8: "low-allow" should be "low-alloy."

p. 144, Table 1, columns 3, 4, 5, and 6: after "yield stress level ( $\sigma_y$ )" put in ksi."

p. 148, line 2: "Fig. 4(c)" should be "Fig. 4(d)."

p. 151, line 15: "routing" should be "routine."

p. 156, Fig. 17: the title should read ". . .  $\sigma_y$  (STUB COL.)/ $\sigma_y$  (MILL) and not  $\sigma_y$  (STUB COL.)/ $\sigma_y$  (MILL).

p. 161, Fig. 23: The figures above the titles of Fig. 23 (a) and 23 (b) should be interchanged.

p. 162, line 2: " $L/r \geq \pi\sqrt{E/\sigma_p}$ " should be " $L/r \leq \pi\sqrt{E/\sigma_p}$ ."

p. 162, line 4: " $L/r \leq \pi\sqrt{E/\sigma_p}$ " should be " $L/r \geq \pi\sqrt{E/\sigma_p}$ ."

pp. 163, 165: These two pages should be interchanged.

p. 170, para. #13: " $(40 \leq L/4 \leq 120)$ " should be " $(40 \leq L/r \leq 120)$ ."

p. 172, line 4: " $\epsilon_{pl}$ " should be " $\epsilon_{pl}$ ."

SHEAR DIAPHRAGMS OF LIGHT GAGE STEEL<sup>a</sup>

---

Discussion by J. Morley English

---

J. MORLEY ENGLISH,<sup>6</sup> M. ASCE.—The publication of the results obtained by Nilson has prompted the writer to offer as discussion the results of a series of tests and conclusions therefrom of a research program that was performed in 1957. The tested section is similar to that of Nilson's type 4, as can be seen in Fig. 17.

The material in this discussion was prepared prior to the publication of Nilson's paper. It is interesting to note that the independently formulated conclusions are in remarkably close agreement to those of the author.

Since shear (equal biaxial tension-compression) may be assumed to be the most significant stress state in a diaphragm, a jig to produce a pure shear field was constructed. It was considered necessary to perform the test on a full-scale panel to avoid problems of scaling and similitude. The jig, Fig. 18, was 16 ft 8 in. square. It was a picture-frame type capable of being loaded across the diagonals (one in tension, the other in compression) by means of hydraulic jacks. The increase or decrease of the diagonal measured between reference points on the corner pins was recorded by means of an Ames dial extensometer.

The test panels were constructed of the same hot-rolled 18 gage sheet stock, roll-formed to the section shown in Fig. 17. The individual sections were welded by intermittent welds 1 in. long and spaced at intervals ranging from 48 in. center to center to as close as 6 in. center to center. The boundaries were welded in the same manner to the jig. A 3 in. wide closure strip was needed to connect the section ends to the jig. In all cases the welds were located to provide a pattern parallel to the jig sides (that is, non-staggered).

A second set of tests was run to ensure that deflections computed on the assumption of pure shear were applicable to the flanged deep-beam case. For these tests the deck was comprised of three panels 16 ft 8 in. long and laid with ribs parallel to the boundary members. These were arbitrarily chosen as channels in order to provide adequate bending resistance for the deck as a whole and still remain sufficiently flexible to provide a minimum of resistance to component forces in the plane of the deck and normal to the boundaries.

A jig to apply third-point concentrated loads was constructed and is shown with the deck in place in Fig. 19. Strain gages were placed in a number of locations throughout the panel in an attempt to determine the stress distribution. However, the results of these measurements were inconclusive.

*Theoretical Strength.*—Failure may occur by yielding, tearing of the welds, local instability of the sheet, or a general instability of the deck. For thin sheet

---

<sup>a</sup> November 1960, by Arthur H. Nilson (Proc. Paper 2650).

<sup>6</sup> Assoc. Prof., Engrg. Dept., Univ. of California, Los Angeles, Calif.



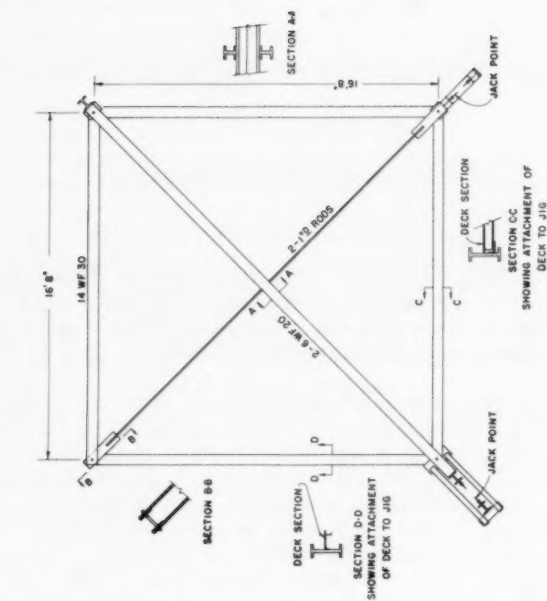


FIG. 18.—PICTURE FRAME JIG

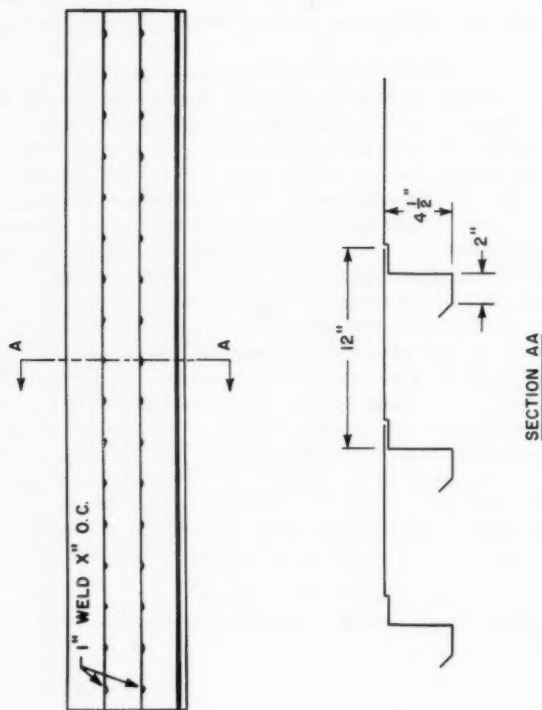


FIG. 17.—DECK SECTION AND WELD PATTERN



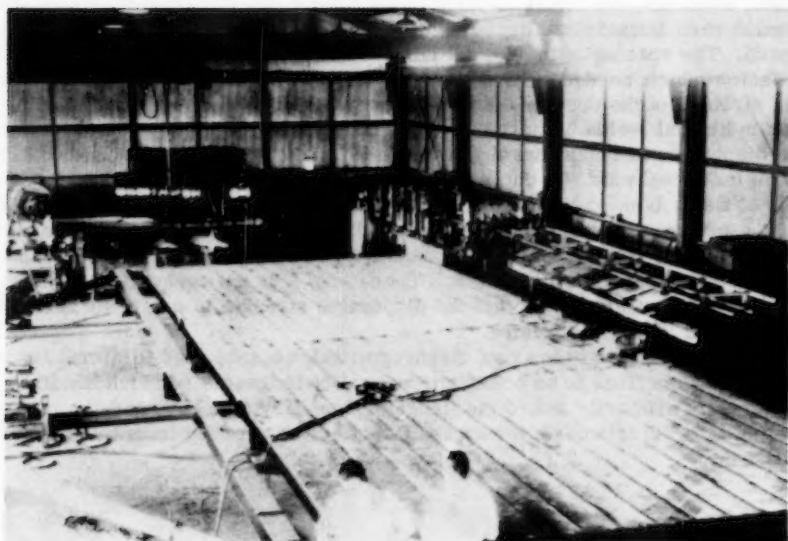


FIG. 19.—JIG WITH DECK IN PLACE

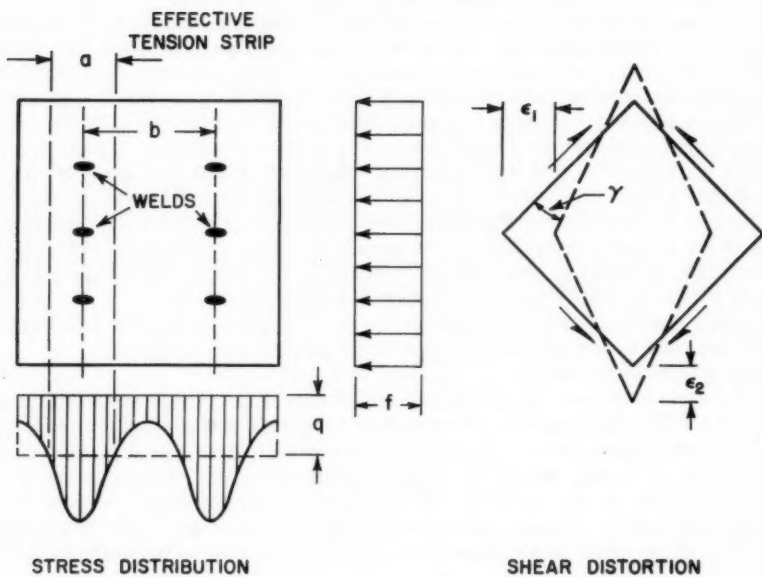


FIG. 20.—STRESS AND SHEAR

metal elements, the metal yielding is not normally a factor which needs to be considered. Local instability is inhibited by proper location of ribs and stiffener beads. The spacing of the  $4 \frac{1}{2}$  in. rib on 12 in. centers eliminated stability as a factor which needed to be considered for normal weld spacing. Therefore, the strength of the deck is reduced to a function of the strength and spacing of the individual welds. In addition, it will depend on the stress pattern within the diaphragm at the instant of failure if the failure is precipitated by the failure of an individual weld. On the other hand, it is apparent that if a sufficient number of welds is used, the failure can be forced into a general instability mode. At the general instability stress level, a rib may be utilized to its full capacity for the sole function of maintaining stability; it would have no reserve for supporting transverse bending loads. Therefore, it is not economical to provide such a close weld spacing that the diaphragm strength is that associated with the general instability failure.

The stress field within a roof diaphragm, which is subjected to lateral forces, is pure shear. This is an accepted idealization for beams in which bending resistance is primarily due to the flange or boundary members and in which the web is thin. In this case, the stress field derives directly from the shear relationship,

$$q = \frac{VQ}{I} = \frac{V}{h} \dots \dots \dots (4)$$

and

$$V = qh = n F_w \dots \dots \dots (5)$$

in which  $n$  is the number of welds in  $h$  and  $F_w$  is the value per weld.

If no flange is provided, but where the shear modulus,  $G$ , is low in comparison to  $E$ , the shear distortion will tend to alter the stress pattern. As a consequence the shear will tend, as for the flanged beam, toward a more uniform distribution across the section. Perhaps more significant, the bending stresses will depart appreciably from a linear distribution across the section. High stresses will concentrate at the edges of the beam. Unless a flange is provided in the form of a positive diaphragm boundary member, high stresses in the outside planks may precipitate failure at much lower loads than might be expected from conventional beam theory. Since the shear across the section tends to be constant regardless of the boundary configuration and since the ultimate value of shear is governed by the weld strengths, it follows that a weld pattern which is uniformly spaced tends to be optimal.

Furthermore, because the bending resistance is provided by the boundaries, the stress field in the diaphragm tends to be that of pure shear.

#### *Theoretical Stiffness.—*

**Shear Deflection.**—It is postulated that shear is the stress state within the diaphragm. The diaphragm is anisotropic; its elastic properties are different in two principal directions. A modulus of Elasticity  $E_1$  in the direction of the plank is that of steel. It will be reduced in the direction perpendicular to the plank, by virtue of the tendency for stress to transmit along narrow paths through the welds. Assume that an effective strip of width  $a$  governs the deformation of the panel when loaded in a direction normal to the plank, Fig. 20. Then

$$\delta = \frac{FL}{EA} = \frac{FL}{Ea t} \dots \dots \dots (6)$$

in which  $A$  is the effective area  $a t$ .

Thus the effective modulus of elasticity for the panel in this direction is

$$E_2 = \frac{a}{b} E_I \dots \dots \dots (7)$$

in which  $b$  is the weld spacing.

With reference to Fig. 20

$$\gamma = \epsilon_1 + \epsilon_2 \dots \dots \dots (8a)$$

$$\epsilon_1 = \frac{f}{E_1} + \frac{\mu f}{E_1} \dots \dots \dots (8b)$$

and

$$\epsilon_2 = \frac{f}{E_2} + \frac{\mu f}{E_2} \dots \dots \dots (8c)$$

from which

$$\gamma = \frac{v}{G} = \frac{f}{G} = (1 + \mu) \left( 1 + \frac{E_1}{E_2} \right) \frac{f}{E_1} \dots \dots \dots (9)$$

Solving

$$G = \frac{E_1}{(1 + \mu) \left( 1 + \frac{E_1}{E_2} \right)} \dots \dots \dots (10)$$

Substituting for  $E_1/E_2$ , using a value of 0.25 for Poisson's ratio, and dropping the subscript, Eq. 10 becomes

$$G = \frac{E}{1.25 \left( 1 + \frac{b}{a} \right)} \dots \dots \dots (11)$$

A curve for  $G$  as a function of weld spacing is plotted in Fig. 21. For general applicability it must now be hypothesized that this value for  $G$  is valid when the direction of principal stresses is other than parallel and normal to the direction of the planks.

**Shear Versus Bending Deflection.**—Third-point loading corresponds approximately to a distributed load. The maximum bending deflection for third-point loading is

$$\delta_B = 0.071 \frac{VL^3}{EI} \dots \dots \dots (12)$$

The shear deflection for the same loading is

$$\delta_V = \frac{1}{3} \frac{VL}{GA_w} \dots \dots \dots (13)$$

from which

$$\frac{\delta_V}{\delta_B} = 4.68 \frac{EI}{GAL^2} \dots \dots \dots (14)$$

Now  $I \approx A_f \frac{h^2}{2}$  for flanged beams.

$$\text{Thus } \frac{\delta_V}{\delta_B} \approx 2.34 \frac{E}{G} \frac{A_f}{A_w} \left(\frac{h}{L}\right)^2$$

In roof and floor systems it is usual that (a)  $A_f/A_w$  is not small, (b) the effective  $G$  has been shown to be quite small as compared to  $E$ , and (c)  $h/L$  is not greater than  $1/3$  for most roof systems.

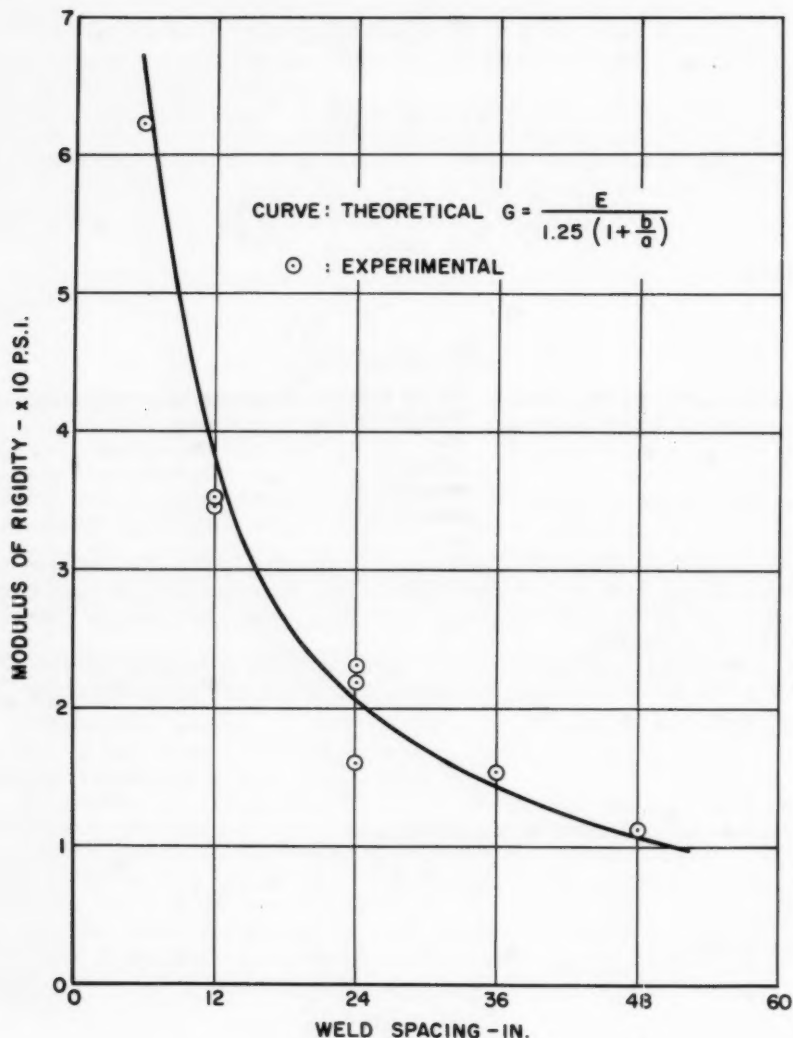


FIG. 21.—MODULUS OF RIGIDITY VERSUS WELD SPACING

Therefore, the shear deflection is more significant than bending deflection. In most cases bending deflection may be ignored completely.

**Test Procedure.**—The test procedure called for full-scale testing. The welding was done on 18 gage hot rolled sheet, roll-formed into the section shown in Fig. 17. It was desired to vary the spacing of welds from that which was needed to produce a general instability to as much as 48 in. A model test was therefore not considered to be particularly useful. Since the main assumption was that such diaphragms could be considered as pure shear fields (that is, equal principal tensions and compressions at  $45^\circ$ ), the deck panel was constructed in the picture-frame type jig previously described.

The deflections were measured by means of two Ames dial extensometers along the diagonals of the jig.

**Analysis of Test Results.**—

**Strength.**—The results of the shear panel tests are given in Table 2. The missing lower-numbered tests are those which were conducted in order to evaluate the vertical-loading capacity of the section; the results are not pertinent. Failure in all cases, with the notable exception of test V-C (the 6-in. weld spacing) failed in shearing of the welds. Tearing of the metal around the weld was characteristic of all weld failures. Failure of the three-panel third-point-loaded beam tests exhibited the same characteristics and developed essentially the same shear values as in the single-panel shear test. On the other hand, for the tests of panels with boundary welding on the same spacing as for the interior seams, failure occurred on the boundary. For tests in which the welds on the boundary were one-half the spacing of those on the interior seams, the average value per weld at failure was 2,780 lb. This was not appreciably greater than that for the tests in which welding on the boundary was the same as on the interior. The value in this case averaged 2,400 lb per weld. This indicates that an increase in number of welds on the boundary of approximately 15% is required to develop the full panel strength and produce a balanced welding design.

A further improvement which resulted from increased boundary welding was a marked increase in the yield limit.

Evidence of the validity of the theory that the stress in the diaphragm is pure shear was obtained from the correlation of data from the single-panel tests, the three-panel tests, and individual weld specimens. All three types of tests fell within the normal scatter of the data. If a non-uniform shear field had occurred in either of the two types of diaphragm tests, a much lower shear strength could have been expected than for the individual weld specimens which failed at an average value of 2,770 lb per weld. Also the three-panel test might have been expected to produce lower values than for the single-panel test.

The first indication of nonlinearity of the load-deflection curve was always accompanied by a slight elastic buckle on the outstanding edge of a plank (Fig. 22). This increased progressively until failure occurred in the weld. It is possible that it contributed to the tearing-out around the weld (Fig. 23) when final failure ultimately developed. An interesting effect was noted, in that these buckles tended to occur toward one end of the space between welds and faded out at the other. A possible explanation of this is that the  $45^\circ$  principal-stress field intersects through the welds. On one side of the weld, the stress is tension and the other side compression. The tension region near a free edge tends to inhibit buckling and vice versa. The actual stress pattern is undoubtedly complex.

TABLE 2.—SUMMARY OF RESULTS

Test	Description	Failure and Remarks	Failure per weld, in pounds	Ultimate load, in pounds per linear foot	G, in $10^6$ psi
II-C	Tension diagonal only Welds 48" c/c & 48" c/c	None	----	----	----
II-D	Tens-Comp Same as II-C	Buckling of 3" end closure strip	2520	630	1.1
II-E	Same as II-D 12" c/c on edge	Welds sheared	2940	760	1.1
III-A	Welds 24" c/c & none on end boundary	None - flexible system	----	----	0.89
III-B	Welds 24" c/c & 24 c/c	Buckle at closure strip 2 welds in panel sheared 2 minutes later	2620	1310	1.63
IV-A	Weld 24" c/c & 12 c/c	None	----	----	1.95
IV-B	IV-a with 12.5/distributed vert load	No effect on vertical load no failure	----	----	2.07
IV-C (1)	Weld 12" c/c & 12 c/c modified IV-a	None	----	----	3.46
IV-D (1)	Repeat IV-C with 12.5/vert load	Failed in welds on boundary - Boundary repaired & welds added to provide 6" c/c on boundary	2030	2030	3.53
			2450	2450	
V-A	Modified boundary to eliminate closure on end weld direct end weld direct to frame welds 24" c/c & 12" c/c	None	----	----	2.98
V-B	Welds 12" c/c & 6" c/c	None	----	----	3.90
V-C	Welds 6" c/c & 6" c/c	General Instability - no weld failure until after buckling	1850	3700	6.25
VI- (2)	Welds 36" c/c & 12" c/c	Weld shear	2880	960	1.56
VII-A	3 panel test 1/3 point load Welds: seams 24" c/c end 12" c/c edges none	Very flexible-loaded to 1000 - extensive elastic buckling, but no permanent set	----	----	----
VII-B	Repeat VII-A with 24" c/c edge & 12" c/c on end	Shear failure	2530	1285	2.33
VII-C					
VIII-A	Weld 12" c/c & 12" c/c 3 panel	End welds sheared suddenly	2400	2400	3.47
IX-	Same as III-B	Shear in welds in area of corner - Extensive buckles	3140	1570	----
X-	Weld 24" c/c & 12" c/c 3 panel weak load point	Shear along end panel about 1/3/in from tension flange	----	----	1.68

In two of the three-panel tests, jacking loads were applied to the jig and transferred directly into the diaphragm in continuous shear along the inner panel transverse boundary. Seismic forces are body forces which distribute in proportion to mass. On the other hand, a wind load may be applied in a manner similar to the jacking loads at definite points of support along an outside wall. For this reason test No. 10 was arranged as for a typical building structure. The loads applied to the cross member of the jig had to find their way into the deck by indeterminate means. A high proportion of load which was applied to the cross beam directly was distributed by tension in the closure strip that joined the end and center panels. A still greater portion must have



FIG. 22.—BUCKLE ON OUTSTANDING EDGE

been introduced by compression through an extensive region in the vicinity of the jacking point. This was evidenced by a tendency of the first two edge planks and the closure strips to buckle. This compression effect was evident throughout the entire compression side of the diaphragm. As the elastic limit was approached, the inner-weld buckles appeared as formerly but were obviously greater toward the end supports. In spite of these severe conditions for load application, the final collapse was typical of all others. The welds failed in shear along the third rib from the tension boundary of one of the end panels (Fig. 24). The failure was sudden, so that it could not be determined whether or not it may have been precipitated by failure of a single weld in the closure strip in the compression zone. In any event, failure along the rib produced a



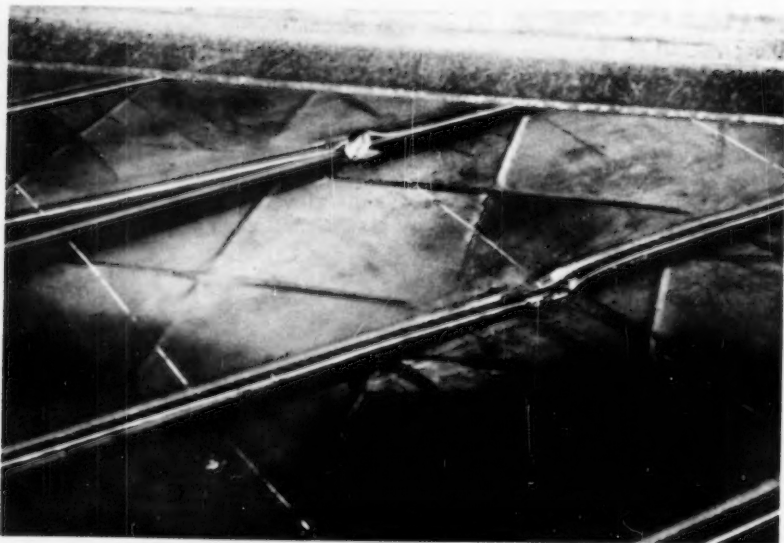


FIG. 23.—TEARING OUT AROUND WELD

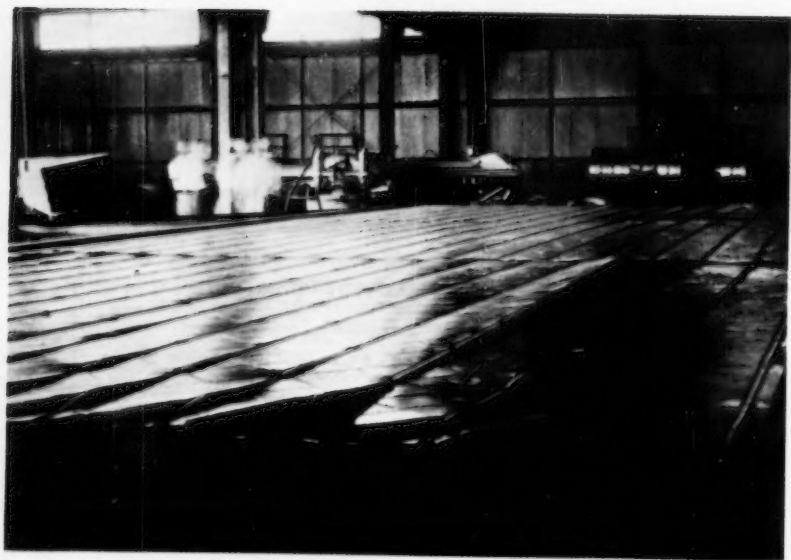


FIG. 24



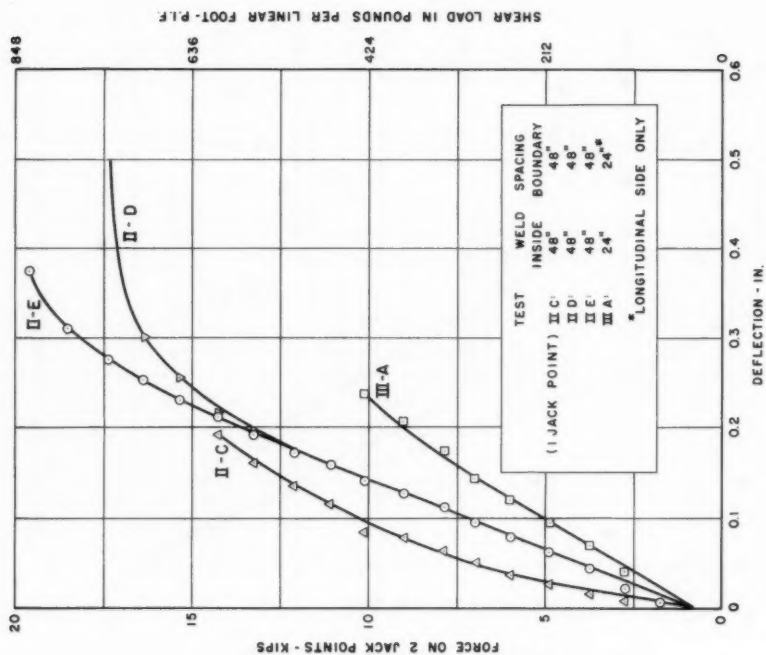


FIG. 26.—DEFLECTION VERSUS SHEAR LOAD

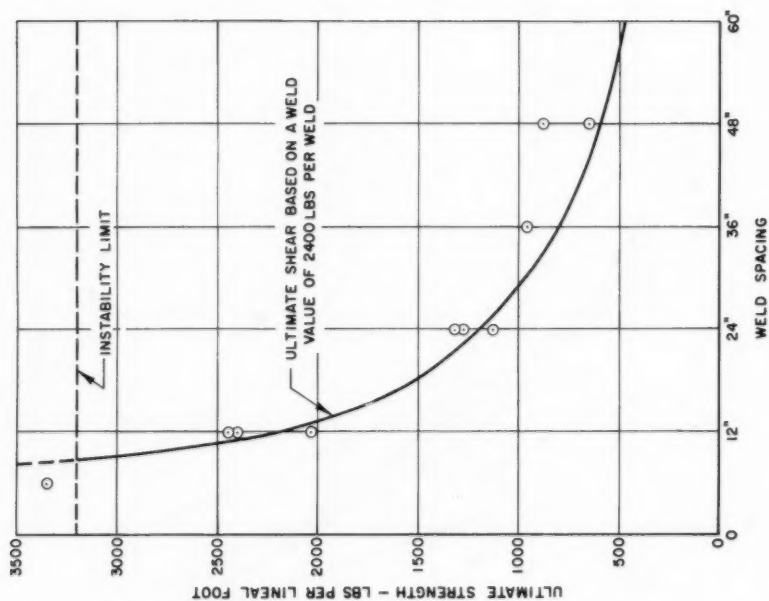


FIG. 25.—ULTIMATE STRENGTH VERSUS WELD SPACING

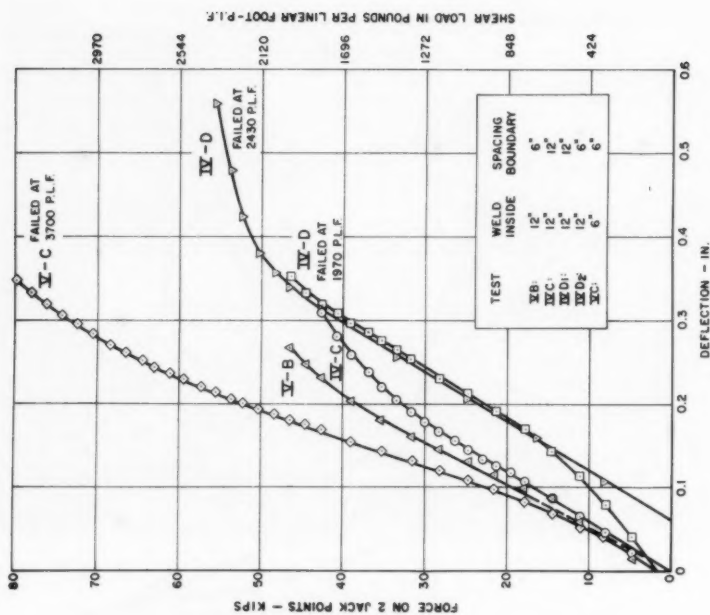


FIG. 28.—DEFLECTION VERSUS SHEAR LOAD

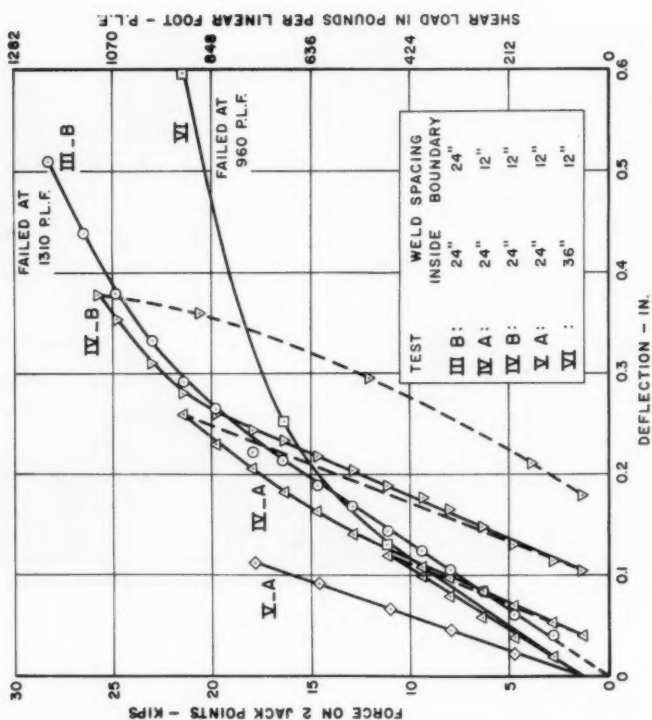


FIG. 27.—DEFLECTION VERSUS SHEAR LOAD

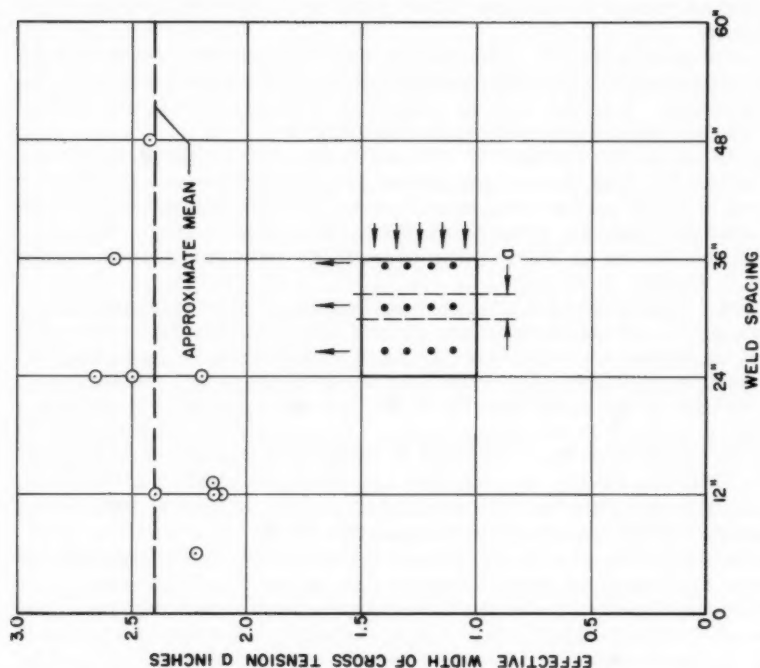


FIG. 30.—EFFECTIVE WIDTH

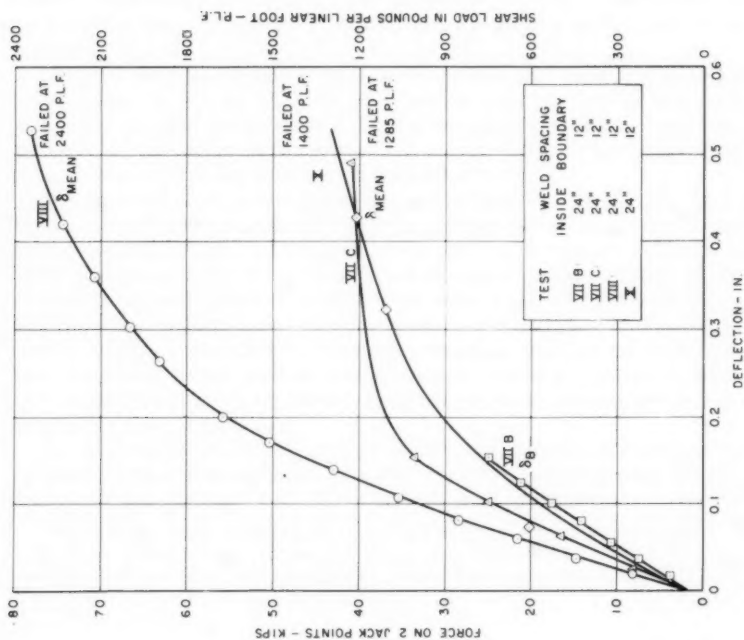


FIG. 29.—DEFLECTION VERSUS SHEAR LOAD

realignment of shears which then caused progressive failure along the inner closure strip.

One three-panel test was conducted to determine the effectiveness of the longitudinal boundaries. No weld connection between the outside plank and the jig was provided. The test was not continued to failure. However, the diaphragm was obviously weaker and much less stiff.

It may be noted that the ratio of ultimate to an offset elastic limit was always less than 3 to 1.85. Since these factors, 3 and 1.85, are usually taken for the factors of safety against ultimate failure and yielding respectively, it may be concluded that ultimate strength should always govern design. This confirms the conclusions of Nilson. The ultimate strength versus weld spacing is shown in Fig. 25.

Stiffness.—The shear-deflection curves, Figs. 26, 27, 28, and 29 are largely self-explanatory. These curves were plotted using the one dial gage on the compression diagonal of the jig only. It was felt that the sag in the tension rod gave unreliable readings on that gage. In a few tests there was stiffening with increasing load in the early loading steps. However, it is believed that this was a result of slack in the testing system. In general there was a linear or elastic portion followed by a reduction in stiffness as the elastic buckles developed. This was usually accompanied by some local yielding at the welds. In fact, the gain in elastic behavior associated with increasing the welds along the boundary may be directly attributable to this effect.

The average value of  $a$  in Eq. 11 was determined from the experimental value of  $G$ . Since no trend with weld spacing is evident, Fig. 30, it may be assumed that Eq. 11 describes the stiffness characteristic reasonably well. The average value of  $a$  was taken as 2.37 and  $G$ , plotted as a function of weld spacing,  $b$ . It is interesting to note how well the theoretical curve fits the test data, Fig. 21.

PERIODS OF FRAMED BUILDINGS FOR EARTHQUAKE ANALYSIS<sup>a</sup>

---

Closure by M. G. Salvadori and E. Heer

---

M. G. SALVADORI,<sup>21</sup> F. ASCE, and E. HEER,<sup>22</sup> A. M. ASCE.—White has proved once again that Rayleigh's method can give good estimates of the lowest frequency of an elastic system. White also questions the practical usefulness of Eqs. 28(a) and 29 because he feels that:

1. Structures with the characteristics assumed in the derivation of Eqs. 28(a) and 29 are rare.
2. The parameters appearing in these equations are easier to define than to evaluate.

As to the first objection, it must be pointed out that modern buildings have large window areas and use lightweight material, with little structural resistance, as partitions. The rigidity of a modern building is mostly due to its structural framing. Because the column sizes depend on the weight they carry, it is logical to assume an approximate linear variation for  $k$  and  $I$ . White must have had in mind an old-fashioned type of building with heavy brickwork partitions when he stated that "the contribution of the structural frame to the stiffness of a normal building is small compared to that of its walls and partitions." In deriving Eqs. 28(a) and 29 the writers visualized exclusively modern-type buildings.

White's second objection has some weight, although the evaluation of the parameters is not as difficult as it may appear. However, the writers must state that the use of Rayleigh's method suggested by White requires the computation of the same parameters, and moreover does not easily give reliable information on the frequencies of the higher modes.

Derrick has contributed illuminating clarifications to many factors influencing earthquake design. The writers agree with all of his statements, but would like to emphasize once more that, as the title of the paper indicates, their results do not present "a new method of dynamic design." Although it would be easy to plot the vibrational modes from their analysis, the formulas they have presented do nothing else but allow the fast evaluation of the first few frequencies of a modern building in its shear, bending, rocking and translational motion. Inasmuch as the periods are among the essential factors in both preliminary and final design, it seems practical to have simple and fairly accurate means for their evaluation.

A. A. Eremin, M. ASCE, indicated that the effects of elastic properties of the foundation on the vibration of structures varies within wide limits, and that, therefore, the inclusion of these effects may decrease the importance of the

---

<sup>a</sup> December 1960, by M. G. Salvadori and E. Heer (Proc. Paper 2680).

<sup>21</sup> Prof. of Civ. Engrg., Columbia Univ., New York, N. Y.

<sup>22</sup> Designing Engr., Paul Weidlinger, Cons. Engineer, New York, N. Y.

period values for other parts of the structure. However, the writers would like to point out that the elastic effects of the foundation on the fundamental period  $T_1$  may be disregarded by setting  $i = 1$  in Eq. 28(b). The range of these effects on  $T_1$  may be estimated by substituting extreme values in Eq. 28(a).

The writers agree that for more refined analysis methods including effects of seismic wave propagations should be considered and developed.

# MOVEMENTS OF A CABLE DUE TO CHANGES IN LOADING<sup>a</sup>

Discussion by D. M. Brotton, N. W. Williamson, M. Millar,  
Hannsharl Bandel, W. E. Adams, and Jackson L. Durkee

D. M. BROTTON,<sup>13</sup> N. W. WILLIAMSON,<sup>14</sup> and M. MILLAR,<sup>15</sup>—The erection of deck structures for suspension bridges is an important application for the calculations described herein. They will be valid until the connections which develop the continuity of the stiffening girders either close as the erection proceeds or are forcibly closed. Thereafter the hanger loads become indeterminate due to the interaction of the cables and stiffening girders.

The problem which usually arises is the determination of the geometry of a free cable when it is subjected to a series of loads of known magnitude which are attached at points whose spacings along the center line of the cable in its "unstrained condition" are known. The system of calculation which has been presented by the authors determines cable displacements due to changes in loading from an equilibrium condition. It could, however, be used to solve the problem mentioned previously by modifying Eq. 5 to

$$\Delta l = \frac{T}{A E} \frac{l_u}{p} \dots \dots \dots (10)$$

in which  $l_u$  is the unstrained length of a segment of the cable.

At the instigation of the engineers who are concerned with the erection of the deck structure for one of the largest suspension bridges in the United Kingdom, this problem was investigated in the Department of Structural Engineering, Manchester College of Science and Technology. The approach was generally similar to that of the authors in that static equilibrium and bending moments provide the basis of the calculation, but its detailed operation seems to be somewhat neater. A computer program which will carry out the calculation entirely automatically has been prepared and the program has been used extensively in carrying out erection calculations for the foregoing and one other major suspension bridge.

*Initial Computer Program Data.*—The precise information on which the calculation is based comprises:

1. The total span, tangent point to tangent point.
2. The unstrained lengths of the segments of the cable between adjacent hangers.

<sup>a</sup> December 1960, by James Michalos and Charles Birnstiel, (Proc. Paper 2674).

<sup>13</sup> Dept. of Structural Engrg., Manchester College of Science and Tech., Manchester, England.

<sup>14</sup> Dept. of Structural Engrg., Manchester College of Science and Tech., Manchester, England.

<sup>15</sup> Dept. of Structural Engrg., Manchester College of Science and Tech., Manchester, England.

3. The cross-sectional area of the cable.
4. The modulus of elasticity of the cable.
5. A pattern of loads applied at the hanger points.

In addition, approximate values are required for:

6. The center-span sag.
7. The horizontal spacings of the hangers, the total corresponding precisely to the span.

*Basis of the Calculation.*—The geometry assumed by the cable under the action of a particular pattern of loading is represented to some scale by the bending moment diagram of a simply supported beam between the tangent points.

The first calculation of the bending moments uses the approximate horizontal spacings and the bending moment values multiplied by the ratio

$$\frac{\text{Approximate center sag}}{\text{Center bending moment}}$$

gives the first approximation to the geometry. The tensions in the segments of the cable and their lengths can readily be calculated and these values together with the area of cross section and modulus of elasticity of the cable enable its "apparent unstrained lengths" to be calculated. The apparent lengths are those for a hypothetical cable which would satisfy the approximate conditions. For the geometry to be correct the total of the apparent unstrained lengths should equal the total of the unstrained lengths of the real cable, the "scale" is therefore altered by calculating an improved value of the center sag.

For a parabolic cable it can be shown that a change in the length of the cable  $\Delta l$  results in a change in the center sag  $\Delta s$  given by

$$\Delta s = \frac{3 L}{16 s} \Delta l \dots\dots\dots (11)$$

(neglecting second order terms)

in which  $s$  is the center sag and  $L$  refers to the span.

The calculation can be repeated until a satisfactory value for the center sag is obtained. At this stage, the calculation based on an assumed set of horizontal spacings has been completed.

In the equilibrium condition the horizontal components of the tensions in the individual sections of the cable must be equal. In order to attain this condition the horizontal spacings are adjusted by amounts calculated from the cable strains and corresponding to the differences between the individual values of the horizontal components of the cable tensions and their mean value. Because these adjustments are not exact, the totals of the spacings may not correspond to the span, it is necessary therefore to make a further linear correction.

This marks the completion of one major cycle of the calculation, the original bending moments and hence the vertical ordinates can now be improved by using the modified horizontal spacings and the procedure repeated. The calculation is terminated when the largest difference between the mean value and the individual values of the horizontal components of the cable tensions is less than a predetermined value.

*Additional Features.*—The preceding description deals with a single main-span calculation. There will, however, be span changes due to tower movement and temperature changes. The program has been extended so that it can repeat



the entire calculation for a new span corresponding to a specified tower movement. The effect of a temperature change can also be included because this merely consists of a calculation repeated for a set of modified "unstrained lengths" and total "unstrained length."

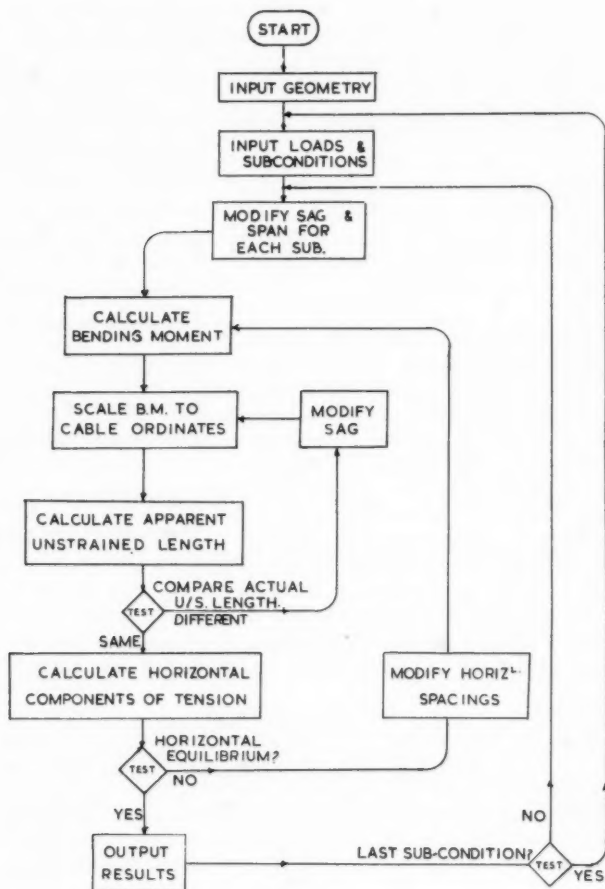


FIG. 4.—CABLE FLOW DIAGRAM

A flow diagram for the entire calculation is shown in Fig. 4. This shows clearly the path which is followed by the computer in solving each problem. Table 6 shows a "print out" of the data tape required for the solution of Example 2 in the paper. The values of the unstrained lengths of the segments of the cable having been obtained by hand calculations based on the tensions  $T_w$  and strained lengths  $l_w$  which appear in lines 8 and 4 respectively of Table 4.

TABLE 6.—DATA TAPE

9					Hanger points
2					Denotes symmetry
100	100	100	100	100	Approximately spaces for half span in ft (not critical)
106.3566	103.8193	101.9302	100.6775	100.0532	U/s lengths for half span in ft
100					Approximately sag in ft (not critical)
0.85					Cable area in sq in.
8482.14					Modulus of elasticity in tons per sq in.
0.0000065					Temperature coefficient
0					Difference in level of supports in ft
111					Load reference
1					Sub-conditions
1					Denotes non-symmetry
332	325	320	8317	316	
317	320	325	332		Loads for whole span in lb
0	0				Temperature and span change

TABLE 7.—FUNICULAR POLYGON

Load Ref.	Temperature Change	Span Change
111	0.000	0.000
9.02 Horizontal component of cable tension in tons		
Hanger Ref.	Ordinates, in feet	Abscissae, in feet
1	31.63	101.69
2	61.01	201.41
3	88.39	299.73
4	114.01	397.23
5	99.23	496.31
6	82.93	595.16
7	65.03	694.36
8	45.36	794.51
9	23.76	896.19
10	0.00	1000.00

The machine time for the solution of this problem was approximately fifteen seconds of which the major part was taken in punching out the results.

The results for this problem are shown in the "print out" of the results tape in Table 7, the interpretation of the various figures being as shown. It can be seen that they are in close agreement with those given in the paper.

*Accuracy of the Calculation.*—The calculation requires the specification of two limits, those for terminating the adjustments to the center sag and the horizontal spacings. They have generally been set as 0.001 ft and 0.5 ton horizontal restraint, respectively, because these figures provide corresponding accuracy. The convergence of the calculation is so rapid that these limits are satisfied in few cycles and it may also be mentioned here that the initial values for sag and horizontal spacings are by no means critical. Values corresponding to a parabolic profile for a cable having the specified total unstrained length and the total span divided equally by the number of horizontal spacings would have a negligible effect on the number of cycles and hence the computing time. The number of decimal places given in the output figure for the problem has been limited to a practical value in the interests of economy in computer output time.

*Sidespan Program.*—In considering the bridge as a whole, the horizontal components of the cable tensions in the main and sidespans are equalized at the main tower saddles. At the lower end of the sidespan cables, however, a further saddle is placed leading to the backstay cable. The sidespan can therefore change due to movements at both ends. It would be impracticable to equalize horizontal components of cable tensions at both ends so in order to simplify the treatment, a backstay stiffness function can be included which will automatically deal with the backstay saddle movement. In effect this further facility allows the computer to do a normal analysis for a specified span; this results in a value for the horizontal component of the sidespan cable tension which enables the span to be modified in accordance with the backstay stiffness function. The process is repeated until the equilibrium condition is attained. The data and output are generally similar in form to that illustrated and this program also has been used extensively on the two bridges mentioned previously.

HANNSHARL BANDEL,<sup>16</sup>—A calculation method for cables with three dimensional loading<sup>17</sup> has been developed by the writer which converges more rapidly than that developed by the authors and is more time saving. Here the three dimensional deformations are obtained by solving the equation system (Eq. 12) which results from the equilibrium at each load point (Fig. 5). Equilibrium equation at loadpoint (i)

$$\begin{aligned}\delta_{i-1,i} u_{i-1} + \delta_{i,i} u_i + \delta_{i,i+1} u_{i+1} &= \bar{X}_i \\ \delta_{i-1,i} v_{i-1} + \delta_{i,i} v_i + \delta_{i,i+1} v_{i+1} &= \bar{Y}_i \dots\dots\dots (12) \\ \delta_{i-1,i} w_{i-1} + \delta_{i,i} w_i + \delta_{i,i+1} w_{i+1} &= \bar{Z}_i\end{aligned}$$

16 Assoc., Severud-Elstad-Krueger-Assocs., New York, N.Y.

17 To be published in "Der Bauingenieur."

in which

$$\delta_{i-1,i} = -k_{i-1,i}; \delta_{i,i+1} = -k_{i,i+1}; \delta_{i,i} = +[k_{i-1,i} + k_{i,i+1}]$$

$$k_{i-1,i} = \frac{S_{i-1,i} + \Delta S_{i-1,i}}{\Delta s_{i-1,i} + \Delta \Delta s_{i-1,i}}; k_{i,i+1} = \frac{S_{i,i+1} + \Delta S_{i,i+1}}{\Delta s_{i,i+1} + \Delta \Delta s_{i,i+1}}$$

$$\Delta \Delta s = \left[ \frac{\Delta S}{EA} + \epsilon t \right] \Delta s$$

$$\bar{X}_i = X_i + \Delta X_i - k_{i-1,i} \Delta x_{i-1,i} + k_{i,i+1} \Delta x_{i,i+1}$$

$$\bar{Y}_i = Y_i + \Delta Y_i - k_{i-1,i} \Delta y_{i-1,i} + k_{i,i+1} \Delta y_{i,i+1}$$

$$\bar{Z}_i = Z_i + \Delta Z_i - k_{i-1,i} \Delta z_{i-1,i} + k_{i,i+1} \Delta z_{i,i+1}$$

The cable forces used in this formula are initially assumed forces, or those resulting from corrected cable reactions, which consider the previously cal-

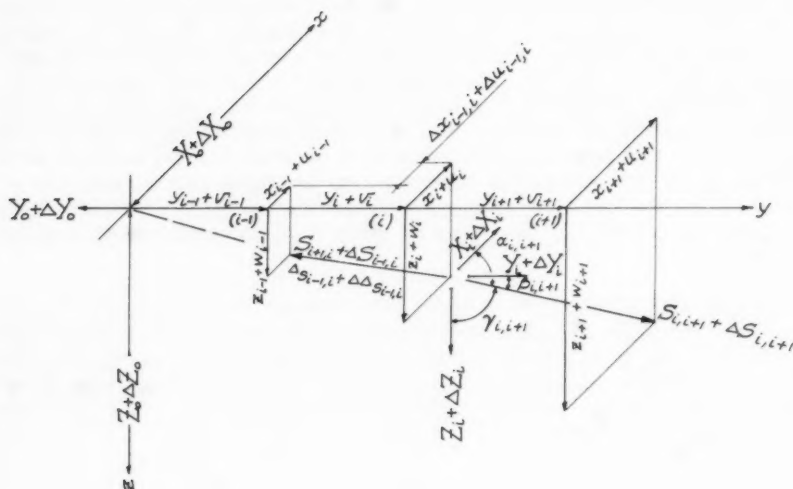
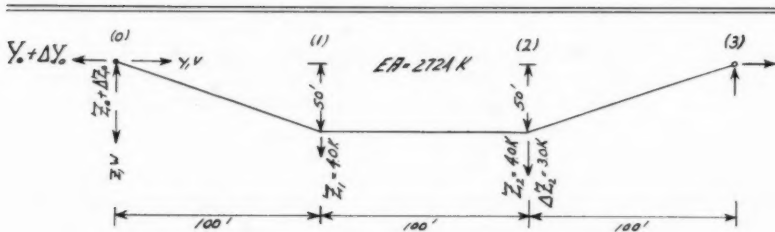


FIG. 5.—EQUILIBRIUM AT LOAD POINT (I)

culated cable deformations. The fast convergence is achieved by linear interpolation of the cable reactions according to

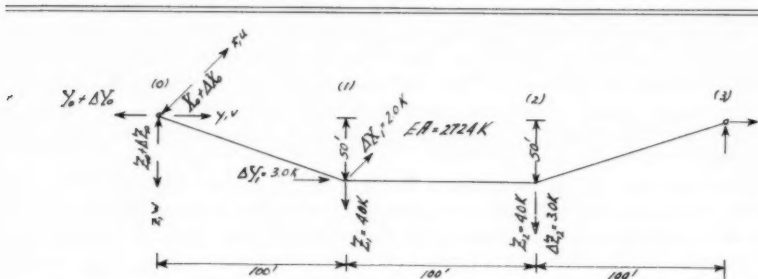
$$N_{r+1} = \frac{(N_{r-1}) \cdot [N_r] - (N_r) \cdot [N_{r-1}]}{(N_{r-1}) + [N_r] - (N_r) - [N_{r-1}]} \dots \dots \dots (13)$$

TABLE 8



r	$(Y_0 + \Delta Y_0)$	$(Z_0 + \Delta Z_0)$	$S_{01} + \Delta S_{01}$	$S_{02} + \Delta S_{02}$	$S_{03} + \Delta S_{03}$	$U_1$	$V_1$	$W_1$	$U_2$	$V_2$	$W_2$	$(X_0 + \Delta X_0)$	$(Z_0 + \Delta Z_0)$
	Kips		Kips			Feet						Kips	
1	10.900	5.000	11.992	10.946	12.442	1.906	-3.953	1.762	4.585	10.918	4.933		
2	11.000	5.000	12.083	11.045	12.530	1.938	-4.284	1.678	4.190	11.004	4.935		
3	11.030	4.933	12.083	11.070	12.589	2.167	-4.363	1.913	4.016	11.029	4.926		
4	11.023	4.926	12.073	11.061	12.586	2.193	-4.337	1.953	4.037	11.023	4.925		
5	11.0216	4.9251	12.072	11.060	12.585	2.193	-4.334	1.954	4.040				

TABLE 9



r	$(Y_0 + \Delta Y_0)$	$(Y_0 + \Delta Y_0)$	$(Z_0 + \Delta Z_0)$	$S_{01} + \Delta S_{01}$	$S_{02} + \Delta S_{02}$	$S_{03} + \Delta S_{03}$	$u_1$	$v_1$	$w_1$	$u_2$	$v_2$	$w_2$	$(X_0 + \Delta X_0)$	$(Y_0 + \Delta Y_0)$	$(Z_0 + \Delta Z_0)$
	Kips			Kips			Feet						Kips		
1	1.333	12.500	5.500	13.721	9.641	10.798	11.685	2.746	-6.387	5.784	2.356	7.553	1.432	12.592	5.345
2	1.432	12.592	5.345	13.754	9.702	11.149	11.632	3.182	-6.659	5.736	2.943	6.982	1.428	12.671	5.332
3	1.429	13.154	5.349	14.260	10.259	11.649	11.777	3.347	-8.238	5.545	2.430	4.604	1.423	13.156	5.316
4	1.436	13.171	5.345	14.276	10.272	11.666	11.163	3.343	-8.288	5.538	2.437	4.531	1.423	13.170	5.315

with

$$N = X_0 + \Delta X_0; Y_0 + \Delta Y_0; Z_0 + \Delta Z_0$$

$[N]$  = initial value of an iteration cycle.

$(N)$  = resulting value of an iteration cycle.

$r$  = number of cycles.

Table 8 shows the values of the iteration for the cable calculated by the authors. The exact values have already been obtained after the fourth cycle of the iteration. Table 9 is the calculation of the same cable under an arbitrary three dimensional loading.

W. E. ADAMS,<sup>18</sup>—The numerical method of determining displacements along a suspended cable resulting from change in load as developed by the authors constitutes an accurate and straightforward type of solution to this problem.

Each logical step by step approach, involving a series of simple calculations, produces a value for one of the well defined physical quantities used in the solution. This method, in common with others, involves a lengthy trial and error procedure, but today some of this disadvantage can be overcome by the use of an electronic digital computer. The fact that this procedure can be easily programmed for a computer adds a great deal to its merit.

One feature which can affect that accuracy of the solution is the method of handling the weight of the cable. In Example 1, the authors have elected to neglect the weight of the cable. This produces an excellent theoretical problem and the results should be accurate to the extent of the given values for the case of a truly weightless cable. Naturally, this could only be done where the cable weight is small in magnitude with respect to the applied loads. However, the writer has never had a case where he felt he could neglect the weight of the cable without distorting the results. In Example 2, the 1,000 ft span has been divided into ten segments for computing cable lengths and weights. This number of segments appears to be well chosen to provide an accurate analysis within the limits of accuracy of the modulus, area, and weight of the cable. Too few segments would introduce inaccuracy into the results and too many segments would needlessly complicate the problem without any practical gain in accuracy.

There are two different types of loading which can be applied to suspended cables, namely, a fixed load and a rolling load. The method developed by the authors comprehends the fixed load type; that is, the load is attached to the cable and undergoes the same displacement as the cable at the point of attachment. This is illustrated in Example 2 where a load placed 400 ft from the left support undergoes a horizontal displacement together with the cable and ends up approximately 397 ft from the left support.

In the case of a rolling load, that is a load which is supported from a movable carriage, it is usually desirable to obtain the vertical deflection of the cable at a given distance from one of the supports, the location to be reckoned after shifting of the cable has taken place. A direct solution to this type of problem does not appear to be readily attainable by the method under study be-

<sup>18</sup> Wire Rope Engr., Amer. Steel and Wire Div., U. S. Steel Corp., New Haven, Conn.

cause the exact location of the point of application of the rolling load before displacement of the cable has occurred is unknown.

JACKSON L. DURKEE,<sup>19</sup> F. ASCE.—This is a valuable paper, containing a new method of solving a problem for which, as the authors state, “. . . no direct solution seems to be available.” The paper is concise and the concepts are readily grasped. In fact, the procedure seems so obvious that many engineers who have struggled with the suspended-cable problem will undoubtedly wonder why they did not think of it first.

As the authors state, the stress and geometric data for the cable in the initial position can be found from statical considerations. However, the changes in stress and geometry caused by changes in loading do not follow from statics alone, and it is this information that is obtained through use of the authors' procedure, which is substantially as follows:

1. The suspended cable carrying the changed loading is cut loose from the right support, and a trial tension force having a specified horizontal component “H” is applied to the free right end of the cable.

2. Under this trial H, the cable has an equilibrium position with the free cable right end falling somewhere on a straight line through the two cable supports. This equilibrium position is found by a rapidly-converging iterative procedure.

3. The horizontal “mismatching” (or “error of closure”) of the free cable right end under the trial H, with respect to the right support, is plotted on a graph.

4. If the first trial H is too large, the equilibrium position of the free cable right end will be to the right of the support, and conversely; so that a second trial value of H, closer than the first, can be selected.

5. The right-end horizontal mismatching corresponding to this second trial value of H is plotted on the graph.

6. Since the “mismatching vs H” curve is nearly linear, a straight line through the two plotted points will indicate a third trial value of H that will be close to the true value, that is, the value that will make the free cable right end coincide with the right support.

7. Thus, the true value of H can be found by iteration. With H known, complete stress and geometric data for the suspended cable in the displaced position follow directly.

This procedure as outlined by the writer is, it should be noted, not precisely the same as that given by the authors, who use a slight variation of the equilibrium concept stated in step 2. The authors use instead the condition that the area of the cable “corresponding simple beam” shear diagram to the left of the cable right support point must equal zero. When this condition is achieved, the cable will not actually be in equilibrium except when the trial H turns out to be the true value of H, that is, when the free cable right end coincides with the support point. This is because the cable will be in equilibrium only when the summation of moments of all forces about some point is zero. Referring to Fig. 6, the authors' procedure sums the moments, about the cable right sup-

---

<sup>19</sup> Asst. Engr., Bethlehem Steel Co., Fabricated Steel Constr., Bethlehem, Pa.



port, of force  $V_A$  and the suspended loads, but omits the moment about this support of left-end force  $N_A$  and of right-end forces  $V_B$  and  $N_B$ . When the cable right end coincides with support-point B, the moment about this point of forces  $N_A$ ,  $V_B$  and  $N_B$  is of course zero, and the authors' cable is then in equilibrium (in accordance with step 2). Prior to this final stage the authors' cable is not in equilibrium, and their corresponding values of  $\xi$  and  $\eta$  are therefore parameters rather than true values.

The authors' procedure is nonetheless convergent and gives the true final value of  $H$ .

$$\Sigma F_H = 0: N_A \cos \alpha = N_B \cos \alpha, N_A = N_B, H_A = H_B = H_w$$

$\Sigma M_B = 0$  shows that  $V_A$  and  $V_B$  of cable are identical to reactions of corresponding simple beam. Taking the portion of cable to left of C as a free body,

$$\Sigma M_C = 0: N_{Ae} \cos \alpha = V_A S_c - W_1 (S_c - S_{w1})$$

or

$$H_w e_c = M_c = \text{moment at point C of corresponding simple beam.}$$

Thus,  $H_w = \frac{M_c}{e_c}$  (exact) -- verifying authors' Eq. 1. However, the writer be-

lieves that an improvement in the physical interpretation of the paper would result from making each trial-H cable position an equilibrium position, in accordance with the 7-step procedure. This change can be made quite simply; it is necessary only to omit correcting the right-end cable-segment horizontal projection  $S_p$  by the right-end  $\xi$ , as called for by the authors. The effect of this change is to move the moment center to the free right end of the cable. When the summation of "corresponding simple beam" shear areas across the cable (that is, from left end to right end) is zero, the cable is in equilibrium and  $\xi$  and  $\eta$  are the true "errors of closure."

The writer has verified the previous reasoning by means of a numerical example, and finds that the correct value of  $H$  is obtained regardless of whether  $\xi$  is added to the right-end  $S_p$  (as done by the authors), or subtracted from  $S_p$ , or not applied at all.

The distinction between "corresponding simple beam" cable shears and true cable shears, as applied in the authors' procedure, is in need of clarification. Under the heading "Computational Procedure" the authors use " $V_p$ " as the symbol for true cable shears, while in the numerical examples they use this same symbol to denote "corresponding simple beam" cable shears. This is technically correct, because for a cable with both support points at the same elevation the "corresponding simple beam" shears are identical with the true shears. However, in order to preclude misunderstandings the writer recommends that the two types of shear be given different symbols, for example " $V_p$ " to represent simple-beam shears and " $\bar{V}_p$ " to denote true shears. The distinction is important, since the authors use " $\bar{V}_p$ " to obtain cable angles  $\psi$ , and " $V_p$ " in obtaining the cable shear-diagram area. With this terminology, lines 10, 20, . . . , 50 in the authors' Table 1 would read " $\bar{V}_p (=V_p)$ ," while lines 19, 29, . . . , 59 would remain " $V_{pSp}$ ." (Similar changes would be needed in Table 4.)



However, in the writer's opinion the best way to handle the distinction between these two types of shear is to use only the simple-beam shears throughout the iteration cycles, and obtain the true shears as a final step at the end of the computations. This can be done simply by changing the authors' Eq. 3 to read

$$\tan \psi = \frac{V_p}{H} + \frac{h}{L} \dots \dots \dots (14)$$

in which  $V_p$  is defined as "corresponding simple beam" cable shear, which for the cable shown in Fig. 6 would be  $V_A$  in segment 1,  $(V_A - W_1)$  in segment 2, and  $V_B$  in segment 3. This equation is identical with the writer's Eq. 16, to be given.

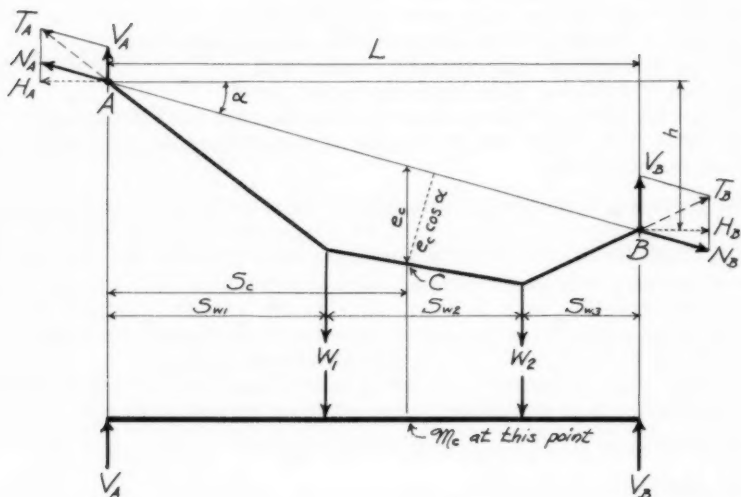


FIG. 6.—WEIGHTLESS CABLE IN EQUILIBRIUM, AND "CORRESPONDING SIMPLE BEAM"

It is perhaps unfortunate that the authors chose special-case cables, having support points at the same elevation, for their numerical examples, rather than the general-case sloping-chord cable as shown in Fig. 1. Had the latter been used, the preceding misunderstandings of terminology could not have arisen.

There are some numerical discrepancies in Example 1, which the writer assumes that the authors have already discovered and will cover in their closing discussion.

Moving on now past these minor criticisms, the writer finds the authors' procedure to have obvious application to the problem of suspension-bridge cable distortions under deck-erection loads. At the time this paper became available, the writer was working with a small single-span suspension bridge.

He therefore programmed the authors' procedure for electronic computation and obtained excellent results, and wishes to endorse the authors' statement that the procedure is "particularly suitable for programming for an electronic digital computer." A brief description of the computer program, along with a flow chart, is presented subsequently.

The program input is as follows:

1.  $N$  = number of suspenders (load-concentration points);
2.  $S_{w1}$  = horizontal distance from left support to first suspender at dead-load condition, feet;
3.  $S_w$  = suspender horizontal spacing (uniform) at deadload, feet;
4.  $L$  = cable span, feet;
5.  $A$  = cable area, square inches;
6.  $E$  = cable modulus of elasticity, kips per square inch;
7.  $Z_A$  = elevation of left cable support, feet;
8.  $Z_B$  = elevation of right cable support, feet;
9.  $Z_{w1}$  = deadload cable-axis elevation at suspender, feet;
10.  $l_{w1}$  = deadload cable-segment length, feet;
11.  $T_{w1}$  = deadload cable-segment tension, feet;
12.  $t$  = temperature change from normal, degrees fahrenheit; and
13.  $(W + P)_i$  = total weight hanging at each suspender point under given erection condition, kips.

The preceding terminology conforms to that used by the authors, wherever possible. Subscripts "i" refer to the  $i$ th suspender or cable segment. Note that the first eleven input items are standard for a given bridge, and that only the last two vary with each problem. Each erection load  $(W + P)_i$  will generally be less than the dead load  $W_i$ , since in the erection condition the "live load"  $P_i$  is an upward load representing absent dead loads (corrected by the weight of any temporary loads such as erection equipment).

The flow chart, illustrating order of calculations and the various "loops," is as follows:

1. Read input  $N, S_{w1}, S_w, L, A, E, Z_A, Z_B, t$
2. Apply  $N$  to loop orders
3.  $h; \tan \alpha = h/L$
4. Read  $Z_{w1}, l_{w1}, T_{w1}$  -- loop  $(N+1)$  times
5. Read  $(W + P)_i$
6. 1st trial  $V_A = \frac{\sum (W + P)_i (L - x_i)}{L}$  (vertical reaction of "corresponding simple beam" at left support)
7. First trial  $H_p : H_{p1} = 2V_A$
8. First trial  $V_{p1} = V_A$  ("simple-beam" shear in first cable segment)
9.  $V_{pi} = V_{pi-1} - (W + P)_{i-1}$  -- loop  $N$  times ("simple-beam" cable shears)
10. Start  $\Delta V$  loop: zero boxes  $\Sigma G_{pi}, \Sigma S_{pi}$  (see steps 17 and 19)

11. Start i loop:  $\tan \psi_1 = \frac{V_{pl}}{H_{pj}} + \tan \alpha$ ;  $\psi_1$ ;  $\sin \psi_1$ ;  $\cos \psi_1$
12.  $T_{pl} = \frac{H_{pj}}{\cos \psi_1}$
13.  $\Delta T_1 = T_{pl} - T_{wl}$
14.  $\Delta l_1 = l_{wl} \left\{ \frac{\Delta T_1}{AE} + \epsilon t \right\}$
15.  $l_{pl} = l_{wl} + \Delta l_1$
16.  $G_{pl} = l_{pl} \sin \psi_1$
17. Contribute to  $\Sigma G_{pl}$
18.  $S_{pl} = l_{pl} \cos \psi_1$
19. Contribute to  $\Sigma S_{pl}$
20. Loop (N+1) times (i loop), starting at step 11 ( $i = 1, 2, \dots, N+1$ )
21. i loop complete: zero  $\Delta M_B$  &  $\Delta V$  boxes (see steps 25 & 27)
22.  $\xi_B = (\Sigma S_{pl}) - L$  ( $\rightarrow = +$ )  
(horizontal displacement of cable right end relative to support)
23.  $\eta_B = (\Sigma G_{pl}) - h$  ( $\downarrow = +$ )  
(vertical displacement of cable right end relative to support)
24.  $\Delta M_1 = V_{pl} \times S_{pl}$  ("simple-beam" shear area)
25.  $\Delta M_B = \Sigma \Delta M_1$  (unbalanced moment about free right end of cable)
26. Loop (N+1) times, starting at step 24
27.  $\Delta V = \frac{-\Delta M_B}{L}$  (shear correction)
28.  $|\Delta V| < .001k$ ? Yes: go to step 31 -- No: go to step 29
29.  $|\Delta V| \geq .001k$ :  $V_{pl}$  revised =  $V_{pl}$  prev +  $\Delta V$  -- loop (N+1) times
30. Go to step 10 ( $\Delta V$  loop, no change in  $H_p$ )
31.  $|\Delta V| < .001k$  ( $\Delta V$  loop complete):  
First time (i.e.  $j = 1$ ): go to step 32  
Subsequent times ( $j = 2, 3, \dots$ ): go to step 35
32.  $j = 1$ : set aside  $H_{pl}$ ,  $\xi_{B1}$ ,  $\eta_{B1}$  in "j-1 boxes"

33. Assume  $H_{p2} = .9 H_{p1}$
34. Go to step 10 (to repeat  $\Delta V$  loop, giving  $\xi_{B2}, \eta_{B2}$  for  $H_{p2}$ )
35.  $j = 2, 3, \dots$ : Set aside  $H_{pj}, \xi_{Bj}, \eta_{Bj}$  in "j boxes"
36.  $\Delta H_j = H_{pj-1} - H_{pj}$
37.  $\Delta \xi_j = \xi_{Bj-1} - \xi_{Bj}$
38.  $\cot \phi_j = \frac{\Delta H_j}{\Delta \xi_j}$
39.  $\delta H_j = \xi_{Bj} \cot \phi_j$
40.  $|\delta H_j| < .01k$ ? Yes: go to step 44 -- No: go to step 41
41.  $|\delta H_j| > .01k$ : revised  $H_p = H_{pj} - \delta H_j$
42. Move  $H_{pj}, \xi_{Bj}, \eta_{Bj}$  into "j-1 boxes"
43. Go to step 10 (to repeat  $\Delta V$  loop, giving  $\xi_{Bj}, \eta_{Bj}$  for revised  $H_p$ )
44.  $\delta H_j < .01k$  ( $\therefore H_p$  now correct value):  $L_p = \sum l_{pi}$  (cable length)
45.  $\bar{V}_{pi} = V_{pi} + H_p \tan \alpha$  -- loop (N+1) times (true cable shears)
46.  $Z_{pi}, \Delta \psi_i, \xi_i, \eta_i$  -- loop N times
47. Punch  $t$  = temp change from normal, F
48. Punch final  $H_p$  = horizontal component of cable tension, kips
49. Punch final  $\xi_B$  = horizontal "error of closure" at right support, ft
50. Punch final  $\eta_B$  = vertical "error of closure" at right support, ft
51. Punch final  $L_p$  = cable length, ft
52. Punch final  $Z_{pi}$  = cable-axis elevation at suspender, ft
53. Punch final  $S_{pi}$  = suspender horizontal spacing, ft
54. Punch final  $l_{pi}$  = cable-segment length, ft
55. Punch final  $\psi_i$  = angle of cable segment with horizontal, deg
56. Punch final  $\Delta \psi_i$  = angle of cable "break" at suspender, deg
57. Punch final  $T_{pi}$  = cable-segment tension, kips

58. Punch final  $\bar{V}_{pi}$  = cable-segment true shear, kips
59. Punch final  $\xi_1$  = horizontal displacement of suspender point, ft
60. Punch final  $\eta_1$  = vertical displacement of suspender point, ft
61. STOP

The program output is indicated by the punch instruction of the flow chart. All output data apply, of course, to the bridge cable in the "liveload" (that is displaced) condition, and give a complete geometric and stress picture of the cable in the particular erection condition.

Some features of the flow chart which may need some comment are as follows:

1. (Step 7) The first-trial value of  $H_p$  is always assumed as  $2V_A$ . This will be a reasonable initial value for any practical case of cable loading.

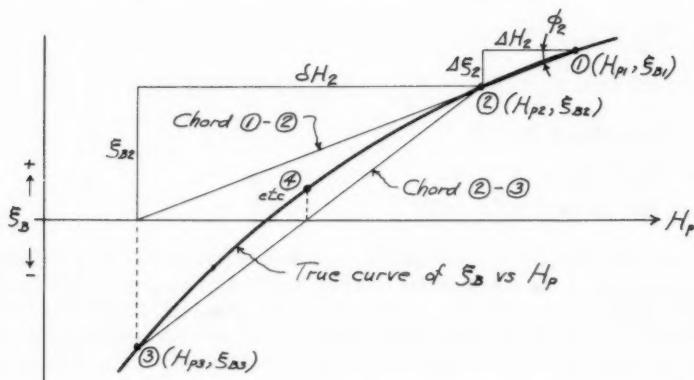


FIG. 7.—ITERATION FOR  $H_p$  (REFER TO FLOW CHART, STEPS 31-43)

2. (Steps 9 & 11) "Corresponding simple beam" shears  $V_{pi}$  are used in the iteration cycles, and true cable shears are computed afterward (step 45), as previously examined. From inspection of Figs. 1 and 6 it can be seen that

$$\tan \psi_1 = \frac{V_A + H_p \tan \alpha}{H_p} = \frac{V_A}{H_p} + \tan \alpha \dots \dots \dots (15)$$

or, in general,

$$\tan \psi_1 = \frac{V_{pi}}{H_p} + \tan \alpha \dots \dots \dots (16)$$

3. (Step 22)  $\xi_B$  is taken as positive to the right (in the direction of positive X) rather than positive to the left as shown by the authors.

4. (Steps 24 & 25) The correction used by the authors, that is, the addition of  $\xi_B$  to  $S_p$  for the last cable segment, is omitted for reasons given previously.

5. (Steps 31-43) The program "plots" point  $(H_{pj}, \xi_{Bj})$  and used a chord through this point and the previous point  $(H_{pj-1}, \xi_{Bj-1})$  to locate the next trial value of  $H_p$ , as shown in Fig. 7. For Fig. 7:

1. Take  $H_{p1} = 2V_A$ ; plot point ①
2. Take  $H_{p2} = .9 H_{p1}$ ; plot point ②
3. Draw chord ① - ②
4.  $\Delta H_2 = H_{p1} - H_{p2}$
5.  $\Delta \xi_2 = \xi_{B1} - \xi_{B2}$
6.  $\cot \phi_2 = \Delta H_2 / \Delta \xi_2$
7.  $\delta H_2 = \xi_{B2} \cot \phi_2$
8. Next trial  $H_p : H_{p3} = H_{p2} - \delta H_2$ ; plot point ③
9. Draw chord ② - ③
10.  $\Delta H_3 = H_{p2} - H_{p3} \dots$   
etc. until  $|\delta H_j| < .01k$

$\xi$  must be used for this plot rather than  $\eta$ , because the values of  $\eta$  will be small in consequence of the equilibrium concept applied in step 25. This is because the free cable right end will come to rest on a straight line through points A and B (Fig. 6), as mentioned previously. If the left and right cable supports are at the same elevation, values of  $\eta$  will be practically zero. For the general case,  $\eta \doteq \xi \tan \alpha$ .

6. (Step 45) Multiplying Eq. 16 by  $H_p$ ,

$$H_p \tan \psi_i = V_{pi} + H_p \tan \alpha = \bar{V}_{pi} \dots \dots \dots (17)$$

which is the true shear in the cable segment.

This procedure could readily be extended to cover the deck-erection problem of a three-span suspension bridge with flexible towers. The tower flexibility equations could be solved in conjunction with the three cable-span solutions to give a compatible solution for the structure as a whole. (Tower-saddle geometry would have to be considered.) The sequence of steps might be as follows:

1. Assume towers deflected shoreward by some amount (for example 0.3 ft), and find mainspan-cable  $H$  using the preceding procedure.
2. Calculate net horizontal force  $Q$  required to hold each tower top in the assumed position.
3. Apply these values of  $Q$  to mainspan  $H$  to obtain a trial value of  $H$  for each side span.

4. Calculate horizontal "error of closure" of lower end of cable in each side span, consistent with sidespan loads and assumed  $H$ .

5. Use these errors of closure to revise assumed tower positions. Iterate until errors of closure approximate zero.

Extension of this procedure to cover the five-span suspension bridge (four flexible towers, straight backstays) would follow these same lines. Such programs would make unnecessary the construction of suspension-bridge models to solve cable problems associated with suspended-deck erection. It is obvious, too, that such programs would perform mathematical analyses that would be thoroughly impractical without the computer.

In conclusion, the writer wishes to commend the authors for presenting a procedure which should prove to be a notable contribution to engineering science. The authors' method, particularly when coupled with the electronic computer, should enable engineers to make significant advances in the field of cable computation.





STRUCTURAL MODEL ANALYSIS BY MEANS OF MOIRE FRINGES<sup>a</sup>

---

Closure by A. J. Durelli and I. M. Daniel

---

A. J. DURELLI<sup>14</sup> and I. M. DANIEL,<sup>15</sup> A. M. ASCE.—The writers are pleased to see that the discussers share their interest in the application of moire fringes to structural model analysis. They were especially impressed with the discussers' results and they regret the fact that the discussers' previous work on the subject had not come to their attention.

The possibility of obtaining a practically instantaneous record of deflections from a model of a linear viscoelastic material is important only when the model is subjected to defined external loads. In the determination of influence lines, however, where given displacements or rotations are introduced in parts of the model, creep does not influence the results. There is only stress relaxation, which does not affect deflections. For this reason it is not absolutely necessary to analyze the fringe patterns from photographic records. It is possible, as was done by the writers, to measure the location of the fringes directly on the model by means of a ruler.

It should be stressed that the use of special deformeters similar to that of Beggs is not necessary. Relatively large displacements can be applied by means of pins and holes drilled on the base board. Errors introduced by large deformations are cancelled out by applying equal and opposite displacements and averaging the results, as was shown by Massonet.<sup>4</sup> The applied displacements or rotations can be easily measured by counting moire fringes. For example, the fringe pattern of the horizontal strip at point B in the model of Fig. 8 gives the rotation of joint B due to the applied vertical displacement.

As far as structural analysis by means of moire fringes is concerned, high density of grid lines is not always desirable. Grids of 50 to 300 lines per in. are usually satisfactory. Finer grids, such as 1,000 lines per in., have been used by the writers in strain analysis problems only.

---

<sup>a</sup> December 1960, by A. J. Durelli and I. M. Daniel (Proc. Paper 2693).

<sup>14</sup> Prof. of Civ. Engrg., Catholic Univ. of America, Washington, D. C.

<sup>15</sup> Armour Research Foundation of Illinois Inst. of Tech., Chicago, Ill.

1. The first part of the paper is devoted to a discussion of the

# STATIC AND DYNAMIC ANALYSIS OF GUY CABLES<sup>a</sup>

Discussion by A. H. Brownfield and John H. Wells

A. H. BROWNFIELD, 12 F. ASCE.—The purpose of this discussion is to emphasize some useful formulas applying to the common catenary rather than present the author's paper in detail.

The material was assembled by the writer and others between 1931 and 1935 and was used for adjusting the strands of the San Francisco-Oakland Bay Bridge, and earlier for correcting some steep slope measurements for a base line on Yerba Buena Island. At that time all of the computations were done on ten bank electric computers and the memory drums were pads of paper and our heads. The formulas presented can be used for computing the H component of several guy cables meeting at a point. The writer would solve the author's problem by plotting three or more computed points for each guy cable on a graph. The intersection should give a close value of H for each guy. All problems involving cables or wires are somewhat indeterminate because they must be referenced back to a no stress length of strand  $L_n$  and also at some given or standard temperature. Trial and error solutions can be made quite rapidly after a computing procedure is established. All catenaries having the same  $h_0$  ( $H = w h_0$ ) are related and may be considered as part of the same curve.

The term " $h_0$ " is the ordinate at the low point X=0, y=0 and also the radius of curvature at this point. The equations can usually be simplified by referring to the mid-span point  $\frac{1}{2}$  of any portion of the curve under study such as Fig. 1. Many of the functions are related by the pathogoranian relation, namely

$$h_0^2 = y^2 - L_0^2 \dots\dots\dots (67)$$

This gives the arc length back to the origin. The intrinsic quation of the catenary is

$$L_0 = h_0 \tan \gamma_0 \dots\dots\dots (68)$$

The vertical sag at mid-span is always given by

$$f = \frac{1}{2} \tanh \frac{1}{4h_0} \dots\dots\dots (69)$$

<sup>a</sup> January 1961, by Donald L. Dean, (Proc. Paper 2703).

<sup>12</sup> Supvr., Structural Engr., Div. of Architecture, State of California, Sacramento, Calif.

The general equation of a catenary is attributed to M. Fujioka of Tokyo, 1915

$$\frac{L^2 - h^2}{l^2} = \frac{2 \cosh u - 1}{u^2} \dots\dots\dots (70)$$

in which

$$u = \frac{l}{h_0} \dots\dots\dots (71)$$

let

$$z = \left( \frac{L^2 - h^2}{l^2} - 1 \right) \dots\dots\dots (72)$$

then

$$u = \sqrt{12z = \frac{24}{5}z^2 + \frac{492}{175}z^3 - \frac{336}{175}z^4 + \frac{480372}{336875}z^5 - 1.116815z^6} \dots\dots\dots (73)$$

Most of the equations given here are exact. Cross checking time can frequently be saved through their use. A short seven place table of  $\frac{2 \cosh u - 1}{u^2}$

was assembled by the writer for work on the San Francisco-Oakland Bay Bridge strands. Values of  $u$  could be taken from this table by using Newton's or Sterling's formula for interpolation. With modern electronic computers a more extensive table could be readily assembled for future projects.

The area between a portion of a catenary and the X axis is given by

$$A_r = h_0 L \dots\dots\dots (74)$$

the average ordinate by

$$Y_a = \frac{h_0 L}{l} \dots\dots\dots (75)$$

and

$$T_a = \frac{w h_0 L}{l} \text{ (nearly)} \dots\dots\dots (76)$$

From this

$$\delta = \frac{w L L_n}{U A E} \dots\dots\dots (77)$$

$\delta$  is the stretch or elongation and

$$L_n = L - \delta \dots\dots\dots (78)$$

The value of  $L$  and  $u$  must be obtained by trial as mentioned earlier.

The writer has used the terms  $X_3$   $Y_3$   $L_3$  and  $\gamma_3$  to define the mid-span point of catenary. Let

$$q = \sqrt{\frac{L+h}{L-h}} \dots\dots\dots (79)$$

for any portion under consideration such as the author's Fig. 1. Then

$$L_3 = h_0 \frac{q^2 - 1}{q} = \frac{h}{2 \sinh \frac{u}{2}} \dots\dots\dots (80)$$

$$\frac{h}{L} = \frac{L_3}{Y_3} \dots\dots\dots (81)$$

$$\tan \gamma_3 = \frac{h}{l} = 2 \frac{L_3}{l} \sinh \frac{u}{2} \dots\dots\dots (82)$$

$$X_3 = h_0 \log_e q \dots\dots\dots (83)$$

$$Y_1 - \frac{h}{2} = Y_3 + f = Y_3 \cosh \frac{u}{2} \dots\dots\dots (84)$$

$$\sin \gamma_3 = \frac{L_3}{Y_3} = \frac{h}{L} \quad \tan \gamma_3 = \sqrt{\frac{h^2}{L^2 - h^2}} \dots\dots\dots (85)$$

and

$$L = 2 Y_3 \sinh \frac{u}{2} \dots\dots\dots (86)$$

At the middle point of the arc

$$L_m = \frac{h}{2 \tanh \frac{u}{2}} \dots\dots\dots (87)$$

The X ordinate of the center of mass of the arc is indicated by the intersection of the terminal tangents and moments about any point on a cable must equal zero. It follows that a suspended weight P equals wL, that is the tangents at a load and the load vector form a closed force triangle.

The foregoing are a few of the several hundred equations that can be written involving any portion of a catenary. They should indicate the steps that can be taken to solve most any problem of a suspended chain or strand of uniform weight and having a constant E. There may be some confusion in  $h_0$  and  $h$  but this is caused by using the author's notation. These conflicts were avoided in the San Francisco-Oakland Bay Bridge charts in which S was used for arc length,  $\phi$  for  $\gamma$  and  $k$  for the author's  $h$ .

---

#### READING REFERENCES

---

1. Transactions of American Inst. of Elect. Engrs., Vol. No. 30, (1911).
2. Smithsonian Mathematical Table Hyperbolic Functions.

3. Mathematical Handbook, by Seaver.
4. Bulletins Nos. 13 & 66, Univ. of Washington, Engrg. Experiment Sta.
5. Civil Engineering by Rankine.
6. Sag Calculations by use of Martins Tables.
7. Vectorial Mechanics, by Louis Brand.
8. Mechanical Engineers Handbook, by Lionel S. Marks.
9. Technical Mechanics, by Maurer.
10. Modern Framed Structures, by Johnson Bryan and Turneaure, Vol. II.
11. Solving the Catenary on the Slide Rule, by Bardsley, Sc.D.

JOHN H. WELLS,<sup>13</sup> F. ASCE.—The author's equations for static analysis of guy cables resemble those presented by D. O. Ehrenburg,<sup>14</sup> in that both use the catenary equations developed into approximate formulas in terms of the parameter  $r$ . However, the Ehrenburg semigraphical method for applying the formulas to numerical problems is somewhat more systematic than the all-numerical method demonstrated by the author.

With  $l$ ,  $h$ , and  $q$  established by the conditions of the problem, the catenary and all its properties are determined if  $(L - \bar{L})$  is prescribed.  $(L - \bar{L})$  is the amount by which the arc exceeds the chord, and is called "slack" and

$$L - \bar{L} = \frac{1}{L} f(r) \dots \dots \dots (88)$$

in which

$$f(r) = \frac{1}{6} \left( r^2 + \frac{r^4}{20} \right) \dots \dots \dots (89)$$

Also, from Eq. 11,  $T_1 = \frac{q}{2} (L \coth r + h)$ , and from Eq. 10,  $T_0 = \frac{q}{2} (L \coth r - h)$ ; so that the average tension,  $T$ , is

$$T = \frac{q}{2} L \coth r \dots \dots \dots (90)$$

Values of  $f(r)$  and  $\coth r$  are given in Table 3.

Because the range of values of  $r$  encountered in practical problems is small, it is easy to calculate values of tension and slack for several assumed values of the parameter  $r$ , and to plot a chart for each of the cable loadings to be considered, using slack as the independent variable. See Tables 1 and 2 for calculation, and Fig. 9 for chart based on the author's numerical examples 1 and 2.

The quantity  $(A_c E_c / L)^*$  is the spring constant of the cable in kips per linear foot, in which the force and deflection are measured along the chord of the guy.

If the terminal points of the guy remain fixed in position, the slack will be changed only by; (a) change in loading, or (b) thermal growth of the cable.

<sup>13</sup> Asst. Head, Structural Div., Jackson & Moreland, Inc., Boston.

<sup>14</sup> "Transmission Line Catenary Calculations," by D. O. Ehrenburg, Transactions AIEE, 1935, p. 719.

If (a) the temperature remains constant and the load  $q$  changes, the average tension in the cable is related to the slack by Hook's law, thus, change in average tension = (change in slack)  $\times A_c E_c / L_u$ , in which  $L_u$  is the unstressed length of the cable. In the author's numerical problems  $L_u = 1649.53$  ft, and  $A_c E_c / L_u = 35,210$  lb per ft. Thus, referring to Fig. 9, if the tension in the cable is 60 kips for  $q = 10.55$  plf., the tension at the same temperature for  $q = 9$  lb per linear foot can be found by drawing line (a) at a slope of 35.21

TABLE 1<sup>a</sup>

$r$	$L - \bar{L}$	H, in kips	T (av.), in kips	$(A_c E_c / L)^*$
0.105	1.006	40.71	70.96	17.56
0.110	1.104	38.86	67.75	16.32
0.115	1.207	37.17	64.83	15.16
0.120	1.314	35.62	62.16	14.06
0.125	1.425	34.20	59.69	13.04
0.130	1.542	32.89	57.42	12.09
0.135	1.663	31.67	55.32	11.20
0.140	1.789	30.54	53.37	10.37
0.145	1.919	29.48	51.55	9.62
0.150	2.053	28.50	49.86	8.92

<sup>a</sup> for  $q = 9.0$  lb per linear foot.

TABLE 2<sup>a</sup>

$r$	$L - \bar{L}$	H, in kips	T (av.), in kips	$(A_c E_c / L)^*$
0.105	1.006	47.73	83.17	18.95
0.110	1.104	45.56	79.42	17.72
0.115	1.207	43.58	75.99	16.54
0.120	1.314	41.76	72.85	15.43
0.125	1.425	40.09	69.97	14.37
0.130	1.542	38.55	67.32	13.37
0.135	1.663	37.12	64.85	12.45
0.140	1.789	35.80	62.57	11.58
0.145	1.919	34.56	60.43	10.77
0.150	2.053	33.41	58.44	10.02

<sup>a</sup> for  $q = 10.55$  lb per linear foot.

kips per ft, and reading  $T = 53.7$  kips at the intersection of (a) with the  $T$  curve for  $q = 9$ .

Case (b), change in length of guy cable due to thermal action at constant loading with terminals remaining fixed in position can be treated by imagining first that the change in slack occurs at constant tension. This will require the imposition of a temporary imaginary load, plus for temperature rise, minus for temperature drop. The second operation is to remove this imaginary load, following the graphical construction described in the preceding paragraph. For example, if the cable of the preceding paragraph experiences a temperature

drop such that the unstressed cable length is reduced by 0.2 ft the new slack and tension can be found by drawing lines (b) and (c), and reading slack = 1.628 ft and  $T = 55.9$  kips.

A change in the guy chord length,  $\bar{L}$ , at constant temperature, due to a small movement of the guy terminals, is equivalent to an equal and opposite thermal

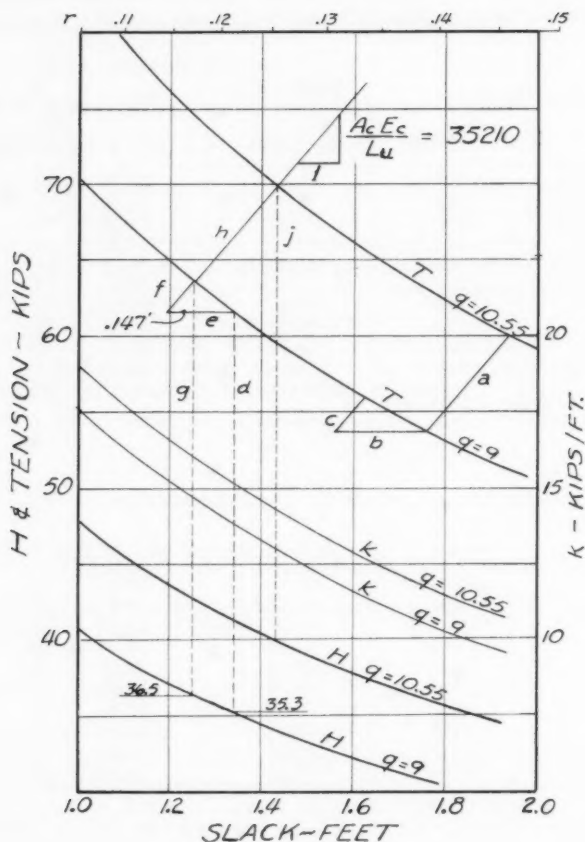


FIG. 9

change of cable length with guy terminals fixed. Starting from a known slack and tension, a new slack and tension associated with a change in  $\bar{L}$  can be found by the same graphical construction as that used for thermal action. Thus, if the direction cosines of the guy of the preceding paragraph referred to some system of orthogonal coordinates  $xyz$  are  $l$ ,  $m$  and  $n$ , and the movements of the upper guy terminal are  $u$ ,  $v$ , and  $w$ , than any set of movements for which



$$\Delta \bar{L} = lu + mv + nw = 0.2$$

can be represented by the construction of lines (b) and (c) of Fig. 9.

A solution of the author's Problem 1 with tower shortening neglected is shown at the left side of Fig. 9. A temperature drop of 40°F affecting the tower and cable but not the ground is equivalent to a 40°F temperature rise affecting the ground (with an assumed coefficient of expansion equal to that for steel) but not the cable or tower.

$$\Delta l = 40 \times 6.7 \times 10^{-6} \times 950 = 0.2546 \text{ ft}$$

and

$$\Delta \bar{L} = 0.2546 \times 950/1649.94 = 0.147 \text{ ft}$$

Enter the chart with  $H_0 = 35.3$  kips for  $q = 9$ , draw lines d, e, f, and g, and find the new  $H = 36.5$  kips. The direction in which line e (= 0.147 ft) should be drawn is obvious from the consideration that the conditions of the problem imply a tightening of the cable.

The approximate influence of tower shortening in Problem 1 can be obtained by noting that the change in cable tension is 2,100 lb, and the corresponding change in force in the tower leg is  $2,100 \times 1349/1650 = 1,720$  lb per cable. The change in length of the tower leg associated with the change of force in two cables is

$$\begin{aligned} \Delta h &= 2 \times 1720 \times 1349/26.4 \times 30 \times 10^6 \\ &= 0.00586 \text{ ft} \end{aligned}$$

whence

$$\Delta \bar{L} = 0.00586 \times 1349/1650 = 0.0048 \text{ ft}$$

This is too small to plot to the scale of Fig. 9, but its influence may be obtained by proportion thus

$$\Delta H = 1.2 \times 0.0048/0.147 = 0.039 \text{ kips}$$

A solution of Problem 2 is represented in Fig. 9 by lines (h) and (j).

The semigraphical method which has been previously outlined is capable of considerable precision if the charts are drawn to reasonably large scale. It is frequently possible to plot up a problem or group of problems to a small scale and then to amplify the portions of the chart in the vicinities of the significant intersections. Such a chart is also useful in supplementing calculations made along the lines demonstrated in the paper.

As the author suggests in his Introduction the static analysis of guyed towers could be greatly simplified if the guys could be treated as straight two-force members. A method for doing this over a small range of tower deflection is to calculate the effective spring constant  $(A_c E_c / L)^*$  for each guy and then to treat the guy-and-tower system as a beam-column on spring supports, using a matrix formulation of the method of Southwell.<sup>15</sup>

Referring to Fig. 9, lines b and c, it will be seen that the actual change in slack corresponding to a change in tension is less than the change in chord

<sup>15</sup> "Relaxation Methods in Engineering Science," by R. V. Southwell.

TABLE 3.—FUNCTIONS OF  $r$ 

$r$	$f(r)$	$\text{Coth } r$	$g(r)$
0.010	0.00001667	100.003	0.0000003
0.015	0.00003750	90.913	0.0000011
0.020	0.00006667	50.007	0.0000027
0.025	0.00010417	40.008	0.0000052
0.030	0.00015001	33.343	0.0000090
0.035	0.00020418	28.583	0.0000143
0.040	0.00026669	25.013	0.0000213
0.045	0.00033753	22.237	0.0000304
0.050	0.00041672	20.017	0.0000417
0.055	0.00050424	18.200	0.0000555
0.060	0.00060011	16.687	0.0000711
0.065	0.0007043	15.406	0.0000917
0.070	0.0008169	14.309	0.0001146
0.075	0.0009378	13.358	0.0001410
0.080	0.001067	12.527	0.0001711
0.085	0.001205	11.793	0.0002053
0.090	0.001351	11.141	0.0002439
0.095	0.001505	10.558	0.0002869
0.100	0.001668	10.033	0.0003348
0.105	0.001839	9.5588	0.0003877
0.110	0.002018	9.1275	0.0004460
0.115	0.002206	8.7339	0.0005099
0.120	0.002402	8.3733	0.0005796
0.125	0.002606	8.0416	0.0006555
0.130	0.002819	7.7356	0.0007377
0.135	0.003040	7.4523	0.0008266
0.140	0.003270	7.1895	0.0009225
0.145	0.003508	6.9448	0.0010255
0.150	0.003754	6.7166	0.0011360
0.155	0.004009	6.5032	0.0012543
0.160	0.004272	6.3032	0.0013805
0.165	0.004544	6.1155	0.0015151
0.170	0.004824	5.9389	0.0016540
0.175	0.005112	5.7725	0.0018103
0.180	0.005409	5.6154	0.0019715
0.185	0.005714	5.4669	0.0021420
0.190	0.006028	5.3263	0.0023223
0.195	0.006350	5.1931	0.0025126
0.200	0.006680	5.0665	0.0027132

length which causes the changes in slack and tension. In the example the change in chord length is 0.2 ft, the change in slack is 0.137 ft, and the change in tension is 2,200 lb. The effective spring constant of the guy over this interval is

$$(A_c E_c / L)^* = 2200 / 0.2 = 11000 \text{ lb per ft}$$

In the triangle formed by lines  $b$ ,  $c$ , and the chord of the T curve

$$b = (L / A_c E_c) \Delta \text{ Tension} - \Delta \text{ Slack} = (L / A_c E_c)^* \times \Delta \text{ Tension}$$

or,

$$0.2 = 2200 / 35210 + 0.137 = 2200 / 11000 \dots \dots \dots (91)$$

(Note that  $\Delta$  Slack on the chart of this problem is negative.)

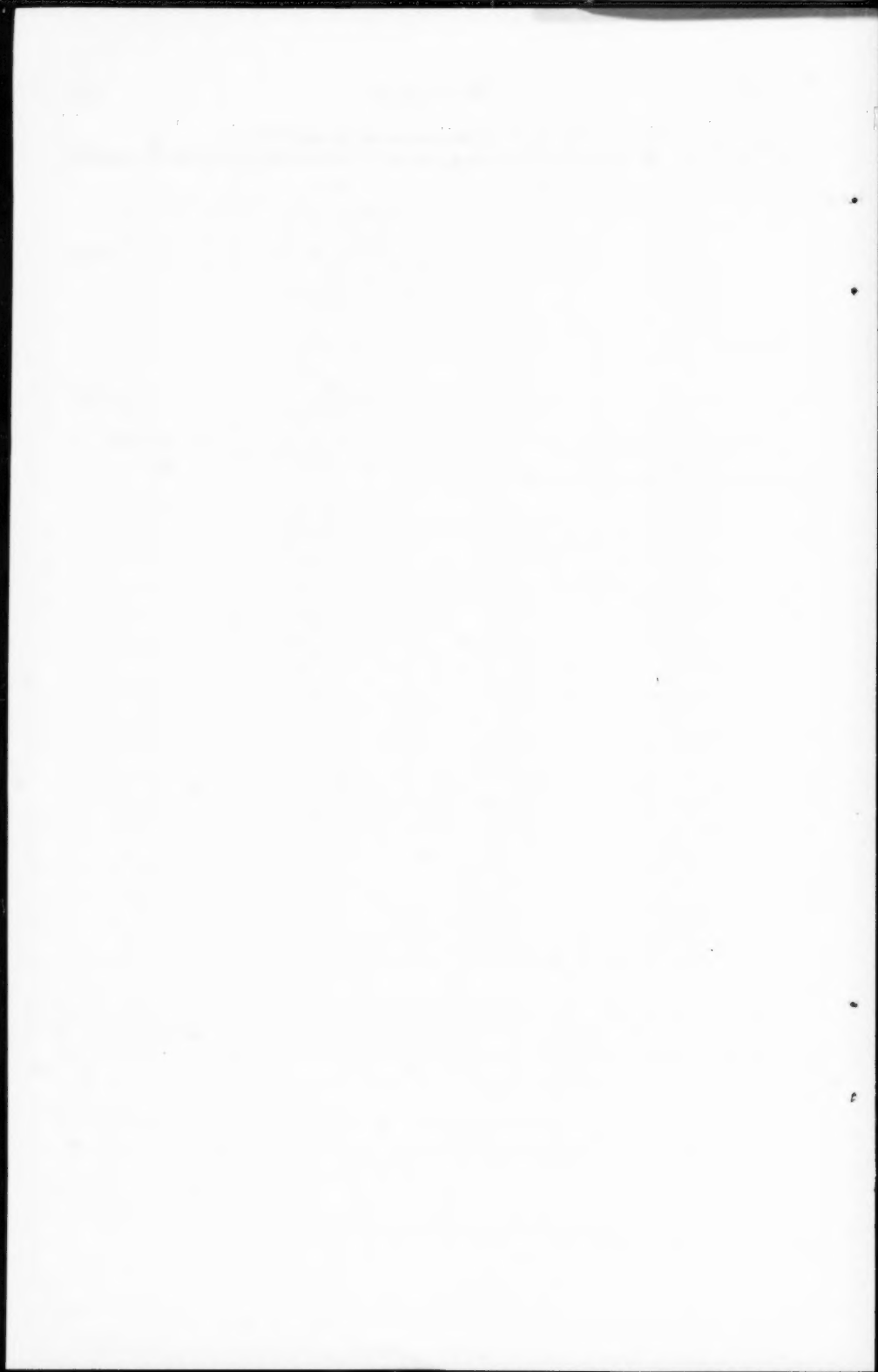
From Eq. 91, by taking derivatives of the approximate formulas for slack and tension

$$\left(\frac{A_c E_c}{L}\right)^* = \frac{\frac{A_c E_c}{L}}{1 + \frac{A_c E_c}{L} \frac{2}{q} \frac{1}{L^2} g(r)} \dots\dots\dots (92)$$

in which

$$g(r) = \left(\frac{r}{3} + \frac{r^3}{30}\right) \text{Sinh}^2 r \dots\dots\dots (93)$$

Values of  $g(r)$  are given in Table 3, and  $k = (A_c E_c / L)^*$  for the author's cables are plotted in Fig. 9.



ANALYSIS OF STRUCTURES BY COMBINING REDUNDANTS<sup>a</sup>

---

Discussion by B. J. Hartz and Phillip L. Gould

---

B. J. HARTZ,<sup>13</sup> M. ASCE.—The interesting procedure presented by the authors for the solution of simultaneous equations reopens for discussion the use of orthogonalizing and related methods for the solution of indeterminate structures. This procedure came to the writer's attention with the publication of a paper,<sup>14</sup> in which this procedure was first presented, with applications to a number of statically indeterminate problems.

Since publication of the paper by Morrison, the writer has used the suggested procedure on a number of occasions. It is appropriate here to study some of the conclusions reached on the basis of this experience. First, it should be noted that the transformation to group redundants proposed by Morrison and the authors is not orthogonal in the sense that the group redundants obtained are not orthogonal, but instead the transformation is one of diagonal congruence. That is, the change of variables is such as to diagonalize the set of simultaneous equations but does not have the additional property that the transpose of the transformation matrix is equal to the inverse. Once this is realized it is possible to use any one of a number of computational procedures for obtaining this congruent transformation, of which the transformation proposed by Morrison and the authors is but one. In addition it becomes a simple matter to extend the analysis to include orthogonal transformations (a special case of diagonal congruence) as well. Orthogonal transformations were applied to structural analysis problems by Wilbur,<sup>15</sup> and others.<sup>9,10</sup>

The writer has found that it may be desirable to use one of the transformations presented previously even when computers may be available for matrix inversion or solution of the simultaneous equations, if the original choice of redundants is such as to yield a "poorly-conditioned" set of simultaneous equations; that is, if the initial redundants are such that some of the equations are almost linearly dependent.

The writer has also found that for a large system of equations in which it may be difficult, or not feasible at all, to solve the set of equations obtained from the analysis, the previous formulation may be used to develop an approximate procedure which is analogous to the Rayleigh-Ritz procedure for continuous structures. This procedure has the advantage that a good approximation to the true solution may sometimes be obtained with only a small order approximation, particularly when an approximate solution is available such as may be

---

<sup>a</sup> January 1961, by Peter P. Gillis and Kurt H. Gerstle (Proc. Paper 2712).

<sup>13</sup> Assoc. Prof. of Civ. Engrg., Univ. of Washington, Seattle, Wash.

<sup>14</sup> "Group Loadings Applied to the Analysis of Frames," by I. F. Morrison, *Transactions*, ASCE, Vol. 119, p. 338, 1954.

<sup>15</sup> "Characteristics Redundants used for Analyzing Statically Indeterminate Structures," by John B. Wilbur, *Proceedings*, ASCE, Vol. 70, No. 6, 1944.

obtained by the portal method or the cantilever method for the analysis of multi-story frames. In this case the solution is in the form of corrections to the approximate solution. Unfortunately, the writer does not have all of the computations completed for a presentation of this procedure and so this must be reserved for a later paper.

Finally, it should be stated that all of the previous discussion and procedures apply equally well to deformation methods of analysis. It is only necessary to interchange forces and displacements, equilibrium and compatibility, etc., as indicated by R. W. Clough,<sup>16</sup> F. ASCE.

The mathematical formulation of the transformations previously studied are presented below in more concise matrix form to illustrate the ideas presented. The notation used is the same as used by Clough and others<sup>15</sup> and is becoming somewhat standard.

The basic equations corresponding to the formulation of Morrison or the authors, except for a change in sign convention, are

$$-D_0 = D X \dots\dots\dots (40)$$

in which

$$D_0 = b_1' f b_0 \dots\dots\dots (41)$$

and

$$D = b_1' f b_1 \dots\dots\dots (42)$$

Making a linear transformation to a "generalized" set of redundants according to the equations (with an obvious change in notation)

$$X = h Y \dots\dots\dots (43)$$

yields, after pre-multiplying both sides by  $h'$  to obtain the virtual work equations,

$$-D_0^* = D^* Y \dots\dots\dots (44)$$

in which

$$D_0^* = h' D_0 \dots\dots\dots (45)$$

and

$$D^* = h' D h \dots\dots\dots (46)$$

These equations may be obtained from Eqs. 41 and 42 because  $b_1^* = b_1 h$  is the set of stresses due to unit values of the  $Y$  redundants. Morrison defines a new matrix (Eq. 6(b))

$$B = D h \dots\dots\dots (47)$$

which has the physical significance of being the displacement of the  $X$  redundants due to unit values of the  $Y$  redundants and are the quantities in Morrison's Eq. 9(b) and the authors' Eq. 11(b). Using this definition, Eq. 46 becomes

<sup>16</sup> "Use of Modern Computers in Structural Analysis," by R. W. Clough, Proceedings, ASCE, Vol. 84, No. ST 3, May 1958, p. 1636.

$$D^* = h' B \dots\dots\dots (48)$$

which is Morrison's Eq. 8. The procedure proposed by Morrison and subsequently by the authors is to find  $h'$  by requiring each of the off-diagonal terms of  $D^*$  from Eq. 48 to be zero; that is,  $h'$  to be orthogonal to  $B$  with the choice of unity for each of the diagonal elements of  $h$ . This yields a set of simultaneous equations in triangular form for  $h$ . The general solution of this set is indicated by Morrison's Eq. 11 or the authors' Eq. 14.

A more commonly used procedure for obtaining this diagonal congruence is to operate directly on Eq. 46 and record by the use of identity matrices the operations necessary to diagonalize  $D$ .

The use of an orthogonal transformation requires finding the characteristic vectors of  $D$ , which may be accomplished by matrix iteration or other procedures. In general this requires more computation than the previous procedures. For the solution of indeterminate structures the fact that for this transformation (if normalized; that is, an orthonormal transformation)  $h' = h^{-1}$  is generally of little value unless it is desired for some reason to solve Eq. 43 for  $Y$  for a given  $X$ .

The Rayleigh-Ritz procedure stated previously involves the choice of a limited number of vectors of  $h$  and the solution of this limited set of equations such as to obtain a minimum energy solution; minimum complementary energy for the force method and minimum potential energy for the deformation method.

In conclusion it is seen that the method proposed by Morrison and the authors is a particular computation procedure for obtaining a diagonal congruence transformation. The type of presentation used in both of these papers gives a physical feeling which may be lacking in a purely mathematical formulation but tends to obscure the generality of transformation procedures of this type. In particular, there may be more efficient computational procedures for accomplishing the same result and in addition these procedures may be applied to any set of linear equations, including both the force and deformation methods of structural analysis.

PHILLIP L. GOULD,<sup>17</sup> A. M. ASCE. *Introduction.*—On examining the application of the method of combining redundants to the indeterminate pin-jointed truss, the most apparent feature is the elimination of the simultaneous equations which are generally associated with the analysis of this type of structure. In order to determine the comparative ease of computation offered by a so-called classical method and by the method of this article, a simple example is presented together with the calculations that are required to compute the indeterminate stresses by each method. No effort is made to obtain exceedingly precise calculations because, in the solution of the design problem, slide-rule accuracy would be sufficient.

Certain corrections required to the column headings in Table 1 are made in Table 5.

One point should be emphasized to avoid any confusion as to the relationship between the classical redundants  $x_1$ ,  $x_2$  and  $x_3$  and the combined redundants of the article  $X_1$ ,  $X_2$  and  $X_3$ . These redundants are, of course, not identical and the classical redundants are readily obtainable from the combined redundants.

<sup>17</sup> Skidmore, Owings and Merrill Inc., Architects, Engrs., Chicago, Ill.

The combined redundants of the example presented herein are converted to the classical redundants in order to illustrate the procedure. As the example illustrates, the numerical values of the combined redundants may be like the classical redundants. In order to further differentiate between the redundants, different symbols are adopted for the purpose of the discussion.

*Analysis by Classical Methods.*—The proposed structure is given in Fig. 5 for which  $\frac{L}{AL} = \text{constant} = 1$  and the classical redundants are shown in Fig. 6. The superposition equations are

$$\Delta G = 0 = \Delta'G + RG \delta G^{1\uparrow G} + S_{CH} \delta G^{1\swarrow CH} + SCF \delta G^{1\searrow CF} \dots (49)$$

$$\Delta CH = 0 = \Delta'CH = RG \delta CH^{1\uparrow G} + S_{CH} \delta CH^{1\swarrow CH} + SCF \delta CH^{1\searrow CF} \dots (50)$$

and

$$\Delta CF = 0 = \Delta'CF = RG \delta CF^{1\uparrow G} + S_{CH} \delta CF^{1\swarrow CH} + SCF \delta CF^{1\searrow CF} \dots (51)$$

The equations required to evaluate the terms in these equations are

$$\Delta'G = \Sigma P u \alpha \dots (52a)$$

$$\Delta'CH = \Sigma P v \alpha \dots (52b)$$

$$\Delta'CF = \Sigma P w \alpha \dots (52c)$$

$$\delta G^{1\uparrow G} = \Sigma u^2 \alpha \dots (53a)$$

$$\delta G^{1\swarrow CH} = \Sigma v u \alpha \dots (53b)$$

$$\delta G^{1\searrow CF} = \Sigma w u \alpha \dots (53c)$$

$$\delta CH^{1\uparrow G} = \Sigma u v \alpha \dots (54a)$$

$$\delta CH^{1\swarrow CH} = \Sigma v^2 \alpha \dots (54b)$$

$$\delta CH^{1\searrow CF} = \Sigma w v \alpha \dots (54c)$$

$$\delta CF^{1\uparrow G} = \Sigma u w \alpha \dots (55a)$$

$$\delta CF^{1\swarrow CH} = \Sigma v w \alpha \dots (55b)$$

$$\delta CF^{1\searrow CF} = \Sigma w^2 \alpha \dots (55c)$$

and

The new notation that is introduced herein is as follows:

$\Delta'n$  = deflection of  $n$ th point to  $12^k$  load applied to determinate truss;

$P$  = stress in  $n$ th bar due to  $12^k$  load applied to determinate truss;



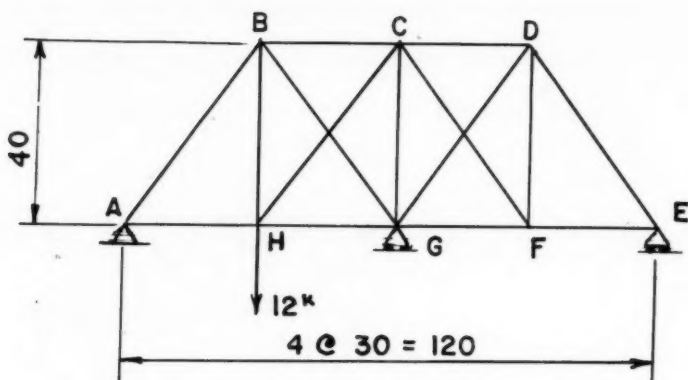
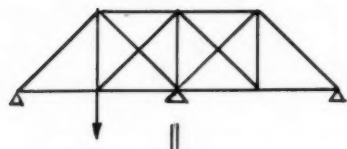
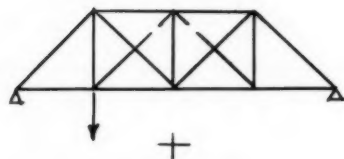


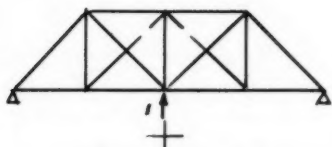
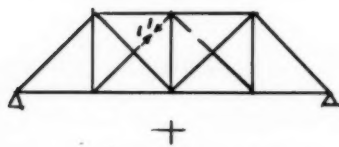
FIG. 5

BAR FORCES

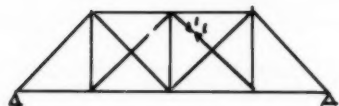
S



x P.

x R<sub>G</sub>

x SCH



x SCF

FIG. 6.—METHOD 1—CLASSICAL METHOD

- $u$  = stress in bars of determinate truss due to  $1k \uparrow @G$ ;  
 $v$  = stress in bars of determinate truss due to  $1k \nearrow @CH$ ;  
 $w$  = stress in bars of determinate truss due to  $1k \searrow @CF$ ;

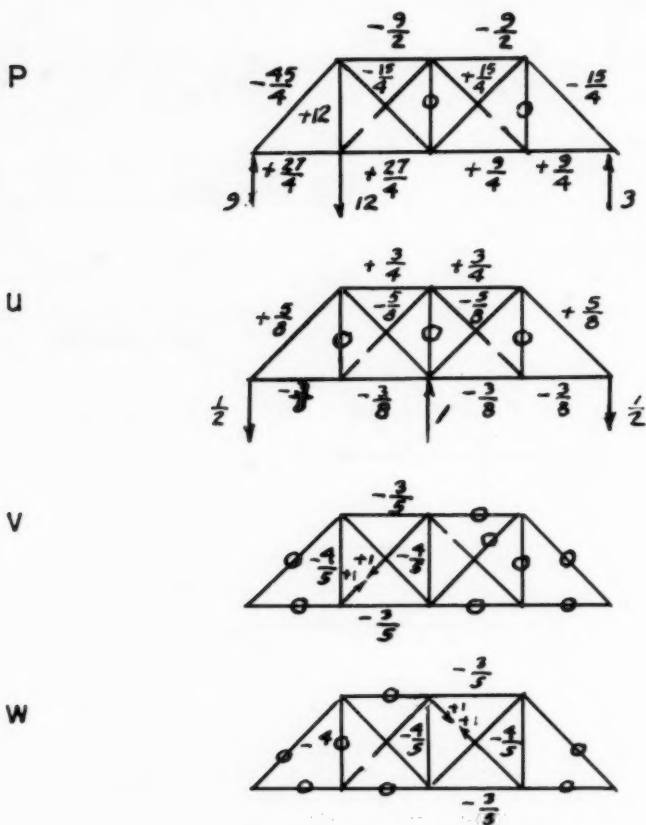


FIG. 7.—SOLUTION FOR UNIT STRESSES

- $\Delta_n$  = deflection of  $n$ th points in original structure (For internal redundants " $n$ " represents two (2) adjacent points in the bar which have been cut and not the panel points);  
 $S_n$  = stress in  $n$ th bar of original structure;  
 $\alpha$  =  $\frac{L}{AE}$  of each member;

$R_n$  = reaction at  $n$ th support; and

$\delta_n$  = deflection of  $n$ th point due 1k load applied to determinate structure in direction of  $S_n$ .

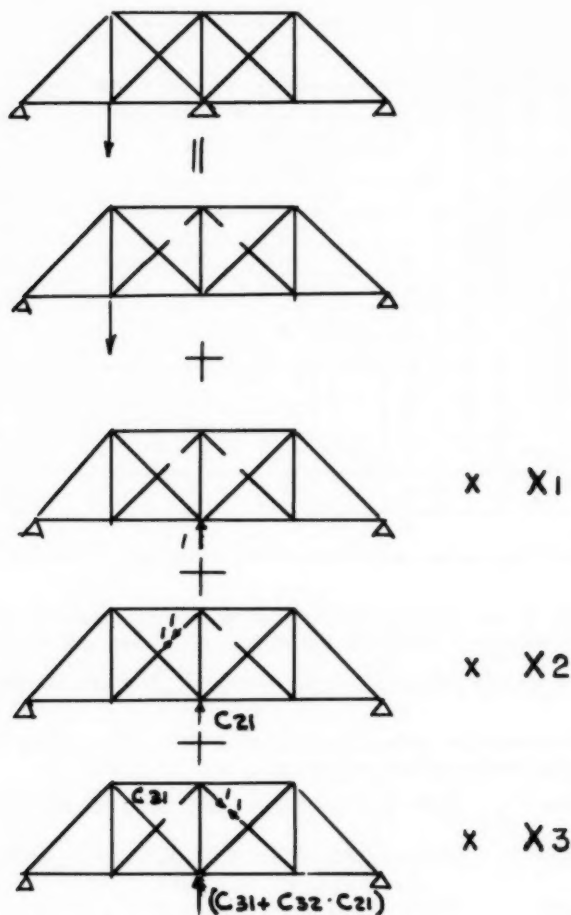


FIG. 8.—METHOD 2—COMBINING REDUNDANTS

It should be noted that the indeterminate internal members are not removed but merely cut and held together by equal and opposite forces, so that  $\Delta_{CH}$  and  $\Delta_{CF}$  can be set equal to zero. Often the classical equations are written with

the indeterminate members removed so that  $\Delta_{CH} = \frac{-S_{CH}L}{A E}$  and  $\Delta_{CF} = \frac{-S_{CF}L}{A E}$ ,

TABLE 4.—SOLUTION BY

	L	A	$\frac{L}{A}$	$\alpha$	P	Unit Stresses			$\Delta'$		
						U	V	W	$\alpha P_u$	$\alpha P_v$	$\alpha P_w$
AB	50	5	10	1	-11.25	+6.25	0	0	- 7.04	- 7.04	0
BC	30	.3	10	1	- 4.5	+ .75	- .60	0	- 3.38	+ 2.70	0
CD	30	.3	10	1	- 4.5	+ .75	0	- .60	- 3.38	0	+2.70
DE	50	.5	10	1	- 3.75	+ .625	0	0	- 2.34	0	0
EF	30	.3	10	1	+ 2.25	- .375	0	0	- 0.84	0	0
FG	30	3	10	1	+ 2.25	- .375	0	- .60	- 0.84	0	-1.35
GH	30	3	10	1	+ 6.75	- .375	- .60	0	- 2.53	- 4.06	0
HA	30	3	10	1	+ 6.75	- .375	0	0	- 2.53	0	0
BG	50	5	10	1	- 3.75	- .625	+1.0	0	+ 2.34	- 3.75	0
DG	50	5	10	1	+ 3.75	- .625	0	+1.0	- 2.34	0	+3.75
BH	40	4	10	1	+12.0	0	- .80	0	0	- 9.60	0
CG	40	4	10	1	0	0	- .80	- .80	0	0	0
DF	40	4	10	1	0	0	0	- .80	0	0	0
CH	50	5	10	1	0	0	+1.0	0	0	0	0
CF	50	5	10	1	0	0	0	+1.0	0	0	0
TOT	-	-	-	-	-	-	-	-	-22.88	-14.71	+5.10
Rg = 8.45						Sch = 5.50					

respectively. If this approach is used, the unit stresses for CH and CF are non-existent and do not appear in the equations. These unit stresses result in  $\frac{SL}{AE}$  terms so that the two methods are identical. The unit stresses are shown in Fig. 7.

The calculations are presented as Table 4. The following eqs show the substitution in the superposition equations:

$$\Delta G = - 22.88 + 3.254 RG - 0.850 SCH - 0.850 SCF = 0. \quad (56)$$

$$\Delta CH^2 = - 14.71 - 0.850 RG + 4.00 SCH + 0.64 SCF = 0 \dots (57)$$

$$\Delta CF = + 5.50 - 0.850 RG + 0.64 SCH + 4.00 SCF = 0 \dots (58)$$

The redundants are  $SCH = +5.50$ ,  $SCF = -0.40$  and  $RG = +8.45$ .

*Analysis by Combining Unit Redundants.*—The combined redundants are shown in Fig. 8. The unit stresses  $s_1$ ,  $s_2$ , and  $s_3$  are the same as  $u$ ,  $v$ , and  $w$  shown in Fig. 7. The superposition equations are given as Eqs. 9(a) through 9(c) in the example given by the authors. By the authors' procedure the superposition equations are reduced to the explicit form given as Eqs. 12(a), 12(b), and 12(c) in their example. The equations for the coefficients and unit redundants are given as Eqs. 59 through 64 with the calculations shown in Table 5.

## CLASSICAL METHOD

$\delta G$			$\delta CH$			$\delta CF$			Rg-u	Sch-v	Scf-w	S
$\alpha u^2$	$\alpha uv$	$\alpha uw$	$\alpha vu$	$\alpha v^2$	$\alpha vw$	$\alpha wu$	$\alpha wv$	$\alpha w^2$				
+ .391	0	0	0	0	0	0	0	0	+5.28	0	0	-5.97
+ .563	- .45	0	- .45	+ .36	0	0	0	0	+6.32	-3.30	+ .24	-1.26
+ .563	0	- .45	0	0	0	- .45	0	+ .36	+6.32	0	0	+1.82
+ .391	0	0	0	0	0	0	0	0	+5.28	0	0	+1.53
+ .141	0	0	0	0	0	0	0	0	-3.17	0	0	- .92
+ .141	0	+ .225	0	0	0	+ .225	0	+ .36	-3.17	0	+ .24	- .68
+ .141	+ .225	0	+ .225	+ .36	0	0	0	0	-3.17	-3.30	0	+ .28
+ .141	0	0	0	0	0	0	0	0	-3.17	0	0	+3.58
+ .391	- .625	0	- .625	+1.0	0	0	0	0	-5.28	+5.50	0	-3.53
+ .391	0	- .625	0	0	0	- .625	0	+1.0	-5.28	0	- .40	-1.93
0	0	0	0	+ .64	0	0	0	0	0	-4.40	0	+7.6
0	0	0	0	+ .64	+ .64	0	+ .64	+ .64	0	-4.40	+ .32	-4.08
0	0	0	0	0	0	0	0	+ .64	0	0	+ .32	+ .32
0	0	0	0	0	0	0	0	0	0	+5.50	0	+5.50
0	0	0	0	+1.0	0	0	0	+1.0	0	0	- .40	- .40
+3.254	- .85	- .85	- .85	+4.00	+ .64	- .850	+ .64	4.00	-	-	-	-

$S_{cf} = 0.40$

$$S_1 = s_1 = u \dots \dots \dots (59)$$

$$C_{21} = - \frac{\sum \alpha S_1 s_2}{\sum \alpha S_1^2} = - \frac{\sum \alpha s_1 s_2}{\sum \alpha s_1^2} = + 0.262 \dots \dots \dots (60)$$

$$S_2 = C_{21} S_1 + s_2 = 0.262 s_1 + s_2 \dots \dots \dots (61)$$

$$C_{31} = - \frac{\sum \alpha S_1 s_3}{\sum \alpha S_1^2} = - \frac{\sum \alpha s_1 s_3}{\sum \alpha s_1^2} = + 0.262 \dots \dots \dots (62)$$

$$C_{32} = - \frac{\sum \alpha S_2 s_3}{\sum \alpha S_2^2} = - \frac{\sum \alpha (0.262 s_1 + s_2) s_3}{\sum \alpha (0.262 s_1 + s_2)^2} = - 0.1105 \dots \dots (63)$$

$$S_3 = C_{31} S_1 + C_{32} S_2 + s_3 = C_{31} s_1 + C_{32} (C_{31} s_1 + s_2) + s_3 \\ = 0.262 s_1 - 0.1105 (0.262 s_1 + s_2) + s_3 \dots \dots \dots (64)$$

TABLE 5.—SOLUTION BY METHOD

	1	2	3	4	5	6	7	8	9	10	11
BAR	$s_1 = S_1$	$s_2$	$s_3$	$\alpha S_1^2$	$\alpha S_1 s_2$	$c_{21} S_1$	$S_2$	$\alpha S_1 s_3$	$\alpha S_2 s_3$	$\alpha S_2^2$	$c_{31} S_1$
AB	+ .625	0	0	+ .391	0	+ .164	+ .164	0	0	+ .027	+ .164
BC	+ .75	- .60	0	+ .563	- .45	+ .197	- .403	0	0	+ .160	+ .197
CD	+ .75	0	- .60	+ .563	0	+ .197	+ .197	- .45	- .118	+ .039	+ .197
DE	+6.25	0	0	+ .391	0	+ .164	+ .164	0	0	+ .027	+ .164
EF	- .375	0	0	+ .141	0	- .098	- .098	0	0	+ .001	- .098
FG	- .375	0	- .60	+ .141	0	- .098	- .098	+ .225	+ .059	+ .001	- .098
GH	- .375	- .60	0	+ .141	+ .225	- .098	- .698	0	0	+ .487	- .098
HA	- .375	0	0	+ .141	0	- .098	- .098	0	0	+ .001	- .098
BG	- .625	+1.0	0	+ .391	- .625	- .164	+ .836	0	0	+ .700	- .164
DG	- .625	0	+1.0	+ .391	0	- .164	- .164	- .625	- .164	+ .027	- .164
BH	0	- .80	0	0	0	0	- .80	0	0	+ .64	0
CG	0	- .80	- .80	0	0	0	- .80	0	+ .64	+ .64	0
DF	0	0	- .80	0	0	0	0	0	0	0	0
CH	0	+1.0	0	0	0	0	+1.0	0	0	+1.0	0
CF	0	0	+1.0	0	0	0	0	0	0	0	0
TOT	-	-	-	+3.25	- .85	-	-	- .85	+ .417	+3.75	-

$$X_1 = 7.07$$

$$X_2 = 5.52$$

$$X_3 = -0.35$$

With reference to Table 5, Eq. 59 is from column 1. Eq. 80 is column 5/column 4; Eq. 61 is from column 7; Eq. 62 is column 8/column 4; Eq. 63 is column 9/column 10; and Eq. 64 is from column 13. Eqs. 65 (col. 16/col. 4), 66 (col. 17/column 10) and 67 (col. 18/col. 14) are used to calculate the values of the redundants.

$$X_1 = - \frac{\sum \alpha S_0 S_1}{\sum \alpha S_1^2} = - \frac{\sum \alpha S_0 s_1}{\sum \alpha s_1^2} \dots \dots \dots (65)$$

$$X_2 = - \frac{\sum \alpha S_0 S_2}{\sum \alpha S_2^2} = - \frac{\sum \alpha S_0 (C_{21} S_1 + s_2)}{\sum \alpha (C_{21} S_1 + s_2)^2}$$

$$= - \frac{\sum \alpha S_0 (0.62 S_1 + s_2)}{\sum \alpha (0.262 S_1 + s_2)^2} \dots \dots \dots (66)$$

## OF COMBINING REDUNDANTS

12	13	14	15	16	17	18	19	20	21	22
$c_3 s_2$	$s_3$	$\alpha s_3^2$	$s_0$	$\alpha s_0 s_1$	$\alpha s_0 s_2$	$\alpha s_0 s_3$	$x_1 s_1$	$x_2 s_2$	$x_3 s_3$	$s$
- .0181	+ .146	+ .021	-11.25	- 7.03	- 1.85	-1.65	+4.42	+0.90	- .06	-5.99
+ .0446	+ .242	+ .059	- 4.50	- 3.37	+ 1.82	-1.09	+5.31	-2.22	-0.08	-1.49
- .0218	+ .425	+ .181	- 4.50	- 3.37	- 0.89	+1.92	+5.31	+1.08	+0.16	+2.05
- .0181	+ .146	+ .021	- 3.75	- 2.35	- 0.62	-0.55	+4.42	+0.90	-0.06	+1.51
+ .0109	- .087	+ .008	+ 2.25	- 0.84	- 0.22	- .20	-2.66	-0.54	+0.03	-0.92
+ .0109	- .687	+ .472	+ 2.25	- 0.84	- 0.22	-1.54	-2.66	-0.54	+0.26	-0.69
+ .0771	- .021	+ .004	+ 6.75	- 2.54	- 4.72	-0.14	-2.66	-3.84	+0.01	+0.26
+ .0109	- .087	+ .008	+ 6.75	- 2.54	- 0.67	-0.59	-2.66	-0.54	+0.03	+3.58
- .0924	- .256	+ .065	- 3.75	+ 2.35	- 3.13	+0.97	-4.42	+4.61	+0.10	-3.16
+ .0181	+ .854	+ .730	+ 3.75	- 2.35	- 0.61	+3.21	-4.42	-0.90	-0.32	-1.89
+ .0885	+ .089	+ .008	+12.0	0	- 9.6	+ .98	0	-4.41	-0.03	+7.56
+ .0885	- .712	+ .507	0	0	0	0	0	-4.41	+0.27	-4.14
0	- .80	+ .640	0	0	0	0	0	+0.30	0	+0.30
- .1105	- .1105	+ .012	0	0	0	0	0	+5.52	+0.04	+5.56
+1.0	+1.00	0	0	0	0	0	0	-0.35	0	-0.35
-	+3.74	-	-	-22.88	-20.71	+1.32	-	-	-	-

$$\begin{aligned}
 x_3 &= - \frac{\sum \alpha s_0 s_3}{\sum \alpha s_3^2} = - \frac{\sum \alpha s_0 [C_{21} s_1 + C_{32} s_2 + s_3]}{\sum \alpha [C_{21} s_1 + C_{32} s_2 + s_3]^2} \\
 &= - \frac{\sum \alpha s_0 [0.262 s_1 - 0.1105 s_2 + s_3]}{\sum \alpha [0.262 s_1 - 0.1105 s_2 + s_3]^2} \dots \dots \dots (67)
 \end{aligned}$$

The combined unit redundants are converted to the classical redundants using Eqs. 68 through 70 as indicated in Fig. 2 by the authors.

$$s_{CF} = x_3 = - 0.35 \dots \dots \dots (68)$$

$$s_{CH} = x_2 + C_{32} x_3 = 5.52 + (-0.1105)(-0.35) = 5.56 \dots \dots (69)$$

$$\begin{aligned}
 R_G &= x_1 + C_{21} x_2 + (C_{31} + C_{32} C_{21}) x_3 \\
 &= 7.08 + 0.262 \cdot 5.56 + [0.262 + (-0.1105)(0.262)] [-0.35] \\
 &= 8.46 \dots \dots \dots (70)
 \end{aligned}$$

*Conclusions.*—In comparing the relative merits of the two methods, it is apparent that the classical equations of superposition yield redundants which have a simple physical meaning and, therefore, enable the designer to understand the behavior more readily. However, the method of combining redundants eliminates the cumbersome procedure of solving simultaneous equations at the expense of increasing numerical calculations. As far as this elementary example is concerned this method does not seem to offer any particular time savings. However, for more complex problems that would result in more than three simultaneous equations if treated classically, the method of combining redundants might offer certain advantages, especially if the simultaneous equations would have to be solved by numerical computation.



RECENT TRENDS IN ULTIMATE STRENGTH DESIGN<sup>a</sup>

Discussion by John G. Merkle, M. Gregory, and A. A. Eremin

JOHN G. MERKLE,<sup>13</sup> A. M. ASCE.—The establishment of ultimate strength criteria for the design of reinforced concrete beams requires that both the shortcomings of the present elastic theory and the advantages of ultimate strength theory be well explained.<sup>14</sup> The stress versus load curves presented by Ferguson clearly show that there can be a considerable difference between the stresses actually developed in a reinforced concrete beam and those predicted by elastic theory. The acceptance of this fact, that elastic theory does not represent actual physical behavior, is a necessary first step in the establishment of a theory which does.

There is another form of graphical presentation from which the economic advantages of ultimate strength theory can be inferred directly. This is a plot

of ultimate strength, expressed as  $\frac{M_{ult}}{bd^2}$ , versus  $p$ , the percentage of steel. The

validity of such a comparison is based on two facts, first, that the stresses at sub-ultimate loads are irrelevant to the determination of ultimate strength, and second, that the value of  $p_i$  (percentage of steel for balanced elastic design) shifts only slightly between the curves for allowable load and those for ultimate load. Thus the allowable loads computed for the same section by each theory bear the same relation to each other as do the predicted ultimate strengths, provided the same safety factor is used. It follows that wherever elastic theory underestimates the ultimate strength of a beam, it also determines a design load which is lower than necessary and causes material to be used uneconomically.

$M_{ult}$  for elastic theory has been assumed as that moment at which  $f_s = f_y$  or  $f_c = f'_c$  or both. On the assumption that an amount of steel in excess of  $p = 0.03$  is often difficult to place, a dashed line has been drawn at this value to delimit the range of principal practical interest. The point at which both  $f_s = f_y$  and  $f'_c$  by ultimate strength theory is labelled  $p_b$ , and corresponds to  $p_i$  by elastic theory. For computation by ultimate strength theory it has been further assumed that concrete fails at an ultimate strain of 0.003.

The following facts can be inferred from Figs. 16-20 in which the solid lines indicate ultimate values and the dashed elastic:

*General Comparison (Figs. 16 and 17).*—Elastic theory and ultimate strength theory agree quite closely for beams with  $p < p_i$ , but beams with  $p > p_i$  are

<sup>a</sup> January 1961, by Phil M. Ferguson (Proc. Paper 2715).

<sup>13</sup> Graduate Student and Teaching Asst., School of Civ. Engrg., Cornell Univ., Ithaca, N. Y.

<sup>14</sup> "Design of Concrete Structures," by Urquhart, O'Rourke and Winter, 5th Ed., McGraw-Hill Book Co., Inc., New York, 1954, p. 438.

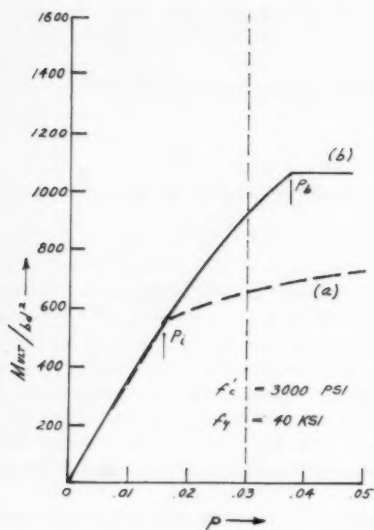


FIG. 16.—ULTIMATE STRENGTH BY (a) ELASTIC THEORY (b) ULTIMATE STRENGTH THEORY; ORDINARY CONCRETE AND STEEL

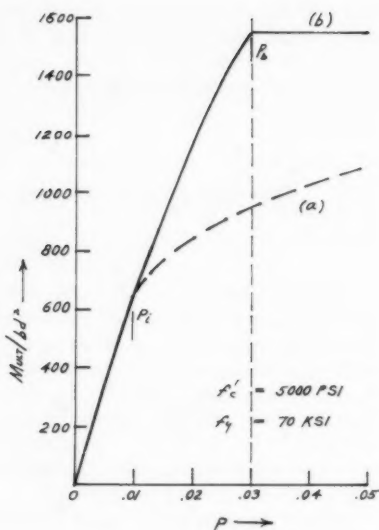


FIG. 17.—ULTIMATE STRENGTH BY (a) ELASTIC THEORY (b) ULTIMATE STRENGTH THEORY; HIGHSTRENGTH CONCRETE AND STEEL

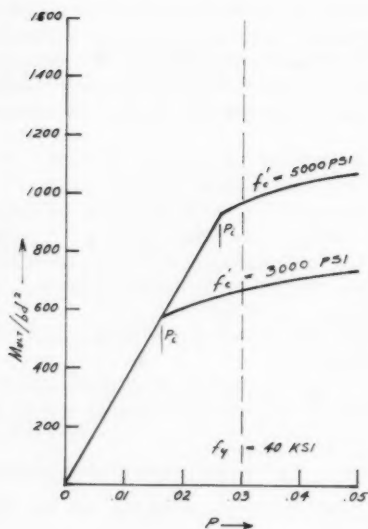


FIG. 18.—EFFECT OF RAISING  $f'_c$  AT CONSTANT  $f_y$  BY ELASTIC THEORY

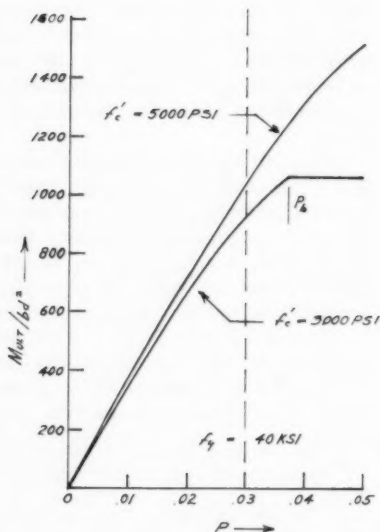


FIG. 19.—EFFECT OF RAISING  $f'_c$  AT CONSTANT  $f_y$  BY ULTIMATE STRENGTH THEORY

actually stronger than as determined by elastic theory. If the full strength of such beams was recognized most compression reinforcement would be unnecessary, and the depth of many beams carrying high moment and low shear could be reduced with a consequent saving in dead weight.

*High Strength Materials (Figs. 18, 19, 20).*

1. Concrete.—Elastic theory (Fig. 18) shows that increasing  $f'_c$  produces a significant increase in  $\frac{M_{ult}}{bd^2}$  for beams with large values of  $p$ . But ultimate

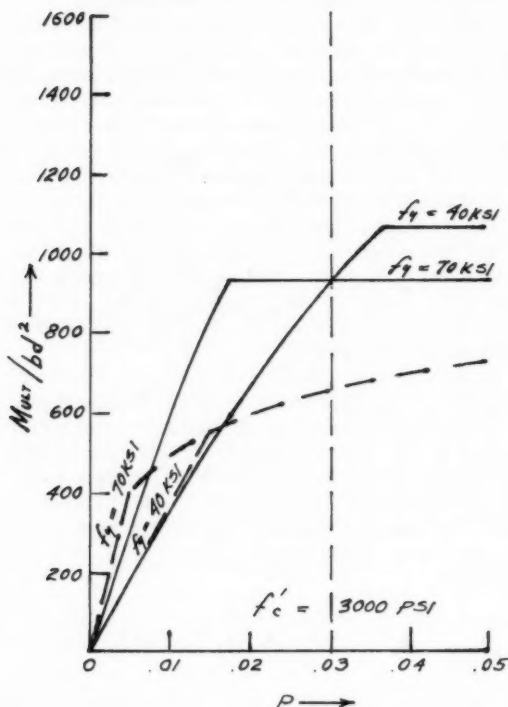


FIG. 20.—EFFECT OF RAISING  $f_y$  AT CONSTANT  $f'_c$  BY BOTH THEORIES

theory (Fig. 19) shows that the beam already possesses the strength which the elastic theory purports to add by means of increasing  $f'_c$ . Ultimate theory shows that the actual gain in strength due to raising  $f'_c$ , within reasonable limits of  $p$ , is rather slight.

2. Steel.—Conversely, elastic theory (Fig. 20) understates the advantage of increasing  $f_y$  at large values of  $p$ , because it underestimates the strength of the concrete compression zone. Ultimate theory shows that high strength reinforcing results in the greatest advantage at almost the same value of  $p$  for which elastic theory says there is no advantage ( $p \approx 0.016$ ).

The most important general conclusion which can be drawn from these facts is that design theory does have a strong influence on material economy, and that a more accurate theory will definitely produce worthwhile savings.

M. GREGORY.<sup>15</sup>—It is gratifying to see the philosophy of ultimate strength design of concrete structures so clearly presented in one paper. One has only to test a few reinforced or prestressed concrete beams to realize the shortcomings of the linear theory and the simplicity of ultimate strength methods. It is certainly true, as Ferguson has stated, that in certain cases the linear theory can point towards added compression steel in a situation where this steel makes an insignificant contribution to the strength.

So far as the choice of the value of  $f'_c$  to be used in design is concerned, adequate statistical methods are available, and they do not need to be precise, especially if one is prepared to tolerate one cylinder in ten falling below the specified  $f'_c$ , which is quite reasonable in most circumstances. However, the problems of practical economic concrete production in order to meet the requirements of the specification with regard to  $f'_c$  may become acute.<sup>16</sup> It has become the practice to achieve safety in design partly by the use of load factors, as studied by Ferguson, ultimate strengths being calculated on the specified value of  $f'_c$ . But, in view of the inherent variability of concrete production, it is necessary, in order to ensure satisfactory concrete, to set the mean concrete strength somewhat above  $f'_c$ . The author has shown how to do this, but in addition it should be stated that the adequacy of the actual method by which the adopted mean strength is arrived at, and the standard of quality control maintained, is extremely important.

With regard to the ultimate strength of tension reinforced concrete beams subject to bending only, axial load being zero, the assumed strain configuration at failure given in Fig. 12 enables simple explicit calculation of the ultimate bending moment. It is not even necessary in this simple case to assume the magnitude of the failure strain in the concrete. If there is one layer of steel  $A_{s1}$  and the steel yields before the concrete crushes (most codes ensure this in order to avoid a brittle-type failure, and in any case, the designer should ensure it), then the force in the steel is  $T = A_{s1} f_y$ . For zero axial force,  $T = C_c$ , and therefore

$$0.85 f'_c b a = A_{s1} f_y = p b d f_y \dots\dots\dots (3)$$

in which  $p$  is the ratio of steel to concrete. The moment is then

$$\begin{aligned} M &= T \left( d - \frac{1}{2} a \right) \\ &= p b d^2 f_y \left( \frac{1 - p f_y}{1.70 f'_c} \right) \dots\dots\dots (4) \end{aligned}$$

<sup>15</sup> Senior Lecturer in Civ. Engrg., Univ. of Tasmania, Nuffield Foundation Fellow visiting the Univ. of Cambridge, England.

<sup>16</sup> "Sequential Analysis Applied to Quality Control of Concrete," by M. Gregory, Commonwealth Engineer Tait Publishing Co., Melbourne, Australia, Vol. 45 No. 8, April, 1958, p. 51.

where only information given in Fig. 12 is used.

It makes little difference whether the Whitney rectangular stress block is used, as in Ferguson's paper, or some other shape of stress block, such as parabolic; the result is substantially the same. In fact, the number which is taken as 1.70 in Eq. 4 should be considered as an empirical factor to be obtained from tests, and it is unnecessary to specify the shape of the stress block, but only to specify its average height relative to  $f'_c$  and the location of its center of gravity. For instance if

$$C_c = K_1 f'_c K_u d b \dots\dots\dots (5)$$

in which  $b K_u d$  is the area of concrete in compression, and the center of gravity of the stress block is located a distance  $K_2 K_u d$  from the top of the beam, then

$$M = p b d^2 f_y \left[ 1 - \left( \frac{p f_y}{f'_c} \right) \left( \frac{K_2}{K_1} \right) \right] \dots\dots\dots (6)$$

and tests show that  $K_1/K_2 = 1.70$  allows a reasonably conservative estimate of  $M$ .

An important point appears here in that the practical range, quite large variations in  $f'_c$  make little difference to  $M$ . If a few graphs (useful for design purposes) of  $M/bd^2 f_y$  against  $p$  are plotted for various values of  $f'_c$ , this soon becomes apparent. This is certainly true for beams with less than 2% tensile steel, and the designer is well advised to think again if he intends to use more than about  $1\frac{1}{2}\%$ , as there is then little chance of proper compaction of the concrete once the necessary laps and stirrups are inserted. In a great deal of the normal reinforced concrete construction, except where axial loads are high, there is little to be gained by using high strength concrete. It is much more important that the concrete should be uniform, properly compacted and properly cured.

If one conducts a test on such a beam and observes the beam when it is carrying maximum moment, then the method of calculating the ultimate moment presents itself in a simple and striking manner. A large crack has formed on the tension side of the beam, and the steel has obviously yielded. Hence the magnitude and the location of the force  $T$  is known and there is as little doubt about the location of the force  $C_c = T$  in the region of crushing of the concrete in the compression side. It must be somewhere between the point to which visible tensile cracks extend and the top of the beam, and any roughly guessed location gives the correct moment. This intrinsic accuracy of the ultimate load method is reflected in the foregoing calculations.

In problems for which axial loads are considerable, or where there is more than one layer of steel, or where high strength steel is used, or where the beam is prestressed, it becomes necessary to specify the strain configuration at failure in order to calculate the ultimate strength, as Ferguson has clearly stated. Even a casual glance at a member approaching failure confirms this. Now, what is needed is a specification of the strain configuration sufficient to define all the forces in the steel and concrete. Tests show that a linear strain diagram across the member is sufficiently correct to do this. It makes little difference to the subsequent calculations whether 0.002 or 0.004 is taken as the

maximum strain in the concrete at failure, and 0.003 is a reasonable value. Nothing more than the equations of statics is now needed in order to produce diagrams such as Figs. 13 through 15, which give all the information necessary for design. This method has also been presented by the writer.<sup>17</sup> But when high tensile steel or prestressing wire is in use, it must not be forgotten that the local strains in the steel may be reduced by the breaking of the bond between the steel and concrete, thus allowing a longer length of steel to stretch. The strain may therefore be rather less than that given by the linear strain diagram.

It is hoped that the preceding remarks may serve to reinforce not only the philosophy presented by Ferguson but also the empirical methods used by him to obtain design formulas.

However, one important point arises which does not appear to be touched on by the author and this is the question of the method of analysis of statically indeterminate structures in order that one can actually use in design of structures the known ultimate bending strength or combined bending and axial load carrying capacity of members. Obviously elastic analysis can be used but this can surely be regarded only as a temporary expedient, and entirely unsatisfactory. Again, a few tests will soon convince the careful observer about the ability of reinforced or prestressed concrete beams to attain large deflections through localized rotation at points of high moment. Measured moment-curvature diagrams have a flat top until surprisingly high strains are reached; perhaps this is not so surprising when the ability of concrete to flow is once realized. One feels already confident enough to apply the simple plastic-theory collapse analysis to beam-type concrete structures. It would be interesting to have Ferguson's comments of this.

Work at the University of Tasmania, using measured moment curvature relations, and this is based on the strain configuration as being fundamental, is proceeding (in 1961). The powerful analysis tool is applied to reinforced concrete structures provided by complementary energy methods, with a view to achieve a realistic method of analysis of the structure as failure is approached, and perhaps being able to place a deflection limitation on design.

A. A. EREMIN,<sup>18</sup> M. ASCE.—Ferguson has shown the elastic stresses theory limitations and advantages of ultimate strength method of design of reinforced concrete structures. Furthermore, Ferguson correctly stated, that for efficient understanding the ultimate strength method of reinforced concrete design, a greater understanding of its background is necessary.

In Figs. 2 to 5, Ferguson has shown relation of increased loading and ultimate stresses in reinforced concrete members. These diagrams may be used in developing either the ultimate load factors, or ultimate bending moment factors in design of beams. The limiting factors of ultimate bending moment may be considered as a simplified step from the elastic stress method to the ultimate strength method.

The block shape distribution of ultimate stresses in compressive zone of reinforced concrete members is well known. Therefore, it may easily be adopted in the codes of design.

Adoption of the block ultimate stress distribution method will facilitate accumulation of experimental study of yet needed more research on ultimate strain problems and distribution of plastic hinges.

<sup>17</sup> "Ultimate Strength Design of Reinforced Concrete Members under Combined Bending and Axial Load," by M. Gregory and G. C. Reynolds, *Commonwealth Engineer*, Vol. 47, No. 2, September, 1959, p. 66.

<sup>18</sup> Cons. Structural Engr., Berkeley, Calif.

In theory of ultimate stresses important consideration shall be given to distribution of shear stresses and provision of shear reinforcement in concrete members. In Figs. 13 to 15 Ferguson specified the quantity of longitudinal reinforcement in concrete columns and briefly mentioned the provision of reinforcing ties.

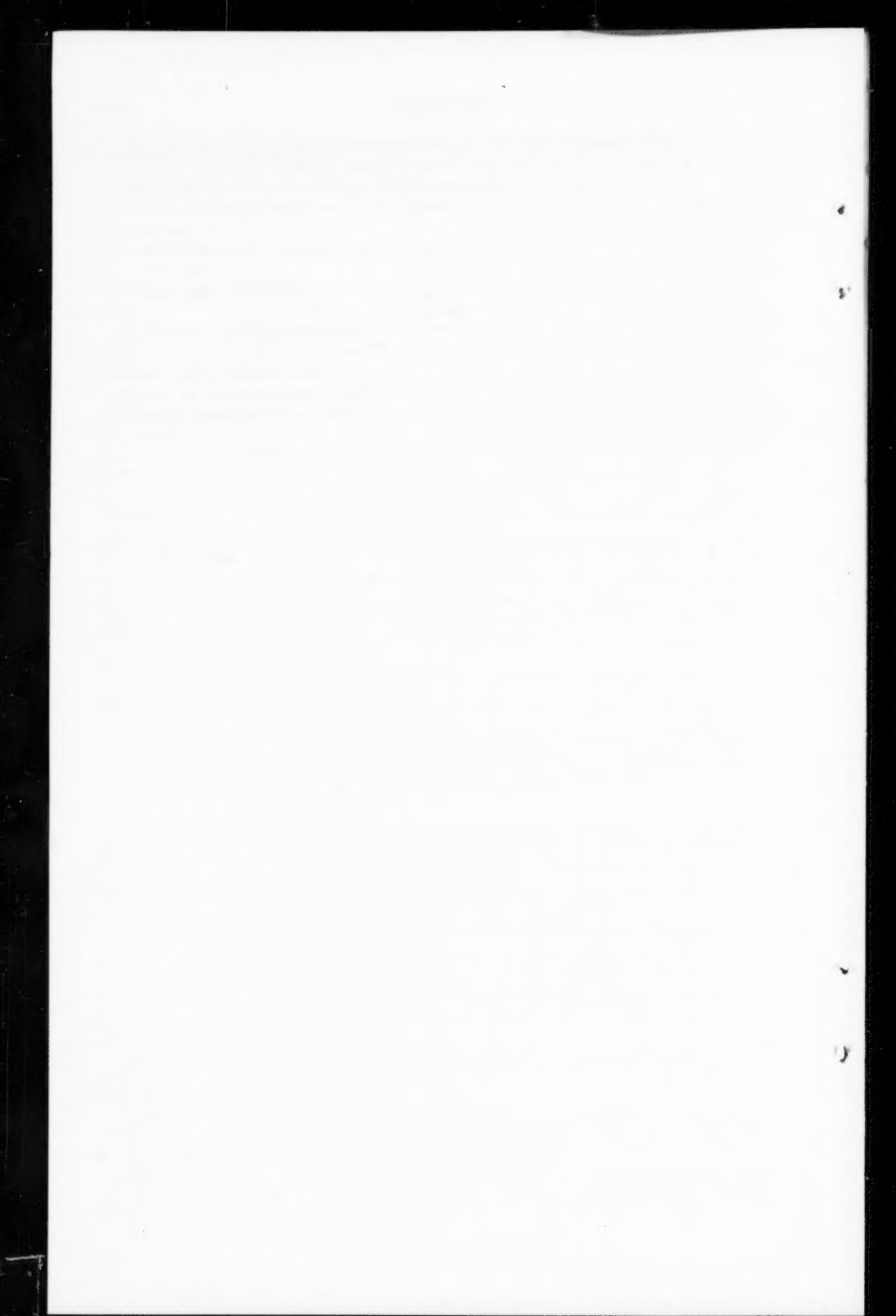
In the compressed members, ties and shear reinforcement often have a prime importance in carrying ultimate stresses.

In testing of concrete for the elastic properties the standard 6 in. cylinder crushing compressive tests furnished excellent results.

In the ultimate strength method of design greater informations may be obtained from the tests of concrete for tensile stresses.

Often, the "ultimate strength" method of design is yet considered as "semi-empirical." Therefore, adoption of ultimate strength theory may be simplified by available tests of reinforced concrete structures for ultimate stresses and strain.







# MOMENT-DISTRIBUTION CONSTANTS FROM CARDBOARD ANALOGS<sup>a</sup>

Discussion by Paul H. Reimer, Jr., and Miguel Angel Macias-Rendón

PAUL H. REIMER, JR.,<sup>5</sup> A. M. ASCE.—Ondra's cardboard analogs for determining moment-distribution constants are a significant contribution to the field of structural design. For the engineer who wants a quick, accurate check on his work, this method is good.

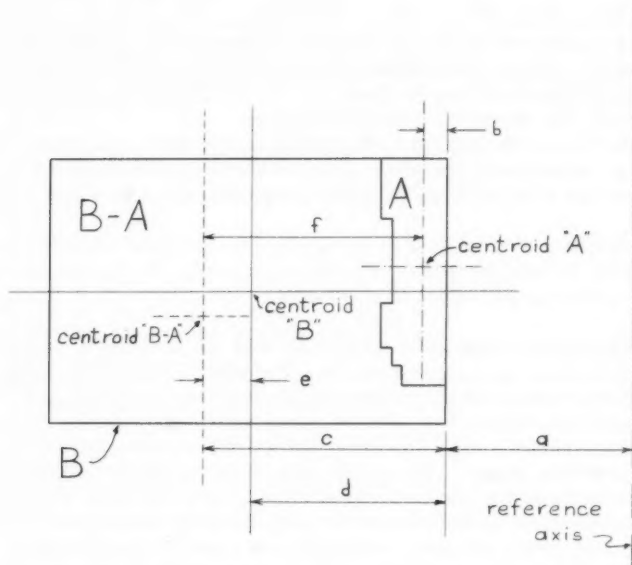


FIG. 21

To make the method a little faster and more accurate, the following modification in the determination of the stiffness factors is proposed. The finding of the area of the  $1/I$  diagram can be simplified if the following system is used.

In Fig. 21, the  $1/I$  diagram is plotted on the rectangular cardboard to some

<sup>a</sup> January 1961, by Otakar Ondra (Proc. Paper 2721).

<sup>5</sup> Graduate Asst., Lehigh Univ., Bethlehem, Pa.

convenient scale. It is then cut out and the centroids of both pieces are found by the method given by Ondra. When the centroids have been located, the distances to the edges of the piece may be scaled and recorded on the cardboard.

For the purpose of derivation only, consider a reference axis at some distance "a" from the edge of the cardboard. It is easily seen that the total area of the cardboard times its centroidal distance to the reference axis must equal the sum of the individual areas times their respective centroidal distances about the reference axis. In terms of the symbols shown, this is

$$B(a+d) = A(a+b) + (B-A)(a+c) \dots\dots\dots (64)$$

Multiplying, combining and cancelling terms in the previous expression gives us the simple identity

$$A = B \frac{(c-d)}{(c-b)} = B \frac{e}{f} \dots\dots\dots (65)$$

in which A is the area of the  $1/I$  diagram, B denotes the original area of cardboard sheet, e refers to the distance from centroid of leftover piece to the centroid of the original cardboard sheet, and f is the distance from centroid of leftover piece to the centroid of the  $1/I$  diagram.

It is thus seen that the only restriction that must be placed on "e" and "f" is that they be measured parallel to each other. Care should be taken to measure "e" so that it is as large as possible. This will tend to reduce the errors involved.

This simple method of finding the area of an irregular shape if not confined to this field. It can be used to determine the area of any section that can be plotted accurately on a sheet of cardboard.

MIGUEL ANGEL MACIAS-RENDÓN.<sup>6</sup>—The determination of moment distribution constants by means of cardboard analogs involves the construction of plane figures representing summations of quantities  $(x/EI)\Delta x$  and  $(x^2/EI)\Delta x$ . The physical significance of these figures and their relation to the various constants are established. Additional helpful information may be found in the author's previous paper.<sup>2</sup> The basic idea of the cardboard-analog method is an experimental evaluation of areas and the location of their centroids.

The construction of the analogs is done either by graphic multiplication or division. The areas and their centroids are found by mechanically balancing cardboard templates and with the aid of simple equations of statics. The unique feature of this experimental method of analysis is that the simplicity of the technique as well as the use of readily available tools and material make it practical for office work.

The author states "The line is then replaced by a continuous curve drawn tangent to the segmented line." In reality, the continuous curve must pass through each of the graphically constructed points. Consequently, the author's statement should read "The line is then replaced by a continuous curve drawn through the individual points, closely following the general trend of the segmented line."

<sup>6</sup> Prof. of Civ. Engrg., Instituto Tecnológico y de Estudios Superiores de Monterrey, N. L., Mexico.

Undoubtedly, the length and scope of the paper made it impractical to illustrate the method by actual examples. To assess independently the merits of Ondra's method the writer has applied the method to a beam previously analyzed in an article<sup>7</sup> by William J. Eney, F. ASCE. The purpose of this particular choice was two-fold, namely, to assess the accuracy of the analog method by comparison with analytically determined results, and to compare results obtained by the analog and mechanical-type deformeter-methods. The data of Eney's beam is given in Fig. 22 and Table 2.

TABLE 2.—PROPERTIES OF EXAMPLE BEAM

Section	0	1	2	3	4	5	6	7	8	9	10
h (ft)	4.83	4.09	3.38	2.87	2.52	2.33	2.18	2.22	2.44	2.97	3.58
I (ft <sup>4</sup> )	28.0	17.0	9.5	6.0	4.0	3.2	2.6	2.7	3.6	6.5	11.5

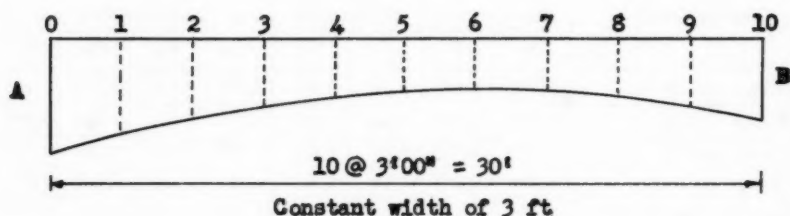


FIG. 22

Scales adopted for the analogs are as follows:

Lengths: 1 cm = 1.2 ft

Moments of Inertia: 1 cm = 1.5 ft<sup>4</sup>

(Moments of Inertia)<sup>-1</sup>: 1 cm = 0.05 ft<sup>-4</sup>

Reference ordinate for graphical division = 1.8 cm

Stiffness areas "A": 1 cm<sup>2</sup> = (1.2 by 0.05) ft<sup>-3</sup> = 0.06 ft<sup>-3</sup>

Fixed-end Moments areas "W": 1 cm<sup>2</sup> =  $\left(\frac{1.2}{1.5 \times 1.8}\right)$  ft<sup>-3</sup> by 1.2 ft

Thus 1 cm<sup>2</sup> = 0.533 ft<sup>-2</sup>

A reference moment of inertia  $I_0$  of 12 ft<sup>4</sup> was adopted to express stiffnesses in terms of  $EI_0/L$ , being  $L$  the total length of the beam.

Three sets of analogs were made and worked out separately in order to avoid checks of partial results. The cardboard used is of the type commercially available, and the analogs were drawn and cut with ordinary scales and scissors. Slide rule was used in all the numerical computations.

<sup>7</sup> "Fixed-End Moments by Cardboard Models," by W. J. Eney, *Engineering News-Record*, December 12, 1935, p. 814.

Table 3 shows the results obtained in the determinations of carry-over factors, stiffnesses and fixed-end moments for a concentrated load  $P$  at two different locations, section 4 and section 6. All analogs were made to give directly the values for end "A," and the proper Eqs. 31, 32 and 41 were used to find the corresponding values for end "B." Stiffnesses are expressed in terms of  $EI_0/L$  and the fixed-end moments are in terms of  $PL$ . Clockwise moments are positive.

It should be noted that even the analytical values contain some error with respect to the exact values. This is due to the fact that numerical integration was used in the analytical work. A rigorous mathematical study requires the treatment of one continuous function of the moment of inertia, ( $I$ ), fulfilling all the values of  $I$  for the different sections of the beam. Therefore, ignoring the sign of the error of the analytical values, it can be said that the differences

TABLE 3

Determination	Carry-over		Stiffnesses		Fixed-end Moments			
	A	B	A	B	$-A_4$	$B_4$	$-A_6$	$B_6$
Analogs (set 1)	0.532	0.885	3.22	1.95	0.243	0.070	0.162	0.155
Analogs (set 2)	0.524	0.865	3.11	1.88	0.230	0.070	0.153	0.158
Analogs (set 3)	0.535	0.864	3.21	1.92	0.233	0.066	0.156	0.152
Average (analogs)	0.530	0.871	3.18	1.92	0.235	0.069	0.157	0.155
Maximum Deviation <sup>a</sup>	1.13%	1.61%	2.20%	2.08%	3.40%	4.35%	3.18%	1.94%
Analytical Values <sup>b</sup>	0.529	0.869	3.17	1.91	0.239	0.072	0.157	0.156
Average Difference <sup>c</sup>	0.19%	0.23%	0.32%	0.52%	1.68%	4.17%	0.00%	0.64%
Maximum Difference <sup>c</sup>	1.14%	1.84%	1.89%	2.09%	3.76%	8.34%	3.18%	2.56%

<sup>a</sup> Maximum deviation from one set with respect to the average value of the three sets.

<sup>b</sup> Values taken from the paper "Elastic Constants for Indeterminate Structures Determined with Cardboard Models," by W. J. Eney, complete original of reference 7.

<sup>c</sup> Differences with respect to the analytical values.

shown in the previous table will, with respect to the exact values, increase or decrease a small amount.

In order to give an idea of the necessary analogs in an ordinary work, those of the first set are reproduced to scale in Figs. 23 through 26, showing the procedures used in finding the characteristic values of the beam.

The evaluations of the area "A" for the stiffness, as well as that "W" for the fixed-end moment due to a concentrated load  $P$  at section 4, are done using Eq. 17. The area "W" for concentrated load  $P$  at section 6 is obtained by the use of a simplified procedure, idea of Paul H. Reimer, A.M. ASCE, that permits the saving of one cut and one balancing operation. Although this last procedure is obviously easier, Eq. 17 is followed in two templates in order to show its use, as well as the advantage of Reimer's procedure.

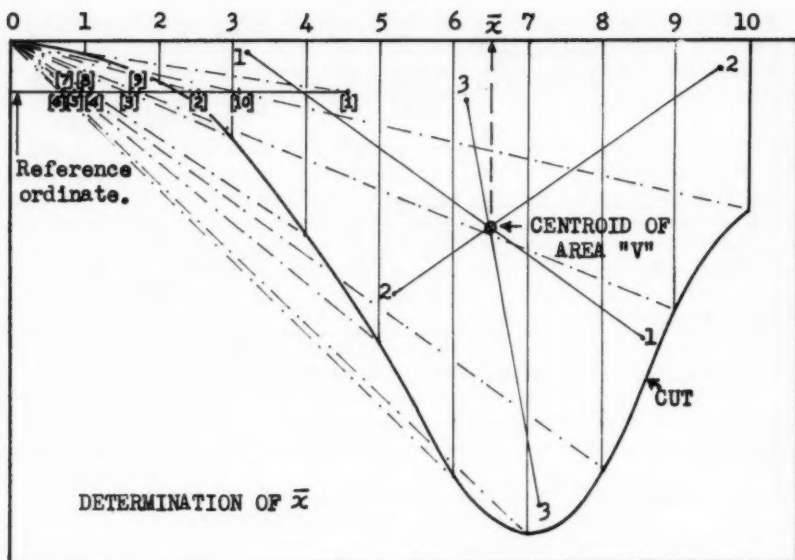


FIG. 23

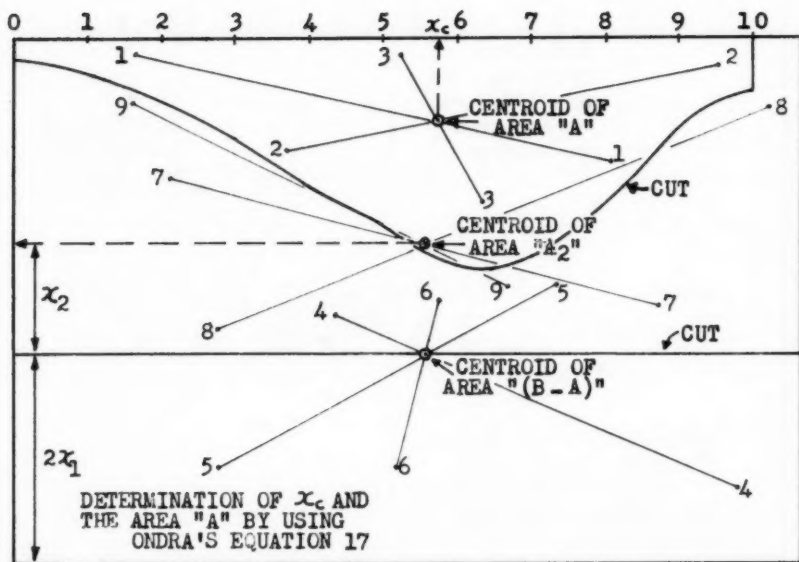


FIG. 24

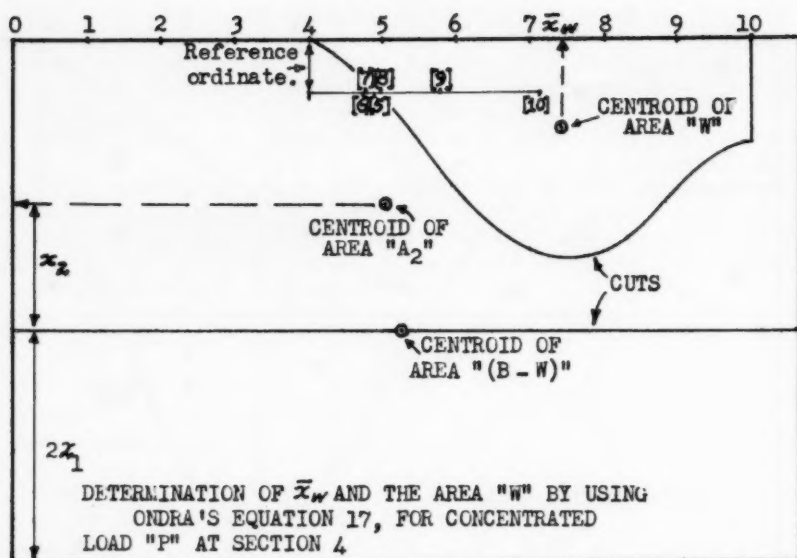


FIG. 25

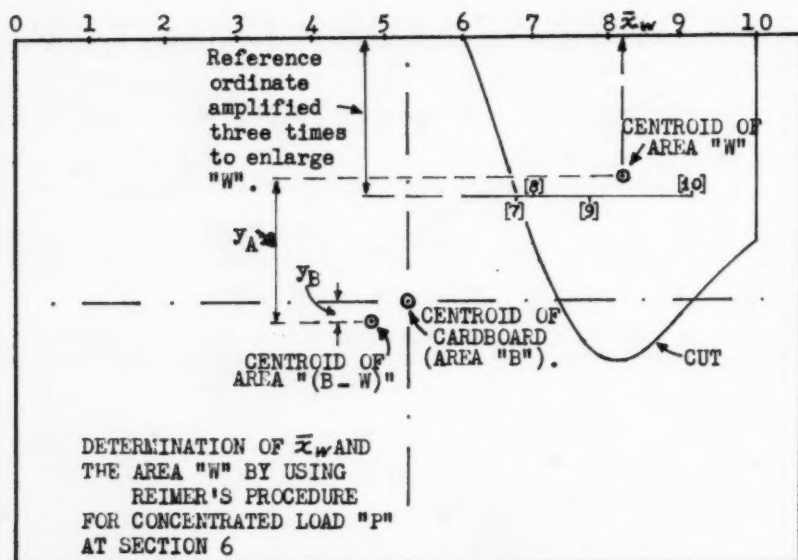
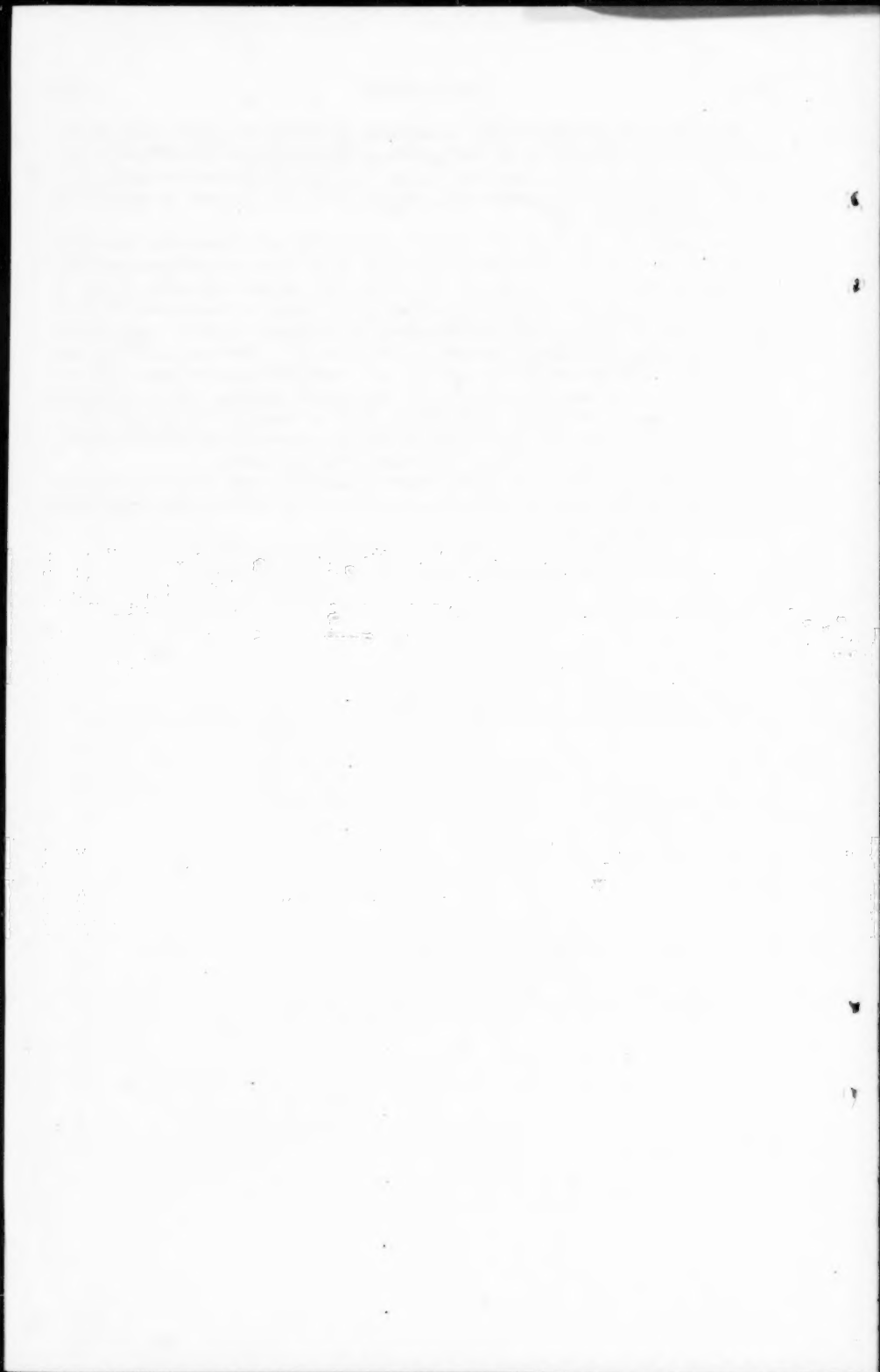


FIG. 26

Because of the constant width of the beam in study, the work could be reduced by using the cube of the depth instead of the moment of inertia as significant parameter. Because the writer's purpose is to show the application of the cardboard analog method for a general case, the moment of inertia was used in the calculations.

The results shown from the example give an idea of the accuracy and simplicity of the method in the determination of carry-over and stiffness factors, and also in dealing with fixed-end moments for concentrated load. It can be seen that for a complete study of a member, three centroid determinations must be made and two cuts must be performed on the cardboard in order to determine the carry-over and stiffness factors for both ends. For fixed-end moments due to a single concentrated load, in addition two centroids must be found with one cardboard cut. In dealing with uniform distributed loading, one centroid and one cut are only additionally required, although the template drawing is a little more time consuming. The operations are based on the assumption that Reimer's procedure will be used in finding the areas of the templates.

With a little practice, a complete study of member subjected to one concentrated load can be made, including the carry-over and stiffness determinations, in about 45 min to 1 hr.





# MATRIX ANALYSIS OF STRUCTURES CURVED IN SPACE<sup>a</sup>

Discussion by Alfredo H. -S. Ang

ALFREDO H. -S. ANG,<sup>4</sup> A. M. ASCE.—In matrix analysis of space structures, transformation from the reference system 1, 2, 3 (Fig. 9), involving the axis of the member to a fixed reference system, XYZ, or vice versa, are often encountered, that is, transformations involving Eq. 5 of the paper. For a given member in space, it is natural to take  $q_1$  to be in the direction of the axis of the member. However, having defined  $q_1$ , there are infinite systems of  $(q_1, q_2, q_3)$  that can be formed which are orthogonal sets of vectors. The author stated that  $q_2$  and  $q_3$  are taken to be along the principal axes of a cross section.

It is the purpose of this discussion to present, in more explicit terms, a transformation matrix,

$$\bar{q} = \bar{q}_1, \bar{q}_2, \bar{q}_3) \dots\dots\dots (118)$$

which would be most useful in practical cases when a member is obliquely oriented with the fixed reference frame. Referring to Fig. 9, specify  $\bar{q}_1$  to be along the axis of the member, that is

$$\bar{q}_1 = l i + m j + n k \dots\dots\dots (119)$$

in which  $l, m, n$  are the direction cosines of member  $ab$ , and  $i, j, k$  are the vectors in the fixed reference system. Choose  $\bar{q}_3$  such that

$$(\bar{q}_1^0 k) \bar{q}_3 = 0 \dots\dots\dots (120)$$

Eq. 120 means that  $\bar{q}_3$  is taken to be in the vertical plane formed by  $\bar{q}_1$  and the Z-axis. The term  $\bar{q}_2$  is perpendicular to this plane and hence lies in the XY-plane. It is readily seen from Fig. 9, that

$$\bar{q}_2 = -m i + l j \dots\dots\dots (121)$$

Finally,

$$\bar{q}_3 = \bar{q}_1 \bar{q}_2 = -lni = mnj + (l^2 + m^2) k \dots\dots\dots (122)$$

<sup>a</sup> March 1961 by Frank Baron (Proc. Paper 2779).

<sup>4</sup> Asst. Prof. of Civ. Engrg., Univ. of Illinois, Urbana, Ill.

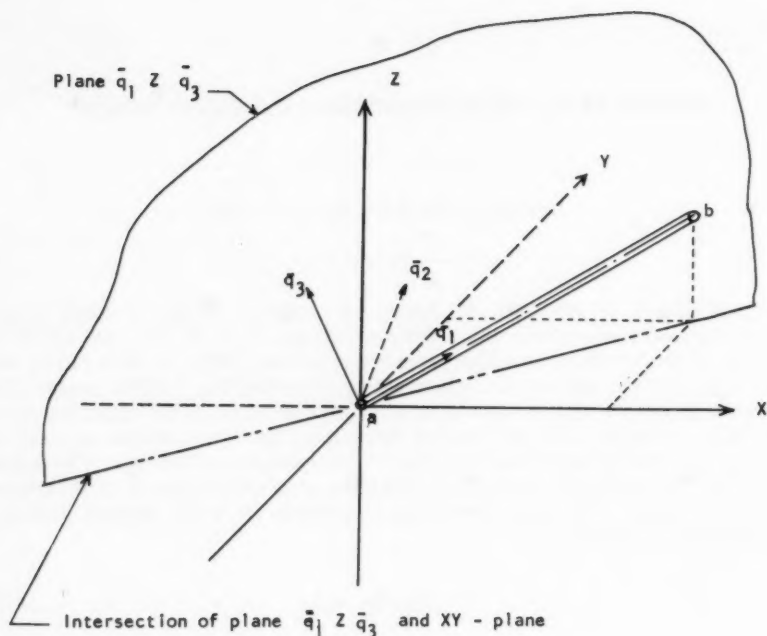


FIG. 9

and the matrix  $\bar{q}$  is

$$\bar{q} = \begin{bmatrix} 1 - m - ln \\ m + 1 - mn \\ n \quad 0 \quad (1^2 + m^2) \end{bmatrix} \dots\dots\dots (123)$$

The matrix  $\bar{q}$  of a member is easily determined when the relative positions or space coordinates of the ends of the member are given. This transformation matrix conforms with the most usual orientation of the principal axes of a cross section; that is, one of the principal axes is oriented in a vertical plane and the other principal axis in the horizontal plane.

For curved members in space, the direction cosines  $(l, m, n)$ , are those of the directed line through the end points of a member.

STEEL FRAME FOLDED PLATE ROOF<sup>a</sup>

Discussion by E. I. Fiesenheiser

E. I. FIESENHEISER,<sup>2</sup> F. ASCE.—The author is certainly to be commended for a remarkably clear and well-explained presentation of the analysis of a steel frame folded plate roof type of structure. With the availability of the newer types of high strength steel, additional economies can be achieved by careful adaptation to new designs. Further studies of structural arrangement to investigate the effects on economy of various height-to-span ratios are no doubt warranted.

Concerning the analysis of such a structure for direct stresses, the writer would like to suggest the influence-coefficient method, whereby a unit load is placed successively at the roof panel points and its effect is tabulated in each case. This would be advantageous particularly for a symmetrical structure, such as that of Fig. 7. Due to symmetry it would only be necessary to place the unit load successively at points N, H, J, and P, for a complete analysis for any vertical roof load.

Baer mentions the necessity for design of the diagonals as compression members when analysis shows them to be subjected to this type of stress. Would it not, however, be possible to use counters where these would prove economical?

As the author comments, careful detailing is essential at the joints. With reference to Fig. 6, in which a partial design is shown, making the two ridge purlins serve as a compression chord appears objectionable when the purlins are seated on top of the rafters, due to the eccentricity introduced. Actually it appears that the centroid of the compression chord should be located as nearly as possible in the plane of rafter centerlines. The writer suggests a single beam be used as the combination ridge purlin and compression chord, dropping it sufficiently so that its outer flange edges coincide with the roof line, and of a depth sufficient so that its centroid is nearly coincident with rafter centerline. Its web would be vertical. Attention should also be given to the eave strut detail so that its centroid is brought as closely as possible to the rafter centerline, thus avoiding eccentricity at this point.

With columns located only around the periphery of the building it is not quite certain that the establishment of full continuity of the rafters where they intersect at the ridge is wise. Such continuity increases the force reaction component at the ridge, reducing it at the outer ends of the rafter span, thus carrying a greater proportion of load toward the interior of the roof structure and a smaller proportion of the load is then delivered to the ends where the columns are located. For example, if in Fig. 1, rafter D-G-M were fully continuous at G, the 1,200 lb load at center of span D-G would produce 825 lb at G, rather

<sup>a</sup> June 1961, by Oliver A. Baer (Proc. Paper 2845).

<sup>2</sup> Prof. and Dir., Dept. of Civ. Engrg., Illinois Inst. of Tech., Chicago, Ill.

than 600 lb. At D the vertical reaction effect would be 487 lb, and there would be an uplift of 112 lb at M. In general, it appears that the rafter continuity at interior points would produce higher stresses in the trusses and that this is one case where continuity is not desirable. On the other hand, continuity developed at the outer column connections might reduce the load carried by the roof trusses.

# PROCEEDINGS PAPERS

The technical papers published in the past year are identified by number below. Technical-division sponsorship is indicated by an abbreviation at the end of each Paper Number, the symbols referring to: Air Transport (AT), City Planning (CP), Construction (CO), Engineering Mechanics (EM), Highway (HW), Hydraulics (HY), Irrigation and Drainage (IR), Pipeline (PL), Power (PO), Sanitary Engineering (SA), Soil Mechanics and Foundations (SM), Structural (ST), Surveying and Mapping (SU); and Waterways and Harbors (WW), divisions. Papers sponsored by the Department of Conditions of Practice are identified by the symbols (PP). For titles and order coupons, refer to the appropriate issue of "Civil Engineering." Beginning with Volume 82 (January 1956) papers were published in Journals of the various Technical Divisions. To locate papers in the Journals, the symbols after the paper number are followed by a numeral designating the issue of a particular Journal in which the paper appeared. For example, Paper 2703 is identified as 2703(ST1) which indicates that the paper is contained in the first issue of the Journal of the Structural Division during 1961.

## VOLUME 86 (1960)

OCTOBER: 2615(EM5), 2616(EM5), 2617(ST10), 2618(SM5), 2619(EM5), 2620(EM5), 2621(ST10), 2622(EM5), 2623(SM5), 2624(EM5), 2625(SM5), 2626(SM5), 2627(EM5), 2628(EM5), 2629(ST10), 2630(ST10), 2631(PO5)<sup>c</sup>, 2632(EM5)<sup>c</sup>, 2633(ST10), 2634(ST10), 2635(ST10)<sup>c</sup>, 2636(SM5)<sup>c</sup>.  
 NOVEMBER: 2637(ST11), 2638(ST11), 2639(CO3), 2640(ST11), 2641(SA6), 2642(WW4), 2643(ST11), 2644(HY9), 2645(ST11), 2646(HY9), 2647(WW4), 2648(WW4), 2649(WW4), 2650(ST11), 2651(CO3), 2652(HY9), 2653(HY9), 2654(ST11), 2655(HY9), 2656(HY9), 2657(SA6), 2658(WW4), 2659(WW4)<sup>c</sup>, 2660(SA6), 2661(CO3), 2662(CO3), 2663(SA6), 2664(CO3)<sup>c</sup>, 2665(HY9)<sup>c</sup>, 2666(SA6)<sup>c</sup>, 2667(ST11)<sup>c</sup>.  
 DECEMBER: 2668(ST12), 2669(IR4), 2670(SM6), 2671(IR4), 2672(IR4), 2673(IR4), 2674(ST12), 2675(EM6), 2676(IR4), 2677(HW4), 2678(ST12), 2679(EM6), 2680(ST12), 2681(SM6), 2682(IR4), 2683(SM6), 2684(SM6), 2685(IR4), 2686(EM6), 2687(EM6), 2688(EM6), 2689(EM6), 2690(EM6), 2691(EM6)<sup>c</sup>, 2692(ST12), 2693(ST12), 2694(HW4)<sup>c</sup>, 2695(IR4)<sup>c</sup>, 2696(SM6)<sup>c</sup>, 2697(ST12)<sup>c</sup>.

## VOLUME 87 (1961)

JANUARY: 2698(PP1), 2699(PP1), 2700(HY1), 2701(SA1), 2702(SU1), 2703(ST1), 2704(ST1), 2705(SU1), 2706(HY1), 2707(HY1), 2708(HY1), 2709(PO1), 2710(HY1), 2711(HY1), 2712(ST1), 2713(HY1), 2714(PO1), 2715(ST1), 2716(HY1), 2717(SA1), 2718(SA1), 2719(SU1)<sup>c</sup>, 2720(SA1)<sup>c</sup>, 2721(ST1), 2722(PP1)<sup>c</sup>, 2723(PO1)<sup>c</sup>, 2724(HY1)<sup>c</sup>, 2725(ST1)<sup>c</sup>.  
 FEBRUARY: 2726(WW1), 2727(EM1), 2728(EM1), 2729(WW1), 2730(WW1), 2731(EM1), 2732(SM1), 2733(WW1), 2734(SM1), 2735(EM1), 2736(EM1), 2737(PL1), 2738(PL1), 2739(PL1), 2740(PL1), 2741(EM1), 2742(ST2), 2743(EM1), 2744(WW1), 2745(WW1), 2746(SM1), 2747(WW1), 2748(EM1), 2749(WW1), 2750(WW1)<sup>c</sup>, 2751(EM1)<sup>c</sup>, 2752(SM1)<sup>c</sup>, 2753(PL1)<sup>c</sup>, 2754(ST2)<sup>c</sup>, 2755(PL1).  
 MARCH: 2756(HY2), 2757(IR1), 2758(AT1), 2759(CO1), 2760(HY2), 2761(IR1), 2762(IR1), 2763(HY2), 2764(ST3), 2765(HY2), 2766(HW1), 2767(SA2), 2768(CO1), 2769(IR1), 2770(HY2), 2771(SA2), 2772(HY2), 2773(CO1), 2774(AT1), 2775(IR1), 2776(HY2), 2777(HY2), 2778(SA2), 2779(ST3), 2780(HY2), 2781(HY2)<sup>c</sup>, 2782(HW1)<sup>c</sup>, 2783(SA2)<sup>c</sup>, 2784(CO1), 2785(CO1)<sup>c</sup>, 2786(IR1)<sup>c</sup>, 2787(ST3)<sup>c</sup>, 2788(AT1)<sup>c</sup>, 2789(HW1).  
 APRIL: 2790(EM2), 2791(SM2), 2792(SM2), 2793(SM2), 2794(SM2), 2795(SM2), 2796(SM2), 2797(SM2), 2798(EM2), 2799(EM2), 2800(EM2), 2801(EM2), 2802(ST4), 2803(EM2)<sup>c</sup>, 2804(SM2)<sup>c</sup>, 2805(ST4)<sup>c</sup>.  
 MAY: 2806(SA3), 2807(WW2), 2808(HY3), 2809(WW2), 2810(HY3), 2811(WW2), 2812(HY3), 2813(WW2), 2814(HY3), 2815(WW2), 2816(HY3), 2817(HY3), 2818(SA3), 2819(WW2), 2820(SA3), 2821(WW2), 2822(WW2)<sup>c</sup>, 2823(HY3), 2824(SA3), 2825(HY3), 2826(SA3)<sup>c</sup>, 2827(HY3)<sup>c</sup>.  
 JUNE: 2828(SM3), 2829(EM3), 2830(EM3), 2831(IR2), 2832(SM3), 2833(HW2), 2834(IR2), 2835(EM3), 2836(IR2), 2837(IR2), 2838(SM3), 2839(SM3)<sup>c</sup>, 2840(IR2)<sup>c</sup>, 2841(HW2)<sup>c</sup>, 2842(EM3)<sup>c</sup>, 2843(ST5), 2844(ST5), 2845(ST5), 2846(ST5)<sup>c</sup>.  
 JULY: 2847(PO2), 2848(SU2), 2849(HY4), 2850(PO2), 2851(HY4), 2852(PO2), 2853(SU2), 2854(HY4), 2855(PO2), 2856(PO2), 2857(PO2), 2858(SA4), 2859(SU2), 2860(SA4), 2861(PO2), 2862(SA4), 2863(HY4), 2864(HY4), 2865(HY4), 2866(HY4), 2867(HY4), 2868(PO2)<sup>c</sup>, 2869(SA4)<sup>c</sup>, 2870(SU2)<sup>c</sup>, 2871(HY4), 2872(HY4)<sup>c</sup>, 2873(SU2), 2874(SA4).  
 AUGUST: 2875(WW3), 2876(WW3), 2877(WW3), 2878(SM4), 2879(ST6), 2880(EM4), 2881(SM4), 2882(EM4), 2883(WW3), 2884(EM4), 2885(SM4), 2886(WW3), 2887(EM4), 2888(WW3), 2889(AT2), 2890(AT2), 2891(AT2), 2892(AT2), 2893(AT2), 2894(AT2), 2895(AT2), 2896(AT2), 2897(AT2), 2898(AT2), 2899(AT2), 2900(AT2), 2901(AT2), 2902(SM4), 2903(ST6), 2904(ST6), 2905(SM4), 2906(ST6), 2907(EM4), 2908(ST6), 2909(EM4), 2910(ST6), 2911(EM4), 2912(SM4), 2913(ST6), 2914(WW3)<sup>c</sup>, 2915(ST6)<sup>c</sup>, 2916(EM4)<sup>c</sup>, 2917(SM4)<sup>c</sup>.  
 SEPTEMBER: 2918(SA5)<sup>c</sup>, 2919(HW3)<sup>c</sup>, 2920(HY5)<sup>c</sup>, 2921(SA5), 2922(PL2), 2923(IR3), 2924(HY5), 2925(HY5), 2926(CP1), 2927(HY5), 2928(IR3), 2929(IR3), 2930(HY5), 2931(CP1), 2932(PL2), 2933(HY5), 2934(HY5), 2935(HY5), 2936(HY5), 2937(HW3), 2938(CP1), 2939(PL2), 2940(SA5), 2941(SA5), 2942(SA5), 2943(HY5), 2944(PL2)<sup>c</sup>, 2945(CP1)<sup>c</sup>, 2946(IR3), 2947(HW3), 2948(IR3), 2949(IR3)<sup>c</sup>.  
 OCTOBER: 2950(PP2), 2951(PP2), 2952(PP2), 2953(ST7), 2954(SM5), 2955(ST7), 2956(ST7), 2957(ST7), 2958(ST7), 2959(SM5), 2960(EM5), 2961(EM5), 2962(ST7), 2963(ST7), 2964(EM5), 2965(SM5), 2966(SM5), 2967(ST7), 2968(ST7), 2969(ST7), 2970(ST7), 2971(SM5), 2972(SM5)<sup>c</sup>, 2973(EM5)<sup>c</sup>, 2974(ST7)<sup>c</sup>, 2975(PP2).

c. Discussion of several papers, grouped by divisions.

# AMERICAN SOCIETY OF CIVIL ENGINEERS

## OFFICERS FOR 1961

### PRESIDENT

GLENN W. HOLCOMB

### VICE-PRESIDENTS

*Term expires October 1961:*

CHARLES B. MOLINEAUX  
LAWRENCE A. ELSENER

*Term expires October 1962:*

DONALD H. MATTERN  
WILLIAM J. HEDLEY

### DIRECTORS

*Term expires October 1961:*

THOMAS J. FRATAR  
EARL F. O'BRIEN  
DANIEL B. VENTRES  
CHARLES W. BRITZIUS  
WAYNE G. O'HARRA  
FRED H. RHODES, JR.  
N. T. VEATCH

*Term expires October 1962:*

ELMER K. TIMBY  
SAMUEL S. BAXTER  
THOMAS M. NILES  
TRENT R. DAMES  
WOODROW W. BAKER  
BERNHARD DORNBLATT

*Term expires October 1963:*

ROGER H. GILMAN  
HENRY W. BUCK  
EARLE T. ANDREWS  
C. MERRILL BARBER  
JOHN D. WATSON  
HARMER E. DAVIS

### PAST PRESIDENTS

*Members of the Board*

FRANCIS S. FRIEL

FRANK A. MARSTON

---

### EXECUTIVE SECRETARY

WILLIAM H. WISELY

### TREASURER

E. LAWRENCE CHANDLER

### ASSISTANT SECRETARY

DON P. REYNOLDS

### ASSISTANT TREASURER

LOUIS R. HOWSON

---

## PROCEEDINGS OF THE SOCIETY

HAROLD T. LARSEN

*Manager of Technical Publications*

PAUL A. PARISI

*Editor of Technical Publications*

MARVIN L. SCHECHTER

*Associate Editor of Technical Publications*

IRVIN J. SCHWARTZ

*Assistant Editor of Technical Publications*

---

### COMMITTEE ON PUBLICATIONS

THOMAS M. NILES, *Chairman*

WAYNE G. O'HARRA, *Vice-Chairman*

BERNHARD DORNBLATT

HENRY W. BUCK

JOHN D. WATSON

HARMER E. DAVIS

